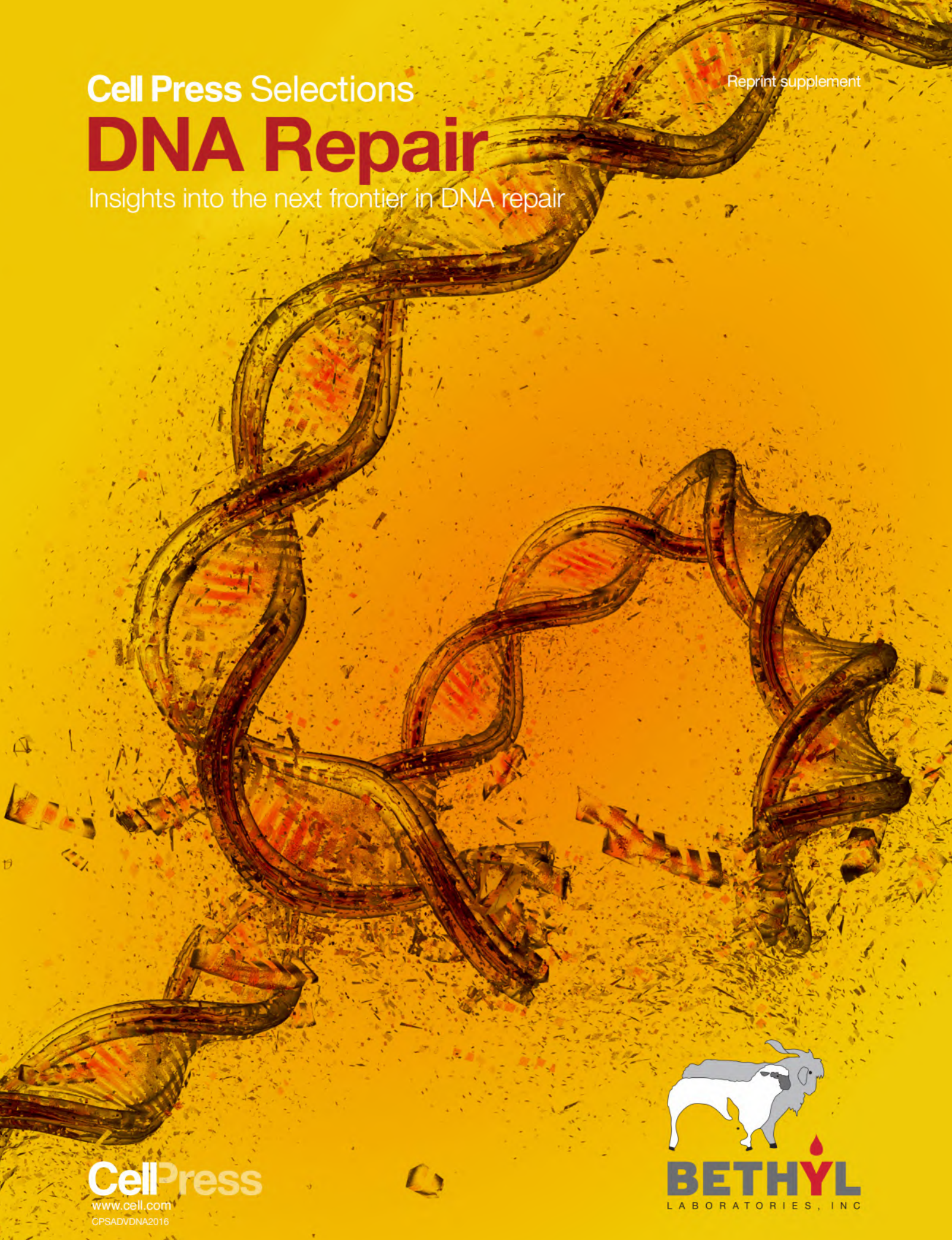


Cell Press Selections

Reprint supplement

# DNA Repair

Insights into the next frontier in DNA repair



**CellPress**

[www.cell.com](http://www.cell.com)  
CPSADVDNA2016



**BETHYL**  
LABORATORIES, INC

QUALIFIED ANTIBODIES | MADE IN THE USA | VALIDATED IN THE USA

&%Y'#  
GOOD!

  
**BETHYL**  
LABORATORIES, INC  
Really Good Antibodies

### Darn Good!—Great Reactions Start with Really Good Antibodies

That's because every antibody is manufactured and validated on-site using a unique process that verifies target specificity with paired antibodies raised against distinct protein epitopes. We've heard our customers' great reactions for over 40 years and now we'd like to hear what you'll say.

Request a free trial size antibody by visiting [bethyl.com/8855](http://bethyl.com/8855)

Terms & Conditions Apply. Please see webpage for complete details.

©2016 Bethyl Laboratories, Inc. All rights reserved.

## Foreword

---

2015 was undoubtedly the year of DNA repair, with five researchers being recognized for their contributions in both the Nobel Prize in Chemistry and the Albert Lasker Basic Medical Research Award. You can read more about the science and scientists behind each of these prizes in the editorial and essays included in this *Cell Press Selections* edition on DNA repair.

The response to DNA damage is complex, eliciting tens of thousands of protein post-translational modifications in the typical mammalian cell. These modifications help the cell to select the appropriate repair mechanisms to fix the damage and minimize the number of mistakes that could lead to mutations or genome rearrangements.

The articles and review that we are reprinting in this collection reveal how DNA repair mechanisms are coordinated with each other and with processes such as DNA replication, transcription, and mitosis. They also explore ways to exploit these connections and dependencies in cancers lacking a particular DNA repair pathway.

Of course, these articles just scratch the surface of what Cell Press has published and will publish in this ever-evolving field, so we hope you'll visit [www.cell.com](http://www.cell.com) on a regular basis to keep up on the latest DNA repair news.

Finally, we are grateful that Bethyl Laboratories has provided generous support to help bring this reprint collection to you.

**For more information about Cell Press Selections:**  
Jonathan Christison  
Program Director, Best of Cell Press  
e: [jchristison@cell.com](mailto:jchristison@cell.com)  
p: 617-397-2893  
t: @cellPressBiz

QUALIFIED ANTIBODIES | MADE IN THE USA | VALIDATED IN THE USA

HOLY  
@Y#!

  
**BETHYL**  
LABORATORIES, INC  
Really Good Antibodies

**Holy Cow!—Great Reactions Start with Really Good Antibodies**

That's because every antibody is manufactured and validated on-site using a unique process that verifies target specificity with paired antibodies raised against distinct protein epitopes. We've heard our customers' great reactions for over 40 years and now we'd like to hear what you'll say.

Request a free trial size antibody by visiting [bethyl.com/8855](http://bethyl.com/8855)

Terms & Conditions Apply. Please see webpage for complete details.

©2016 Bethyl Laboratories, Inc. All rights reserved.

# DNA Repair

Insights into the next frontier in DNA repair

## Editorial

2015: The Year of DNA Repair

*Brian Plosky*

## BenchMarks

Celebrating DNA's Repair Crew

*Thomas A. Kunkel*

Deciphering the DNA Damage Response

*James E. Haber*

## Forum

The Journey of DNA Repair

*Natalie Saini*

## Review

Targeting the DNA Damage Response in Cancer

*Mark J. O'Connor*

## Articles

**Mutational Strand Asymmetries in Cancer Genomes Reveal Mechanisms of DNA Damage and Repair**

*Nicholas J. Haradhvala, Paz Polak, Petar Stojanov, Kyle R. Covington, Eve Shinbrot, Julian M. Hess, Esther Rheinbay, Jaegil Kim, Yosef E. Maruvka, Lior Z. Braunstein, Atanas Kamburov, Philip C. Hanawalt, David A. Wheeler, Amnon Koren, Michael S. Lawrence, and Gad Getz*

**Non-catalytic Roles for XPG with BRCA1 and BRCA2 in Homologous Recombination and Genome Stability**

*Kelly S. Trego, Torsten Groesser, Albert R. Davalos, Ann C. Parplys, Weixing Zhao, Michael R. Nelson, Ayesu Hlaing, Brian Shih, Björn Rydberg, Janice M. Pluth, Miaw-Sheue Tsai, Jan H.J. Hoeijmakers, Patrick Sung, Claudia Wiese, Judith Campisi, and Priscilla K. Cooper*

**Chromothripsis and Kataegis Induced by Telomere Crisis**

*John Maciejowski, Yilong Li, Nazario Bosco, Peter J. Campbell, and Titia de Lange*

**HELB Is a Feedback Inhibitor of DNA End Resection**

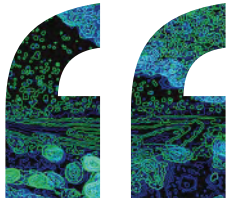
*Ján Tkáč, Guotai Xu, Hemanta Adhikary, Jordan T.F. Young, David Gallo, Cristina Escribano-Díaz, Jana Krietsch, Alexandre Orthwein, Meagan Munro, Wendy Sol, Abdallah Al-Hakim, Zhen-Yuan Lin, Jos Jonkers, Piet Borst, Grant W. Brown, Anne-Claude Gingras, Sven Rottenberg, Jean-Yves Masson, and Daniel Durocher*

**Targeting BRCA1 and BRCA2 Deficiencies with G-Quadruplex-Interacting Compounds**

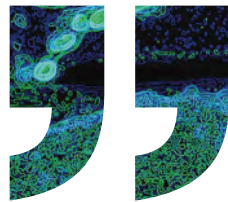
*Jutta Zimmer, Eliana M.C. Tacconi, Cecilia Folio, Sophie Badie, Manuela Porru, Kerstin Klare, Manuela Tumiati, Enni Markkanen, Swagata Halder, Anderson Ryan, Stephen P. Jackson, Kristijan Ramadan, Sergey G. Kuznetsov, Annamaria Biroccio, Julian E. Sale, and Madalena Tarsounas*

**The Fanconi Anemia Pathway Maintains Genome Stability by Coordinating Replication and Transcription**

*Rebekka A. Schwab, Jadwiga Nieminuszczy, Fenil Shah, Jamie Langton, David Lopez Martinez, Chih-Chao Liang, Martin A. Cohn, Richard J. Gibbons, Andrew J. Deans, and Wojciech Niedzwiedz*



# We won't waste your time.



Our hands-on approach means we're more responsive, the review process is more efficient and turnaround times are shorter.

**When you choose Cell Press you get the attention you deserve.**

For more information visit: [www.cell.com/values](http://www.cell.com/values)

Your **work** is our **life**



## 2015: The Year of DNA Repair

I started my undergraduate education at Colgate University in 1993, and by then, each of the 2015 Nobel Laureates in Chemistry, Paul Modrich, Thomas Lindahl, and Aziz Sancar, had already made the core discoveries for which they were appropriately recognized last month. Armed with my copy of *Genes V* (Lewin, 1994; Oxford University Press) for my seminar course on molecular biology, I was introduced to the mechanisms of base excision repair (BER), nucleotide excision repair (NER), and mismatch repair (MMR) for which the prize was awarded.

The Nobel announcement prompted me to open my now rather sun-bleached copy of *Genes V* (which still finds its home in my office). In the light of our current knowledge of these systems and the looming complexity of eukaryotic DNA repair, it's remarkable to me how much we already understood back then about the bacterial systems. At one point during my undergraduate course, we discussed a series of papers on MMR, including several from Paul Modrich's group, and I was struck by the conservation between prokaryotic and eukaryotic MMR and by the link between MMR and a form of hereditary colon cancer, which had recently been described in a pair of *Cell* papers. Reading and discussing those papers with the professor and the rest of the class was the start of my long-standing interest in DNA repair.

The repair mechanisms that this year's laureates elucidated are seemingly simple and elegant mechanisms that all make use of the fact that one strand of the double helix can serve as a template for its replication (as alluded to by Watson and Crick) and for its repair (as Phil Hanawalt often reminds us). Yet the key unifying theme in their discoveries was really the recognition and removal of the damaged or incorrect nucleotides. While each of the laureates has contributed in many ways to the field over the years, I'd like to delve a bit deeper into why they are being recognized for "mechanistic studies of DNA repair."

Tomas Lindahl discovered DNA glycosylases, which initiate BER, and his group has worked out many of the key factors involved in BER. Cells are equipped with a variety of glycosylases with diverse specificity to remove many modified base from the DNA backbone to start the repair process. Many of these enzymes are also critical in the active removal of cytosine methylation and the regulation of gene expression in plants and animals.

Paul Modrich characterized the bacterial MMR system to understand how replication errors are corrected by a network of proteins that recognize both the mismatch and nascent DNA strand as well as factors for removal of the incorrect strand. His lab has also explored the role of MMR in hereditary colon cancer and other cancers. Seemingly paradoxically, while loss of MMR can cause cancer, it can also result in the resistance of some cancers to certain types of chemotherapy.

Aziz Sancar has focused mainly on DNA damage caused by ultraviolet light (UV). Most notably, he characterized the bacterial NER proteins, and his group has also contributed to our understanding of mammalian responses to UV including NER and the replication checkpoint. They also explored prokaryotic enzymes that carry out light-dependent reversal of UV-induced DNA damage. These photolyases have homologs in mammals, which despite having no apparent role in DNA repair are key light receptors in circadian biology known as cryptochromes or CRY proteins.

As a graduate student, I focused on the contributions of NER and BER to the repair of alkylated DNA bases, and so the names Lindahl and Sancar were used liberally throughout the introduction to my thesis. With roughly ten years of research experience in the DNA repair field and nine more as an editor handling many DNA repair papers, it is personally tremendously exciting to see the recognition of the whole field in 2015 by the Nobel and Lasker committees. Also, this year, the use of the PARP inhibitor, olaparib, that exploits tumor-specific changes in the DNA damage response has been approved for the treatment of ovarian cancer (stay tuned for a Review of this topic in our next issue). All of this provides extraordinary validation of the power of basic research and the need for a balance among basic, translational, and clinical science.

*Molecular Cell* has been privileged to publish so much exciting work from so many scientists in this field (including Lindahl and Modrich). Without the pioneering biochemistry on the enzymes that initiate repair by the removal of individual bases or stretches of nucleotides, it would have been extremely difficult to interpret the genetics and cell biology of these pathways or understand their importance in human disease.

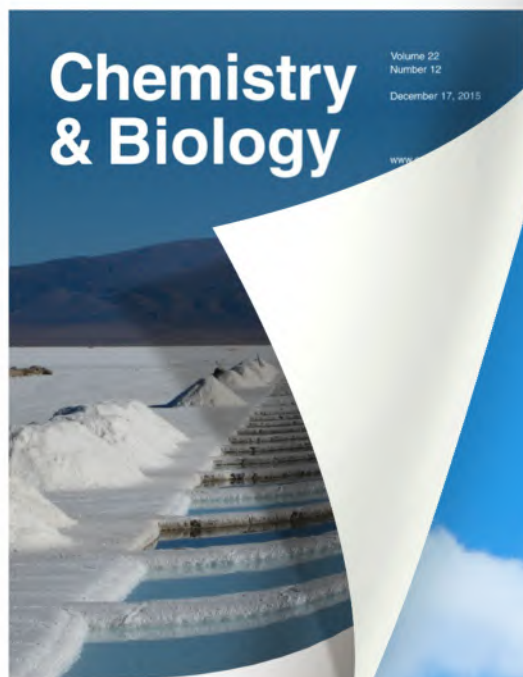
Congratulations to Paul, Tomas, Aziz, and the whole DNA repair field!

### Brian Plosky

Deputy Editor, *Molecular Cell*

<http://dx.doi.org/10.1016/j.molcel.2015.10.034>

# FAREWELL



# HELLO



# Introducing Cell Chemical Biology

As the first journal in the field, our focus has always been on chemical biology, and now we have a title that reflects that. *Cell Chemical Biology* draws on the rich heritage of the Cell Press portfolio and reflects our vision for the journal – today and tomorrow.

To learn more about the aims and scope of *Cell Chemical Biology* visit:  
[cell.com/cell-chemical-biology](http://cell.com/cell-chemical-biology)

## Celebrating DNA's Repair Crew

Thomas A. Kunkel<sup>1,\*</sup>

<sup>1</sup>Genome Integrity and Structural Biology Laboratory, National Institute of Environmental Health Sciences, NIH, Research Triangle Park, NC 27709, USA

\*Correspondence: kunkel@niehs.nih.gov

<http://dx.doi.org/10.1016/j.cell.2015.11.028>

**This year, the Nobel Prize in Chemistry has been awarded to Tomas Lindahl, Aziz Sancar, and Paul Modrich for their seminal studies of the mechanisms by which cells from bacteria to man repair DNA damage that is generated by normal cellular metabolism and stress from the environment. These studies beautifully illustrate the remarkable power of DNA repair to influence life from evolution through disease susceptibility.**

When Watson and Crick described the structure of DNA in 1953, their initial Nobel-Prize-winning studies did not discuss how DNA damage and its repair affect its information content. More than 60 years later, we know that, in the time it takes you to read this article, each cell in your body will generate a very large number and a wide diversity of lesions in DNA. This DNA degradation is not limited to human beings but occurs in all organisms on earth. Fortunately, we also know that organisms from bacteria to man have developed several pathways to repair these lesions and that these repair pathways are extremely important for a wide variety of biological processes from the evolution of species to the modulation of human disease susceptibility. The Royal Swedish Academy of Sciences now celebrates the incredible value of DNA repair by awarding the 2015 Nobel Prize in Chemistry to three pioneers of basic research on DNA repair mechanisms, Tomas Lindahl, Aziz Sancar, and Paul Modrich.

Even as the central dogma positing DNA to RNA to protein was being elucidated, the amazing contributions of DNA repair to genome integrity were being discovered. For example, studies performed by several truly outstanding investigators before and during the 1950s and 1960s (reviewed in Friedberg et al., 2006) revealed that treating bacterial or eukaryotic cells with exogenous agents that damage DNA results in cell death or mutagenesis and that these effects are suppressed by DNA repair. Then, in 1972, Tomas Lindahl published that the glycosylic bond between a purine base and the DNA backbone can spontane-

ously be cleaved at a readily detectable rate (Lindahl and Nyberg, 1972), thereby generating an apurinic site that can be lethal or mutagenic if not repaired. He also showed that large numbers of oxidized, alkylated, and deaminated bases are produced in DNA as a consequence of normal processes that occur in cells every day and that spontaneous or enzymatic release of these modified bases can form large numbers of abasic sites. These elegant studies highlighted the need to repair DNA lesions resulting not only from external environmental stress but also from normal cellular metabolism.

Importantly, Lindahl did not stop there and, by 1993, he had defined the basic mechanism of base excision repair (BER), which repairs the lesions he had quantified (Lindahl, 1993). BER can be initiated by any of several DNA glycosylases that remove a modified base. Lindahl's first example was removal of a uracil generated by deamination of cytosine in a G-C base pair (Figure 1A), which is a reaction catalyzed by uracil DNA glycosylase. Abasic site endonuclease, discovered in the late 1960s and early 1970s, then cleaves this site, or abasic sites that are generated spontaneously, to generate a DNA end with sugar-phosphate group lacking a base, i.e., a deoxyribosephosphate (dRP) group. DNA polymerase fills the gap and the dRP group is removed, after which DNA ligation completes BER. These mechanistic studies have led to the award of this year's prize to Lindahl. Based on his work and the work of several other outstanding investigators, we now know there are several variations on this BER theme, depending on the lesions being re-

paired, the DNA glycosylase that removes the lesion, the nuclease that cuts the DNA backbone, the polymerase that performs the DNA synthesis reaction, the enzyme that removes the dRP group, and the ligase that seals the gap. As a consequence, the number of nucleotides replaced can vary from a single nucleotide replacement during "short-patch" BER (as in Figure 1A) to cleavage of a slightly longer flap by an endonuclease that results in "long-patch" BER (e.g., see Prasad et al., 2011). We also know that BER is incredibly important biologically. Defects in the proteins that participate in BER are associated with lethality and/or mutagenesis in organisms from bacteria to man, and mutations that result from defective BER can affect evolution, the aging process, and susceptibility to human diseases such as cancer and neurodegenerative diseases.

The wealth of early studies of DNA repair also revealed that exposure of DNA or cells to UV light generates DNA photoproducts. In bacteria, DNA photoproducts can be converted back to normal base pairs either through direct reversal by DNA photolyase or by removal and replacement during another type of repair, nucleotide excision repair (NER). A large body of work on the mechanisms of action and the integration of these two repair processes has garnered a share of this year's Nobel Prize for Aziz Sancar. While working as a graduate student with C.S. Rupert in the mid-1970s, Sancar cloned the *E. coli* photolyase gene (Sancar and Rupert, 1978). Then, working as a principal investigator in the 1980s, he performed seminal studies describing the mechanism of action of photolyase

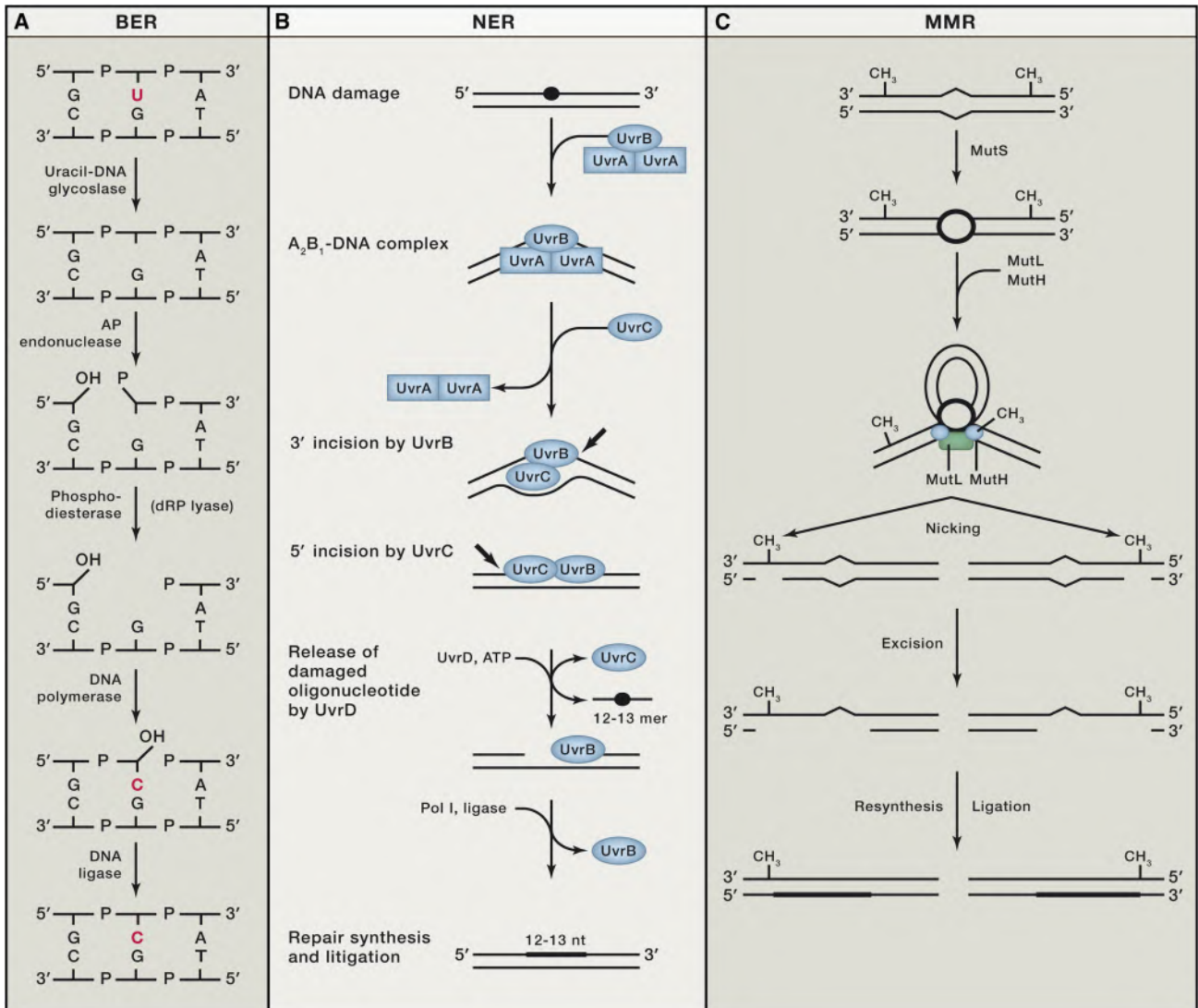


**Figure 1. The Mechanisms of *Escherichia coli* BER, NER, and MMR**

(A) The mechanism of single-nucleotide BER of uracil arising from deaminated cytosine, as described by Lindahl (1993).

(B) The basic mechanism of NER described by Sancar (Petit and Sancar, 1999).

(C) The basic mechanism of *E. coli* MMR (Modrich, 1991). See text for full descriptions and for additional studies of eukaryotic repair mechanisms.

in reversing photoproducts (see Sancar et al., 1987 and references therein). He also examined a role for the mammalian homolog of bacterial photolyase in circadian rhythm—i.e., the regulation of biological processes in response to light. Equally importantly, Sancar cloned several genes required for nucleotide excision repair in *E. coli*, and he and his colleagues then described their mechanism of action (Petit and Sancar, 1999). He showed that lesions resulting from exposure to sunlight or certain chemicals are recognized by the Uvr proteins to

initiate NER (Figure 1B). The pathway begins with lesion recognition by the UvrA and UvrB proteins. This recognition reshapes the DNA to allow the nuclease activities of the UvrB and UvrC proteins to incise the DNA backbone on both sides of the lesion, permitting the UvrD helicase to release an oligonucleotide containing the lesion. After this release, re-synthesis of DNA and ligation completes NER.

Sancar also performed seminal studies to identify and characterize the proteins involved in eukaryotic NER. Eukaryotic NER is mechanistically similar to prokary-

otic NER, but it requires many more gene products and removes a larger damaged oligonucleotide than does prokaryotic NER. Moreover, eukaryotic NER is differentiated into global NER of the whole genome and transcription-coupled NER that specifically operates on transcribed genes. We now know that the protein requirements for these two types of NER differ somewhat (Schärer, 2013). This fact is of great continuing interest not only mechanistically, but also because the health consequences of the failure of the two types of NER differ. In addition,

Sancar has more recently found and is vigorously investigating the role of a mammalian homolog of bacterial photolyase in circadian control of mammalian NER, with one possible goal being chrono-chemotherapy (Sancar et al., 2010).

The third Nobel laureate in Chemistry for 2015 is Paul Modrich. He too richly deserves this honor for his studies elucidating the mechanisms underlying a third, very important type of DNA repair, mismatch repair (MMR). By 1980, elegant studies by several outstanding bacterial geneticists had demonstrated that mismatched base pairs in the DNA of certain bacteria are corrected by MMR that is directed to one of the two DNA strands by unmethylated adenines present in GATC sequences and that this repair requires the products of the *MutS*, *MutL*, *MutH*, and *UvrD* genes. These facts prompted a series of studies in which Modrich began to unravel the mechanisms underlying MMR in *E. coli*. By 1989 (Lahue et al., 1989), Modrich reported that MMR is initiated when MutS protein binds to a mismatch (Figure 1C). The mediator protein MutL then binds to MutS-DNA, allowing these proteins, with assistance from the beta clamp protein, to perform an ATP-dependent search of the DNA for GATC sequences containing adenines that are transiently hemimethylated for a very short time after replication. MutS and MutL then interact with MutH, allowing the endonuclease activity of MutH to incise the DNA backbone of the transiently unmethylated—i.e., newly replicated—DNA strand. This incision can be introduced either 5' or 3' of the mismatch, allowing the UvrD helicase to promote excision of the newly replicated DNA containing the mismatch by any of four nucleases. Correct DNA re-synthesis and ligation then complete *E. coli* MMR (Modrich, 1991).

In the late 1980s, Modrich also began to use cell free extracts to examine the mechanism of eukaryotic MMR. Just as his colleagues had shown for BER and NER, Modrich showed that the mechanisms of prokaryotic and eukaryotic MMR share many common features but that eukaryotic MMR is more complicated. He shared in the discovery of

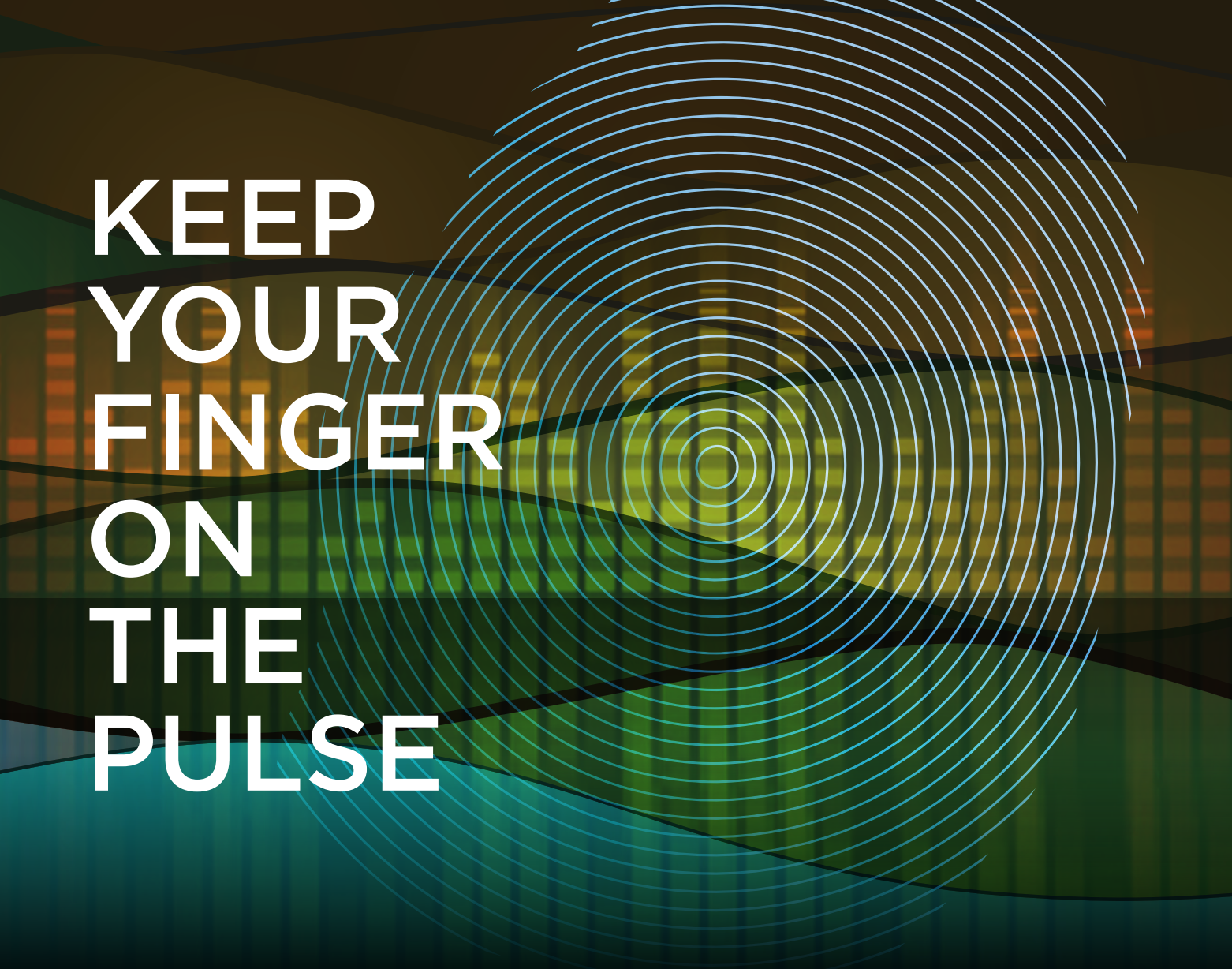
eukaryotic MutS $\alpha$  in 1993, and he has led the field in describing how this heterodimer cooperates with a second heterodimer, MutL $\alpha$ , to promote MMR recognition, signaling for strand discrimination and mismatch excision. Among Modrich's most important recent findings is that the PCNA sliding clamp that encircles DNA and participates in both replication and MMR, working in conjunction with MutS $\alpha$  bound to a mismatch, activates an endonuclease activity in MutL $\alpha$ . This nuclease activity nicks the DNA in only one strand, thereby allowing nuclear DNA replication errors in the newly synthesized strand to be repaired very efficiently (Kadyrov et al., 2006). Remarkably, endonuclease activity is also present in most prokaryotic MutL homologs. This strongly implies that, for most organisms on earth, the major strand discrimination signal and entry point for mismatch excision during MMR involves sliding clamp-dependent nicking of the newly replicated DNA strand by bacterial MutL or eukaryotic MutL $\alpha$ . The many interesting questions that remain in this field can now be examined with an appreciation of the general mechanism of MMR outlined by Modrich's work.

Each of this year's Nobel laureates in chemistry share with their many colleagues the knowledge that DNA repair comes in many forms that sometimes overlap. Sancar and Modrich have co-authored articles showing that NER and MMR can sometimes repair the same lesions (e.g., see Mu et al., 1997), and they have shown that the proteins involved in NER and MMR have additional functions in cellular checkpoint responses to DNA damage (Lindsey-Boltz et al., 2014; Liu et al., 2010). The mechanistic studies by all three Nobel laureates are also beautifully complemented by extensive studies of additional types of DNA repair conducted by other talented investigators. This includes the repair of DNA double-stranded breaks by homologous recombination and by non-homologous end joining, repair of DNA-DNA and DNA-protein crosslinks, and repair of ribonucleotides incorporated into DNA. Moreover, the various types of DNA repair are controlled and coordinated with each other in space and time and with other

cellular transactions, including replication, transcription, and cellular signaling mechanisms. Obviously, after only a few decades of work to sort out how evolution has gotten us to this point in the lives of many and very different organisms on earth, we still have much to learn. That said, it is a great pleasure to celebrate what we already know at this moment, thanks in large measure to the outstanding mechanistic studies of DNA repair conducted for several decades by Tomas Lindahl, Aziz Sancar, and Paul Modrich. As we eagerly look forward to what will be discovered in the future, we, their colleagues and friends, congratulate them!

## REFERENCES

- Friedberg, E.C., Walker, G.C., Siede, W., Wood, R.C., Schultz, R., and Ellenberger, T. (2006). DNA Repair and Mutagenesis, Second Edition (American Society for Microbiology).
- Kadyrov, F.A., Dzantiev, L., Constantin, N., and Modrich, P. (2006). *Cell* 126, 297–308.
- Lahue, R.S., Au, K.G., and Modrich, P. (1989). *Science* 245, 160–164.
- Lindahl, T. (1993). *Nature* 362, 709–715.
- Lindahl, T., and Nyberg, B. (1972). *Biochemistry* 11, 3610–3618.
- Lindsey-Boltz, L.A., Kemp, M.G., Reardon, J.T., DeRocco, V., Iyer, R.R., Modrich, P., and Sancar, A. (2014). *J. Biol. Chem.* 289, 5074–5082.
- Liu, Y., Fang, Y., Shao, H., Lindsey-Boltz, L., Sancar, A., and Modrich, P. (2010). *J. Biol. Chem.* 285, 5974–5982.
- Modrich, P. (1991). *Annu. Rev. Genet.* 25, 229–253.
- Mu, D., Tursun, M., Duckett, D.R., Drummond, J.T., Modrich, P., and Sancar, A. (1997). *Mol. Cell. Biol.* 17, 760–769.
- Petit, C., and Sancar, A. (1999). *Biochimie* 81, 15–25.
- Prasad, R., Beard, W.A., Batra, V.K., Liu, Y., Shock, D.D., and Wilson, S.H. (2011). *Mol. Biol. (Mosk.)* 45, 586–600.
- Sancar, A., and Rupert, C.S. (1978). *Gene* 4, 295–308.
- Sancar, G.B., Jorns, M.S., Payne, G., Fluke, D.J., Rupert, C.S., and Sancar, A. (1987). *J. Biol. Chem.* 262, 492–498.
- Sancar, A., Lindsey-Boltz, L.A., Kang, T.H., Reardon, J.T., Lee, J.H., and Ozturk, N. (2010). *FEBS Lett.* 584, 2618–2625.
- Schärer, O.D. (2013). *Cold Spring Harb. Perspect. Biol.* 5, a012609.



# KEEP YOUR FINGER ON THE PULSE

## With Cell Press Reviews

Looking for authoritative reviews on the forefront of science? Turn to Cell Press. Our editors stay abreast of the latest developments so they can commission expert, cutting-edge reviews.

To propel your research forward, faster, turn to Cell Press Reviews. Our insightful, authoritative reviews—published across the life sciences in our primary research and *Trends* journals—go beyond synthesis and offer a point of view.

Find your way  
with Cell Press Reviews

[www.cell.com/reviews](http://www.cell.com/reviews)

**CellPress**  
Your work is our life

## Deciphering the DNA Damage Response

James E. Haber<sup>1,\*</sup>

<sup>1</sup>Department of Biology and Rosenstiel Basic Medical Sciences Research Center, Brandeis University, Waltham, MA 02454, USA

\*Correspondence: haber@brandeis.edu

<http://dx.doi.org/10.1016/j.cell.2015.08.034>

**This year's Albert Lasker Basic Medical Research Award honors Evelyn Witkin and Stephen J. Elledge, two pioneers in elucidating the DNA damage response, whose contributions span more than 40 years.**

Bacterial or human cells devote significant resources to maintain the integrity of their genomes. Among the most severe challenges are sources of DNA damage such as ultraviolet (UV) light and other chemical agents that alter DNA bases. Crosslinking of DNA bases creates blocks to normal DNA replication that must be removed or bypassed. Genome integrity is also assaulted by ionizing radiation and other clastogens that cause double-strand breaks that must be rejoined, either by nonhomologous end-joining or by homologous recombination. For repair to be successful, it must be completed before the cell divides; incompletely replicated chromosomes become trapped, while acentric broken chromosome segments get lost or mis-segregated. Failures of the DNA damage response are a common cause of cancer in humans. To assure that repair is accomplished before cell division, cells have evolved complex surveillance mechanisms to identify DNA damage, to impose checkpoints that arrest cell division until repair is completed, and to assure that an appropriate DNA repair response is launched. This year's Lasker prize honors two visionary scientists whose experiments and revolutionary insights set the stage for our present understanding of these critical processes.

Evelyn Witkin's contributions to the field of DNA repair began with her first publication, in 1946, identifying a mutant *E. coli* strain that is resistant to both UV light and X-rays. She noted that this strain does not show the usual delay in cell division or the filamentous elongation before cell division that is normally seen in wild-type strains. Subsequently, she noted many similarities between UV-induced filament formation and the UV-induced activation of the dormant phage  $\lambda$ . After moving from Cold Spring Harbor

Laboratory to the State University of New York Downstate Medical Center, Witkin pursued these ideas while also providing key insights into the process of UV-induced mutagenesis, identifying a "dark repair" process in addition to the photo-reversal of pyrimidine dimers and suggesting the existence of error-prone DNA polymerases.

In her seminal paper (Witkin, 1967), Evelyn Witkin invoked the ideas recently proposed by Jacob and Monod of a repressor that inhibits both UV-induced phenomena and that itself would be inactivated by UV irradiation. By this time, it was already known that phage  $\lambda$  itself has a repressor that is inactivated by UV light. Witkin proposed that the presence of UV photodimers triggers the inactivation of a common repressor that would then allow the expression of genes, which in turn would promote both the arrest of cell division and the induction of the

phage. Subsequently, Miro Radman, a postdoctoral fellow in Paris, circulated a letter in 1971 to leading scientists in the field, proposing the concept of a general "SOS response." Radman's ideas were not formally published and widely available until 1975, but Witkin quickly embraced this idea. She summarized the rapidly growing body of knowledge in a comprehensive review on "Ultraviolet mutagenesis and inducible DNA repair in *Escherichia coli*" (Witkin, 1976).

Soon after Witkin advanced her hypothesis, several labs identified key elements of this regulation. Activation of phage  $\lambda$  and inhibition of cell division depend on the recombination protein RecA. Witkin herself, now at Rutgers University, showed that UV-induced mutagenesis depends on an apparently UV-induced error-prone form of DNA replication controlled by LexA (Witkin and George, 1973), which proved to be the repressor of many SOS genes. The induction of phage  $\lambda$  depends on the proteolytic cleavage of the  $\lambda$  repressor, a process involving RecA. Initially RecA was thought to be a protease as well as the central recombination protein, but subsequent work has shown that RecA, which forms a filament on single-stranded DNA that is created at stalled replication forks (i.e., after UV irradiation) or on the resected single-stranded ends of X-ray broken DNA ends, acts as an allosteric effector to promote the autocleavage of both LexA and the  $\lambda$  repressor.

In the more than 40 years since Witkin's hypothesis began to take molecular shape, the SOS response has emerged as a much more complex network of responses to DNA damage. Nearly 70 genes have been identified that either regulate LexA response or are regulated directly by LexA and are induced by



**Witkin and Elledge at Graham Walker's induction into the National Academy of Sciences in 2013. Photo credit: Gordon Walker.**

DNA damage. These genes have been identified by reporter gene fusions to various promoters and subsequently by gene expression profiling or by bioinformatics approaches using the consensus SOS repressor sequence. Among the processes controlled by SOS are cell division, nucleotide excision repair, DNA repair by recombination, and translesion DNA polymerases. Witkin's decisive role in understanding the bacterial DNA damage response has been recognized by many awards, most notably the National Medal of Science in 2004.

One particular LexA-regulated "bypass" DNA polymerase, encoded by the UmuDC operon, provides the link between Evelyn Witkin and Stephen Elledge. Witkin had generously supported the research of young researchers such as Graham Walker (in his case, Witkin carried a sensitive UV dose meter from Paris to Cambridge, MA, so that Walker could carry out his experiments). Elledge and Walker (Elledge and Walker, 1983) cloned the UmuC and UmuD open reading frames. UmuD is cleaved in a RecA-dependent fashion to a smaller, active form called UmuD'. Witkin herself showed that there is a third key RecA-mediated activity, independent of the operon's induction by LexA or the cleavage of UmuD.

In Walker's lab, Elledge first displayed his remarkable facility in creating novel genetic screens and molecular tools for the analysis of complex regulation, inventing phasmid vectors for the complementation of *E. coli* mutants. Indeed, throughout his career, Elledge has invented remarkable research tools and genetic screens, most recently a powerful new method for profiling human populations with a drop of blood, using a synthetic human virome to detect anti-viral antibodies.

After earning his Ph.D., Elledge moved to Ron Davis' lab at Stanford for his postdoctoral work, making the transition from prokaryotes to the emerging eukaryotic model system, budding yeast. Elledge's initial goal was to use phage-expression techniques to screen for yeast's RecA on the assumption that an anti-RecA antibody would find the gene. Instead, he accidentally pulled out the gene encoding the small subunit of ribonucleotide reductase, Rnr2 (Elledge and Davis, 1987). (It would take another 5 years

before yeast's Rad51 protein would be shown to be similar to RecA.) Elledge demonstrated that *RNR2* mRNA is strongly induced by DNA damage and realized that this might be a tool through which he could interrogate the regulatory pathway responsible for *RNR2*'s induction.

Elledge's characterization of *RNR2* regulation quickly established that it does not fit the paradigm of the *E. coli* response: its expression is still induced by UV in the absence of protein synthesis. A 42-bp regulatory region would confer damage inducibility to a reporter gene but does not share sequence similarity with the LexA binding site. Importantly, a protein kinase, Dun1, was found to be a key regulator of RNR gene expression after blocking DNA replication (Zhou and Elledge, 1993). Dun1 itself is activated for autophosphorylation in response to DNA damage. This finding established that DNA damage is indeed transduced by signal transduction, through a protein kinase, and was the first demonstration of what is now called the DNA damage response (DDR) pathway.

The concept of a DNA-damage-dependent cell-cycle delay in eukaryotes was intuited by Tobey (Tobey, 1975) studying drug and UV-sensitive mutants in fission yeast, and the concept of a DNA damage checkpoint was first articulated by Weinert and Hartwell (Weinert and Hartwell, 1988), who demonstrated that mutants in the *RAD9* gene, while proficient for repair of X-ray induced lesions, are X-ray sensitive because they fail to arrest prior to mitosis and thus give cells sufficient time to repair lesions before chromosome segregation. Several additional mutations, including mutants in *MEC1* (mitotic entry checkpoint) and *RAD53* (originally identified as an X-ray sensitive mutation), had been identified by Weinert et al. (Weinert et al., 1994), but the biochemical activities of these gene products were unknown. Elledge's lab contemporaneously identified S-phase arrest-defective (*sad*) mutants, including an allele of *RAD53* and an allele of *MEC1*, which later proved to be yeast's homolog of the ATR kinase (Allen et al., 1994). Allen et al. showed first that Rad53 is itself a protein kinase. Second, Rad53's kinase activity is required for the activation of Dun1, and Dun1 remains unphosphorylated in the *rad53*

mutant. Third, Rad53 is involved in the control of three distinct checkpoints: a pause in G1 after DNA damage, the failure to induce RNR genes in response to a replication block, and a failure to delay mitosis in the face of unrepaired DNA damage. At this point, it became clear that the response to DNA damage in eukaryotes was not going to be similar to the regulation of the LexA repressor. The studies of eukaryotic regulation "implicate protein phosphorylation in the cellular response to DNA damage and replication blocks" (Allen et al., 1994).

Indeed, the notion of a cascade of phosphorylation signals, and the counteracting dephosphorylations that must help terminate the checkpoint response, is the primary theme of eukaryotic cell-cycle regulation in response to DNA damage. On top of this scheme is another feature especially of higher eukaryotes, the self-destruction of cells with DNA damage by apoptosis, mediated principally through the p53 gene.

When Elledge set up his own lab at Baylor College of Medicine in 1989, he soon began to work on mammalian cells as well as yeast, embracing questions of the role of cyclin-dependent kinases in cell-cycle control. The yeast work quickly informed recent discoveries in the DNA damage response in mammalian cells. Soon thereafter, Elledge's lab showed that Mec1 and another kinase Tel1 phosphorylate and regulate Rad53 (Sanchez et al., 1996) and later that Tel1 phosphorylates yet another protein kinase Chk1. In collaboration with Errol Friedberg's lab, they established that Mec1 is a homolog of the mammalian ATM gene, whose mutant cells show many defects in response to DNA damage. In fact, Mec1 later proved to be the homolog of another PI3K-like kinase, ATR, while Tel1 is the closer homolog to the ATM-related ATR gene. As the work progressed, it became evident that the PI3K-like kinases Mec1 and Tel1 sat atop a protein kinase cascade whose immediate downstream targets include Rad53 and Chk1 (Matsuoka et al., 1998). In a flurry of other papers, the Elledge lab demonstrated the parallels between the Mec1/Tel1 regulation of Rad53 and Chk1 with the mammalian ATM/ATR control of Chk1 and Rad53's mammalian homolog, Chk2, respectively (Liu et al., 2000; Matsuoka et al., 1998;

Sanchez et al., 1999). The link between ATR and cell-cycle control became stronger when Elledge's lab, in collaboration with Helen Piwnica-Worms, demonstrated that Chk1 phosphorylates the key Cdk2 regulator, Cdc25 phosphatase (Sanchez et al., 1997), and later, with Elledge's long-time collaborator Wade Harper, showed that this phosphorylation triggers the degradation of Cdc25 and imposes cell-cycle arrest (Jin et al., 2003). Of course, while celebrating Stephen Elledge, it is important to remember that there were many important contributions by other labs as these ideas blossomed. To cite only a few, Yosef Shiloh's group first cloned and sequenced ATM; Michael Kastan demonstrated a key control by ATM of p53; Antony Carr and Karlene Cimprich characterized ATR; and Paul Russell and Paul Nurse outlined the phosphoregulation of the Cdk2 kinase.

The outlines of the full DDR are still being inked in. After moving to Harvard Medical School, Elledge's lab continued to enlarge the domain of DDR responses. A phosphoproteomic screen identified more than 700 *in vivo* substrates of ATM and ATR, implicating ATM/ATR control of processes as diverse as kinetochore

function, regulation of the cytoskeleton, control of ubiquitylation, and protein degradation by both the proteasome and autophagy. Most recently, his lab has carried out an analysis of proteins recruited to DNA-damaged chromatin and a quantitative "atlas" of ubiquitylation and acetylation associated with the DDR. In addition, Elledge's masterful reviews have guided the field. Stephen Elledge's insights into the eukaryotic DNA damage response have led to many awards, most recently the Rosenstiel Award and the Canada Gairdner Award in 2013.

Both bacteria and eukaryotes exhibit a complex DDR, but this is one of those fascinating instances in which there has been little evolutionary conservation of the mechanisms to achieve a common goal. Our present understanding of these processes owes much to Evelyn Witkin and Stephen Elledge, the two winners of this year's Albert Lasker Award in Basic Medical Research.

#### REFERENCES

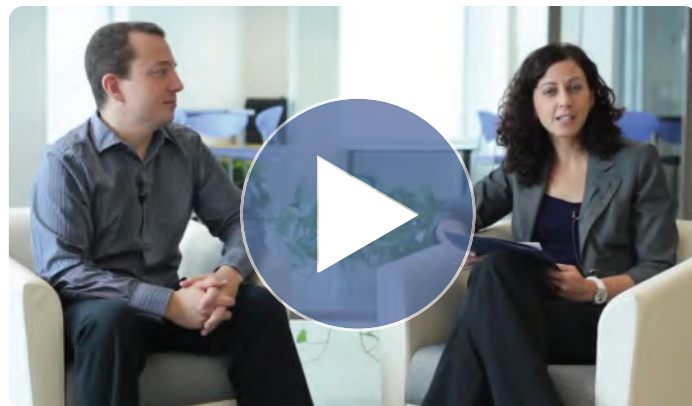
- Allen, J.B., Zhou, Z., Siede, W., Friedberg, E.C., and Elledge, S.J. (1994). *Genes Dev.* *8*, 2401–2415.
- Elledge, S.J., and Davis, R.W. (1987). *Mol. Cell. Biol.* *7*, 2783–2793.
- Elledge, S.J., and Walker, G.C. (1983). *J. Mol. Biol.* *164*, 175–192.
- Jin, J., Shirogane, T., Xu, L., Nalepa, G., Qin, J., Elledge, S.J., and Harper, J.W. (2003). *Genes Dev.* *17*, 3062–3074.
- Liu, Q., Guntuku, S., Cui, X.S., Matsuoka, S., Cortez, D., Tamai, K., Luo, G., Carattini-Rivera, S., DeMayo, F., Bradley, A., et al. (2000). *Genes Dev.* *14*, 1448–1459.
- Matsuoka, S., Huang, M., and Elledge, S.J. (1998). *Science* *282*, 1893–1897.
- Sanchez, Y., Desany, B.A., Jones, W.J., Liu, Q., Wang, B., and Elledge, S.J. (1996). *Science* *271*, 357–360.
- Sanchez, Y., Wong, C., Thoma, R.S., Richman, R., Wu, Z., Piwnica-Worms, H., and Elledge, S.J. (1997). *Science* *277*, 1497–1501.
- Sanchez, Y., Bachant, J., Wang, H., Hu, F., Liu, D., Tetzlaff, M., and Elledge, S.J. (1999). *Science* *286*, 1166–1171.
- Tobey, R.A. (1975). *Nature* *254*, 245–247.
- Weinert, T.A., and Hartwell, L.H. (1988). *Science* *241*, 317–322.
- Weinert, T.A., Kiser, G.L., and Hartwell, L.H. (1994). *Genes Dev.* *8*, 652–665.
- Witkin, E.M. (1967). *Proc. Natl. Acad. Sci. USA* *57*, 1275–1279.
- Witkin, E.M. (1976). *Bacteriol. Rev.* *40*, 869–907.
- Witkin, E.M., and George, D.L. (1973). *Genetics* *73* (Suppl 73), 73, 91–10.
- Zhou, Z., and Elledge, S.J. (1993). *Cell* *75*, 1119–1127.

# Want to learn how to prepare, submit and publish an article in a Cell Press journal?

Watch the Cell Press publication guide.



*Chapter 1: Before manuscript submission*



*Chapter 2: After initial submission*



*Chapter 3: Decision process*



*Chapter 4: After manuscript acceptance*

for more information visit  
[www.cell.com/publicationguide](http://www.cell.com/publicationguide)



## Forum

## The Journey of DNA Repair

Natalie Saini<sup>1,\*</sup>

**Twenty one years ago, the DNA Repair Enzyme was declared ‘Molecule of the Year’. Today, we are celebrating another ‘year of repair’, with the 2015 Nobel Prize in Chemistry being awarded to Aziz Sancar, Tomas Lindahl, and Paul Modrich for their collective work on the different DNA repair pathways.**

The integrity of DNA is constantly under threat by many genotoxic agents both within and outside the cell. It is estimated that the DNA in a typical mammalian cell is exposed to  $10^4$  to  $10^5$  lesions every day in the form of altered bases, abasic sites, inter- or intrastrand crosslinks, bulky adducts, mismatches and small insertions and deletions, and single- or double-strand breaks [1]. Given the vast repertoire of damage encountered by the genome, it is hardly surprising that cells have evolved a multitude of repair pathways to maintain integrity. Either the absence or erroneous repair of such damage has dire consequences for the organism in the form of increased mutation load and chromosomal rearrangements. Unrepaired double-strand breaks can also lead to loss of entire chromosomes. These phenomena have been implicated in cancers and various hereditary diseases. Examples include predisposition to hereditary non-polyposis colon cancer in individuals with defects in mismatch repair (MMR); colorectal cancer and sporadic glioblastomas associated with mutations in base excision repair (BER); breast cancer in carriers of mutations in *BRCA1* or *BRCA2*; Nijmegen breakage syndrome; cancer-prone ataxia telangiectasia; and Bloom and Werner syndromes due to defective recombination repair. Furthermore, increased mutation loads resulting from

the lack of, or error-prone repair, have been proposed to play a role in aging. In support of this theory are several studies demonstrating that DNA damage and mutations accumulate in aging cells, as well as recent work linking defective DNA repair with premature aging phenotypes and an increased incidence of cancer (reviewed in [2]).

**DNA Repair: The Early Days**

The discovery that DNA and its replication form the predominant basis of heritability triggered an avalanche of studies seeking to elucidate the factors that influence its stability. The knowledge of deleterious effects of mutagenic chemicals and radiation on DNA, accumulated mostly from classical genetics, soon led to the realization that repairing DNA lesions is critical. Among the first DNA repair pathways to be discovered was enzymatic photoreactivation – the process of reverting UV-induced pyrimidine dimers to monomers by photolyase in the presence of light. The cloning of the *Escherichia coli* gene *phr* and its biochemical characterization by Aziz Sancar [3] was crucial in understanding the function of this remarkable enzyme. Thereafter, Sancar went on to study other mechanisms of DNA repair that are activated post-UV exposure. His work along with others in the cloning and biochemical analysis of the bacterial *uvr* proteins steered the discovery of the nucleotide excision repair (NER) pathway [4]. Similarly, the 1974 discovery of DNA glycosylases in *E. coli* by Tomas Lindahl pioneered studies on the BER pathway [5]. Subsequently, nucleases dedicated to the cleavage and consequent repair of abasic sites formed in DNA after the action of glycosylases have been found in various other systems. Today, there are 11 known glycosylases in mammalian cells.

The existence of an enzymatic mechanism correcting abnormally paired bases in DNA was first postulated by Robin Holliday in 1964 to explain the fate of such mismatches formed in the process of meiotic recombination in ascomycetes [6]. It was

later noted that MMR was also required to assure the fidelity of DNA replication by correcting nucleotide misincorporation and primer–template misalignment by the replicative polymerases. However, a key question remained unanswered: How is MMR able to distinguish between the parental and the newly synthesized strands of DNA? Using elegant biochemical and genetic approaches, Paul Modrich demonstrated that strand discrimination in *E. coli* is achieved by differential methylation of the parental strand at adenines in the GATC context [7]. Modrich’s subsequent work on both eukaryotic and prokaryotic MMR has been seminal in revealing the roles for the major players involved in this repair system.

**DNA Repair: The Current Era**

The past few decades have witnessed a tremendous advancement in our understanding of DNA repair. Current technological breakthroughs have enabled us to address several unresolved questions regarding the intricate mechanistic details underlying various repair pathways: How is DNA damage sensed by these pathways? Which are the key components of these pathways and what are their roles in repairing different lesions? Where in the cell do the different pathways operate? How do cells regulate error-free versus error-prone repair mechanisms? We now have valuable insight on a few of these problems, as illustrated briefly through the following examples.

The development of live cell imaging has led to the elucidation of the spatiotemporal interactions of repair proteins with DNA lesions in real time. Utilization of fluorescently tagged repair proteins with the ability to engineer damage at defined loci in the genome has enabled researchers to decipher the dynamics of DNA repair. Analogous approaches using fluorescent tagging of double-strand breaks in the genome have further revealed that broken chromosomes have increased mobility within the nucleus and that breaks tend to localize at the nuclear periphery during repair [8].

Another powerful approach gaining widespread popularity is the analysis of DNA repair at the single-molecule level, which allows researchers to stretch and visualize individual DNA molecules, and study the dynamics of DNA repair. This method was recently used to demonstrate that break-induced replication, a double-strand break–repair pathway used to repair one-ended breaks, proceeds via a conservative mode of inheritance unlike the canonical semiconservative DNA synthesis [9]. Other single-molecule techniques include the use of ‘DNA curtains’ wherein individual DNA molecules are tethered at one end to help understand how proteins traverse the length of DNA; tethered particle motion to study the change in DNA length upon interaction with enzymes; and the use of molecular tweezers to study the mechanical properties of DNA–protein and protein–protein interactions (reviewed in [10]).

With the advent of the ‘omics’ era it is now possible to analyze the mutagenic potential of various endogenous and exogenous mutagens and to study repair efficacy across the genome. Chromatin immunoprecipitation (ChIP) using antibodies against lesions, in combination with Next-Gen sequencing, has been extremely valuable in determining the global pervasiveness of damaging lesions such as RNA:DNA hybrids [11]. ChIP has been additionally used with antibodies

against various DNA repair factors to measure their accessibility to different genomic regions. Additionally, high-throughput sequencing of cancer genomes has immensely helped in detection of the mutational mechanisms operative in them. For instance, cancers with defective MMR demonstrate elevated levels of microsatellite instability. By contrast, increased clusters of A/T mutations have been attributed to the translesion polymerase Pol $\eta$  and this signature is detectable in some blood cancers, such as multiple myeloma, chronic leukemia, and B cell lymphoma. Furthermore, evidence of impaired repair can be gleaned from the elevated amount of mutations attributable to known mutagens. Notable examples include UV-induced C→T changes in TC or CC contexts or A:T→T:A mutations induced by mutagenic aristolactam adducts formed by aristolochic acid that are repaired by NER (reviewed in [12]).

### Concluding Remarks

The availability of cutting edge technology has ushered in a new era of DNA repair research where studies from model organisms serve as a basis to elucidate the mechanisms underlying repair in complex systems including human cancers. The future holds great promise for the field as we continue to seek better understanding of the cellular mechanisms employed to preserve

genome integrity. This is truly a great time to be in the field of DNA repair!

<sup>1</sup>Genome Integrity and Structural Biology Laboratory, National Institute of Environmental Health Sciences, Research Triangle Park, NC 27709, USA

\*Correspondence: natalie.saini@nih.gov (N. Saini).  
<http://dx.doi.org/10.1016/j.trecan.2015.11.001>

### References

1. Hoeijmakers, J.H. (2009) DNA damage, aging, and cancer. *N. Engl. J. Med.* 361, 1475–1485
2. Lombard, D.B. *et al.* (2005) DNA repair, genome stability, and aging. *Cell* 120, 497–512
3. Sancar, A. and Rupert, C.S. (1978) Cloning of the *phr* gene and amplification of photolyase in *Escherichia coli*. *Gene* 4, 295–308
4. Sancar, A. and Rupp, W.D. (1983) A novel repair enzyme: UVRABC excision nuclease of *Escherichia coli* cuts a DNA strand on both sides of the damaged region. *Cell* 33, 249–260
5. Lindahl, T. (1974) An N-glycosidase from *Escherichia coli* that releases free uracil from DNA containing deaminated cytosine residues. *Proc. Natl. Acad. Sci. U.S.A.* 71, 3649–3653
6. Holliday, R. (2007) A mechanism for gene conversion in fungi. *Genet. Res.* 89, 285–307
7. Lu, A.L. *et al.* (1983) Methyl-directed repair of DNA base-pair mismatches in vitro. *Proc. Natl. Acad. Sci. U.S.A.* 80, 4639–4643
8. Oza, P. *et al.* (2009) Mechanisms that regulate localization of a DNA double-strand break to the nuclear periphery. *Genes Dev.* 23, 912–927
9. Saini, N. *et al.* (2013) Migrating bubble during break-induced replication drives conservative DNA synthesis. *Nature* 502, 389–392
10. Robison, A.D. and Finkelstein, I.J. (2014) High-throughput single-molecule studies of protein–DNA interactions. *FEBS Lett.* 588, 3539–3546
11. Chan, Y.A. *et al.* (2014) Genome-wide profiling of yeast DNA:RNA hybrid prone sites with DRIP-chip. *PLoS Genet.* 10, e1004288
12. Roberts, S.A. and Gordenin, D.A. (2014) Hypermutation in human cancer genomes: footprints and mechanisms. *Nat. Rev. Cancer* 14, 786–800

# Targeting the DNA Damage Response in Cancer

Mark J. O'Connor<sup>1,\*</sup>

<sup>1</sup>Senior Principal Scientist, Head of the DNA Damage Response Biology Area, Oncology IMED, AstraZeneca, Mereside, Alderley Park, Macclesfield SK10 4TG, United Kingdom

\*Correspondence: mark.j.oconnor@astrazeneca.com

<http://dx.doi.org/10.1016/j.molcel.2015.10.040>

An underlying hallmark of cancers is their genomic instability, which is associated with a greater propensity to accumulate DNA damage. Historical treatment of cancer by radiotherapy and DNA-damaging chemotherapy is based on this principle, yet it is accompanied by significant collateral damage to normal tissue and unwanted side effects. Targeted therapy based on inhibiting the DNA damage response (DDR) in cancers offers the potential for a greater therapeutic window by tailoring treatment to patients with tumors lacking specific DDR functions. The recent approval of olaparib (Lynparza), the poly (ADP-ribose) polymerase (PARP) inhibitor for treating tumors harboring *BRCA1* or *BRCA2* mutations, represents the first medicine based on this principle, exploiting an underlying cause of tumor formation that also represents an Achilles' heel. This review highlights the different concepts behind targeting DDR in cancer and how this can provide significant opportunities for DDR-based therapies in the future.

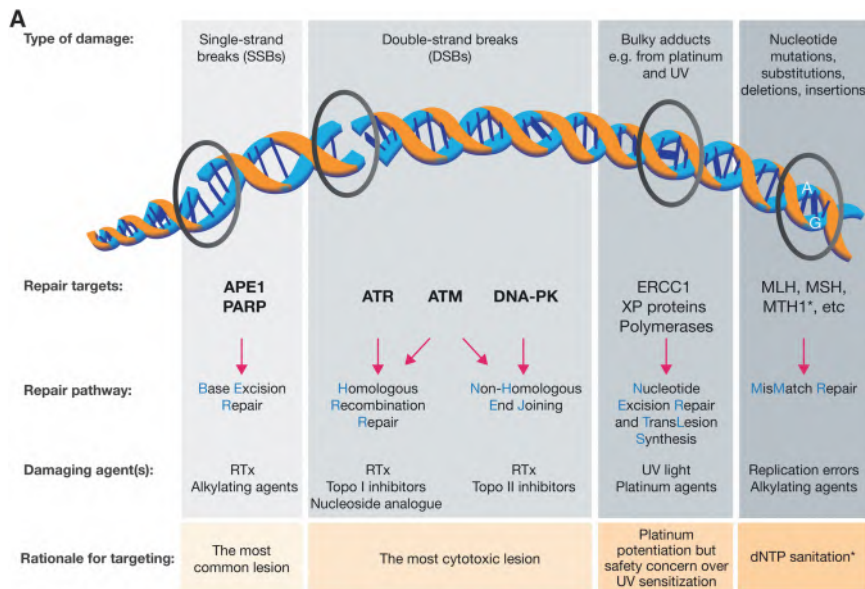
## The DNA Damage Response as a Source of Anticancer Drug Targets

Tens of thousands of DNA damage events occur every day in our cells, and many different mechanisms have evolved to deal with them (Ciccia and Elledge, 2010; Jackson and Bartek, 2009). The DNA damage response (DDR) is a collective term for the plethora of different intra- and inter-cellular signaling events and enzyme activities that result from the induction and detection of DNA damage. These include events that lead to cell-cycle arrest, regulation of DNA replication, and the repair or bypass of DNA damage. Should DNA repair not be possible or suboptimal repair lead to an unsupportable level of genomic instability, DDR can also impact on downstream cell fate decisions, such as cell death or senescence that can either be dependent or independent of the immune system (d'Adda di Fagagna et al., 2003; Freund et al., 2010; Kang et al., 2015). Recent analyses suggest that there are at least 450 proteins integral to DDR (Pearl et al., 2015), and the choice of optimal drug target within DDR will be based on what type of DNA damage repair is to be inhibited and when in the cell cycle that damage is likely to occur (Figure 1).

Different forms of DNA damage evoke responses by different repair mechanisms and signaling pathways (Hoeijmakers, 2001), and while there is not an absolute redundancy as such, different DDR pathways may potentially compensate in the absence of the optimal or bespoke repair pathway. An analogy might be carpentry tools where, in the absence of a specific tool for a repair job, another tool can be used, although that tool may not be quite as effective and the results not quite so accurate. In human cells there are five major repair pathways. Modified bases, abasic sites, and the DNA single-strand breaks (SSBs) primarily generated from their processing are the most common form of DNA damage, estimated at more than 20,000 events per cell per day (Lindahl et al., 1995), and these are repaired by the base excision repair (BER) pathway (Caldecott, 2014; Wilson et al., 2010). There are two major forms of repair when dealing with DNA double-strand breaks (DSBs) (Shibata and Jeggo, 2014), the

most genotoxic form of DNA lesion due to the issues associated with accurate chromosome segregation during cell division. Homologous recombination repair (HRR) is a relatively accurate and efficient repair pathway but depends upon the presence of undamaged sister chromatid DNA (Moynahan and Jasin, 2010), while the non-homologous end-joining (NHEJ) pathways (C-NHEJ and alt-NHEJ) are not dependent on the presence of replicated DNA and, while still effective, are less accurate, potentially introducing DNA rearrangements (Ceccaldi et al., 2015; Lieber, 2010; Radhakrishnan et al., 2014). The nucleotide excision repair (NER) pathway deals with modified nucleotides that distort the structure of the double helix (Hoeijmakers, 2009) and is the pathway that primarily deals with UV-induced damage but also plays an important role in dealing with DNA damage induced by platinum salts as well. The mismatch repair (MMR) pathway deals with replication errors, including mismatch base-pairing as well as nucleotide insertions and deletions (Jiricny, 2006). Another common event during the replication process is the incorporation of ribonucleotides. Removal by RNase H2 prevents the increased likelihood of DNA strand breaks that would otherwise form due to the greater susceptibility of ribonucleotides to hydrolysis compared with deoxynucleotides (Reijns et al., 2012).

In addition to these major pathways, nucleotide damage in the form of adducts that can block replication fork progression, either occurring naturally through environmental mutagens or from chemotherapy such as platinum agents, can be bypassed as a short-term solution by a mechanism known as translesion synthesis (Goodman and Woodgate, 2013; Waters et al., 2009). Other mechanisms of DNA damage tolerance that allow DNA replication to proceed in the presence of damage include convergence of adjacent replicons, discontinuous synthesis of Okazaki fragments on the lagging DNA strand, and re-priming of DNA synthesis downstream of lesions on the leading strand (Bianchi et al., 2013; Heller and Marians, 2006). DNA inter-strand cross-links that can also impair replication are repaired through the activities of the Fanconi anemia (FA) complex



\*MTH1/dNTP sanitation proposed as an opportunity but emerging data have not been able to provide validation  
Shown in bold are SSB and DSB repair targets that are currently being evaluated in clinical trials

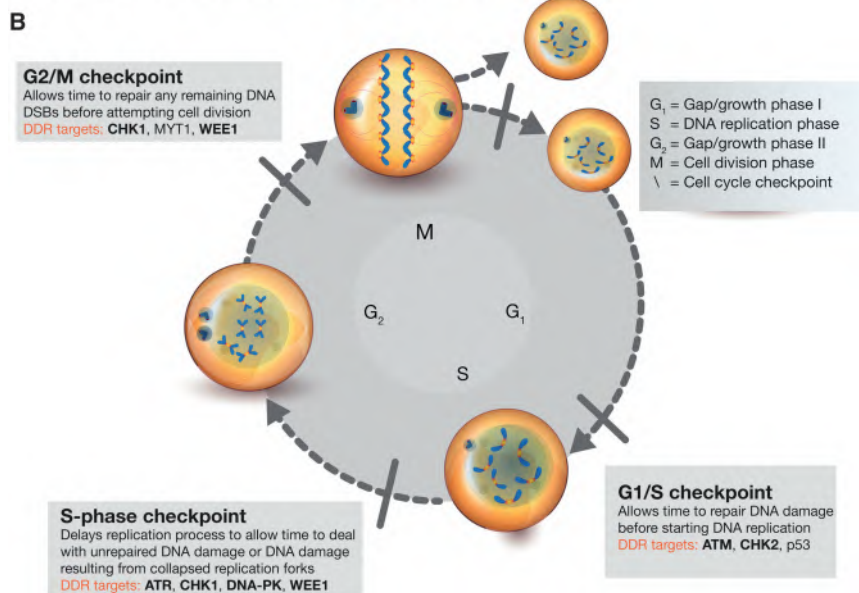


**Figure 1. DDR Pathway and Cell-Cycle Targets**

(A) DDR pathway targets, including the rationale for targeting these pathways. Shown in bold are SSB and DSB repair targets that are currently being evaluated in clinical trials. \*MTH1/dNTP sanitation proposed as an opportunity, but emerging data have not been able to provide validation (Alwan et al., 2015).

(B) DDR cell-cycle targets. DDR targets are shown for each cell-cycle checkpoint, with those in bold currently being evaluated in clinical trials. APE1, AP endonuclease 1; ATM, ataxia-telangiectasia mutated; ATR, ataxia-telangiectasia and Rad3-related; DNA-PK, DNA-dependent protein kinase; PARP, poly(ADP-ribose) polymerase; RTx, radiotherapy; Topo, topoisomerase.

ATM, CHK2, and p53. The intra-S phase checkpoint proteins ATR, CHK1, DNA-PK, and WEE1 can delay replication origin firing to provide time to deal with any unrepaired DNA damage that has occurred, thus preventing under-replicated DNA regions being taken beyond S-phase. The activities of the G2/M checkpoint proteins including CHK1, MYT1, and WEE1 lead to an increase in phosphorylated CDK1, thereby keeping it in its inactive state and delaying mitotic entry. The G2/M checkpoint really represents the last major opportunity for preventing DNA damage being taken into mitosis where unrepaired DSBs and under-replicated DNA may result in mitotic catastrophe and cell death (Castedo et al., 2004).

Given the fundamental role of the DDR, one could be forgiven for wondering why DDR represents a good source of anti-cancer drug targets at all. The explanation lies in the fact that there are at least three key aspects of DDR that are different in cancers compared with normal cells, which in turn makes DDR an attractive

source for drug targets that can (and indeed currently are) being exploited to generate new cancer therapies (Figure 2).

of proteins (Kee and D'Andrea, 2010). Finally, three common forms of base damage (O6-methylguanine, 1-methyladenine, and 3-methylcytosine) can be repaired directly (Sedgwick et al., 2007).

The response to DNA damage will be different depending on the cell-cycle status. For example, cells in G1 will not have sister chromatid DNA available as an undamaged template and therefore will be dependent upon NHEJ pathways for the repair of DSBs. In addition, there are important differences in the primary roles of checkpoints at different stages of the cell cycle and in the DDR factors that are involved. For example, the G1/S checkpoint allows the repair of DNA damage prior to the start of DNA replication in order to remove obstacles to DNA synthesis, and key DDR factors regulating this checkpoint include

source for drug targets that can (and indeed currently are) being exploited to generate new cancer therapies (Figure 2).

### Loss of DDR Capability in Cancer Can Lead to an Exploitable DDR Dependency

The first aspect of cancer DDR that is different from normal cells is that most (if not all) cancers will have lost one or more DDR pathway or capability during their generation, leading to a greater dependency on the remaining pathways (Jackson and Bartek, 2009). Figure 3 outlines the underlying concept as well as the opportunity for exploitation using DDR inhibitors.

An early step in tumorigenesis is the deregulation of cell proliferation that can result, for example, from oncogenic stress (Hahn et al., 1999). This has been shown to lead to the activation

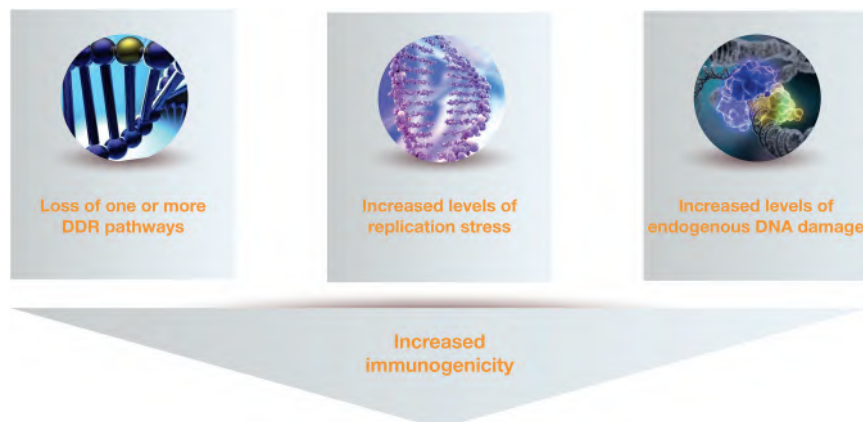


**Figure 2. Key Differences in Cancer DDR that Provide a Rationale for Drug Targeting**

Loss of one or more DDR pathways, increased replication stress and higher levels of endogenous DNA damage are all differentiating aspects of cancer DDR that can be targeted therapeutically. Left image, ©Suravid. Dreamstime.com - Golden Gene In DNA Photo; middle image, ©paulista/Shutterstock.com.

of a DDR, particularly activation of ataxia telangiectasia mutated (ATM) and ataxia telangiectasia and rad3-related (ATR) pathways, characterized by constitutive phosphorylation of ATM, CHK2, histone H2AX, and p53 (Bartkova et al., 2010; Bartkova et al., 2005; Gorgoulis et al., 2005). While this activation of the DDR in precancerous cells has been proposed to represent a barrier to uncontrolled cell growth, in cells that have progressed to form tumors, this barrier will have been removed through loss of one or more DDR capabilities (Halazonetis et al., 2008). As a consequence, cancer cells demonstrate increased genomic instability and a greater dependency on remaining DDR pathways to deal with both endogenous and exogenous DNA damage.

A cancer cell that harbors a DDR deficiency resulting in a dependency on a particular DDR target or pathway for survival in this way, provides the potential for single-agent activity of an inhibitor of that target or pathway—an approach that has been described as synthetic lethality (Ashworth, 2008; Curtin, 2012). The original context for synthetic lethality in *Drosophila* involved two genetic loss-of-function events, either of which alone was compatible with viability but together in the same cell resulted in lethality (Lucchesi, 1968). The concept has been developed further with the idea that yeast could be used for the discovery of anticancer drugs by screening compounds in specifically defined genetic backgrounds (Hartwell et al., 1997). In the context of DDR therapeutics illustrated in Figure 3, one event is genetic and specific to the tumor and not found in normal cells; the second loss-of-function event is achieved pharmacologically through treatment with a DDR inhibitor. This approach of targeting a gene product that is synthetic lethal to a cancer-relevant mutation is predicted to preferentially kill cancer cells and spare normal cells, providing a significant patient benefit over conventional cancer chemotherapeutic approaches (Curtin, 2012; Kaelin, 2005; Lord and Ashworth, 2012; O'Connor et al., 2007). The realization of this prediction in the form of clinical validation has been provided by the recent regulatory approval of olaparib (Lynparza), the first poly (ADP ribose) polymerase or PARP inhibitor to market (EMA, 2014; FDA, 2015).

PARP is a major factor in the repair of SSBs, and the mechanism of action of inhibitors currently being developed in the clinic as a monotherapy (Table 1) involves the inhibition of PARP enzymatic activity (formation of poly ADP-ribose chains from NAD<sup>+</sup>)

that is required for both relaxing chromatin and PARP dissociation from the DNA that occurs following auto-modification. Both of these events are required to facilitate SSB repair, and the structures of the PARP inhibitors are built around an NAD<sup>+</sup> mimetic core. Consequently,

competitive inhibition prevents NAD<sup>+</sup> utilization on PARP protein that is bound to SSBs, preventing repair by trapping the inactivated enzyme onto the SSB and generating a potential block for cellular DNA replication (Helleday, 2011; Murai et al., 2012). An important consequence of this is that trapped PARP-DNA complexes can lead to the stalling and/or collapsing of replication forks, resulting in the generation of more deleterious DSBs (Murai et al., 2012). As described above, in replicating cells these DSBs would normally be repaired by HRR. In cancers with HRR deficiency (HRD), the use of lower fidelity forms of DNA repair such as NHEJ will result in a significant increase in genomic instability that over multiple rounds of replication will become unsustainable and result in tumor cell death (Ceccaldi et al., 2015; Mateos-Gomez et al., 2015; Patel et al., 2011) (Figure 4).

Probably the best-known disease-associated examples of defective components of HRR are the breast- and ovarian-associated tumor suppressor genes *BRCA1* and *BRCA2* (Miki et al., 1994; Wooster et al., 1995). Both *BRCA1* and *BRCA2* proteins are critical for the repair of DSBs by HRR (Prakash et al., 2015), and loss of function results in increased mutation and genome instability (Venkitaraman, 2014). It is this increased genomic instability that is thought to be responsible for the significantly increased cancer risk of patients with familial or germline *BRCA* (*gBRCA*) mutations. However, the lack of functional *BRCA1* or *BRCA2* in tumors also represents an opportunity for targeted treatment with PARP inhibitors.

Published data in 2005 (Bryant et al., 2005; Farmer et al., 2005) demonstrated the potential for PARP inhibitors to induce cell death in *BRCA*-deficient cells through the concept of synthetic lethality. In Farmer et al. (2005), the differential PARP inhibitor activity seen between *BRCA* homozygous mutant (*BRCA1*<sup>-/-</sup>) cells and *BRCA* heterozygous (*BRCA1*<sup>-/+</sup>) and wild-type (*BRCA1*<sup>+/+</sup>) cells was approximately 1,000-fold. PARP inhibition in *BRCA*-deficient cancers was therefore predicted to have significantly reduced effects on normal cells that were wild-type or heterozygous for *BRCA1* or *BRCA2*. In patients with *gBRCA* mutations, normal tissues will carry only one mutated copy of the relevant *BRCA* gene, but their tumors will have lost both functional copies. This is integral for the selective therapeutic window of PARP inhibitors (i.e., the effect on the tumor versus that on normal tissue).

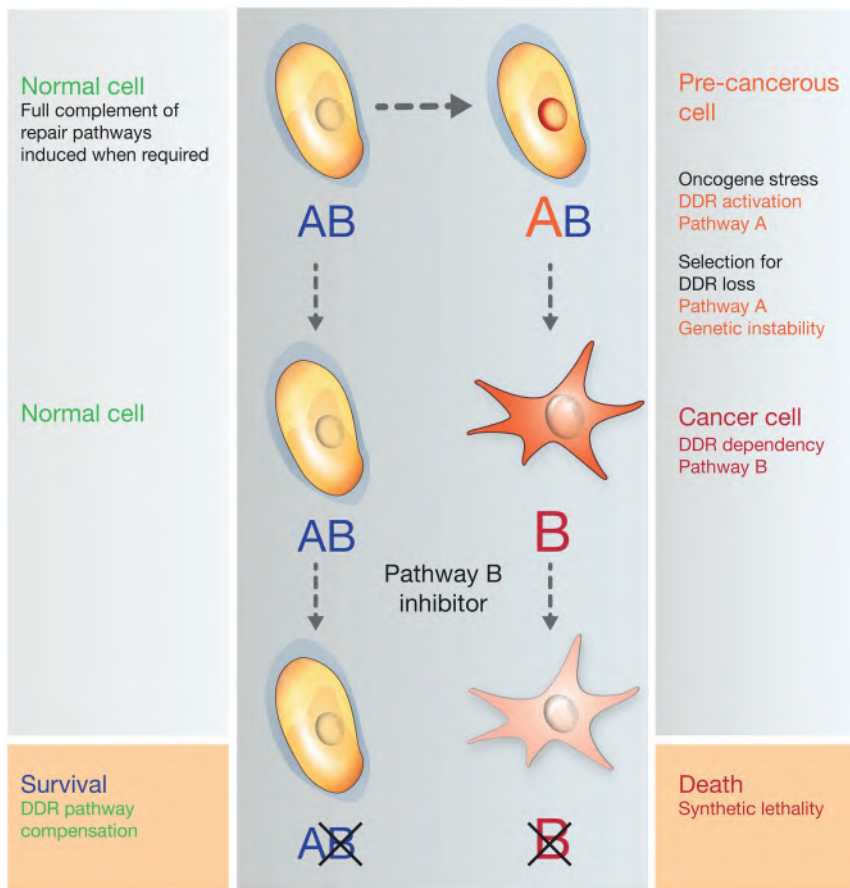


**Figure 3. Loss of DDR Pathways during Tumorigenesis Results in DDR Dependencies that Can Be Targeted in the Resulting Cancer**

With a full complement of repair pathways, normal cells can compensate for the loss of individual DDR pathways. However, loss of one or more DDR pathway(s) in response to oncogenic stress can leave cancer cells vulnerable to inhibition of remaining pathways and induce cancer-specific cell death through the process of synthetic lethality.

many different potential opportunities have been identified through preclinical screens, and a number are now being investigated in the clinic (Martin et al., 2009). One question that remains to be answered is how often examples of true therapeutic synthetic lethality, such as that seen with PARP inhibitor treatment of *BRCA* mutant tumors, will be identified. The term synthetic lethality is often used quite loosely to describe either a scenario in which a tumor genetic lesion only increases sensitivity to a targeted agent but still requires another (chemotherapeutic) agent to induce cancer cell death, or where two targeted agents are being used in the absence of a tumor-specific lesion (so-called ‘contextual’ synthetic lethality). The distinction is important from a drug development point of view because in the former case there will not

Consistent with the basic science, the first PARP inhibitor to test this hypothesis in the clinic demonstrated both an exciting level of antitumor activity combined with tolerability, providing clinical validation for the concept of synthetic lethality (Fong et al., 2009). This was followed by consistent clinical data from two further Phase II trials in *gBRCA* patients with breast (Tutt et al., 2010) and ovarian (Audeh et al., 2010) cancer and extension into the maintenance setting in platinum-sensitive relapsed ovarian cancer patients (Ledermann et al., 2012; Ledermann et al., 2014). There are currently six PARP inhibitors in late clinical development being investigated in more than 20 Phase III clinical trials (Table 1), and the majority involve monotherapy studies in *BRCA*-mutated tumors.

PARP inhibitors are also being tested in non-*BRCA* HRD settings, but patient selection based on loss of a DDR pathway is not trivial, and multiple different approaches are currently being investigated in the clinic that include DNA sequence analysis of a panel of HRR genes (Hodgson et al., 2015), an analysis of genomic scars based on DNA rearrangements or mutational patterns resulting from the loss of the HRR pathway (Abkevich et al., 2012), or selection of a single non-*BRCA* HRR-associated deficiency using an immunohistochemistry approach (Bang et al., 2015).

Although synthetic lethality based on PARP inhibitors in *BRCA* mutant tumors represents the first example of this concept to be exploited by a DDR inhibitor, it is not likely to be the last, and

be an opportunity for monotherapy and in the latter there will be a significant reduction in therapeutic index.

### Exploiting Replication Stress in Cancers Using DDR Inhibitors

Replication stress is a hallmark of cancer (Macheret and Halazonetis, 2015) and, as well as representing an important aspect of cancer etiology (Bartkova et al., 2005, 2010; Gorgoulis et al., 2005), has the potential to be exploited to generate cancer therapies (Dobbelstein and Sørensen, 2015; Lecona and Fernández-Capetillo, 2014). A molecular definition of replication stress is the uncoupling of the DNA polymerase from the replisome helicase activity (Byun et al., 2005; Zeman and Cimprich, 2014). This results in the generation of extended single-strand DNA (ssDNA) at the replication fork, the presence of which leads to binding by replication protein A (RPA) and the induction of a DDR, regulated primarily by the ATR kinase (Cimprich and Cortez, 2008).

There are a number of intrinsic, as well as extrinsic, forms of replication stress (Figure 5), but all have in common the potential to directly or indirectly slow or stall DNA polymerase progression and result in DNA polymerization being uncoupled from the helicase that is unwinding the DNA. Factors that can induce replication stress include insufficiency in nucleotide pools or other replication factors. In cancer cells deficient in G1/S cell-cycle checkpoints resulting from deficiencies in pRB, deletion of the *CDKN2A* locus

(Bester et al., 2011), or amplification of Cyclin D1 or Cyclin E (Macheret and Halazonetis, 2015), premature entry into S-phase and DNA replication can occur before the necessary resources for replication have been generated, and this is a particular issue in early S-phase (Buisson et al., 2015). Nucleoside analogs used in cancer chemotherapy also reduce the size or the relative amounts of the four dNTPs, leading to a reduction in the speed of DNA synthesis and an increase in replication stress. For example, gemcitabine inhibits ribonucleotide reductase, while 5-FU inhibits thymidylate synthetase (Ewald et al., 2008).

Cyclin E amplification also increases replication initiation that can lead to a clash between the replication and transcription processes (Jones et al., 2013). The same is true for other oncogenic drivers such as *KRAS* mutations or *MYC* amplification, where the latter also leads to an increase in replication origin firing (Rohban and Campaner, 2015; Vafa et al., 2002) as well as increased transcription. Another important aspect of *MYC* overexpression is the generation of increased reactive oxygen species (ROS) (Vafa et al., 2002). High levels of ROS is an underlying feature in cancers (Sabharwal and Schumacker, 2014) that leads to an increase in damaged nucleotides, the most frequent being the generation of 8-oxoguanine. Oxidized bases are the cause of mismatch mutations, and their detection by the MMR pathway and removal by BER or bypass by translesion synthesis following polymerase switching all have the potential to increase replication stress. Other DNA lesions or secondary structures in the template strand, whether intrinsic due to endogenous DNA damage or extrinsic resulting from chemotherapies such as platinum agents or topoisomerase inhibitors, can also induce replication stress.

The causes outlined here provide an explanation as to why replication stress generated by chemotherapy will be greater in cancers than in normal cells, since cancers but not normal cells will also be associated with cell-cycle checkpoint loss, oncogenic drivers, and higher levels of intrinsic ROS. While this, together with the potential loss of additional DDR capabilities in cancers, provides the basis of therapeutic index for such chemotherapies, there will still be collateral damage in rapidly dividing normal cells such as gut epithelia, hematopoietic cells, and hair follicles. The goal for targeting cancer DDR dependencies associated with the replication stress response is therefore to understand which DDR targets provide an improved therapeutic index over standard chemotherapies and how best to select cancers that will demonstrate the greatest susceptibility to those DDR-targeted agents.

As mentioned previously, the initial activation of a DDR response to replication stress begins with the association of RPA with the extended ssDNA region generated at the stalled replication fork (Byun et al., 2005). This leads to both the protection of the ssDNA from cleavage (Fanning et al., 2006), the recruitment by ATRIP of ATR (Ball et al., 2005; Zou and Elledge, 2003) and the replication fork remodelling protein SMARCAL1 (Bhat et al., 2015). ATR prevents replication fork collapse and the generation of DSBs through multiple mechanisms. These include ATR inhibiting new origin firing under conditions of replication stress via its effector kinase CHK1 (Couch et al., 2013; Maya-Mendoza et al., 2007; Petermann et al., 2010; Shechter et al., 2004). In addition to suppressing origin firing, ATR also coordinates the increase of ribonucleotide reductase M2 or RRM2 (Buisson et al., 2015). Together, this helps to prevent the accumulation of excessive ssDNA and conse-

quently the exhaustion of RPA. The reason that this is critical is because it has been demonstrated that when all RPA becomes sequestered on to ssDNA, every active replicon generates unprotected ssDNA that is then rapidly converted into DSBs, resulting in replication catastrophe and cell death (Toledo et al., 2013). In addition, ATR directly regulates the activity of fork remodelling enzymes, such as SMARCAL1, to prevent the generation of DSBs resulting from fork cleavage by structure-specific nucleases (Couch et al., 2013; Ragland et al., 2013).

The significant body of evidence for the role of the ATR-CHK1 pathway in the stabilization and repair of replication forks (and the prevention of early entry into mitosis with under-replicated genomes) has meant much of the current focus around pharmacological targeting of replication stress has been on these two kinases. Inhibitors of ATR (AZD6738 and VX-970) and CHK1 (GDC-0575, LY2606368, and MK-8776) are currently being investigated in clinical trials (Table 1). However, replication origin firing is also regulated by CDKs and the WEE1 tyrosine kinase phosphorylates, and consequently inhibits both CDK1 and CDK2 activity. When WEE1 is inhibited pharmacologically, CDK1 and CDK2 will be deregulated, and the enhanced activity will lead to increased replication origin firing, a decrease in nucleotide availability, and an increase in DSBs mediated through MUS81 endonuclease activity (Beck et al., 2012). Moreover, because CDK1 is a major regulator of the G2/M checkpoint, WEE1 inhibition and the subsequent CDK1 activation can also result in premature entry into mitosis, even in the presence of under-replicated DNA or DSBs, thus promoting mitotic catastrophe and cancer cell death (Aarts et al., 2012; Do et al., 2013). For this reason, it would be more accurate to consider both the ATR-CHK1 pathway and the WEE1-CDK1/2 pathway as core pathways for targeting replication stress in cancers, and the WEE1 inhibitor AZD1775 (previously known as MK-1775) is also being investigated in clinical trials as a monotherapy to test this hypothesis directly (Table 1).

Differences between the effects of the ATR and the CHK inhibitor on cycling cells have been described where ATR inhibition only induced  $\gamma$ H2AX in a small fraction of cells compared to CHK1 inhibition, the latter inducing massive  $\gamma$ H2AX accumulation in a large fraction of the cells (Toledo et al., 2011). This observation raised the possibility that ATR and CHK1 might not always function in a linear pathway, and this hypothesis has been confirmed in a recent study where cells treated with an ATR inhibitor were found to still be able to prevent replication origin firing in the majority of cells via a backup pathway involving DNA-PK and CHK1, with ATM also playing a role (Buisson et al., 2015). This study further suggested that this backup pathway provides a threshold effect, such that an ATR inhibitor selectively kills cells under high levels of replication stress, whereas a CHK1 inhibitor induces cell death at a lower threshold. In addition, the authors provided evidence that CHK1 suppresses origin firing by inhibiting CDK2, since WEE1 inhibition was shown to induce activation of CDK2 in ATR-inhibitor-treated cells and this prevented their recovery (Buisson et al., 2015). These findings also imply that a WEE1 inhibitor should, like a CHK1 inhibitor, induce cell death at a lower threshold than an ATR inhibitor, although this has not yet been formally tested. Together, the new data suggest that in addition to ATR, CHK1, and WEE1, the DDR proteins DNA-PK and potentially ATM could also represent DDR targets of

**Table 1. DDR Inhibitors in Clinical Development**

Pathway	Target	Compound	Latest Stage of Development and Trial Details	Clinical Trial Identifier(s)
<b>BER</b>				
	APE1	Methoxyamine	Phase II in combination with TMZ in glioblastoma	NCT02395692
	PARP	E7016	Phase II in combination with TMZ in melanoma	NCT01605162
	PARP	Niraparib	Phase III as monotherapy in breast cancer and as maintenance monotherapy in ovarian cancer	NCT01847274; NCT01905592
	PARP	Olaparib	Olaparib licensed for use. Olaparib Phase IV as maintenance monotherapy NCT0247696.	NCT02476968
	PARP	Olaparib	Phase III as monotherapy, maintenance monotherapy and in combination with chemotherapy or cediranib in multiple tumor types (ovarian, breast, gastric, pancreatic)	NCT01844986; NCT01874353; NCT01924533; NCT02000622; NCT02032823; NCT02184195; NCT02282020; NCT02392676; NCT02446600; NCT02477644; NCT02502266
	PARP	Olaparib	Phase I in combination with RTx (or RTx plus chemotherapy) in various tumor types	NCT01460888; NCT01562210; NCT01758731; NCT02308072; NCT02227082; NCT02229656
	PARP	Olaparib	Phase I in combination with AZD1775 in refractory solid tumors	NCT02511795
	PARP	Rucaparib	Phase III as maintenance monotherapy in ovarian cancer	NCT01968213
	PARP	Talazoparib	Phase III as monotherapy in metastatic breast cancer	NCT01945775
	PARP	Veliparib	Phase III in combination with chemotherapy in multiple tumor types	NCT02032277; NCT02106546; NCT02152982; NCT02163694; NCT02264990; NCT02470585
	PARP	Veliparib	Phase I and II in combination with RTx (or RTx plus chemotherapy) in various tumor types	NCT01264432; NCT01477489; NCT01514201; NCT01618357; NCT01908478; NCT02412371
<b>NHEJ</b>				
	DNA-PKcs	CC-115	Phase I as monotherapy in ASTs	NCT01353625
	DNA-PKcs	MSC2490484A	Phase I as monotherapy or in combination with RTx in ASTs and CLL	NCT02316197; NCT02516813
<b>HRR</b>				
	ATR	AZD6738	Phase I as monotherapy or in combination with RTx, cytotoxic chemotherapy or olaparib in various tumor types	NCT01955668; NCT02223923; NCT02264678
	ATR	VX-970	Phase II in combination with topotecan or cytotoxic chemotherapy in various tumor types	NCT02567409; NCT02487095
	ATR	VX-970	Phase I in combination with RTx and cisplatin in HNSCC	NCT02567422
<b>Checkpoint inhibitors</b>				
	ATM	AZD0156	Phase I as monotherapy or in combination with cytotoxic chemotherapy, olaparib or novel anti-cancer therapies in advanced tumors	NCT02588105
	ATR (see above)			
	CHK1	GDC-0575	Phase I as monotherapy and in combination with cytotoxic chemotherapy in ASTs or lymphoma	NCT01564251
	CHK1	MK-8776	Phase II in combination with cytarabine in myeloid leukemia	NCT01870596
	CHK1 and CHK2	LY2606368	Phase II as monotherapy in breast and ovarian cancer	NCT02203513
	WEE1	AZD1775	Phase II as monotherapy and in combination with chemotherapy or olaparib in multiple tumor types	NCT01164995; NCT01357161; NCT01827384; NCT02037230; NCT02087176; NCT02087241; NCT02095132; NCT02101775; NCT02196168; NCT02272790; NCT02448329; NCT02513563; NCT02576444
	WEE1	AZD1775	Phase I in combination with RTx and TMZ in GBM	NCT01849146
	WEE1	AZD1775	Phase I in combination with olaparib in refractory solid tumors	NCT02511795

(Continued on next page)

**Table 1. Continued**

Pathway	Target	Compound	Latest Stage of Development and Trial Details	Clinical Trial Identifier(s)
Topoisomerase inhibitors				
	Topo I	Belotecan	Licensed for use	
	Topo I	CRLX101	Phase II as monotherapy and in combination with RT, cytotoxic chemotherapy or bevacizumab in various tumor types	NCT00333502; NCT01380769; NCT01652079; NCT01803269; NCT02010567; NCT02187302
	Topo I	Irinotecan	Licensed for use	
	Topo I	LMP 400	Phase I as monotherapy in ASTs and lymphomas	NCT01051635; NCT01794104
	Topo I	LMP 776	Phase I as monotherapy in ASTs and lymphomas	NCT01051635
	Topo I	NKTR-102	Phase III as monotherapy in locally recurrent or metastatic breast cancer	NCT01492101
	Topo I	Topotecan	Licensed for use	
	Topo II	Doxorubicin	Licensed for use	
	Topo II	Epirubicin	Licensed for use	
	Topo II	Etoposide	Licensed for use	
	Topo II	Idarubicin	Licensed for use	
	Topo II	Mitoxantrone	Licensed for use	
	Topo II	Teniposide	Licensed for use	

APE1, AP endonuclease 1; AST, advanced solid tumors; ATM, ataxia-telangiectasia mutated; ATR, ataxia-telangiectasia and Rad3-related; BER, base excision repair; CLL, chronic lymphocytic leukemia; DDR, DNA damage response; GBM, glioblastoma multiforme; HNSCC, head and neck squamous cell carcinoma; HRR, homologous recombination repair; NHEJ, non-homologous end-joining; NSCLC, non-small-cell lung cancer; PARP, poly(ADP-ribose) polymerase; RTx, radiation therapy; TMZ, temozolomide; Topo, topoisomerase.

interest, either in a subset of cancers with genetic backgrounds where there is lower ATR activity and higher levels of replication stress, or in combination with ATR inhibitors. The DNA-PK inhibitors CC-115 and MSC2490484A are now being investigated in Phase I trials, as is the ATM inhibitor AZD0156 (Table 1).

Additional DDR targets for exploiting replication stress in cancers are also likely to be identified by the very powerful combination of iPOND technology (Dungrawala and Cortez, 2015) combined with differential proteomics, as was recently showcased by a study that characterized human replisome dynamics and replication stress response proteomes in response to fork stalling, using an improved iPOND protocol combined with SILAC mass spectrometry (Dungrawala et al., 2015). This approach has the potential to identify new DDR dependencies that could be exploited therapeutically. It could also be used to identify combination opportunities with ATR, CHK1, or WEE1 inhibitors that, if successful, could potentially replace current standard of care chemotherapies, provided an improved therapeutic index was demonstrated. In all likelihood, to achieve this it will be important to understand the cancer genetic backgrounds that correlate with sensitivity.

Our understanding of the replication stress response in cancer cells, and therefore the potential to exploit this by generating therapeutic agents, has made significant progress over recent years. However, the majority of the work has been carried out in 2D *in vitro* cell culture and often in the same small number of cell lines. Going forward, this work will benefit from complementary studies in relevant *vivo* models, such as patient-derived explant (PDX) models, where different tumor types and genetic backgrounds can be tested. In addition, there still needs to be a greater understanding of how best to select patients that have tumors with high levels of replication stress.

ATR inhibitor treatment has been shown to increase both the generation of G1-specific 53BP1 nuclear bodies (Lukas et al., 2011) as well as S-phase ssDNA (Buisson et al., 2015), and both could be considered as readouts of replication stress and susceptibility to an ATR inhibitor. However, it is not clear at this point if these readouts would be seen for other DDR inhibitors and, just like the situation with PARP and HRD, a functional readout of replication stress will have the same cancer diagnostic issues, because in general, only the patient's formalin-fixed, paraffin-embedded (FFPE) tumor samples from the initial cancer diagnosis are likely to be available for testing. The challenge of identifying susceptible cancers for DDR agents therefore remains an important objective if patients are to benefit from DDR inhibitors that can exploit cancer replication stress.

### Combining DDR Inhibitors with DNA-Damaging Therapeutic Agents

Other than surgery, the mainstay of cancer treatment to date has involved the use of DNA-damaging agents in the form of radiation and systemic chemotherapy. Radiation is responsible for approximately 40% of all cures achieved in cancer patients (Einhorn et al., 1996), and this anticancer efficacy is due to the ionization effect that generates DNA-damaging oxygen free radicals—either directly from atoms within the DNA helix or indirectly through the ionization of water. Studies suggest 1 Gy of ionizing radiation will generate approximately 1,000 SSBs and 35 DSBs (Rothkamm and Löbrich, 2003; Ward, 1998). While there have been significant improvements in reducing normal tissue exposure through both improved treatment planning and image-guided delivery of the radiation to the tumor, the acute and chronic normal tissue toxicities are still the limiting factor for radiation dose delivery.

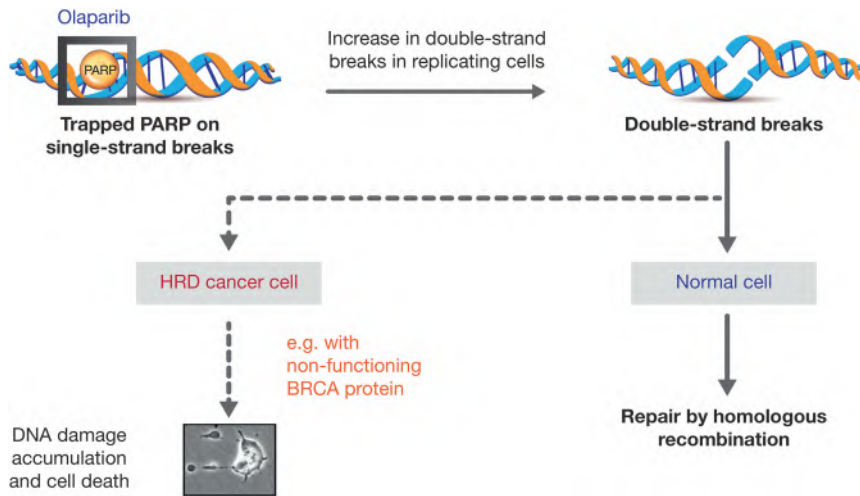


**Figure 4. Olaparib Synthetic Lethality in BRCAm Tumors**

Poly(ADP-ribose) polymerases (PARPs) repair DNA SSBs through the BER pathway. PARP inhibitors, such as olaparib, prevent repair by trapping the inactivated PARP onto the SSB, resulting in the generation of DNA DSBs during the replication process. In tumors with a homologous recombination deficiency (HRD), such as a *BRCA1/2* mutation, the low-fidelity repair mechanism of NHEJ leads to increasing genetic instability and ultimately death of the tumor cell.

One aspect of improving radiation treatment would be to better understand and measure a tumor's intrinsic radiosensitivity, which would represent a major advance and allow individualized treatment to reduce dose and/or omit chemotherapy radiation combinations in patients with sensitive tumors, or conversely to intensify treatment against resistant tumors. Gene expression signatures from cell lines demonstrating different levels of radiosensitivity are currently being assessed, but to date, there has been only limited success in identifying correlations (Hall et al., 2014).

An alternative strategy to enhance the efficacy of radiotherapy is focused on combinations with novel targeted agents, including DDR inhibitors. These could modulate radiosensitivity with the aim of expanding the therapeutic index by increasing radiosensitization of tumors to a greater extent than normal tissue, rather than just causing increased sensitivity in all cells (Begg et al., 2011). There are a number of examples of DDR-targeted agents combined with radiation that have demonstrated preclinical efficacy (Barazzuol et al., 2013; Reaper et al., 2011; Sarcar et al., 2011; Senra et al., 2011) and that are now being tested in clinical trials (Table 1). However, at the moment, our current knowledge of how best to use DDR agents in combination with radiation treatment is significantly behind our understanding of how to use them as monotherapies. For example, what dose of DDR agent will act as an effective radiosensitizer, how much benefit will be obtained from extended exposure to the DDR agent following delivery of radiation-induced damage, and whether radiosensitization by the DDR agent is different in specific DDR-deficient genetic backgrounds are all critically important questions. A recent preclinical study has provided some insights into these questions using clonogenic assays to assess radiosensitization of the PARP inhibitor olaparib in *BRCA2*-deficient and *BRCA2*-complemented isogenic cells, and in a panel of human head and neck squamous cell carcinoma cell lines (Verhagen et al., 2015). The conclusions from this study were that 7 hr of PARP inhibitor exposure following the radiation treatment was sufficient to induce radiosensitization. Moreover, the radiosensitizing effects could be observed at much lower PARP inhibitor doses than those required to induce cell death as a single agent, although they were still sufficient to inhibit the increased PAR resulting from radiation treatment. Finally, in

the isogenic mouse *BRCA2* knockout and complemented cell lines, the data showed that the *BRCA2*-deficient cells were radiosensitized by much lower doses of PARP inhibitor than the *BRCA2*-complemented cells (Verhagen et al., 2015).

The effects of DDR agents in combination with ionizing radiation on normal tissue will still need to be investigated to understand whether improved antitumor cell efficacy is matched by increases in normal tissue toxicity, or whether there is indeed evidence to suggest an improved therapeutic index. One of the challenges for this kind of preclinical work is that a true appreciation of the therapeutic window will require an immune competent host, since radiation-induced toxicities such as pneumonitis in normal lung tissue involve a host inflammatory response. While antitumor activity and normal tissue toxicity can be assessed in different models, ideally a syngeneic or orthotopic immune competent rodent model should be used in which both antitumor activity and normal tissue toxicity can be assessed at the same time. Although this approach will limit the number of models available, it will be of considerable benefit in providing guidance for clinical combination testing. This is because clinical trials involving targeted agents and radiation combinations have significant challenges, not least because the dose escalation phase can take a long time in order to assess the chronic radiation induced toxicities (usually a 3-month follow-up on a particular dose cohort is required before further dose escalation). In addition, efficacy readouts are not straightforward, since local regional disease control does not always reflect overall survival in patients, and the latter can take years to assess because radiation is primarily used in early line therapy. These and other challenges for radiation combination clinical trials have meant that relatively few targeted agent combinations with radiation have been undertaken by the pharmaceutical industry (Ataman et al., 2012). However, targeted DDR agents have significant opportunities in combination with radiation treatment, and so, there does need to be a concerted effort to address these challenges.

Combination of DDR agents with DNA-damage-inducing chemotherapies also has its difficulties. There are two primary reasons for this: the first is that chemotherapies are delivered systemically, and the second is that they tend to have the same overlapping toxicities as DDR inhibitors, namely gastrointestinal (GI) and bone marrow toxicity, for the reasons outlined in the previous section. This has resulted in many clinical trials being terminated due to unacceptable adverse events.

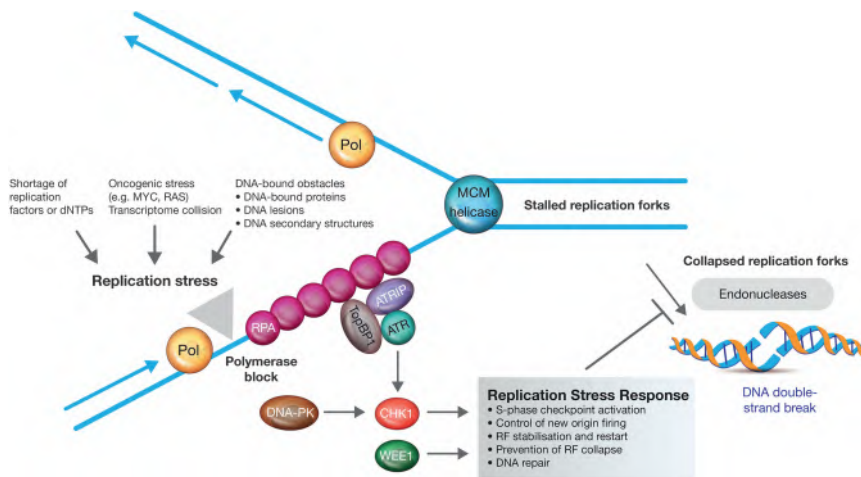


**Figure 5. Activation of DDR in Response to Replication Stress**

Replication fork (RF) stress can cause the polymerase (Pol) to stall leading to extended stretches of ssDNA that are coated by replication protein A (RPA). ATR-interacting protein (ATRIP) binds to the RPA-coated ssDNA, recruiting ATR to the site of DNA damage. Once the ATR-ATRIP complex interacts with TopBP1, ATR signaling can be activated with CHK1 as a key substrate. The replication stress response when activated helps to prevent replication fork collapse and the generation of cytotoxic DNA DSBs.

Commonly used DNA-damage-inducing chemotherapies include platinum salts (carboplatin, cisplatin, and oxaliplatin) that generate covalent cross-links between DNA bases (Jung and Lipard, 2007), alkylating agents such as temozolomide that modify DNA bases (Siddik, 2002), and inhibitors of topoisomerase (Top) 1 (such as the camptothecin, topotecan, and irinotecan) and Top 2 (such as etoposide and doxorubicin) that generate Top-DNA adducts and DNA-strand breaks (Caldecott, 2014; Pommier et al., 2010). Both Top 1 and Top 2 are required to relieve the potentially inhibitory DNA supercoiling that would result following DNA-strand separation during the processes of transcription and replication, while Top 2 can also carry out DNA decatenation and unknotting. Both enzymes achieve DNA relaxation through generating a DNA break, controlled rotation, and re-ligation. The difference in activities between the two classes of enzymes is due to the fact that Top 2 cleaves both DNA strands, while Top 1 cleaves only one strand. In both cases, the Top inhibitors currently approved for cancer therapy generate non-productive Top-DNA cleavage complexes (Topcc) after DNA has been cleaved, but before re-ligation occurs. Top 1 inhibitors induce SSBs, while Top 2 inhibitors induce DSBs. However, the Top 1-induced SSBs are converted into DSBs during replication when met by the replication fork.

At first sight there are clear similarities between the activities of PARP inhibitors that trap PARP onto DNA and topoisomerase inhibitors that generate Top-DNA adducts. However, the primary roles of Top 1 and Top 2 enzymes are not in the DDR, and the normal activity of these enzymes is an error-free process. Moreover, the currently approved inhibitors of Top 1 and Top 2 that are used as standard of care therapy are associated with significant side effects. The smaller therapeutic window of topoisomerase inhibitors compared to PARP inhibitors almost certainly reflects the broad roles that Top enzymes play in both DNA replication and transcription. Consequently, topoisomerase inhibitors should be considered DNA-damaging chemotherapies rather than DDR-targeted agents.

The choice of which DDR agent to combine with which chemotherapy is about aligning the type of DNA damage induced by the chemotherapy with the DDR repair mechanism. For example, in combination with inhibitors of Top 1, the use of ATM inhibitors (Hickson et al., 2004), ATR inhibitors (Jossé et al., 2014), or

PARP inhibitors (Murai et al., 2014) would all be appropriate, since all three DDR agents are involved in the repair of the DNA damage that results from Top 1 inhibition. For TMZ-induced DNA damage,

PARP inhibitor combination would be the obvious choice since there is a direct role for PARP in the repair of the ssDNA breaks induced by this agent, and indeed, there are currently 12 clinical trials ongoing that are investigating this potential therapeutic approach. A nice summary of DNA damage, repair pathway, and DDR target alignment is provided in Curtin (2012).

The generation of preclinical evidence demonstrating efficacy does not, however, guarantee that a DDR agent chemotherapy combination will be successfully deployed in the clinic. A number of trials, for example, have failed to identify an effective combination dose and schedule due to dose-related increases in neutropenia (Samol et al., 2012). However, in spite of the challenges, combinations of DDR inhibitors with chemotherapy still represent a clearly important clinical opportunity, because preclinical data (Curtin et al., 2004; Erice et al., 2015; Tentori et al., 2014) and clinical data (Leijen et al., 2015) have shown chemo-resistant cancers can be re-sensitized through combinations with DNA-damaging agents. In a clinical example, data from Leijen et al. (2015) demonstrated significant activity (41% objective response rate [ORR]) in the most platinum-resistant ovarian cancer patients when platinum retreatment was combined with a WEE1 inhibitor, and although there were some dose reductions in a number of cases, responses were sustained for many months and even years. In addition, for the near future at least, chemotherapies will continue to be part of the standard of care treatment for early line cancer therapies. There is, therefore, a real need to better identify strategies that can lead to enhanced anti-tumor efficacy with DDR-chemotherapy combinations while mitigating the unacceptable normal tissue toxicities.

One approach being taken to achieve better tolerated combinations of chemotherapy and DDR agents is to use gapped schedules, where the chemotherapy is given first, followed by a 2- to 3-day gap before treatment with the targeted agent. This approach is based on preclinical data that demonstrate differential effects of the platinum-induced DNA damage in tumor versus bone marrow. In the former case,  $\gamma$ H2AX was shown to be detectable beyond 72 hr following chemotherapy treatment, whereas the DNA damage appeared to be resolved in bone marrow within 48 hr (O'Connor et al., 2013). Another approach is to use formulations of chemotherapy that selectively deliver

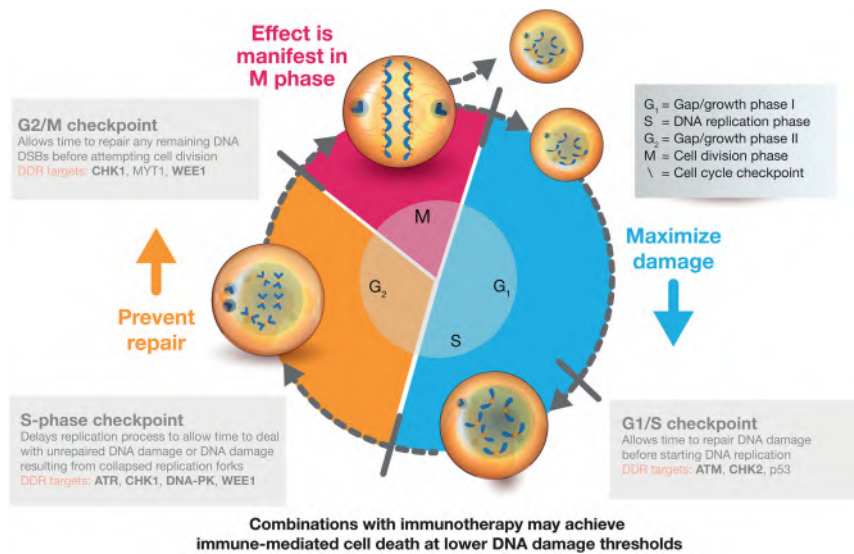


**Figure 6. Strategy for the Use of DDR Inhibitors as Anticancer Agents**

The strategy for the development of DDR-targeted agents is to cause the maximum amount of DNA damage during the G<sub>1</sub> and S phases of the cell cycle, and then prevent DNA repair during G<sub>2</sub>. This strategy maximizes the amount of DNA damage that is taken into mitosis.

ability of inhibitors that can abrogate the G<sub>2</sub>/M checkpoint, such as inhibitors of CHK1 and WEE1, provides an opportunity to overcome this important cancer defense mechanism, and these agents are already being used in the clinic in combination with chemotherapies such as carboplatin and irinotecan, focusing on p53 deficiency as the targeted selection criteria (Table 1).

The goal for the use of DDR-targeted agents in cancer treatment should, therefore,

be, at its simplest level, to maximize DNA damage in G<sub>1</sub> and S-phase and prevent repair in G<sub>2</sub> in order to ensure the damage is taken through into mitosis where the effects will be manifest (Figure 6). A recently published example from the clinic really provides an excellent exemplification of these principles in which a patient with a metastatic small-cell bladder cancer demonstrated an outlier curative response following the combination with a CHK1/CHK2 inhibitor and irinotecan (Al-Ahmadie et al., 2014; Peng et al., 2014). Genetic and functional analyses demonstrated the tumor carried a deleterious mutation in RAD50, which is a DDR gene whose product is part of a complex that detects DNA DSBs and subsequently activates ATM to initiate DSB repair. The tumor also had a functionally relevant p53 mutation. This combination of mutations, DDR inhibitor, and DNA-damaging chemotherapy effectively produced a perfect storm in which an abrogated G<sub>1</sub>/S checkpoint, DSB repair deficiency, exogenous S-phase damage, and G<sub>2</sub>/M checkpoint over-ride resulted in a patient cure.

### Strategies for the Use of DDR Inhibitors as Anticancer Agents

As outlined in this review, all three of the concepts behind targeting DDR in cancer have, as an underlying theme, the increased susceptibility of cancers to S-phase-induced DNA damage. In the one clinically validated example of synthetic lethality, it is the deficiency in HRR and therefore the inability to effectively deal with S-phase DSBs induced by a PARP inhibitor. Replication stress is by definition an S-phase-specific effect, while the higher levels of endogenous DNA damage are due for the most part to a combination of factors associated with increased proliferation (loss of cell-cycle checkpoints, higher levels of transcription, and higher levels of metabolic and replication stress). As described in the previous sections, these are the same characteristics that give rise to the higher level of cancer cell sensitivity to exogenous DNA damage compared to normal cells.

If the levels of S-phase damage are sufficient, this can lead to cell death through replication catastrophe (Toledo et al., 2013) or the induction of apoptosis. Cancer cell death may also occur if DNA damage in the form of DSBs is carried through into mitosis, resulting in mitotic catastrophe. This would explain why chemotherapies such as taxanes that exert their effects in mitosis are particularly effective when coupled with agents such as platinum salts that increase S-phase DNA damage. Increased DNA damage in S-phase cancer cells therefore places a much greater dependency on the G<sub>2</sub>/M checkpoint. Sufficient DNA damage may be generated to exceed the threshold where cancer cells survive, even with an intact G<sub>2</sub>/M checkpoint. However, the avail-

ability of inhibitors that can abrogate the G<sub>2</sub>/M checkpoint, such as inhibitors of CHK1 and WEE1, provides an opportunity to overcome this important cancer defense mechanism, and these agents are already being used in the clinic in combination with chemotherapies such as carboplatin and irinotecan, focusing on p53 deficiency as the targeted selection criteria (Table 1).

The goal for the use of DDR-targeted agents in cancer treatment should, therefore, be, at its simplest level, to maximize DNA damage in G<sub>1</sub> and S-phase and prevent repair in G<sub>2</sub> in order to ensure the damage is taken through into mitosis where the effects will be manifest (Figure 6). A recently published example from the clinic really provides an excellent exemplification of these principles in which a patient with a metastatic small-cell bladder cancer demonstrated an outlier curative response following the combination with a CHK1/CHK2 inhibitor and irinotecan (Al-Ahmadie et al., 2014; Peng et al., 2014). Genetic and functional analyses demonstrated the tumor carried a deleterious mutation in RAD50, which is a DDR gene whose product is part of a complex that detects DNA DSBs and subsequently activates ATM to initiate DSB repair. The tumor also had a functionally relevant p53 mutation. This combination of mutations, DDR inhibitor, and DNA-damaging chemotherapy effectively produced a perfect storm in which an abrogated G<sub>1</sub>/S checkpoint, DSB repair deficiency, exogenous S-phase damage, and G<sub>2</sub>/M checkpoint over-ride resulted in a patient cure.

Achieving similar successes in the clinic should be possible using targeted DDR agents but most likely in combination with other DNA-damaging agents, or targeted therapies, and will require correctly identifying cancer-specific genetic deficiencies that will be associated with susceptibility to the specific DDR-targeted agent. For companion diagnostics that can be used in concert with a DDR agent, there are the challenges that have already been outlined, namely that it will be the diagnostic FFPE sample that will have to be used. However, this situation should improve in parallel with the advanced capabilities for DNA sequencing of formalin-fixed samples, as well as emerging capabilities for sequencing circulating tumor cell DNA or plasma tumor DNA that can complement current diagnostic approaches based on immunohistochemistry. In addition to targeting the right tumors with DDR agents, it will also be important to maximize the therapeutic window by identifying the correct dose and schedule for treating patients, and this in turn will require an understanding of the drug mechanism of action, target engagement, and downstream pharmacodynamic biomarkers that can be used in the clinic.

### The Evolution of DDR-Inhibitor-Based Treatment of Cancer

The initial focus for DDR inhibitors in cancer therapy was in combination with chemotherapy. Some of the earlier clinical trials were with the MGMT inhibitor *O*<sup>6</sup>-benzylguanine in combination with BCNU (Friedman et al., 1998), although clinical benefit was marginal and the combination poorly tolerated (Curtin, 2012). Combination of the PARP inhibitor rucaparib with temozolomide in metastatic melanoma started soon after in 2003 (Plummer et al., 2008). However, in the case of rucaparib, there was no selection of specific tumor genetic deficiencies that would provide an enhanced tumor-specific activity (and therefore the necessary therapeutic window), and so no follow up Phase III trial was initiated. The synthetic lethality data generated with PARP inhibitors in BRCA-deficient backgrounds and clinical validation of olaparib monotherapy activity in *BRCA* mutant cancers really highlights the importance of exploiting known DDR deficiencies to build an effective therapeutic differential between cancer and normal tissue.

In the last 10 years there has been a significant increase in the number of DDR inhibitors generated and entering the clinic (Table 1 highlights a large number of these, but does not capture them all). In addition, there has been an appreciation that replication stress represents another differentiating factor between cancers and normal cells and therefore another opportunity for developing cancer therapies based on DDR inhibitors. Moreover, G2/M checkpoint abrogation by CHK and WEE1 inhibitors is being tested in the clinic in combination with chemotherapy. In the short term, we will begin to see more DDR agents tested as monotherapy in specifically selected genetic backgrounds, where it is believed that there is the corresponding single-agent DDR dependency (for example, PARP inhibitors in non-BRCA HRD tumors, ATR inhibitors in ATM-deficient tumors and WEE1 inhibitors in Cyclin E and MYC amplified tumors).

Even though ultimately DDR agents are likely to be used in combination, an appreciation of which genetic backgrounds they demonstrate single-agent activity in will be pivotal in developing the right combination and patient selection strategy for their use in the clinic. DDR-DDR agent combinations have the potential to provide broader and more effective response than DDR-based monotherapy. An exciting example is the combination of a PARP inhibitor with a WEE1 inhibitor, where impressive preclinical data have led to the initiation of clinical trials (Table 1). DDR combinations with targeted agents affecting other validated hallmarks of cancer also have great therapeutic potential. The recent publication of the Phase II trial data from the combination of olaparib and cediranib, a VEGF inhibitor, is a case in point (Liu et al., 2014). In this study, the activity of the targeted agent combination was greater in *BRCA* wild-type tumors than the standard of care platinum treatment. This example highlights the potential of DDR-based therapy to supplant more toxic chemotherapy in earlier lines of therapy, thus providing a better quality of life for longer in patients with cancer.

DDR agents have also been studied in combination with epigenetic compounds that can modulate the expression of genes involved in the DDR in cancer (Orta et al., 2014; Wu et al., 2015). These studies have shown that epigenetic drugs can enhance the effects of DDR agents; for example, histone lysine methyltransferase (HKMT) inhibitors have been shown to

prevent the retention of the BRCA1/BARD1 complex at DSBs, promoting NHEJ and thereby enhancing the effects of PARP inhibitors (Wu et al., 2015). Finally, the multiple links between DDR and the immune response suggest DDR-immunotherapy combinations could represent a dramatic change in the effectiveness of cancer therapy. Immunotherapy currently appears to provide longer term responses, but in a relatively small proportion of the patient population. Initial studies demonstrated that the combination of radiation with anti-CTLA4 and anti-PD-L1 immunotherapy led to improved tumor responses (Twyman-Saint Victor et al., 2015), while a recent Phase II study in patients with progressive metastatic carcinoma demonstrated that mismatch-repair status was predictive of improved clinical benefit from immune checkpoint blockade with a PD-1 inhibitor (Le et al., 2015). Combinations of DDR and immunotherapy agents have the potential to broaden and deepen cancer patient responses, and the first clinical trials investigating the combination of a PARP inhibitor with immunotherapy are now in progress.

In conclusion, the approval of the first medicine to treat cancer based on a targeted DDR inhibitor in a defined tumor-specific DDR-deficient background is likely to be only the beginning of what could be a significant role for DDR-based agents in future cancer therapy.

### ACKNOWLEDGMENTS

Editorial assistance was provided by Ben Clarke, from Mudskipper Business Ltd, funded by AstraZeneca.

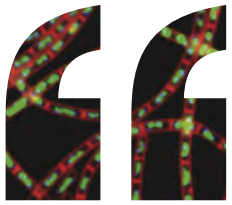
### REFERENCES

- Aarts, M., Sharpe, R., Garcia-Murillas, I., Gevensleben, H., Hurd, M.S., Shumway, S.D., Toniatti, C., Ashworth, A., and Turner, N.C. (2012). Forced mitotic entry of S-phase cells as a therapeutic strategy induced by inhibition of WEE1. *Cancer Discov.* 2, 524–539.
- Abkevich, V., Timms, K.M., Hennessy, B.T., Potter, J., Carey, M.S., Meyer, L.A., Smith-McCune, K., Broaddus, R., Lu, K.H., Chen, J., et al. (2012). Patterns of genomic loss of heterozygosity predict homologous recombination repair defects in epithelial ovarian cancer. *Br. J. Cancer* 107, 1776–1782.
- Al-Ahmadie, H., Iyer, G., Hohl, M., Asthana, S., Inagaki, A., Schultz, N., Hanrahan, A.J., Scott, S.N., Brannon, A.R., McDermott, G.C., et al. (2014). Synthetic lethality in ATM-deficient RAD50-mutant tumors underlies outlier response to cancer therapy. *Cancer Discov.* 4, 1014–1021.
- Alwan, H., Eckersley, K., Goodwin, L., Lau, A., Jones, D., Kettle, J., Nissink, W.M., Read, J., Scott, J.S., Taylor, B.J.M., Walker, G.E., and Foote, K.M. (2015). Role of MTH1 (NUTD1) in cancer cell survival. *Proceedings of the 2015 AACR-NCI-EORTC International Conference on Molecular Targets and Cancer Therapeutics*, pp. 45.
- Ashworth, A. (2008). A synthetic lethal therapeutic approach: poly(ADP) ribose polymerase inhibitors for the treatment of cancers deficient in DNA double-strand break repair. *J. Clin. Oncol.* 26, 3785–3790.
- Ataman, O.U., Sambrook, S.J., Wilks, C., Lloyd, A., Taylor, A.E., and Wedge, S.R. (2012). The clinical development of molecularly targeted agents in combination with radiation therapy: a pharmaceutical perspective. *Int. J. Radiat. Oncol. Biol. Phys.* 84, e447–e454.
- Audeh, M.W., Carmichael, J., Penson, R.T., Friedlander, M., Powell, B., Bell-McGuinn, K.M., Scott, C., Weitzel, J.N., Oaknin, A., Loman, N., et al. (2010). Oral poly(ADP-ribose) polymerase inhibitor olaparib in patients with BRCA1 or BRCA2 mutations and recurrent ovarian cancer: a proof-of-concept trial. *Lancet* 376, 245–251.
- Ball, H.L., Myers, J.S., and Cortez, D. (2005). ATRIP binding to replication protein A-single-stranded DNA promotes ATR-ATRIP localization but is dispensable for Chk1 phosphorylation. *Mol. Biol. Cell* 16, 2372–2381.

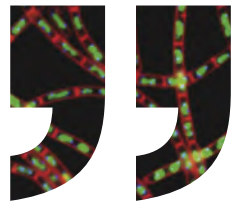
- Bang, Y.J., Im, S.A., Lee, K.W., Cho, J.Y., Song, E.K., Lee, K.H., Kim, Y.H., Park, J.O., Chun, H.G., Zang, D.Y., et al. (2015). Randomized, Double-Blind Phase II Trial With Prospective Classification by ATM Protein Level to Evaluate the Efficacy and Tolerability of Olaparib Plus Paclitaxel in Patients With Recurrent or Metastatic Gastric Cancer. *J. Clin. Oncol.* Published online August 17, 2015.
- Barazzuol, L., Jena, R., Burnet, N.G., Meira, L.B., Jeynes, J.C., Kirkby, K.J., and Kirkby, N.F. (2013). Evaluation of poly (ADP-ribose) polymerase inhibitor ABT-888 combined with radiotherapy and temozolomide in glioblastoma. *Radiat. Oncol.* 8, 65.
- Bartkova, J., Horejsi, Z., Koed, K., Krämer, A., Tort, F., Zieger, K., Guldborg, P., Sehested, M., Nesland, J.M., Lukas, C., et al. (2005). DNA damage response as a candidate anti-cancer barrier in early human tumorigenesis. *Nature* 434, 864–870.
- Bartkova, J., Hamerlik, P., Stockhausen, M.T., Ehrmann, J., Hlobilkova, A., Laursen, H., Kalita, O., Kolar, Z., Poulsen, H.S., Broholm, H., et al. (2010). Replication stress and oxidative damage contribute to aberrant constitutive activation of DNA damage signalling in human gliomas. *Oncogene* 29, 5095–5102.
- Beck, H., Nähse-Kumpf, V., Larsen, M.S., O'Hanlon, K.A., Patzke, S., Holmberg, C., Mejlvang, J., Groth, A., Nielsen, O., Syljuåsen, R.G., and Sørensen, C.S. (2012). Cyclin-dependent kinase suppression by WEE1 kinase protects the genome through control of replication initiation and nucleotide consumption. *Mol. Cell. Biol.* 32, 4226–4236.
- Begg, A.C., Stewart, F.A., and Vens, C. (2011). Strategies to improve radiotherapy with targeted drugs. *Nat. Rev. Cancer* 11, 239–253.
- Bester, A.C., Roniger, M., Oren, Y.S., Im, M.M., Sami, D., Chaoat, M., Bensimon, A., Zamir, G., Shewach, D.S., and Kerem, B. (2011). Nucleotide deficiency promotes genomic instability in early stages of cancer development. *Cell* 145, 435–446.
- Bhat, K.P., Bétous, R., and Cortez, D. (2015). High-affinity DNA-binding domains of replication protein A (RPA) direct SMARCAL1-dependent replication fork remodeling. *J. Biol. Chem.* 290, 4110–4117.
- Bianchi, J., Rudd, S.G., Jozwiakowski, S.K., Bailey, L.J., Soura, V., Taylor, E., Stevanovic, I., Green, A.J., Stracker, T.H., Lindsay, H.D., and Doherty, A.J. (2013). PrimPol bypasses UV photoproducts during eukaryotic chromosomal DNA replication. *Mol. Cell* 52, 566–573.
- Bryant, H.E., Schultz, N., Thomas, H.D., Parker, K.M., Flower, D., Lopez, E., Kyle, S., Meuth, M., Curtin, N.J., and Helleday, T. (2005). Specific killing of BRCA2-deficient tumours with inhibitors of poly(ADP-ribose) polymerase. *Nature* 434, 913–917.
- Buisson, R., Boisvert, J.L., Benes, C.H., and Zou, L. (2015). Distinct but Concerted Roles of ATR, DNA-PK, and Chk1 in Countering Replication Stress during S Phase. *Mol. Cell* 59, 1011–1024.
- Byun, T.S., Pacek, M., Yee, M.C., Walter, J.C., and Cimprich, K.A. (2005). Functional uncoupling of MCM helicase and DNA polymerase activities activates the ATR-dependent checkpoint. *Genes Dev.* 19, 1040–1052.
- Caldecott, K.W. (2014). DNA single-strand break repair. *Exp. Cell Res.* 329, 2–8.
- Castedo, M., Perfettini, J.L., Roumier, T., Andreau, K., Medema, R., and Kroemer, G. (2004). Cell death by mitotic catastrophe: a molecular definition. *Oncogene* 23, 2825–2837.
- Ceccaldi, R., Rondinelli, B., and D'Andrea, A.D. (2015). Repair Pathway Choices and Consequences at the Double-Strand Break. *Trends Cell Biol.* <http://dx.doi.org/10.1016/j.tcb.2015.07.009>.
- Ciccia, A., and Elledge, S.J. (2010). The DNA damage response: making it safe to play with knives. *Mol. Cell* 40, 179–204.
- Cimprich, K.A., and Cortez, D. (2008). ATR: an essential regulator of genome integrity. *Nat. Rev. Mol. Cell Biol.* 9, 616–627.
- Couch, F.B., Bansbach, C.E., Driscoll, R., Luzwick, J.W., Glick, G.G., Bétous, R., Carroll, C.M., Jung, S.Y., Qin, J., Cimprich, K.A., and Cortez, D. (2013). ATR phosphorylates SMARCAL1 to prevent replication fork collapse. *Genes Dev.* 27, 1610–1623.
- Curtin, N.J. (2012). DNA repair dysregulation from cancer driver to therapeutic target. *Nat. Rev. Cancer* 12, 801–817.
- Curtin, N.J., Wang, L.Z., Yiakoukaki, A., Kyle, S., Arris, C.A., Canan-Koch, S., Webber, S.E., Durkacz, B.W., Calvert, H.A., Hostomsky, Z., and Newell, D.R. (2004). Novel poly(ADP-ribose) polymerase-1 inhibitor, AG14361, restores sensitivity to temozolomide in mismatch repair-deficient cells. *Clin. Cancer Res.* 10, 881–889.
- d'Adda di Fagagna, F., Reaper, P.M., Clay-Farrace, L., Fiegler, H., Carr, P., Von Zglinicki, T., Saretzki, G., Carter, N.P., and Jackson, S.P. (2003). A DNA damage checkpoint response in telomere-initiated senescence. *Nature* 426, 194–198.
- Do, K., Doroshov, J.H., and Kummar, S. (2013). Wee1 kinase as a target for cancer therapy. *Cell Cycle* 12, 3159–3164.
- Dobbelstein, M., and Sørensen, C.S. (2015). Exploiting replicative stress to treat cancer. *Nat. Rev. Drug Discov.* 14, 405–423.
- Dungrawala, H., and Cortez, D. (2015). Purification of proteins on newly synthesized DNA using iPOND. *Methods Mol. Biol.* 1228, 123–131.
- Dungrawala, H., Rose, K.L., Bhat, K.P., Mohni, K.N., Glick, G.G., Couch, F.B., and Cortez, D. (2015). The Replication Checkpoint Prevents Two Types of Fork Collapse without Regulating Replisome Stability. *Mol. Cell* 59, 998–1010.
- Einhorn, J., Frodin, J.E., and Müller, T. (1996). Radiotherapy for Cancer. Summary. *Acta Oncol.* 35 (Suppl 6), 9–23.
- EMA (2014). Lynparza recommended for approval in ovarian cancer. [http://www.ema.europa.eu/ema/index.jsp?curl=pages/news\\_and\\_events/news/2014/10/news\\_detail\\_002196.jsp&mid=WC0b01ac058004d5c1](http://www.ema.europa.eu/ema/index.jsp?curl=pages/news_and_events/news/2014/10/news_detail_002196.jsp&mid=WC0b01ac058004d5c1).
- Erice, O., Smith, M.P., White, R., Goicoechea, I., Barriuso, J., Jones, C., Margison, G.P., Acosta, J.C., Wellbrock, C., and Arozarena, I. (2015). MGMT Expression Predicts PARP-Mediated Resistance to Temozolomide. *Mol. Cancer Ther.* 14, 1236–1246.
- Ewald, B., Sampath, D., and Plunkett, W. (2008). Nucleoside analogs: molecular mechanisms signaling cell death. *Oncogene* 27, 6522–6537.
- Fanning, E., Klimovich, V., and Nager, A.R. (2006). A dynamic model for replication protein A (RPA) function in DNA processing pathways. *Nucleic Acids Res.* 34, 4126–4137.
- Farmer, H., McCabe, N., Lord, C.J., Tutt, A.N., Johnson, D.A., Richardson, T.B., Santarosa, M., Dillon, K.J., Hickson, I., Knights, C., et al. (2005). Targeting the DNA repair defect in BRCA mutant cells as a therapeutic strategy. *Nature* 434, 917–921.
- FDA (2015). FDA approves Lynparza to treat advanced ovarian cancer. <http://www.fda.gov/NewsEvents/Newsroom/PressAnnouncements/ucm427554.htm>.
- Fong, P.C., Boss, D.S., Yap, T.A., Tutt, A., Wu, P., Mergui-Roelvink, M., Mortimer, P., Swaisland, H., Lau, A., O'Connor, M.J., et al. (2009). Inhibition of poly(ADP-ribose) polymerase in tumors from BRCA mutation carriers. *N. Engl. J. Med.* 361, 123–134.
- Freund, A., Orjalo, A.V., Desprez, P.Y., and Campisi, J. (2010). Inflammatory networks during cellular senescence: causes and consequences. *Trends Mol. Med.* 16, 238–246.
- Friedman, H.S., Kokkinakis, D.M., Pluda, J., Friedman, A.H., Cokgor, I., Hagglund, M.M., Ashley, D.M., Rich, J., Dolan, M.E., Pegg, A.E., et al. (1998). Phase I trial of O6-benzylguanine for patients undergoing surgery for malignant glioma. *J. Clin. Oncol.* 16, 3570–3575.
- Goodman, M.F., and Woodgate, R. (2013). Translesion DNA polymerases. *Cold Spring Harb. Perspect. Biol.* 5, a010363.
- Gorgoulis, V.G., Vassiliou, L.V., Karakaidos, P., Zacharatos, P., Kotsinas, A., Liloglou, T., Venere, M., Dittullo, R.A., Jr., Kastrinakis, N.G., Levy, B., et al. (2005). Activation of the DNA damage checkpoint and genomic instability in human precancerous lesions. *Nature* 434, 907–913.
- Hahn, W.C., Counter, C.M., Lundberg, A.S., Beijersbergen, R.L., Brooks, M.W., and Weinberg, R.A. (1999). Creation of human tumour cells with defined genetic elements. *Nature* 400, 464–468.

- Halazonetis, T.D., Gorgoulis, V.G., and Bartek, J. (2008). An oncogene-induced DNA damage model for cancer development. *Science* 319, 1352–1355.
- Hall, J.S., Iype, R., Senra, J., Taylor, J., Armenoult, L., Oguejiofor, K., Li, Y., Stratford, I., Stern, P.L., O'Connor, M.J., et al. (2014). Investigation of radiosensitivity gene signatures in cancer cell lines. *PLoS ONE* 9, e86329.
- Hartwell, L.H., Szankasi, P., Roberts, C.J., Murray, A.W., and Friend, S.H. (1997). Integrating genetic approaches into the discovery of anticancer drugs. *Science* 278, 1064–1068.
- Helleday, T. (2011). The underlying mechanism for the PARP and BRCA synthetic lethality: clearing up the misunderstandings. *Mol. Oncol.* 5, 387–393.
- Heller, R.C., and Mariani, K.J. (2006). Replication fork reactivation downstream of a blocked nascent leading strand. *Nature* 439, 557–562.
- Hickson, I., Zhao, Y., Richardson, C.J., Green, S.J., Martin, N.M., Orr, A.I., Reaper, P.M., Jackson, S.P., Curtin, N.J., and Smith, G.C. (2004). Identification and characterization of a novel and specific inhibitor of the ataxia-telangiectasia mutated kinase ATM. *Cancer Res.* 64, 9152–9159.
- Hodgson, D.R., Dougherty, B., Lai, Z., Grinstead, L., Spencer, S., O'Connor, M.J., Ho, T.W., Robertson, J.D., Lanchbury, J., Timms, K., et al. (2015). Candidate biomarkers of PARP inhibitor sensitivity in ovarian cancer beyond the BRCA genes. *Eur. J. Cancer* 51, abstr 435.
- Hoeijmakers, J.H. (2001). Genome maintenance mechanisms for preventing cancer. *Nature* 411, 366–374.
- Hoeijmakers, J.H. (2009). DNA damage, aging, and cancer. *N. Engl. J. Med.* 361, 1475–1485.
- Jackson, S.P., and Bartek, J. (2009). The DNA-damage response in human biology and disease. *Nature* 461, 1071–1078.
- Jiricny, J. (2006). The multifaceted mismatch-repair system. *Nat. Rev. Mol. Cell Biol.* 7, 335–346.
- Jones, R.M., Mortusewicz, O., Afzal, I., Lorvellec, M., Garcia, P., Helleday, T., and Petermann, E. (2013). Increased replication initiation and conflicts with transcription underlie Cyclin E-induced replication stress. *Oncogene* 32, 3744–3753.
- Jossé, R., Martin, S.E., Guha, R., Ormanoglu, P., Pfister, T.D., Reaper, P.M., Barnes, C.S., Jones, J., Charlton, P., Pollard, J.R., et al. (2014). ATR inhibitors VE-821 and VX-970 sensitize cancer cells to topoisomerase I inhibitors by disabling DNA replication initiation and fork elongation responses. *Cancer Res.* 74, 6968–6979.
- Jung, Y., and Lippard, S.J. (2007). Direct cellular responses to platinum-induced DNA damage. *Chem. Rev.* 107, 1387–1407.
- Kaelin, W.G., Jr. (2005). The concept of synthetic lethality in the context of anticancer therapy. *Nat. Rev. Cancer* 5, 689–698.
- Kang, C., Xu, Q., Martin, T.D., Li, M.Z., Demaria, M., Aron, L., Lu, T., Yankner, B.A., Campisi, J., and Elledge, S.J. (2015). The DNA damage response induces inflammation and senescence by inhibiting autophagy of GATA4. *Science* 349, aaa5612.
- Kee, Y., and D'Andrea, A.D. (2010). Expanded roles of the Fanconi anemia pathway in preserving genomic stability. *Genes Dev.* 24, 1680–1694.
- Le, D.T., Uram, J.N., Wang, H., Bartlett, B.R., Kemberling, H., Eyring, A.D., Skora, A.D., Luber, B.S., Azad, N.S., Laheru, D., et al. (2015). PD-1 Blockade in Tumors with Mismatch-Repair Deficiency. *N. Engl. J. Med.* 372, 2509–2520.
- Lecona, E., and Fernández-Capetillo, O. (2014). Replication stress and cancer: it takes two to tango. *Exp. Cell Res.* 329, 26–34.
- Ledermann, J., Harter, P., Gourley, C., Friedlander, M., Vergote, I., Rustin, G., Scott, C., Meier, W., Shapira-Frommer, R., Safra, T., et al. (2012). Olaparib maintenance therapy in platinum-sensitive relapsed ovarian cancer. *N. Engl. J. Med.* 366, 1382–1392.
- Ledermann, J., Harter, P., Gourley, C., Friedlander, M., Vergote, I., Rustin, G., Scott, C.L., Meier, W., Shapira-Frommer, R., Safra, T., et al. (2014). Olaparib maintenance therapy in patients with platinum-sensitive relapsed serous ovarian cancer: a preplanned retrospective analysis of outcomes by BRCA status in a randomised phase 2 trial. *Lancet Oncol.* 15, 852–861.
- Leijen, S., van Geel, R., Sonke, G.S., de Jong, D., Rosenberg, E.H., Marchetti, S., Pluim, D., van Werkhoven, E.D., Rose, S., Lee, M.A., et al. (2015). Phase II study with Wee1 inhibitor AZD1775 plus carboplatin in patients with p53 mutated ovarian cancer refractory or resistant (<3 months) to standard first line therapy. *J. Clin. Oncol.* 33, abstr2507.
- Lieber, M.R. (2010). The mechanism of double-strand DNA break repair by the nonhomologous DNA end-joining pathway. *Annu. Rev. Biochem.* 79, 181–211.
- Lindahl, T., Satoh, M.S., Poirier, G.G., and Klungland, A. (1995). Post-translational modification of poly(ADP-ribose) polymerase induced by DNA strand breaks. *Trends Biochem. Sci.* 20, 405–411.
- Liu, J.F., Barry, W.T., Birrer, M., Lee, J.M., Buckanovich, R.J., Fleming, G.F., Rimel, B., Buss, M.K., Nattam, S., Hurteau, J., et al. (2014). Combination cediranib and olaparib versus olaparib alone for women with recurrent platinum-sensitive ovarian cancer: a randomised phase 2 study. *Lancet Oncol.* 15, 1207–1214.
- Lord, C.J., and Ashworth, A. (2012). The DNA damage response and cancer therapy. *Nature* 481, 287–294.
- Lucchesi, J.C. (1968). Synthetic lethality and semi-lethality among functionally related mutants of *Drosophila melanogaster*. *Genetics* 59, 37–44.
- Lukas, C., Savic, V., Bekker-Jensen, S., Doil, C., Neumann, B., Pedersen, R.S., Grofte, M., Chan, K.L., Hickson, I.D., Bartek, J., and Lukas, J. (2011). 53BP1 nuclear bodies form around DNA lesions generated by mitotic transmission of chromosomes under replication stress. *Nat. Cell Biol.* 13, 243–253.
- Macheret, M., and Halazonetis, T.D. (2015). DNA replication stress as a hallmark of cancer. *Annu. Rev. Pathol.* 10, 425–448.
- Martin, S.A., McCarthy, A., Barber, L.J., Burgess, D.J., Parry, S., Lord, C.J., and Ashworth, A. (2009). Methotrexate induces oxidative DNA damage and is selectively lethal to tumour cells with defects in the DNA mismatch repair gene MSH2. *EMBO Mol. Med.* 1, 323–337.
- Mateos-Gomez, P.A., Gong, F., Nair, N., Miller, K.M., Lazzarini-Denchi, E., and Sfeir, A. (2015). Mammalian polymerase  $\theta$  promotes alternative NHEJ and suppresses recombination. *Nature* 518, 254–257.
- Maya-Mendoza, A., Petermann, E., Gillespie, D.A., Caldecott, K.W., and Jackson, D.A. (2007). Chk1 regulates the density of active replication origins during the vertebrate S phase. *EMBO J.* 26, 2719–2731.
- Miki, Y., Swensen, J., Shattuck-Eidens, D., Futreal, P.A., Harshman, K., Tavtigian, S., Liu, Q., Cochran, C., Bennett, L.M., Ding, W., et al. (1994). A strong candidate for the breast and ovarian cancer susceptibility gene BRCA1. *Science* 266, 66–71.
- Moynahan, M.E., and Jasin, M. (2010). Mitotic homologous recombination maintains genomic stability and suppresses tumorigenesis. *Nat. Rev. Mol. Cell Biol.* 11, 196–207.
- Murai, J., Huang, S.Y., Das, B.B., Renaud, A., Zhang, Y., Doroshow, J.H., Ji, J., Takeda, S., and Pommier, Y. (2012). Trapping of PARP1 and PARP2 by Clinical PARP Inhibitors. *Cancer Res.* 72, 5588–5599.
- Murai, J., Zhang, Y., Morris, J., Ji, J., Takeda, S., Doroshow, J.H., and Pommier, Y. (2014). Rationale for poly(ADP-ribose) polymerase (PARP) inhibitors in combination therapy with camptothecins or temozolomide based on PARP trapping versus catalytic inhibition. *J. Pharmacol. Exp. Ther.* 349, 408–416.
- O'Connor, M.J., Martin, N.M., and Smith, G.C. (2007). Targeted cancer therapies based on the inhibition of DNA strand break repair. *Oncogene* 26, 7816–7824.
- O'Connor, M.J., Mason, H., Horner, S., Slater, I., Lau, A., Cadogan, E., and Oplustilova, L. (2013). Generating preclinical models to assess bone marrow toxicity induced by the PARP inhibitor olaparib in combination with chemotherapy. *Cancer Res.* 73, <http://dx.doi.org/10.1158/1538-7445.AM2013-4420>.
- Orta, M.L., Höglund, A., Calderón-Montaño, J.M., Domínguez, I., Burgos-Morón, E., Visnes, T., Pastor, N., Ström, C., López-lázaro, M., and Helleday, T. (2014). The PARP inhibitor Olaparib disrupts base excision repair of 5-aza-2'-deoxycytidine lesions. *Nucleic Acids Res.* 42, 9108–9120.
- Patel, A.G., Sarkaria, J.N., and Kaufmann, S.H. (2011). Nonhomologous end joining drives poly(ADP-ribose) polymerase (PARP) inhibitor lethality in

- homologous recombination-deficient cells. *Proc. Natl. Acad. Sci. USA* **108**, 3406–3411.
- Pearl, L.H., Schierz, A.C., Ward, S.E., Al-Lazikani, B., and Pearl, F.M. (2015). Therapeutic opportunities within the DNA damage response. *Nat. Rev. Cancer* **15**, 166–180.
- Peng, G., Woodman, S.E., and Mills, G.B. (2014). RADical response puts an exceptional responder in CHKmate: a synthetic lethal curative response to DNA-damaging chemotherapy? *Cancer Discov.* **4**, 988–990.
- Petermann, E., Woodcock, M., and Helleday, T. (2010). Chk1 promotes replication fork progression by controlling replication initiation. *Proc. Natl. Acad. Sci. USA* **107**, 16090–16095.
- Plummer, R., Jones, C., Middleton, M., Wilson, R., Evans, J., Olsen, A., Curtin, N., Boddy, A., McHugh, P., Newell, D., et al. (2008). Phase I study of the poly(ADP-ribose) polymerase inhibitor, AG014699, in combination with temozolomide in patients with advanced solid tumors. *Clin. Cancer Res.* **14**, 7917–7923.
- Pommier, Y., Leo, E., Zhang, H., and Marchand, C. (2010). DNA topoisomerases and their poisoning by anticancer and antibacterial drugs. *Chem. Biol.* **17**, 421–433.
- Prakash, R., Zhang, Y., Feng, W., and Jasin, M. (2015). Homologous recombination and human health: the roles of BRCA1, BRCA2, and associated proteins. *Cold Spring Harb. Perspect. Biol.* **7**, a016600.
- Radhakrishnan, S.K., Jette, N., and Lees-Miller, S.P. (2014). Non-homologous end joining: emerging themes and unanswered questions. *DNA Repair (Amst.)* **17**, 2–8.
- Ragland, R.L., Patel, S., Rivard, R.S., Smith, K., Peters, A.A., Bielinsky, A.K., and Brown, E.J. (2013). RNF4 and PLK1 are required for replication fork collapse in ATR-deficient cells. *Genes Dev.* **27**, 2259–2273.
- Reaper, P.M., Griffiths, M.R., Long, J.M., Charrier, J.D., McCormick, S., Charlton, P.A., Golec, J.M., and Pollard, J.R. (2011). Selective killing of ATM- or p53-deficient cancer cells through inhibition of ATR. *Nat. Chem. Biol.* **7**, 428–430.
- Reijns, M.A., Rabe, B., Rigby, R.E., Mill, P., Astell, K.R., Lettice, L.A., Boyle, S., Leitch, A., Keighren, M., Kilanowski, F., et al. (2012). Enzymatic removal of ribonucleotides from DNA is essential for mammalian genome integrity and development. *Cell* **149**, 1008–1022.
- Rohban, S., and Campaner, S. (2015). Myc induced replicative stress response: How to cope with it and exploit it. *Biochim. Biophys. Acta* **1849**, 517–524.
- Rothkamm, K., and Löbrich, M. (2003). Evidence for a lack of DNA double-strand break repair in human cells exposed to very low x-ray doses. *Proc. Natl. Acad. Sci. USA* **100**, 5057–5062.
- Sabharwal, S.S., and Schumacker, P.T. (2014). Mitochondrial ROS in cancer: initiators, amplifiers or an Achilles' heel? *Nat. Rev. Cancer* **14**, 709–721.
- Samol, J., Ranson, M., Scott, E., Macpherson, E., Carmichael, J., Thomas, A., and Cassidy, J. (2012). Safety and tolerability of the poly(ADP-ribose) polymerase (PARP) inhibitor, olaparib (AZD2281) in combination with topotecan for the treatment of patients with advanced solid tumors: a phase I study. *Invest. New Drugs* **30**, 1493–1500.
- Sarcar, B., Kahali, S., Prabhu, A.H., Shumway, S.D., Xu, Y., Demuth, T., and Chinnaiyan, P. (2011). Targeting radiation-induced G(2) checkpoint activation with the Wee-1 inhibitor MK-1775 in glioblastoma cell lines. *Mol. Cancer Ther.* **10**, 2405–2414.
- Sedgwick, B., Bates, P.A., Paik, J., Jacobs, S.C., and Lindahl, T. (2007). Repair of alkylated DNA: recent advances. *DNA Repair (Amst.)* **6**, 429–442.
- Senra, J.M., Telfer, B.A., Cherry, K.E., McCrudden, C.M., Hirst, D.G., O'Connor, M.J., Wedge, S.R., and Stratford, I.J. (2011). Inhibition of PARP-1 by olaparib (AZD2281) increases the radiosensitivity of a lung tumor xenograft. *Mol. Cancer Ther.* **10**, 1949–1958.
- Shechter, D., Costanzo, V., and Gautier, J. (2004). ATR and ATM regulate the timing of DNA replication origin firing. *Nat. Cell Biol.* **6**, 648–655.
- Shibata, A., and Jeggo, P.A. (2014). DNA double-strand break repair in a cellular context. *Clin. Oncol. (R Coll Radiol)* **26**, 243–249.
- Siddik, Z.H. (2002). Mechanisms of action of cancer chemotherapeutic agents: DNA-interactive alkylating agents and antitumor platinum-based drugs. In *The Cancer Handbook*, M.R. Alison, ed. (John Wiley and Sons, Ltd.).
- Tentori, L., Ricci-Vitiani, L., Muzi, A., Ciccarone, F., Pelacchi, F., Calabrese, R., Runci, D., Pallini, R., Caiafa, P., and Graziani, G. (2014). Pharmacological inhibition of poly(ADP-ribose) polymerase-1 modulates resistance of human glioblastoma stem cells to temozolomide. *BMC Cancer* **14**, 151.
- Toledo, L.I., Murga, M., Zur, R., Soria, R., Rodríguez, A., Martínez, S., Oyarzabal, J., Pastor, J., Bischoff, J.R., and Fernandez-Capetillo, O. (2011). A cell-based screen identifies ATR inhibitors with synthetic lethal properties for cancer-associated mutations. *Nat. Struct. Mol. Biol.* **18**, 721–727.
- Toledo, L.I., Altmeyer, M., Rask, M.B., Lukas, C., Larsen, D.H., Povlsen, L.K., Bekker-Jensen, S., Mailand, N., Bartek, J., and Lukas, J. (2013). ATR prohibits replication catastrophe by preventing global exhaustion of RPA. *Cell* **155**, 1088–1103.
- Tutt, A., Robson, M., Garber, J.E., Domchek, S.M., Audeh, M.W., Weitzel, J.N., Friedlander, M., Arun, B., Loman, N., Schmutzler, R.K., et al. (2010). Oral poly(ADP-ribose) polymerase inhibitor olaparib in patients with BRCA1 or BRCA2 mutations and advanced breast cancer: a proof-of-concept trial. *Lancet* **376**, 235–244.
- Twyman-Saint Victor, C., Rech, A.J., Maity, A., Rengan, R., Pauken, K.E., Stelekati, E., Benci, J.L., Xu, B., Dada, H., Odorizzi, P.M., et al. (2015). Radiation and dual checkpoint blockade activate non-redundant immune mechanisms in cancer. *Nature* **520**, 373–377.
- Vafa, O., Wade, M., Kern, S., Beeche, M., Pandita, T.K., Hampton, G.M., and Wahl, G.M. (2002). c-Myc can induce DNA damage, increase reactive oxygen species, and mitigate p53 function: a mechanism for oncogene-induced genetic instability. *Mol. Cell* **9**, 1031–1044.
- Venkitaraman, A.R. (2014). Cancer suppression by the chromosome custodians, BRCA1 and BRCA2. *Science* **343**, 1470–1475.
- Verhagen, C.V., de Haan, R., Hageman, F., Oostendorp, T.P., Carli, A.L., O'Connor, M.J., Jonkers, J., Verheij, M., van den Brekel, M.W., and Vens, C. (2015). Extent of radiosensitization by the PARP inhibitor olaparib depends on its dose, the radiation dose and the integrity of the homologous recombination pathway of tumor cells. *Radiother. Oncol.* **116**, 358–365.
- Ward, J.F. (1998). Nature of lesions formed by ionizing radiation. In *DNA Damage and Repair*, J.A. Nickoloff and M.F. Hoekstra, eds. (Humana Press), pp. 265–284.
- Waters, L.S., Minesinger, B.K., Wiltrout, M.E., D'Souza, S., Woodruff, R.V., and Walker, G.C. (2009). Eukaryotic translesion polymerases and their roles and regulation in DNA damage tolerance. *Microbiol. Mol. Biol. Rev.* **73**, 134–154.
- Weiss, G.J., Chao, J., Neidhart, J.D., Ramanathan, R.K., Bassett, D., Neidhart, J.A., Choi, C.H., Chow, W., Chung, V., Forman, S.J., et al. (2013). First-in-human phase 1/2a trial of CRLX101, a cyclodextrin-containing polymer-camptothecin nanopharmaceutical in patients with advanced solid tumor malignancies. *Invest. New Drugs* **31**, 986–1000.
- Wilson, S.H., Beard, W.A., Shock, D.D., Batra, V.K., Cavanaugh, N.A., Prasad, R., Hou, E.W., Liu, Y., Asagoshi, K., Horton, J.K., et al. (2010). Base excision repair and design of small molecule inhibitors of human DNA polymerase  $\beta$ . *Cell. Mol. Life Sci.* **67**, 3633–3647.
- Wooster, R., Bignell, G., Lancaster, J., Swift, S., Seal, S., Mangion, J., Collins, N., Gregory, S., Gumbs, C., and Micklem, G. (1995). Identification of the breast cancer susceptibility gene BRCA2. *Nature* **378**, 789–792.
- Wu, W., Nishikawa, H., Fukuda, T., Vittal, V., Asano, M., Miyoshi, Y., Kleivit, R.E., and Ohta, T. (2015). Interaction of BARD1 and HP1 Is Required for BRCA1 Retention at Sites of DNA Damage. *Cancer Res.* **75**, 1311–1321.
- Young, C., Schlupe, T., Hwang, J., and Eliasof, S. (2011). CRLX101 (formerly IT-101)-A Novel Nanopharmaceutical of Camptothecin in Clinical Development. *Curr. Bioact. Compd.* **7**, 8–14.
- Zeman, M.K., and Cimprich, K.A. (2014). Causes and consequences of replication stress. *Nat. Cell Biol.* **16**, 2–9.
- Zou, L., and Elledge, S.J. (2003). Sensing DNA damage through ATRIP recognition of RPA-ssDNA complexes. *Science* **300**, 1542–1548.



# We are editors and scientists too.



We are in your lab, at meetings and talking by phone to get to know as many of you as possible in all corners of the world and at all points of your career.

**When you choose Cell Press you get the attention you deserve.**

For more information visit: [www.cell.com/values](http://www.cell.com/values)

Your **work** is our **life**



# Mutational Strand Asymmetries in Cancer Genomes Reveal Mechanisms of DNA Damage and Repair

Nicholas J. Haradhvala,<sup>1,2,8</sup> Paz Polak,<sup>1,2,3,8</sup> Petar Stojanov,<sup>4</sup> Kyle R. Covington,<sup>5</sup> Eve Shinbrot,<sup>5</sup> Julian M. Hess,<sup>2</sup> Esther Rheinbay,<sup>1,2</sup> Jaegil Kim,<sup>2</sup> Yosef E. Maruvka,<sup>1,2</sup> Lior Z. Braunstein,<sup>2</sup> Atanas Kamburov,<sup>1,2,3</sup> Philip C. Hanawalt,<sup>6</sup> David A. Wheeler,<sup>5</sup> Amnon Koren,<sup>2,7</sup> Michael S. Lawrence,<sup>2,9,\*</sup> and Gad Getz<sup>1,2,3,9,\*</sup>

<sup>1</sup>Massachusetts General Hospital Cancer Center and Department of Pathology, 55 Fruit Street, Boston, MA 02114, USA

<sup>2</sup>Broad Institute of Harvard and MIT, 415 Main Street, Cambridge, MA 02142, USA

<sup>3</sup>Harvard Medical School, 25 Shattuck Street, Boston, MA 02115, USA

<sup>4</sup>Carnegie Mellon University School of Computer Science, 5000 Forbes Avenue, Pittsburgh, PA 15213, USA

<sup>5</sup>Baylor College of Medicine, 1 Baylor Plaza, Houston, TX 77030, USA

<sup>6</sup>Stanford University Department of Biology, 450 Serra Mall, Stanford, CA 94305, USA

<sup>7</sup>Cornell University Department of Molecular Biology and Genetics, 526 Campus Road, Ithaca, NY 14853, USA

<sup>8</sup>Co-first author

<sup>9</sup>Co-senior author

\*Correspondence: lawrence@broadinstitute.org (M.S.L.), gadgetz@broadinstitute.org (G.G.)

<http://dx.doi.org/10.1016/j.cell.2015.12.050>

## SUMMARY

Mutational processes constantly shape the somatic genome, leading to immunity, aging, cancer, and other diseases. When cancer is the outcome, we are afforded a glimpse into these processes by the clonal expansion of the malignant cell. Here, we characterize a less explored layer of the mutational landscape of cancer: mutational asymmetries between the two DNA strands. Analyzing whole-genome sequences of 590 tumors from 14 different cancer types, we reveal widespread asymmetries across mutagenic processes, with transcriptional (“T-class”) asymmetry dominating UV-, smoking-, and liver-cancer-associated mutations and replicative (“R-class”) asymmetry dominating POLE-, APOBEC-, and MSI-associated mutations. We report a striking phenomenon of transcription-coupled damage (TCD) on the non-transcribed DNA strand and provide evidence that APOBEC mutagenesis occurs on the lagging-strand template during DNA replication. As more genomes are sequenced, studying and classifying their asymmetries will illuminate the underlying biological mechanisms of DNA damage and repair.

## INTRODUCTION

A thorough understanding of mutational density and patterns in cancer genomes is important for studying the mechanisms of mutagenesis (Plesance et al., 2010a, 2010b), for modeling the evolution of cancer genomes (Alexandrov et al., 2013; Nik-Zainal et al., 2012b), and for identifying cancer genes (Lawrence et al.,

2013). In cancer genomes, somatic mutations exhibit heterogeneity in total mutation density, in mutation spectra among tumors and cancer types, and in mutation density along the genome within a given tumor (Lawrence et al., 2013; Plesance et al., 2010a, 2010b). This heterogeneity is caused by underlying mutational processes that reflect different genetic backgrounds and mutagenic exposures and by a non-uniform epigenomic landscape with variation in DNA replication timing, chromatin structure, and gene expression levels across the genome (Lawrence et al., 2013; Plesance et al., 2010a, 2010b; Polak et al., 2014, 2015; Waddell et al., 2015).

One challenge inherent in the analysis of genomic mutations is the loss of strand information that occurs between the initial occurrence of a mutagenic lesion and the ultimate readout by DNA sequencing. For instance, consider a mutational process whose initiating event is oxidative attack on the guanine of a C:G base pair. In principle, if we isolated the DNA immediately after such an attack, we could directly observe the lesion; however, in genomic sequencing data, we don't encounter mutations until many cell divisions later. The result of such a lesion is generally an A:G mismatch after the first cell division, leading to a stable A:T base pair after an additional round of replication. Since approximately half of C:G base pairs are oriented with the cytosine on the reference (Watson) and half on the anti-reference (Crick) strand, roughly equal numbers of “G→T” and “C→A” mutations are seen. A lesion at the cytosine of a C:G base pair could produce exactly the same result, so working backward, we cannot determine the base of the original DNA damage. This is because using the genomic reference strand as the “frame of reference” for base-pair orientation is merely an arbitrary convention.

However, we can recover some strand information by considering a more biologically meaningful reference frame. In regions that undergo DNA transcription, the DNA can be oriented with respect to the transcribed strand. Thus, we would consider a C:G→A:T base pair change to be a “C→A” or “G→T” mutation

depending on whether the C or the G is in the template strand for transcription. Alternatively, we can use DNA replication to define a frame of reference. In this case, whether the C of a C:G base pair is on the leading or the lagging strand of DNA replication would determine the type of mutation. Because replication and transcription are each associated with opportunities for the asymmetric (strand-specific) introduction and repair of DNA damage, they each have the potential to leave their footprints in a patient's mutational profile in the form of unequal rates and patterns of mutations on the two strands of DNA (Francioli et al., 2015; Green et al., 2003; Lobry, 1996; Lujan et al., 2012; Pleasance et al., 2010a, 2010b; Polak and Arndt, 2008; Polak et al., 2010; Shinbrot et al., 2014; Touchon et al., 2005).

Strand asymmetry has already been well studied in the context of transcription. DNA lesions encountered on the transcribed ("template") strand can stall progression of the RNA polymerase, leading to the recruitment of a nucleotide excision repair (NER) complex that can correct the damage (Donahue et al., 1994; Fousteri and Mullenders, 2008; Hanawalt and Spivak, 2008; Jiang and Sancar, 2006; Mellon et al., 1987; Spivak and Ganesan, 2014). Importantly, higher transcription levels of a gene are associated with more opportunities for transcription-coupled repair (TCR), leading to an inverse correlation between the expression level of a gene and its mutation density (Chapman et al., 2011; Lawrence et al., 2013; Pleasance et al., 2010a). Conversely, damage on the non-template ("sense") strand may fail to stall the RNA polymerase and therefore could escape repair by TCR. In addition, the non-template strand remains single-stranded during the process of transcription and is therefore more vulnerable to damage (Jinks-Robertson and Bhagwat, 2014). In combination, these mechanisms lead to differences in mutation densities and spectra on the transcribed and non-transcribed strands (Pleasance et al., 2010a, 2010b). Notably, transcriptional strand asymmetry provides information regarding damage and TCR beyond what can be gathered from the correlation of mutational densities with expression, since the latter is convolved with other genomic factors such as chromatin-state and replication-timing-dependent mismatch repair (MMR; Suppek and Lehner, 2015).

Strand asymmetry can also be viewed in the reference frame of DNA replication. The DNA replication fork is composed of a leading strand, copied in a largely continuous fashion, and a lagging strand, copied as a discontinuous series of Okazaki fragments. DNA polymerases  $\alpha$ ,  $\delta$ , and  $\epsilon$  work together to replicate the DNA but have distinct roles in synthesis and proofreading. The resulting asymmetry reflects an imbalance in the types of mutations introduced on the leading versus lagging strand, although it is still a matter of debate whether this occurs due to the division of labor of distinct polymerases in DNA synthesis (Miyabe et al., 2011; Nick McElhinny et al., 2008) or due to specialized polymerase proofreading properties (Johnson et al., 2015; Stillman, 2015). Additionally the lagging strand endures longer exposure as single-stranded DNA (ssDNA; Yu et al., 2014) and, as such, may be more vulnerable to ssDNA-targeting mutagens. These factors lead to replication-associated mutational asymmetry that flips (i.e., inverts which strand has the higher mutation density) at replication origins. Replication-strand asymmetries were observed as local skews in nucleotide

composition in the chromosomes of bacterial (Lobry, 1996; McLean et al., 1998) and eukaryotic (Touchon et al., 2005) species, are associated with robustly programmed yeast replication origins (Koren et al., 2010), and have also been experimentally demonstrated in yeast (Lujan et al., 2012; Pavlov et al., 2002).

## RESULTS

### A Framework for Analysis of Replicative and Transcriptional Asymmetries

We partitioned the human genome in two ways: first, by transcription direction, using RefSeq gene definitions (Figure 1A). We annotated genomic regions as tx(+) when they encoded genes on the reference strand and as tx(-) when they encoded genes on the complementary strand. We considered the patterns of mutations in smoking-associated lung cancers, combining mutation data from seven lung adenocarcinomas (LUAD) that exhibited a strong smoking signature. Mutational densities of C:G  $\rightarrow$  A:T are highest in both tx(+) and tx(-) genes when the guanine is on the non-transcribed strand (Figure 1C). This is consistent with the known mechanism of the smoking signature, driven by carcinogen attack at guanines (Denissenko et al., 1996). TCR lowers the mutational densities of C:G base pairs in which the guanine serves as the transcription template (denoted  $C_{ntx}:G_{tx}$ ), relative to intergenic regions (IGR). In contrast,  $G_{ntx}:C_{tx}$  base pairs do not benefit from this extra opportunity for repair, resulting in undiminished mutation density of  $G_{ntx}:C_{tx} \rightarrow T_{ntx}:A_{tx}$ , as shown previously (Pleasance et al., 2010b).

The second form of genome partitioning was by DNA replication direction. Since the entire genome is replicated every time a cell divides (but only a portion is transcribed), replication direction has the potential to exert larger asymmetries in mutational data. However, determining direction is much more challenging for replication than transcription, since the precise locations of replication origins in the human genome are not known. This has precluded a comprehensive analysis of replicative strand asymmetry thus far.

To enable an analysis of replication direction and strand asymmetry, we utilized high-resolution genomic replication timing data from deep DNA sequencing of S- and G1-phase cells from lymphoblastoid cell lines of six individuals (Koren et al., 2012). These data exhibit valleys and peaks in a timing-versus-location landscape that correspond to the approximate locations of replication origins (or origin clusters) and replication termini (Figure 1B). The regions between valleys and peaks correspond, in principle, to regions that replicate predominantly in a single direction (from origin to termination zone) and for which predominant replication direction can be assigned. This approach has previously been used to reveal compositional skews and asymmetric evolutionary germline mutations in the human genome (Chen et al., 2011). However, there are inherent limitations in the identification of replication origins based on replication timing valleys, and there is a lack of a gold standard (i.e., a set of replication origins with known locations) with which to benchmark this approach.

The valleys and peaks (constant-timing regions) are the source of most tissue-specific variation in the profiles (Rhind and

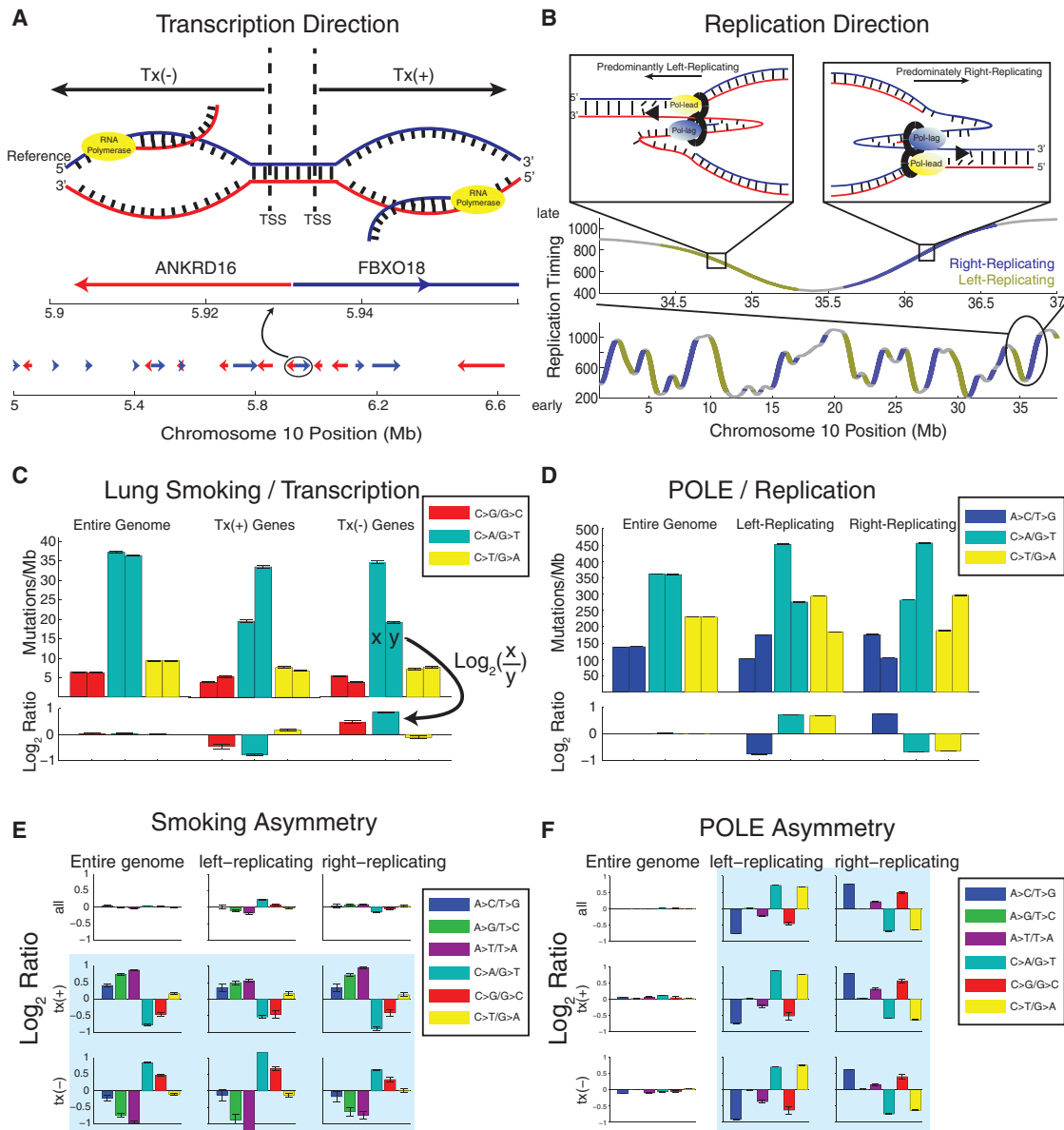


**Figure 1. Mutational Strand Asymmetry Associated with Transcription and Replication**

Transcription is shown on the left and replication on the right.

(A) Transcription direction: Tx(+) regions carry the coding sequence of a gene on the genomic reference strand, and Tx(-) regions carry the coding sequence on the genomic complement strand.

(B) Replication direction: positive slope in replication timing data indicates general rightward movement of the replication complex (“right-replicating”), while negative slope indicates left-replicating.

(C) Lung cancers show strong transcriptional (“T-class”) asymmetry. Each pair of bars (upper axis) shows the density of mutations at C:G (left bar) and G:C (right bar) base pairs. When summing across the entire genome, base-pair orientation does not affect mutational densities. In tx(+) regions, G:C base pairs show a higher density of G → T transversions than C:G base pairs; the opposite is true in tx(-) regions. Lower axis shows the log<sub>2</sub> ratio of each pair of bars.

(D) POLE mutant cancers (colorectal and endometrial) show strong replicative (“R-class”) asymmetry. Left-replicating regions show a higher density of mutations at C:G base pairs, and right-replicating regions show a higher density at G:C.

(E) Lung cancers show strong T-class asymmetry but little R-class.

(F) POLE mutant cancers show strong R-class strand asymmetry but little T-class.

Error bars represent 95% confidence interval.

Gilbert, 2013; Ryba et al., 2010) and, furthermore, present no clear direction of replication. Therefore, we excluded these regions from our analysis and focused on “timing transition re-

gions” (TTRs), which are highly conserved (Rhind and Gilbert, 2013; Ryba et al., 2010) and have a prominent slope that indicates the general direction of replication, either “left-replicating”

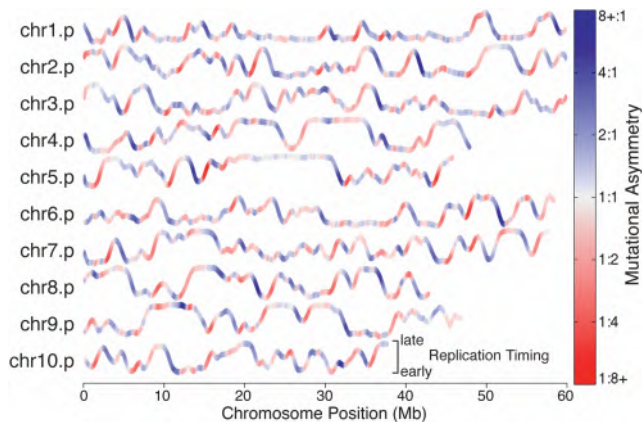


**Figure 2. Strand Asymmetry in POLE Mutant Cancers Reflects Directionality of DNA Replication TTRs**

Replication timing profiles are shown for the p arms (up to 60 Mb) of the first ten chromosomes. Profiles are colored by the local ratio of C→A to G→T mutations in a cohort of 12 mutant-POLE genomes (colorectal and endometrial). Strikingly, late-to-early TTRs (where slope is negative) frequently have a strong bias toward C→A mutations (blue), consistent with leading-strand synthesis using the reference strand as template. Conversely, early-to-late TTRs (positive slopes) show bias toward G→T mutations (red), consistent with lagging-strand synthesis using the reference strand as template (Shinbrot et al., 2014).

or “right-replicating.” (We use the terms “left” and “right” when viewing the DNA in the standard orientation.) While TTRs were first thought to represent regions that are entirely uni-directional in replication (Ryba et al., 2010), it was later suggested that the vast majority of these regions are replicated too quickly for a single replication fork and are more likely replicated by origins that fire in close succession (Guilbaud et al., 2011; Rhind and Gilbert, 2013). For any pair of sequentially firing origins, the greater portion of the inter-origin distance is replicated by the fork originating from the earlier of the two origins. The result is that, in aggregate, the larger portion of a TTR is synthesized in the early-to-late direction (Figure S1). Thus, TTRs have a predominant replication direction given by the sign of their slope. Restricting analysis to these regions enabled us to assign the predominant replication direction to 38% of the genome.

To validate our ability to measure replicative asymmetry using these left- and right-replicating definitions, we considered the one known case of replicative mutational asymmetry: tumors carrying functional mutations in the proofreading exonuclease domain of *POLE*, the gene encoding polymerase  $\epsilon$  (designated as “POLE tumors”; Shinbrot et al., 2014). The exonuclease domain of polymerase  $\epsilon$  is responsible for proofreading during synthesis of the leading strand (Nick McElhinny et al., 2008; Shinbrot et al., 2014), and POLE tumors were previously reported to have high rates of C:G mutations (to A:T or T:A) asymmetrically introduced at cytosines replicated on the leading-strand template near three well-characterized origins of replication (Shinbrot et al., 2014). As a consequence, in these tumors we would expect to see predominantly C→A mutations in left-replicating regions and G→T in right-replicating regions, since we hypothesized these regions to be enriched for leading- and lagging-strand synthesis of the reference strand, respectively.

Indeed, when asymmetry is visualized along the chromosome, asymmetric C:G→A:T mutations, in a pooled cohort of 12 mutant-POLE colorectal and endometrial tumors, correspond strikingly to the slope of the replication timing profile (Figure 2). Higher densities of C→A mutations occur in regions of negative slope, while higher G→T densities occur in regions of positive slope. In TTRs (see Experimental Procedures), the magnitude and direction of this imbalance correlates well with the slope of the profile ( $R^2 = 0.53$ ), while in constant-timing regions, no such correlation exists ( $R^2 = 0.08$ ). Comparing left- and right-replicating regions, we measured a near 2-fold enrichment for the expected mutation type (Figure 1D). This is consistent with the recently reported preference for mutations at C:G base pairs where the cytosine is on the leading template strand measured next to three well-localized origins of replication (we will denote such base pairs  $C_{left}:G_{right}$ ) (Shinbrot et al., 2014), and this validates our ability to extract replication direction from replication timing profiles. Furthermore, we tested our method on replication timing datasets from various cell types, including embryonic stem cells, induced pluripotent stem cells, neural precursor cells, and lymphoblast cell lines (Figure S2) (Ryba et al., 2010). All yielded very similar patterns of asymmetry, demonstrating the robustness of our method to tissue-specific variations in replication timing profiles.

Having analyzed each reference frame separately, we jointly considered transcriptional (T-class) and replicative (R-class) asymmetry. By focusing the analysis on regions that are both transcribed and located in TTRs, we can control for potential confounding factors such as chromatin state, since transcribed regions are typically in open chromatin and TTRs often reside at boundaries between open and closed chromatin (Lawrence et al., 2013). Surprisingly, we observed near-complete mutual exclusivity of R- and T-class asymmetries in the smoking-associated (lung) and POLE-associated (colorectal, endometrial) cohorts. In smoking-associated genomes, the direction of mutational asymmetries flips with transcription direction but shows little dependence on replication direction, even when controlling for transcription direction (Figure 1E). These observations show that smoking-associated lung cancers have a mutational pattern dominated by T-class asymmetry and with very little contribution from R-class asymmetry.

The opposite pattern was seen in POLE-associated cancers, in which mutational asymmetries depended entirely on replication direction and showed little response to change in transcription direction (Figure 1F). Thus, POLE-associated cancers have a mutational pattern dominated by R-class asymmetry and with almost zero T-class asymmetry.

### The Asymmetry Map of Cancer Genomics

Having established that we can observe and separate transcriptional and replicative strand asymmetries for two well-understood mutational processes, we performed a comprehensive analysis of mutational strand asymmetries across many tumor types. We analyzed somatic mutations in 590 whole-genome sequences across 14 tumor types, partitioned into 18 patient cohorts (separating out POLE and microsatellite-instability [MSI] cases in the colorectal and endometrial cohorts and separating smokers from non-smokers in the two

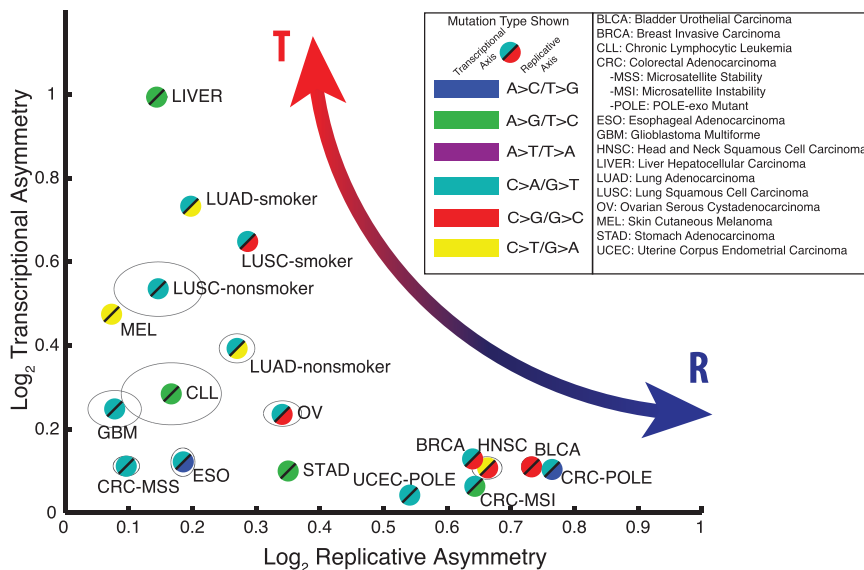


**Figure 3. Cancer Cohorts Vary Widely across the Asymmetry Map**

For each cohort listed, the maximal replicative asymmetry (x axis) and the maximal transcriptional asymmetry (y axis) were measured and plotted. Gray ellipses denote 95% confidence intervals for cohorts in which these extend beyond the bounds of the plot symbols.

lung cohorts; Table S1). For each cohort, we identified the mutation type having the largest asymmetry, with respect to transcription and to replication (Figure 3). This revealed a continuum of tumor types, ranging from tumors with predominant transcriptional (T-class) asymmetry to those with predominant replicative (R-class) asymmetry. For example, the melanoma, liver, and lung cohorts fell on the T-class side of the spectrum, while tumors frequently associated with an APOBEC signature (BLCA, BRCA, and HNSC) or MSI (CRC-MSI) showed R-class asymmetries at levels comparable to those of POLE tumors (CRC-POLE and UCEC-POLE).

The genomic asymmetry profiles of R-class tumors are strikingly concordant among each other within TTRs (POLE-APOBEC  $R^2 = 0.50$ , POLE-MSI  $R^2 = 0.66$ , APOBEC-MSI  $R^2 = 0.42$ ) as well as with the slope of the replication timing profile (POLE  $R^2 = 0.56$ , APOBEC  $R^2 = 0.47$ , MSI  $R^2 = 0.49$ ) (Figure 4), a trend robust to substituting replication timing profiles from various cell types (Ryba et al., 2010) (Figures S3 and S4). Importantly, we were able to detect statistically significant levels of asymmetry in all cohorts in at least one mutation type, and 8/15 showed either T-class or R-class asymmetry with greater than 50% enrichment ( $>0.58$  in Figure 3) for at least one mutation type. Overall, these results demonstrate that mutational strand asymmetries are widespread across cancer.

### Trends in Mutational Asymmetries

Next, we explored how mutational asymmetries depend on other variables such as expression levels, replication timing, and distance from transitions in replication or transcription direction. We focused on mutational processes that we identified as being the chief sources of asymmetry and identified the samples in which these processes were the major contributor to the overall mutational burden (Table S2). First, we analyzed transcriptional asymmetry as a function of gene expression level and replicative asymmetry as a function of DNA replication timing (Experimental Procedures). For most processes, we observed a decrease in

mutational burden at higher expression levels (Figure 5A). Transcriptional asymmetry, which reflects TCR activity, was seen in a subset of these cohorts (liver A→G, smoking C→A, and UV C→T) and was maximal in highly expressed regions. In other cohorts (e.g., POLE C→A, microsatellite stable cancers [MSS] C→T), no transcriptional asymmetry was seen, perhaps due to the fact that other covariates (such as replication timing and chromatin state) correlate

with expression levels but affect mutational burden via repair mechanisms that are independent of transcription. Similarly, for most processes, we observed a decrease in mutational burden in earliest-replicating regions (Figure 5B). Replicative asymmetry was seen in a subset of cohorts (MSI, APOBEC, POLE) and was strongest in earliest-replicating regions (especially in the case of POLE) but absent in other cohorts. To control for differences in chromatin state of TTRs and transcribed regions, in all of these cohorts we again performed a joint analysis of T- and R-class asymmetries (Figure S5).

We also analyzed the effect of genomic position with respect to transitions in transcription or replication direction. We examined transcriptional asymmetry around minus-to-plus transcription-direction transitions (Figure 5C), typically representing bidirectional promoters (Trinklein et al., 2004), and replicative asymmetry around left-to-right replication-direction transitions (Figure 5D), i.e., replication timing minima (Experimental Procedures). Mutations associated with smoking, UV, and liver cancer showed transcriptional strand asymmetries that flipped sign at transitions in transcription direction. Other cancers maintained balanced mutation densities on both sides of these transitions. Conversely, mutations associated with POLE, MSI, and APOBEC showed replicative strand asymmetries that flipped sign at replication timing minima. Other cohorts showed no such behavior at changes in replication direction. Exploring each of these asymmetries further can shed light on the operational mechanisms of mutagenesis and repair in these tumors.

### Mutational Asymmetries Reveal Mechanisms of Mutagenesis

The above analyses led to insights into the mechanisms of incompletely understood mutational processes, such as the APOBEC and liver signatures. The APOBEC signature consists of C→G and C→T mutations in the context TCW (W = A or T) and is thought to reflect the activity of APOBEC-family cytidine

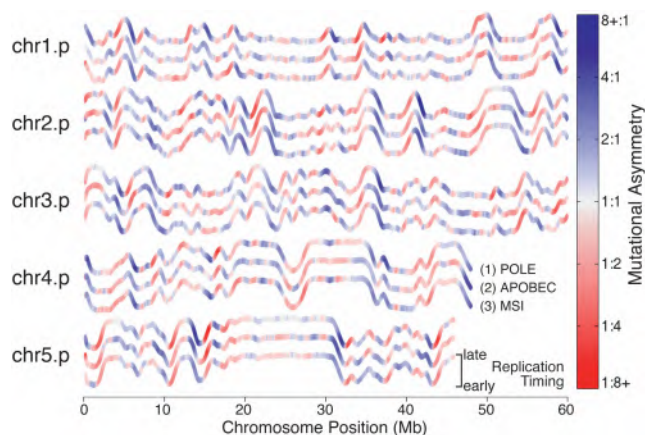


**Figure 4. Replicative Asymmetry Is Concordant across Three Distinct R-Class Mutational Processes**

Color representing mutational asymmetry is overlaid on replication timing profiles as in Figure 2. Profiles are shown in triplets colored by: (1) C→A:G→T asymmetry in 12 mutant-POLE colorectal and endometrial genomes, (2) G→C:C→G asymmetry in 22 APOBEC-enriched bladder, breast, and head-and-neck genomes, and (3) A→G:T→C asymmetry in 9 MSI-associated colon genomes.

deaminase enzymes (Alexandrov et al., 2013; Lawrence et al., 2013; Roberts et al., 2013). While the precise details of this phenomenon in cancer are not completely understood, a large body of work has characterized many aspects of this form of mutagenesis. APOBEC enzymes target ssDNA (Conticello, 2012), cause mutation clusters termed kataegis (Nik-Zainal et al., 2012a), and do not cause the usual increase in mutational densities in late-replicating, open-chromatin, and highly expressed regions (Kazanov et al., 2015). The main occurrences of ssDNA in human cells have been speculated to be at double-strand breaks (DSBs), R loops in transcription bubbles, and the lagging strand of the DNA replication fork. Experiments in model organisms have shown that APOBEC enzymes are indeed capable of inducing mutagenesis at DSBs (Taylor et al., 2013) and transcription bubbles (Lada et al., 2015; Taylor et al., 2014).

Our results suggest that, in humans, APOBEC mutagenesis primarily occurs on the lagging-strand template during DNA replication. The APOBEC signature shows strong R-class asymmetry, with a higher rate of C→G and C→T mutations in right-replicating regions (Figures 3 and 5), where reference-strand DNA is predicted to be replicated as the lagging-strand template, exposed as ssDNA between Okazaki segments. The magnitude of this asymmetry increases with enrichment of the APOBEC signature (Figure 6A), and joint analysis of both classes of asymmetry placed APOBEC squarely at the R-class end of the spectrum (Figure 6B). Note that, in all breast, bladder, and head and neck samples, even when the fraction of APOBEC mutations is low, significant R-class asymmetry is observed, suggesting that it is not merely a property of hypermutation. These findings are further supported by research in model organisms concurrent with this study. Bhagwat et al. (2016) found that overexpression of APOBEC3G in *E. coli* leads to a C:G→T:A signature that shows a replicative strand bias consistent with cytosine deami-

nation of the lagging-strand template. Additionally, in a yeast model, Roberts and colleagues (Hoopes et al., 2016) showed that overexpression of APOBEC3A and B produces a similar replicative asymmetry.

Taken together, these findings suggest that the R-class model is the primary mechanism for APOBEC mutagenesis in humans. In this model, APOBEC-family enzymes deaminate cytosines on the lagging-strand template during DNA replication, likely while it is single stranded (Figure 6C). The resulting uracil is excised, and subsequent replication either incorporates an adenine across from this abasic site, resulting in a C→T mutation, or (mediated by REV1 activity) incorporates a cytosine, resulting in a C→G mutation (Helleday et al., 2014). This model is also supported by the unusual lack of increase in mutational densities in late-replicating regions (Figure 5) (Kazanov et al., 2015). As MMR has been suggested to underlie this variation in mutational densities (Supek and Lehner, 2015), this may imply that APOBEC-associated mutagenesis evades the MMR machinery. This is consistent with the R-class model, in which the lagging-strand template (i.e., the parental strand) is deaminated; MMR, which relies on the parental strand to correct mistakes on the nascent strand, would be unable to correct this error without a correct template. Genome-wide, we observed only a small amount of APOBEC T-class asymmetry (Figure 6C), but a previous report showed that overexpressing APOBEC in yeast resulted in mutations that were transcriptionally asymmetric (Lada et al., 2015). Indeed, when we restricted to 5' UTRs (the regions reported to have the strongest transcriptional asymmetry), we revealed APOBEC T-class asymmetry also in humans (Figure S6). However, in the genome-wide analysis, the T-class asymmetry is dwarfed by the contributions from the R-class model.

Intriguingly, we observed a similar APOBEC mutational R-class asymmetry in the human germline. We measured replicative asymmetry in a set of 11,020 de novo germline mutations (Francioli et al., 2015) and found that C→G and C→T mutations showed no significant R-class asymmetry outside of the TCW context (1127 C→G/T versus 1171 G→A/C, in the leading-strand reference frame,  $p = 0.35$ ). When we focused on the TCW context (the preferred target of APOBEC mutagenesis), we were able to detect a significant level of R-class asymmetry (109 TCW→G/T versus 151 WGA→A/C mutations, in the leading-strand reference frame,  $p = 0.014$ ; Figure S7). Further studies analyzing a larger number of mutations will be required to fully understand the potential impact of APOBEC enzymes on germline mutagenesis and its evolutionary implications.

#### A Mechanism of Transcription-Coupled DNA Damage

In contrast to APOBEC- and MSI-associated mutations, liver A:T→G:C mutations showed little replicative asymmetry but instead showed transcriptional asymmetry similar to that seen in lung cancer (LUSC and LUAD in Figure 3; smoking C→A versus G→T in Figure 5). Closer inspection of transcriptional strand asymmetry revealed a distinction between the liver A→G signature and the two other T-class examples: UV-associated C→T and smoking-associated G→T. Mutations generated by UV light and smoking are lower in density on the transcribed

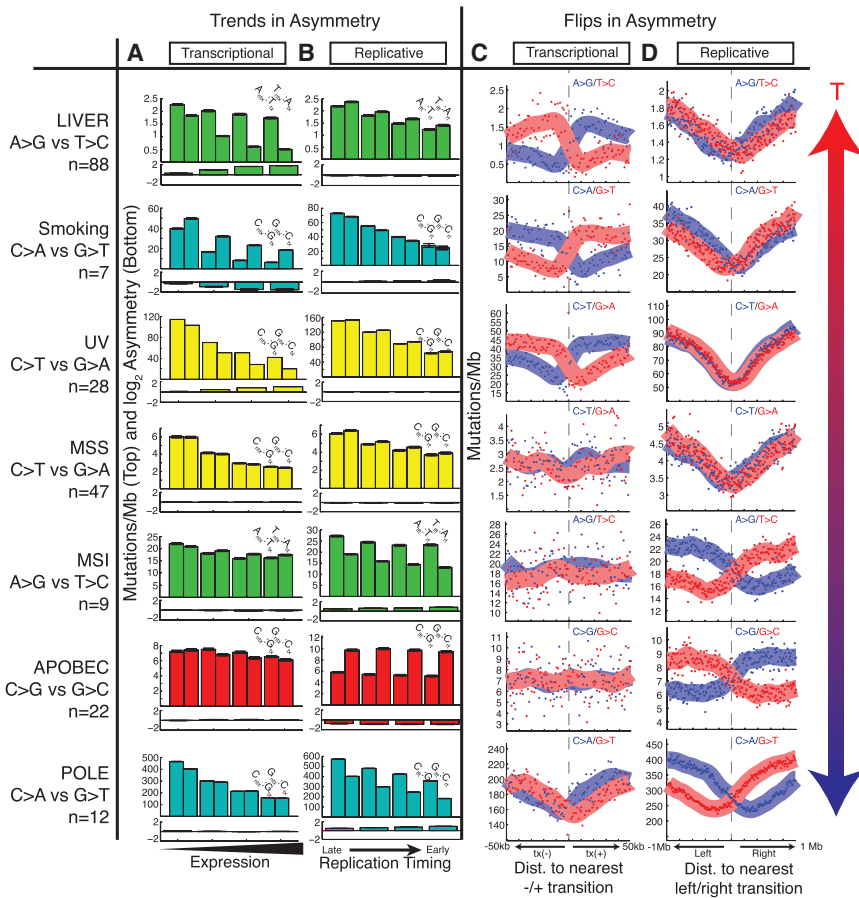


**Figure 5. Trends and Flips in Asymmetry**

(A) Transcriptional strand asymmetry measured across four quartiles of expression levels. Total mutational density tends to decrease with expression level, and T-class asymmetry (liver, smoking, UV) is maximal at highest expression. (B) Replicative strand asymmetry measured across four quartiles of replication timing. Total mutational density tends to decrease with earlier replication, and R-class asymmetry (MSI, APOBEC, POLE) is maximal at earliest replication. (C) Strand-specific mutational density measured in the vicinity of bidirectional promoters. T-class asymmetry flips at transitions from tx(-) to tx(+) regions. (D) Strand-specific mutational density measured in the vicinity of replication timing minima. R-class asymmetry flips at these left-to-right transitions. Error bars represent 95% confidence intervals.

strand compared to proximal IGR (due to TCR), while mutational densities on the non-transcribed strand remain constant regardless of transcription (Figure 7A). The liver A → G signature also shows the expected TCR effect on the transcribed strand; however, mutational densities of A → G on the non-transcribed strand drastically increase in transcribed regions. This suggests that transcriptional asymmetry in liver is not only due to repair of the transcribed strand but is also compounded by damage to the complementary non-transcribed strand, a phenomenon we call transcription-coupled damage (TCD).

At the extreme, we observed one liver cancer sample, HX17T, which showed a 3-fold transcription-dependent increase in A → G mutational densities on the non-transcribed strand (Figure 7B). This is in contrast to the usual trend in which non-transcribed strand mutational densities decrease with expression due to more effective global genome repair (GGR) and MMR in open-chromatin and early-replicating regions. This effect is unique to the A → G signature. In that same sample, C → A mutational densities (driven by carcinogen attack; Alexandrov et al., 2013) showed the usual decrease on both strands (Figure 7C). In our cohort of 88 liver cancer samples, we examined the slope of this response of mutational density to expression level for each of the 12 possible mutation types (Figure 7D). In a two-tailed test, we found that 25/88 of the liver patients showed a significant increase in A → G mutational densities on the non-

transcribed strand (Experimental Procedures), while only 9/88 showed a significant decrease, showing that, in the majority of samples, the A → G signature does not show the usual repair (Table S3). As mentioned before, the contributions of MMR and GGR are confounding factors when considering the effect of expression levels on mutational densities, since higher expression is correlated with earlier replication timing and a more open chromatin state. As a result, on the non-transcribed strand, higher expression could lead to both increased damage by TCD and higher levels of repair by MMR and GGR. Different contributions of these damage and repair processes likely underlie the variation that we observed across patients.

While the strong transcriptional asymmetry of the A → G signature in liver cancer has been noted (Alexandrov et al., 2013), we propose that this is due to two separate processes operating on different strands—TCD and TCR (Figure 7E). This explains the extreme transcriptional asymmetry of liver A → G compared to other signatures (Figure 3). Furthermore these results suggest that the A → G signature is caused by a mutational process distinct from typical bulky-adduct damage. Finally, we noticed that one colorectal patient (“CRC-B”) from an earlier study of nine colorectal whole genomes (Bass et al., 2011) showed the same signature of TCD. Thus, this phenomenon may be enriched in liver but not exclusive to it.

**Mismatch Repair Balances Mutational Asymmetry**

Colorectal cancers with functional MMR (i.e., MSS) show little replicative asymmetry of any mutation type (aside from C → G mutations, which are in part due to low levels of APOBEC signature). As mentioned above, loss of functional polymerase ε proof-reading results in R-class asymmetry. MSI colorectal tumors, typically resulting from damage to the MMR system (Kane et al., 1997; Shinbrot et al., 2014; Vilar and Gruber, 2010), also

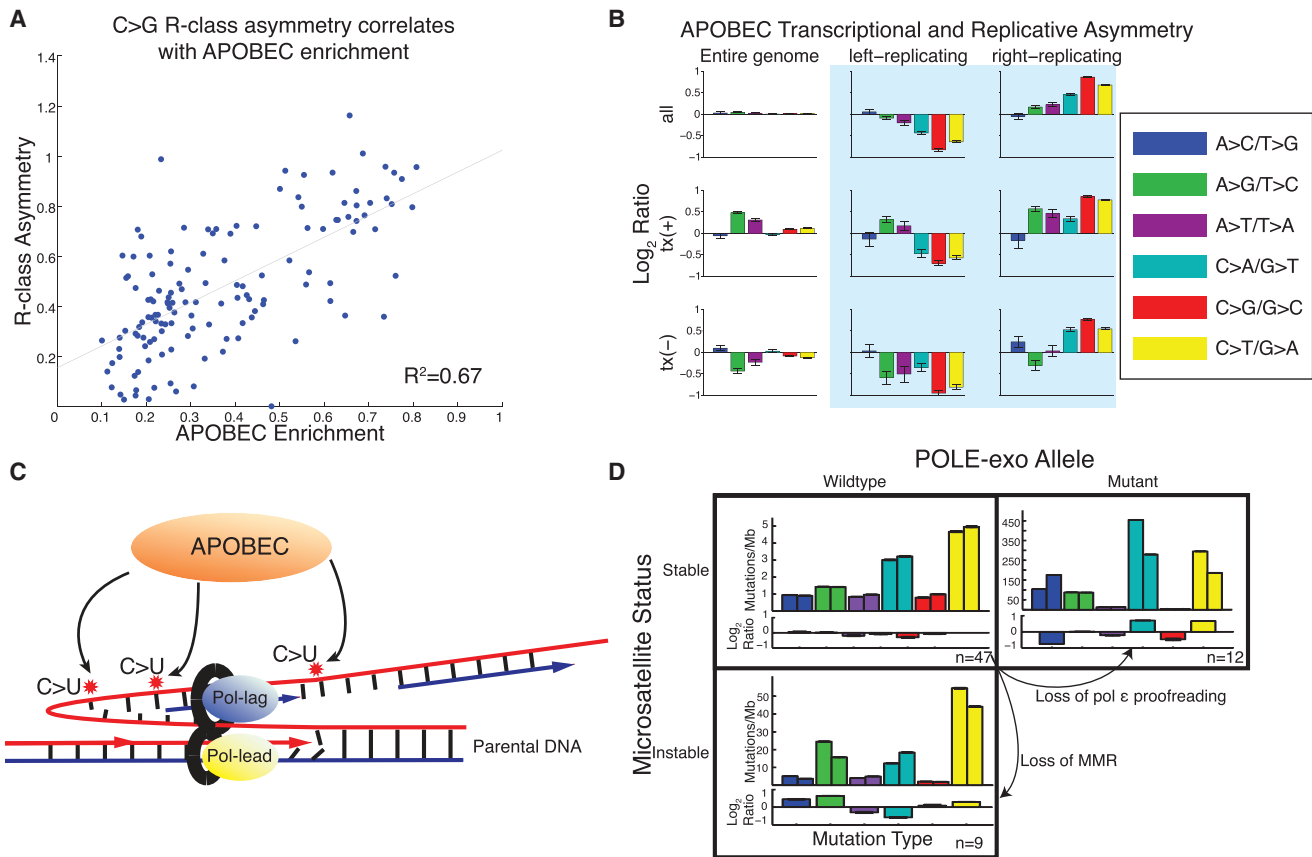


**Figure 6. R-Class Asymmetries Associated with APOBEC and MSI**

(A) Bladder, breast, and head-and-neck cohorts. Samples with highest enrichment of APOBEC signature show highest replicative asymmetry of C→G mutations.

(B) APOBEC-enriched samples are dominated by replicative asymmetry (as in Figures 1E and 1F)

(C) Proposed model: APOBEC deaminates cytosine to uracil on the ssDNA of the lagging-strand template during DNA replication.

(D) R-class asymmetry in MSS, MSI, and POLE mutant cohorts. MSS samples have little asymmetry. Loss of MMR or pol  $\epsilon$  proofreading leads to imbalance in mutations between the leading and lagging strands.

Error bars represent 95% confidence interval.

show replicative asymmetry (Figure 6D). This would suggest that MMR (in addition to exonuclease proofreading) is required to balance mutational asymmetries generated during DNA replication. This phenomenon has also been reported in yeast (Lujan et al., 2012), and our results suggest that the same is true in humans.

The implications of this role for MMR reach beyond the realm of cancer research. Without such balancing, asymmetric introduction of germline mutations would result in local depletion of specific nucleotides over evolution. Indeed, a slight replicative imbalance can be detected in the reference genome:  $C_{\text{left}}:G_{\text{right}}$  base pairs outnumber  $G_{\text{left}}:C_{\text{right}}$  base pairs by 2.1% on average, and  $A_{\text{left}}:T_{\text{right}}$  base pairs outnumber  $T_{\text{left}}:A_{\text{right}}$  base pairs by 3.7%. This is in line with a previous result measuring a mean compositional skew of 3.72% (Chen et al., 2011). However, the relative mildness of these imbalances, compared to the much stronger mutational asymmetries seen in MMR-deficient tumors, suggests that MMR has played an important role throughout evolution in maintaining genome symmetry.

## DISCUSSION

Our results highlight the widespread mutational strand asymmetries observed in cancer genomes, mediated by DNA replication, RNA transcription, and their associated repair pathways. Study of these prominent sources of asymmetry has mostly been performed in model organisms (Lobry, 1996; Lujan et al., 2012; McLean et al., 1998; Pavlov et al., 2002; Touchon et al., 2005), and here, we extend this analysis to humans via cancer genomics. Our work addresses several of the most prominent processes in cancer and provides insight into their biological mechanisms. Analysis of asymmetries associated with the growing number of mutational processes discovered by sophisticated signature decoupling approaches (Alexandrov et al., 2013; Kasar et al., 2015; Lawrence et al., 2013) will provide a deeper view of these processes and will further illuminate their underlying sources. Our ability to detect mutational asymmetries will improve with higher-resolution replication timing and transcription maps and with improving knowledge of human replication origins. Finally, we note that there may

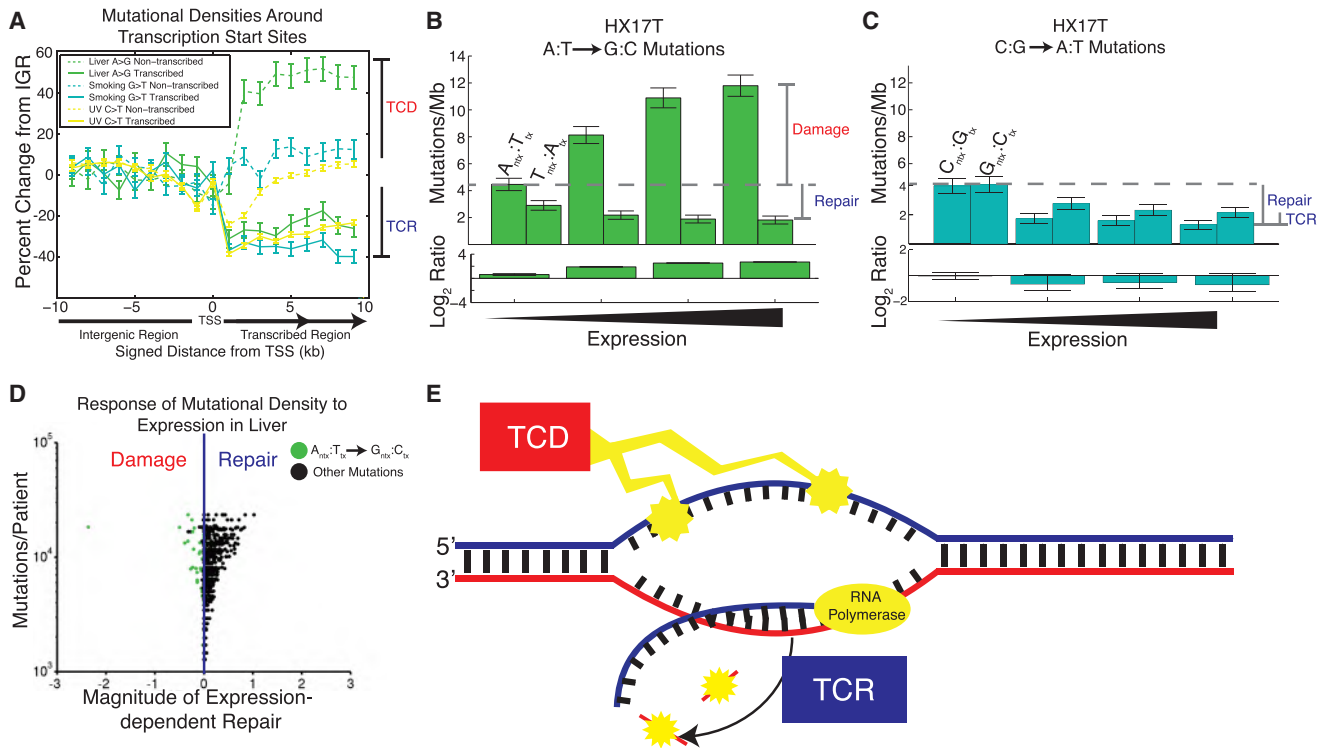


**Figure 7. Transcription-Coupled Damage in Liver Cancer**

(A) Mutational densities in the vicinity of promoters. When crossing from non-transcribed intergenic regions (IGR) to transcribed regions, mutational densities on the transcribed strand fall, reflecting TCR. On the non-transcribed strand there is usually little change from IGR levels, with the notable exception of liver cancer, in which mutational densities increase from IGR levels, consistent with transcription-coupled damage (TCD).  
 (B) Liver cancer patient HX17T shows a dramatic expression-dependent increase in A → G mutational densities on the non-transcribed strand only.  
 (C) In the same patient, G → T mutational densities show only the usual expression-dependent decrease on both strands.  
 (D) Most liver patients show dominant TCR. However, for A → G mutations on the non-transcribed strand (green dots), some show the opposite trend, reflecting dominant TCD. The leftmost dot is patient HX17T.  
 (E) TCD damages the non-transcribed strand, exposed as ssDNA during transcription. TCR repairs the transcribed strand. Both of these processes contribute to T-class asymmetry.  
 Error bars represent 95% confidence interval.

be additional useful reference frames for symmetry breaking beyond the two used here.

Classifying patients according to their patterns of mutational strand asymmetry may have clinical relevance. Tumors with defects in DNA repair mechanisms have been shown to be vulnerable to synthetically lethal therapeutic interventions that further disrupt genome stability (Carreras Puigvert et al., 2015; Curtin, 2012; Middleton et al., 2015). As discussed, R-class asymmetries can be introduced either by asymmetric damage at the replication fork or by deficiency in the proof-reading and repair of DNA synthesis. In the latter case, R-class asymmetry may serve as a proxy for replicative stress and could suggest synthetic lethality as an effective avenue for treatment. Similarly, individual patients of T-class tumor types (such as melanoma) that do not themselves exhibit T-class asymmetry potentially reveal a deficiency of TCR. Thus, analyzing asymmetries of both classes may facilitate a better match between patients and treatments.

Additionally, patient-specific responses to classic chemotherapy drugs are often poorly understood and are difficult to

predict. Analyzing responses to these drugs in conjunction with mutation rates and asymmetries at the replication fork or transcription bubble may provide useful insights into these drugs' functionality. This, in turn, could allow for more targeted use of the drugs, as well as better control of unintended side effects.

Strand asymmetry may be particularly impactful in the earliest driving events of cancer, due to that defining feature of carcinogenesis, the transformation of cells into an aberrantly proliferative state. A particular DNA lesion may push the cell from a resting state (without DNA replication) into active mitosis, and the initial strand hit by that driver lesion is crucial; due to absent (or infrequent DNA) replication in these pre-malignant cells, DNA damage of the non-transcribed strand may wait a very long time to be propagated as a mutation to the transcribed strand where it can exert its driving effect. We also note that the strand asymmetries we observe in cancer may inform the debate on the "immortal DNA strand hypothesis" and its possible relevance to cancer (Cairns, 2006; Yadlapalli and Yamashita, 2013; Tomasetti and Bozic, 2015).

Beyond cancer, somatic mutational processes play an important role in a broad range of diseases, including aging (Kennedy et al., 2012; Kenyon, 2010), autoimmune disease (Ross, 2014), and neurological disorders (Poduri et al., 2013). Many of the same background mutational processes are active in cancerous and non-cancerous cells (such as methylated CpG deamination/“aging,” UV damage, and environmental mutagens), and the lessons learned from the clonal expansion of mutations in cancer will aid in the understanding of these universal processes. Novel mutational and repair processes continue to emerge from cancer genome sequencing studies, and viewing them through the lens of mutational strand asymmetry can provide immediate insights into their molecular mechanisms.

## EXPERIMENTAL PROCEDURES

### Data Provenance

We assembled a collection of 590 whole-genome sequences from 14 tumor types by combining published data from the Cancer Genome Atlas (TCGA; dbGAP: phs000178.v1.p1) with other published datasets (Alexandrov et al., 2013; Dulak et al., 2013; Lawrence et al., 2014; Bass et al., 2011; Berger et al., 2012; Wang et al., 2011).

### Statistical Analysis

MATLAB code to generate asymmetry metrics and figures is available at [www.broadinstitute.org/cancer/cga/AsymTools](http://www.broadinstitute.org/cancer/cga/AsymTools).

### Determining Transcription and Replication Direction and Calculating Densities

Transcription direction was determined according to the Refseq database. Replication direction was defined using replication timing profiles generated in six lymphoblastoid cell lines, as published in Koren et al. (2012). We determined left- and right-replicating regions based on the sign of the derivative of the profile (negative is left-replicating and positive is right-replicating). To only define regions in TTRs, we required a slope with a magnitude of at least 250 replication timing units (“rtu”) per Mb. These arbitrary units range from 100 to 1,200, denoting the beginning and end of S phase.

Mutational densities for a given base pair change  $b1:b2 \rightarrow m1:m2$  and its complementary mutation  $b2:b1 \rightarrow m2:m1$  in a given list of regions were determined by the formula:

$$r_{b1:b2 \rightarrow m1:m2} = \frac{n_{b1 \rightarrow m1}}{p * N_{b1}}$$

$$r_{b2:b1 \rightarrow m2:m1} = \frac{n_{b2 \rightarrow m2}}{p * N_{b2}}$$

where  $n_{b \rightarrow m}$  is the number of observations of  $b \rightarrow m$  mutations with respect to the genomic reference strand,  $N_b$  is the number of chances for this mutation to happen, i.e., the number of occurrences of the motif  $b$  in the given region of the reference genome (on the genomic reference strand), and  $p$  is the number of patients analyzed. Asymmetry was then calculated in a given region by:

$$a_{b \rightarrow m} = \log_2 \left( \frac{r_{b1:b2 \rightarrow m1:m2}}{r_{b2:b1 \rightarrow m2:m1}} \right)$$

as seen in Figure 1.

### Calculating Global Mutational Asymmetries

When calculating global mutational asymmetries, redundant mutations with respect to a given strand are summed together. For example, to calculate global genome mutational densities with respect to the leading strand, we calculate:

$$r_{b1:b2 \rightarrow m1:m2} = \frac{n_{l,b1 \rightarrow m1} + n_{r,b2 \rightarrow m2}}{p * (N_{l,b1} + N_{r,b2})}$$

$$r_{b2:b1 \rightarrow m2:m1} = \frac{n_{l,b2 \rightarrow m2} + n_{r,b1 \rightarrow m1}}{p * (N_{l,b2} + N_{r,b1})}$$

$$a_{b \rightarrow m} = \log_2 \left( \frac{r_{b1:b2 \rightarrow m1:m2}}{r_{b2:b1 \rightarrow m2:m1}} \right)$$

where subscripts “l” and “r” refer to events in left- and right-replicating regions, respectively. Essentially, this approach distinguishes a  $b1:b2$  base pair by whether base  $b1$  is on the presumed leading/lagging strand rather than the genomic reference. The same approach is used for calculating asymmetry with respect to the sense strand, using tx(+) and tx(-) regions instead of left- and right-replicating, respectively.

### Correlation of R-Class Asymmetry with Direction of TTRs

Replication timing data and POLE, APOBEC, and MSI asymmetry metrics were aggregated in 100 kb bins and smoothed using a moving average over 10 bins. The replication timing data were plotted, and the profiles were colored by the asymmetry metrics in the POLE cohort (Figure 2) or all three R-class cohorts (Figure 4). Correlations restricted to TTRs were calculated by only considering regions with a slope of  $>250$  rtu/Mb.

### Binning by Expression and Replication Timing

Expression profiles were an average of many cell lines, as used in Lawrence et al., (2013). To perform binning by functional covariates as seen in Figures 5A and 5B, expression and replication timing values were projected onto 20 kb intervals. These intervals were then sorted by expression for Figure 5A and replication timing for Figure 5B and separated into bins with an even number of intervals, and mutational rates and asymmetry were calculated for the intervals in each bin.

### Identifying Transcription and Replication Direction Transitions

Minus-to-plus transcription transitions were identified by taking all bidirectional gene pairs (opposing genes with transcription start sites within 1 kb of each other; Trinklein et al., 2004) in the Refseq database and calculating the midpoint of their transcription start sites. Left-to-right replication transitions were similarly identified by calculating the midpoint between the right and left boundaries of defined left- and right-replicating regions, respectively.

### Determining Response of Mutational Densities to Increasing Expression

Response of mutational densities to increasing expression, as shown in Figures 7B and 7C, was performed for each patient and for each of the six possible mutations, creating a figure as shown in Figure 7D. Then linear regression was performed separately on each series of bars (the left bars for the non-transcribed strand and the right bars for the transcribed strand). For these two regressions, we calculated a 95% confidence interval for the slope and assessed significance based on whether zero fell inside of the interval. Then for each regression, we plotted the more conservative bound of the corresponding confidence interval, i.e., the value closer to or equal to zero.

### Creating a Hypothetical Replication Timing Distribution

The hypothetical replication timing curve shown in Figure S1A was created by first taking its real counterpart in Figure S1B. Then the locations of origins of replication were randomly assigned, assuming a density of one origin per 40 kb. From these origins, a more detailed profile was drawn by assuming constant polymerase speed and smoothing the result.

## SUPPLEMENTAL INFORMATION

Supplemental Information includes seven figures and three tables and can be found with this article online at <http://dx.doi.org/10.1016/j.cell.2015.12.050>.

## AUTHOR CONTRIBUTIONS

Conceptualization, M.S.L., P.P., G.G., N.J.H., P.S., D.A.W., E.S., K.R.C., A. Koren, and J.K.; Methodology, M.S.L., P.P., N.J.H., and P.S.; Software, N.J.H. and M.S.L.; Formal Analysis, N.J.H., M.S.L., and P.P.; Investigation, N.J.H., P.P., and M.S.L.; Resources, M.S.L., G.G., A. Koren, and D.A.W.; Data Curation, E.R., N.J.H., P.P., M.S.L., and A. Koren; Writing – Original Draft, N.J.H., M.S.L., A. Koren, P.P., and G.G.; Writing – Review & Editing, N.J.H., M.S.L., A. Koren, P.P., G.G., D.A.W., P.C.H., E.S., K.R.C., E.R., J.M.H., P.S., Y.E.M., A. Kamburov, and L.Z.B.; Visualization, N.J.H. and M.S.L.; Supervision, G.G., M.S.L., P.P., A. Koren, D.A.W., and P.C.H.

## ACKNOWLEDGMENTS

We thank Ashok Bhagwat and Steven Roberts and their collaborators for sharing their unpublished data with us and allowing us to reference them in this work. We thank John Iafra for valuable insights about the relevance of strand asymmetry in carcinogenesis. G.G. was partially funded by the Paul C. Zamecnik, MD, Chair in Oncology at Massachusetts General Hospital. G.G. and M.S.L. were partially funded by the NIH TCGA Genome Data Analysis Center (U24CA143845). M.S.L. was partially funded by the NHGRI Genome Sequencing Center (U54HG003067). E.S., K.R.C., and D.A.W. were partially funded by NHGRI grant (U54HG003273). N.J.H., P.P., Y.E.M., and A. Kamburov were funded by G.G.'s startup funds at MGH.

Received: November 13, 2015

Revised: December 21, 2015

Accepted: December 24, 2015

Published: January 21, 2016

## REFERENCES

- Alexandrov, L.B., Nik-Zainal, S., Wedge, D.C., Aparicio, S.A., Behjati, S., Biankin, A.V., Bignell, G.R., Bolli, N., Borg, A., Borresen-Dale, A.L., et al.; Australian Pancreatic Cancer Genome Initiative; ICGC Breast Cancer Consortium; ICGC MMML-Seq Consortium; ICGC PedBrain (2013). Signatures of mutational processes in human cancer. *Nature* **500**, 415–421.
- Bass, A.J., Lawrence, M.S., Brace, L.E., Ramos, A.H., Drier, Y., Cibulskis, K., Sougnez, C., Voet, D., Saksena, G., Sivachenko, A., et al. (2011). Genomic sequencing of colorectal adenocarcinomas identifies a recurrent VTI1A-TCF7L2 fusion. *Nat. Genet.* **43**, 964–968.
- Berger, M.F., Hodis, E., Heffernan, T.P., Deribe, Y.L., Lawrence, M.S., Protopopov, A., Ivanova, E., Watson, I.R., Nickerson, E., Ghosh, P., et al. (2012). Melanoma genome sequencing reveals frequent PREX2 mutations. *Nature* **485**, 502–506.
- Bhagwat, A.S., Hao, W., Townes, J.P., Lee, H., Tang, H., and Foster, P.L. (2016). Strand-biased Cytosine deamination at the Replication Fork causes Cytosine to Thymine Mutations in *Escherichia coli*. *Proc. Natl. Acad. Sci. USA*. <http://dx.doi.org/10.1073/pnas.1522325113>.
- Cairns, J. (2006). Cancer and the immortal strand hypothesis. *Genetics* **174**, 1069–1072.
- Carreras Puigvert, J., Sanjiv, K., and Helleday, T. (2015). Targeting DNA repair, DNA metabolism and replication stress as anti-cancer strategies. *FEBS J.* Published online October 28, 2015. <http://dx.doi.org/10.1111/febs.13574>.
- Chapman, M.A., Lawrence, M.S., Keats, J.J., Cibulskis, K., Sougnez, C., Schinzel, A.C., Harview, C.L., Brunet, J.P., Ahmann, G.J., Adli, M., et al. (2011). Initial genome sequencing and analysis of multiple myeloma. *Nature* **471**, 467–472.
- Chen, C.L., Duquenne, L., Audit, B., Guilbaud, G., Rappailles, A., Baker, A., Huvet, M., d'Aubenton-Carafa, Y., Hyrien, O., Arneodo, A., and Thermes, C. (2011). Replication-associated mutational asymmetry in the human genome. *Mol. Biol. Evol.* **28**, 2327–2337.
- Conticello, S.G. (2012). Creative deaminases, self-inflicted damage, and genome evolution. *Ann. N Y Acad. Sci.* **1267**, 79–85.
- Curtin, N.J. (2012). DNA repair dysregulation from cancer driver to therapeutic target. *Nat. Rev. Cancer* **12**, 801–817.
- Denissenko, M.F., Pao, A., Tang, M., and Pfeifer, G.P. (1996). Preferential formation of benzo[a]pyrene adducts at lung cancer mutational hotspots in P53. *Science* **274**, 430–432.
- Donahue, B.A., Yin, S., Taylor, J.S., Reines, D., and Hanawalt, P.C. (1994). Transcript cleavage by RNA polymerase II arrested by a cyclobutane pyrimidine dimer in the DNA template. *Proc. Natl. Acad. Sci. USA* **91**, 8502–8506.
- Dulak, A.M., Stojanov, P., Peng, S., Lawrence, M.S., Fox, C., Stewart, C., Bandla, S., Imamura, Y., Schumacher, S.E., Shefler, E., et al. (2013). Exome and whole-genome sequencing of esophageal adenocarcinoma identifies recurrent driver events and mutational complexity. *Nat. Genet.* **45**, 478–486.
- Fousteri, M., and Mullenders, L.H. (2008). Transcription-coupled nucleotide excision repair in mammalian cells: molecular mechanisms and biological effects. *Cell Res.* **18**, 73–84.
- Francioli, L.C., Polak, P.P., Koren, A., Menelaou, A., Chun, S., Renkens, I., van Duijn, C.M., Swertz, M., Wijmenga, C., van Ommen, G., et al.; Genome of the Netherlands Consortium (2015). Genome-wide patterns and properties of de novo mutations in humans. *Nat. Genet.* **47**, 822–826.
- Green, P., Ewing, B., Miller, W., Thomas, P.J., and Green, E.D.; NISC Comparative Sequencing Program (2003). Transcription-associated mutational asymmetry in mammalian evolution. *Nat. Genet.* **33**, 514–517.
- Guilbaud, G., Rappailles, A., Baker, A., Chen, C.L., Arneodo, A., Goldar, A., d'Aubenton-Carafa, Y., Thermes, C., Audit, B., and Hyrien, O. (2011). Evidence for sequential and increasing activation of replication origins along replication timing gradients in the human genome. *PLoS Comput. Biol.* **7**, e1002322.
- Hanawalt, P.C., and Spivak, G. (2008). Transcription-coupled DNA repair: two decades of progress and surprises. *Nat. Rev. Mol. Cell Biol.* **9**, 958–970.
- Helleday, T., Eshtad, S., and Nik-Zainal, S. (2014). Mechanisms underlying mutational signatures in human cancers. *Nat. Rev. Genet.* **15**, 585–598.
- Hoopes, J., Cortez, L., Mertz, T., Malc, E.P., Mieczkowski, P.A., and Roberts, S.A. (2016). APOBEC3A and APOBEC3B Deaminate the Lagging Strand Template during DNA Replication. *Cell Reports*. Published online January 28, 2016. <http://dx.doi.org/10.1016/j.celrep.2016.01.021>.
- Jiang, G., and Sancar, A. (2006). Recruitment of DNA damage checkpoint proteins to damage in transcribed and nontranscribed sequences. *Mol. Cell Biol.* **26**, 39–49.
- Jinks-Robertson, S., and Bhagwat, A.S. (2014). Transcription-associated mutagenesis. *Annu. Rev. Genet.* **48**, 341–359.
- Johnson, R.E., Klassen, R., Prakash, L., and Prakash, S. (2015). A Major Role of DNA Polymerase  $\delta$  in Replication of Both the Leading and Lagging DNA Strands. *Mol. Cell* **59**, 163–175.
- Kane, M.F., Loda, M., Gaida, G.M., Lipman, J., Mishra, R., Goldman, H., Jessup, J.M., and Kolodner, R. (1997). Methylation of the hMLH1 promoter correlates with lack of expression of hMLH1 in sporadic colon tumors and mismatch repair-defective human tumor cell lines. *Cancer Res.* **57**, 808–811.
- Kasar, S., Kim, J., Improgo, R., Tiao, G., Polak, P., Haradhvala, N., Lawrence, M.S., Kiezun, A., Fernandes, S.M., Bahl, S., et al. (2015). Whole-genome sequencing reveals activation-induced cytidine deaminase signatures during indolent chronic lymphocytic leukaemia evolution. *Nat. Commun.* **6**, 8866.
- Kazanov, M.D., Roberts, S.A., Polak, P., Stamatoyannopoulos, J., Klimczak, L.J., Gordenin, D.A., and Sunyaev, S.R. (2015). APOBEC-Induced Cancer Mutations Are Uniquely Enriched in Early-Replicating, Gene-Dense, and Active Chromatin Regions. *Cell Rep.* **13**, 1103–1109.
- Kennedy, S.R., Loeb, L.A., and Herr, A.J. (2012). Somatic mutations in aging, cancer and neurodegeneration. *Mech. Ageing Dev.* **133**, 118–126.
- Kenyon, C.J. (2010). The genetics of ageing. *Nature* **464**, 504–512.
- Koren, A., Tsai, H.J., Tirosh, I., Burrack, L.S., Barkai, N., and Berman, J. (2010). Epigenetically-inherited centromere and neocentromere DNA replicates earliest in S-phase. *PLoS Genet.* **6**, e1001068.
- Koren, A., Polak, P., Nemesh, J., Michaelson, J.J., Sebat, J., Sunyaev, S.R., and McCarroll, S.A. (2012). Differential relationship of DNA replication timing

- to different forms of human mutation and variation. *Am. J. Hum. Genet.* **97**, 1033–1040.
- Lada, A.G., Kliver, S.F., Dhar, A., Polev, D.E., Masharsky, A.E., Rogozin, I.B., and Pavlov, Y.I. (2015). Disruption of Transcriptional Coactivator Sub1 Leads to Genome-Wide Re-distribution of Clustered Mutations Induced by APOBEC in Active Yeast Genes. *PLoS Genet.* **11**, e1005217.
- Lawrence, M.S., Stojanov, P., Polak, P., Kryukov, G.V., Cibulskis, K., Sivachenko, A., Carter, S.L., Stewart, C., Mermel, C.H., Roberts, S.A., et al. (2013). Mutational heterogeneity in cancer and the search for new cancer-associated genes. *Nature* **499**, 214–218.
- Lawrence, M.S., Stojanov, P., Mermel, C.H., Robinson, J.T., Garraway, L.A., Golub, T.R., Meyerson, M., Gabriel, S.B., Lander, E.S., and Getz, G. (2014). Discovery and saturation analysis of cancer genes across 21 tumour types. *Nature* **505**, 495–501.
- Lobry, J.R. (1996). Asymmetric substitution patterns in the two DNA strands of bacteria. *Mol. Biol. Evol.* **13**, 660–665.
- Lujan, S.A., Williams, J.S., Pursell, Z.F., Abdulovic-Cui, A.A., Clark, A.B., Nick McElhinny, S.A., and Kunkel, T.A. (2012). Mismatch repair balances leading and lagging strand DNA replication fidelity. *PLoS Genet.* **8**, e1003016.
- McLean, M.J., Wolfe, K.H., and Devine, K.M. (1998). Base composition skews, replication orientation, and gene orientation in 12 prokaryote genomes. *J. Mol. Evol.* **47**, 691–696.
- Mellon, I., Spivak, G., and Hanawalt, P.C. (1987). Selective removal of transcription-blocking DNA damage from the transcribed strand of the mammalian DHFR gene. *Cell* **51**, 241–249.
- Middleton, F.K., Patterson, M.J., Elstob, C.J., Fordham, S., Herriott, A., Wade, M.A., McCormick, A., Edmondson, R., May, F.E., Allan, J.M., et al. (2015). Common cancer-associated imbalances in the DNA damage response confer sensitivity to single agent ATR inhibition. *Oncotarget* **6**, 32396–32409.
- Miyabe, I., Kunkel, T.A., and Carr, A.M. (2011). The major roles of DNA polymerases epsilon and delta at the eukaryotic replication fork are evolutionarily conserved. *PLoS Genet.* **7**, e1002407.
- Nick McElhinny, S.A., Gordenin, D.A., Stith, C.M., Burgers, P.M., and Kunkel, T.A. (2008). Division of labor at the eukaryotic replication fork. *Mol. Cell* **30**, 137–144.
- Nik-Zainal, S., Alexandrov, L.B., Wedge, D.C., Van Loo, P., Greenman, C.D., Raine, K., Jones, D., Hinton, J., Marshall, J., Stebbings, L.A., et al.; Breast Cancer Working Group of the International Cancer Genome Consortium (2012a). Mutational processes molding the genomes of 21 breast cancers. *Cell* **149**, 979–993.
- Nik-Zainal, S., Van Loo, P., Wedge, D.C., Alexandrov, L.B., Greenman, C.D., Lau, K.W., Raine, K., Jones, D., Marshall, J., Ramakrishna, M., et al.; Breast Cancer Working Group of the International Cancer Genome Consortium (2012b). The life history of 21 breast cancers. *Cell* **149**, 994–1007.
- Pavlov, Y.I., Newlon, C.S., and Kunkel, T.A. (2002). Yeast origins establish a strand bias for replicational mutagenesis. *Mol. Cell* **10**, 207–213.
- Pleasance, E.D., Cheetham, R.K., Stephens, P.J., McBride, D.J., Humphray, S.J., Greenman, C.D., Varela, I., Lin, M.L., Ordóñez, G.R., Bignell, G.R., et al. (2010a). A comprehensive catalogue of somatic mutations from a human cancer genome. *Nature* **463**, 191–196.
- Pleasance, E.D., Stephens, P.J., O’Meara, S., McBride, D.J., Meynert, A., Jones, D., Lin, M.L., Beare, D., Lau, K.W., Greenman, C., et al. (2010b). A small-cell lung cancer genome with complex signatures of tobacco exposure. *Nature* **463**, 184–190.
- Poduri, A., Evrony, G.D., Cai, X., and Walsh, C.A. (2013). Somatic mutation, genomic variation, and neurological disease. *Science* **341**, 1237758.
- Polak, P., and Arndt, P.F. (2008). Transcription induces strand-specific mutations at the 5’ end of human genes. *Genome Res.* **18**, 1216–1223.
- Polak, P., Querfurth, R., and Arndt, P.F. (2010). The evolution of transcription-associated biases of mutations across vertebrates. *BMC Evol. Biol.* **10**, 187.
- Polak, P., Lawrence, M.S., Haugen, E., Stoletzki, N., Stojanov, P., Thurman, R.E., Garraway, L.A., Mirkin, S., Getz, G., Stamatoyannopoulos, J.A., and Sunyaev, S.R. (2014). Reduced local mutation density in regulatory DNA of cancer genomes is linked to DNA repair. *Nat. Biotechnol.* **32**, 71–75.
- Polak, P., Karlić, R., Koren, A., Thurman, R., Sandstrom, R., Lawrence, M.S., Reynolds, A., Rynes, E., Vlahoviček, K., Stamatoyannopoulos, J.A., and Sunyaev, S.R. (2015). Cell-of-origin chromatin organization shapes the mutational landscape of cancer. *Nature* **518**, 360–364.
- Rhind, N., and Gilbert, D.M. (2013). DNA replication timing. *Cold Spring Harb. Perspect. Biol.* **5**, a010132.
- Roberts, S.A., Lawrence, M.S., Klimczak, L.J., Grimm, S.A., Fargo, D., Stojanov, P., Kiezun, A., Kryukov, G.V., Carter, S.L., Saksena, G., et al. (2013). An APOBEC cytidine deaminase mutagenesis pattern is widespread in human cancers. *Nat. Genet.* **45**, 970–976.
- Ross, K.A. (2014). Coherent somatic mutation in autoimmune disease. *PLoS ONE* **9**, e101093.
- Ryba, T., Hiratani, I., Lu, J., Itoh, M., Kulik, M., Zhang, J., Schulz, T.C., Robins, A.J., Dalton, S., and Gilbert, D.M. (2010). Evolutionarily conserved replication timing profiles predict long-range chromatin interactions and distinguish closely related cell types. *Genome Res.* **20**, 761–770.
- Shinbrot, E., Henninger, E.E., Weinhold, N., Covington, K.R., Göksenin, A.Y., Schultz, N., Chao, H., Doddapaneni, H., Muzny, D.M., Gibbs, R.A., et al. (2014). Exonuclease mutations in DNA polymerase epsilon reveal replication strand specific mutation patterns and human origins of replication. *Genome Res.* **24**, 1740–1750.
- Spivak, G., and Ganesan, A.K. (2014). The complex choreography of transcription-coupled repair. *DNA Repair (Amst.)* **19**, 64–70.
- Stillman, B. (2015). Reconsidering DNA Polymerases at the Replication Fork in Eukaryotes. *Mol. Cell* **59**, 139–141.
- Supek, F., and Lehner, B. (2015). Differential DNA mismatch repair underlies mutation rate variation across the human genome. *Nature* **521**, 81–84.
- Taylor, B.J., Nik-Zainal, S., Wu, Y.L., Stebbings, L.A., Raine, K., Campbell, P.J., Rada, C., Stratton, M.R., and Neuberger, M.S. (2013). DNA deaminases induce break-associated mutation showers with implication of APOBEC3B and 3A in breast cancer kataegis. *eLife* **2**, e00534.
- Taylor, B.J., Wu, Y.L., and Rada, C. (2014). Active RNAP pre-initiation sites are highly mutated by cytidine deaminases in yeast, with AID targeting small RNA genes. *eLife* **3**, e03553.
- Tomasetti, C., and Bozic, I. (2015). The (not so) immortal strand hypothesis. *Stem Cell Res. (Amst.)* **14**, 238–241.
- Touchon, M., Nicolay, S., Audit, B., Brodie of Brodie, E.B., d’Aubenton-Carafa, Y., Arneodo, A., and Thermes, C. (2005). Replication-associated strand asymmetries in mammalian genomes: toward detection of replication origins. *Proc. Natl. Acad. Sci. USA* **102**, 9836–9841.
- Trinklein, N.D., Aldred, S.F., Hartman, S.J., Schroeder, D.I., Otilar, R.P., and Myers, R.M. (2004). An abundance of bidirectional promoters in the human genome. *Genome Res.* **14**, 62–66.
- Vilar, E., and Gruber, S.B. (2010). Microsatellite instability in colorectal cancer—the stable evidence. *Nat. Rev. Clin. Oncol.* **7**, 153–162.
- Waddell, N., Pajic, M., Patch, A.M., Chang, D.K., Kassahn, K.S., Bailey, P., Johns, A.L., Miller, D., Nones, K., Quek, K., et al.; Australian Pancreatic Cancer Genome Initiative (2015). Whole genomes redefine the mutational landscape of pancreatic cancer. *Nature* **518**, 495–501.
- Wang, L., Lawrence, M.S., Wan, Y., Stojanov, P., Sougnez, C., Stevenson, K., Werner, L., Sivachenko, A., DeLuca, D.S., Zhang, L., et al. (2011). SF3B1 and other novel cancer genes in chronic lymphocytic leukemia. *N. Engl. J. Med.* **365**, 2497–2506.
- Yadlapalli, S., and Yamashita, Y.M. (2013). DNA asymmetry in stem cells – immortal or mortal? *J. Cell Sci.* **126**, 4069–4076.
- Yu, C., Gan, H., Han, J., Zhou, Z.X., Jia, S., Chabes, A., Farrugia, G., Ordog, T., and Zhang, Z. (2014). Strand-specific analysis shows protein binding at replication forks and PCNA unloading from lagging strands when forks stall. *Mol. Cell* **56**, 551–563.

# Cell Career Network just got better!



- Additional reach via extended network
- Post a job within 5 minutes via self service
- More intuitive feel and easier navigation
- New vacancy packages and pricing

Your recruitment process just became even easier.  
**Get started today!**

[careers.cell.com/recruiters](https://careers.cell.com/recruiters)



**Cell**  
PRESS

# Non-catalytic Roles for XPG with BRCA1 and BRCA2 in Homologous Recombination and Genome Stability

Kelly S. Trego,<sup>1</sup> Torsten Groesser,<sup>1,6</sup> Albert R. Davalos,<sup>2</sup> Ann C. Parpys,<sup>1,7</sup> Weixing Zhao,<sup>3</sup> Michael R. Nelson,<sup>1,8</sup> Ayesu Hlaing,<sup>1</sup> Brian Shih,<sup>1</sup> Björn Rydberg,<sup>1,10</sup> Janice M. Pluth,<sup>1</sup> Miaw-Sheue Tsai,<sup>1</sup> Jan H.J. Hoeijmakers,<sup>4</sup> Patrick Sung,<sup>3</sup> Claudia Wiese,<sup>1,5,9</sup> Judith Campisi,<sup>1,2,5</sup> and Priscilla K. Cooper<sup>1,5,\*</sup>

<sup>1</sup>Biosciences, Lawrence Berkeley National Laboratory, Berkeley, CA 94720, USA

<sup>2</sup>The Buck Institute for Research on Aging, Novato, CA 94945, USA

<sup>3</sup>Department of Molecular Biophysics and Biochemistry, Yale University School of Medicine, New Haven, CT 06520, USA

<sup>4</sup>Department of Genetics, Erasmus University Medical Center, 3000 CA Rotterdam, the Netherlands

<sup>5</sup>Co-senior author

<sup>6</sup>Present address: Technical University of Denmark at Risø, DTU Nutech, 4000 Roskilde, Denmark

<sup>7</sup>Present address: Campus Science 27, University Medical Centre Hamburg-Eppendorf, 20246 Hamburg, Germany

<sup>8</sup>Present address: Biomedical Engineering, Georgia Institute of Technology, Atlanta, GA 30332, USA

<sup>9</sup>Present address: Environmental and Radiological Health Sciences, Colorado State University, Fort Collins, CO 80523, USA

<sup>10</sup>Deceased

\*Correspondence: pkcooper@lbl.gov

<http://dx.doi.org/10.1016/j.molcel.2015.12.026>

## SUMMARY

XPG is a structure-specific endonuclease required for nucleotide excision repair, and incision-defective XPG mutations cause the skin cancer-prone syndrome xeroderma pigmentosum. Truncating mutations instead cause the neurodevelopmental progeroid disorder Cockayne syndrome, but little is known about how XPG loss results in this devastating disease. We identify XPG as a partner of BRCA1 and BRCA2 in maintaining genomic stability through homologous recombination (HRR). XPG depletion causes DNA double-strand breaks, chromosomal abnormalities, cell-cycle delays, defective HRR, inability to overcome replication fork stalling, and replication stress. XPG directly interacts with BRCA2, RAD51, and PALB2, and XPG depletion reduces their chromatin binding and subsequent RAD51 foci formation. Upstream in HRR, XPG interacts directly with BRCA1. Its depletion causes BRCA1 hyper-phosphorylation and persistent chromatin binding. These unexpected findings establish XPG as an HRR protein with important roles in genome stability and suggest how XPG defects produce severe clinical consequences including cancer and accelerated aging.

## INTRODUCTION

Unrepaired DNA lesions from both environmental and endogenous sources impede replication fork progression and result in replication stress (Magdalou et al., 2014; Zeman and Cimprich, 2014). Repair intermediates, e.g., single-strand breaks, also can interfere with replication and be processed by it into more

severe lesions, DNA double-strand breaks (DSBs). In addition, encounters with transcription pose a major problem for the replication machinery (Bermejo et al., 2012; Helmrich et al., 2013), which is likely a more severe problem when transcription itself is stalled. Thus, defects in coordination between DNA replication and DNA repair can lead to genomic instability, developmental and immunological abnormalities, and cancer and/or aging (Marteijn et al., 2014; Zeman and Cimprich, 2014).

A major mechanism for rescuing stalled replication forks involves homologous recombination repair (HRR) of the resulting DSB mediated by RAD51 (Prakash et al., 2015; San Filippo et al., 2008). HRR is essential for cell survival, and in its absence, lethal chromosome breaks occur during replication (Sonoda et al., 1998). HRR is initiated by nucleolytic processing of the broken DNA ends to give single-stranded (ss) DNA tails, which become coated by the major eukaryotic ssDNA binding protein, replication protein A (RPA). RAD51 is recruited to ssDNA and loaded onto it through displacement of RPA by the breast cancer-associated protein BRCA2 (Jensen et al., 2010; Liu et al., 2010; Thorslund et al., 2010) in partnership with PALB2 (Xia et al., 2006). In contrast (Roy et al., 2012), the breast cancer-associated protein BRCA1 functions early in HRR to regulate end resection (Coleman and Greenberg, 2011) and to recruit BRCA2 through interaction with PALB2 (Sy et al., 2009). The RAD51 nucleoprotein presynaptic filament catalyzes the search for homology between the ssDNA end and the intact sister chromatid, invading the duplex DNA to form a DNA joint called the D-loop in a process that also requires PALB2 and RAD51AP1 (Buisson et al., 2010; Dray et al., 2010; Wiese et al., 2007). Accessory proteins including RAD52 (Feng et al., 2011) and five RAD51 paralogs, XRCC2/3 and RAD51B/C/D (Chun et al., 2013), are important in the critical early step of RPA displacement and RAD51 filament formation, which manifests at the cellular level as RAD51 foci.

The DNA repair protein XPG was first identified as a structure-specific endonuclease required for nucleotide excision repair (NER). Initiation of NER requires binding of XPC to the helix distortion caused by a lesion, followed by further opening of

the DNA by the transcription/repair factor TFIIH to form an NER bubble, then lesion verification by TFIIH together with XPA. Sequential cuts at the bubble junctions by ERCC1/XPF and XPG excise the lesion-containing strand (Marteijn et al., 2014). Transcription-coupled repair (TCR) is a specialized process that preferentially removes transcription-blocking lesions from transcribed DNA strands through recognition of stalled RNA polymerase by the CSB protein, rather than recognizing the lesion itself (Fousteri and Mullenders, 2008; Vermeulen and Fousteri, 2013). TCR therefore does not involve XPC, but requires other NER proteins including XPG.

Defects in NER result in the skin cancer-prone, sun-sensitive disorder xeroderma pigmentosum (XP), and point mutations in XPG (*ERCC5*) that inactivate its endonuclease (XP-G patients) cause XP (Nouspikel et al., 1997; O'Donovan and Wood, 1993). In contrast, patients with rare truncating mutations in XPG have the combined diseases of XP with Cockayne syndrome (CS), the signature molecular defect of which is loss of TCR (Emmert et al., 2002; Lindenbaum et al., 2001; Nouspikel et al., 1997). Rather than cancer susceptibility, XP-G/CS presents as severe, primarily postnatal, progressive neurodevelopmental abnormalities with mental retardation, dramatic growth failure, greatly accelerated symptoms of aging, and death in early childhood (Schärer, 2008). Mouse models recapitulate the patient phenotypes. The original *Xpg* (*Ercc5*) knockout resulted in death before weaning (Harada et al., 1999), but a recent conditional knockout mouse in a hybrid strain background survives to 15–18 weeks and displays many progressive progeroid features, including early cessation of growth, cachexia, kyphosis, and extensive neurodegeneration (Barnhoorn et al., 2014). In striking contrast, mice with point mutations inactivating XPG enzymatic activity are UV sensitive, but otherwise normal (Shiomi et al., 2004; Tian et al., 2004), similar to XP-G patients. Thus, distinct from its NER incision function, XPG is essential for normal postnatal development in mammals. However, the nature of this requirement has been unclear.

XPG has multiple non-enzymatic functions outside its role in NER that might contribute to the fatal postnatal phenotype associated with its loss. It interacts directly with both RNA polymerase II and the CSB protein that is essential for initiation of TCR, and it has been implicated in early steps of TCR (Sarker et al., 2005) beyond its requirement for repair per se. In addition, XPG forms a complex with TFIIH and has been reported to be important for its stable association with the CAK kinase subunit (Ito et al., 2007). XPG also has a role in the early steps of base excision repair (BER) of oxidative DNA damage through direct interaction with, and stimulation of, the NTH1 glycosylase (Klungland et al., 1999; Weinfeld et al., 2001).

To better understand the critical postnatal function(s) of XPG, we undertook a series of biochemical and cell biological studies directed toward identifying other protein partners of XPG and elucidating the consequences of its absence. Our unexpected findings establish XPG as a member of the HRR pathway whose loss results in an inability to recover from replication stress, leading to DNA damage and genomic instability. These results suggest a basis for the hitherto unexplained, unusually severe phenotypes of *Xpg* knockout mice and, importantly, of XP-G/CS patients.

## RESULTS

### Loss of XPG Causes Spontaneous DNA Damage Independent from Defective NER

We compared the growth rate of normal (wild-type, WT) primary human fibroblasts to that of primary fibroblasts from two unrelated XP-G/CS patients, each with severely truncating XPG mutations (Nouspikel et al., 1997; Okinaka et al., 1997) and no detectable XPG protein (Figure 1B). The XP-G/CS cells had a much slower proliferation rate (Figure 1A), with a doubling time of 38 hr compared to 22 hr for WT, and they accumulated in G2/M (Figure S1A).

We examined XP-G/CS cells for increased pRPA32 as a sign of replication stress (Zeman and Cimprich, 2014). Stalled replication forks lead to formation of stretches of ssDNA, and hence to loading of RPA, which is rapidly phosphorylated in the RPA32 subunit (Binz et al., 2004). Consistent with high replication stress, undamaged patient cells lacking XPG had a dramatic increase in pRPA32 compared to undamaged WT (Figure 1B, lanes 3 and 4 versus 2), similar to WT after 1 hr treatment with 2  $\mu$ M camptothecin (CPT; lane 1), which causes ssDNA breaks that are converted to DSBs by replication.

Use of patient cells has the disadvantage of absence of isogenic WT controls. In addition, there is a possibility that compensatory secondary mutations or epigenetic changes may have occurred during cell culture. Therefore, we used three independent small interfering (si)RNAs to transiently reduce XPG protein to barely detectable levels in U2OS cells (Figure 1C) and compared them to a non-specific siRNA (Control) and untransfected cells (UNTF). XPG depletion caused reduced growth rate and accumulation in G2/M, but no change in the fraction of S phase cells (Figures 1D, S1B, and S1C). Depletion of XPG strongly induced pRPA32 (Figure 1C, lanes 4–6). A similar outcome was observed in XPG-depleted HeLa cells, where the increase was approximately equal to that caused by the addition of 1  $\mu$ M mitomycin C (MMC) to controls (Figure S1D).

We also measured the impact of XPG loss on foci formation for common markers of DNA damage. XPG-depleted U2OS cells had both significantly elevated 53BP1 foci (Figures 1E and 1F) and  $\gamma$ H2AX foci (Figure 1G), as well as increased  $\gamma$ H2AX by western analysis (Figure 1H). Large numbers of  $\gamma$ H2AX foci and increased  $\gamma$ H2AX were also observed in SV40-transformed XPCS1RO cells from an XP-G/CS patient (Ellison et al., 1998), but not in SV40-transformed WT (VA13) cells (Figures 1G and S1F, lane 2 versus 1). Importantly, we similarly observed elevated  $\gamma$ H2AX in primary dermal fibroblasts derived from *Xpg*<sup>-/-</sup> mice (Barnhoorn et al., 2014) compared to WT littermate controls (Figures 1H and S1G).

Together these results strongly suggest that loss of XPG, either genetically in human or mouse cells or by siRNA depletion from two different human cell lines, leads to large numbers of DSBs. To exclude that the effects were due to loss of NER, we similarly depleted U2OS cells of either XPC or XPA, since both are essential for global NER and the latter is also essential for TCR. Neither depletion increased pRPA32 (Figure S1E), 53BP1 foci formation (Figure 1F), or G2/M accumulation (Figures 1D and S1C). We conclude that the DNA damage responses

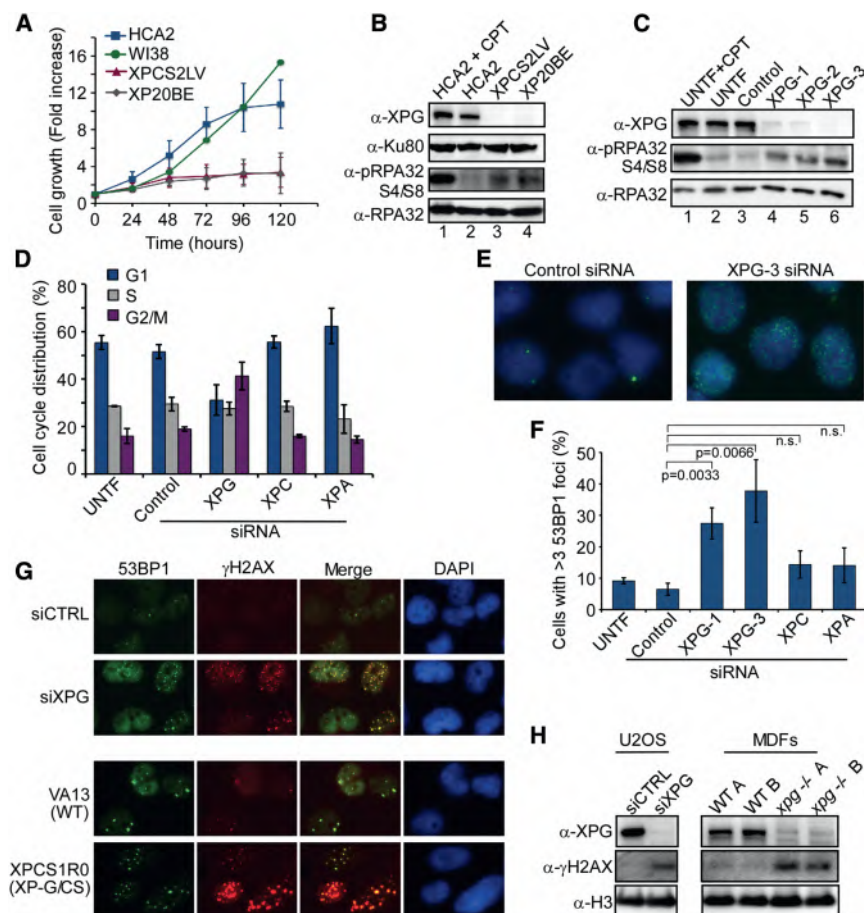


**Figure 1. Loss of XPG Causes Spontaneous DNA Damage Independent from Defective NER**

(A) Impaired cell growth of XP-G/CS patient primary fibroblasts, XPCS2LV and XP20BE, compared to normal human fibroblasts, HCA2 and WI38, of the same population doubling age. The data are mean  $\pm$  SD (N = 3); XP20BE (N = 2); and WI38 was a single experiment.

(B) pRPA32 (S4/S8) amount in undamaged XP-G/CS patient cells, XPCS2LV and XP20BE, compared to normal human fibroblasts, HCA2. The HCA2 cells treated with CPT (2  $\mu$ M for 1 hr and harvested after 4 hr) were a positive control. The Ku80 was a loading control. (C) pRPA32 amounts in U2OS cells untransfected (UTF) with or without CPT treatment (2  $\mu$ M, 1 hr) or transfected with control siRNA or three different siRNAs targeting XPG.

(D) Cell-cycle progression of siRNA transfected U2OS cells. The knock down of XPG was with a mixture of two siRNAs, XPG-1 and XPG-3. The data are the mean  $\pm$  SD for N = 3. While the depletion of XPG, but not of other NER proteins, resulted in G2/M accumulation, the S phase fraction did not change (28.5%, 29.5%, and 27.5% for untransfected, control KD, and XPG siRNA, respectively).

(E and F) Immunostaining for 53BP1 in U2OS cells transfected with siRNAs, fixed after 72 hr, and quantified for cells with >5 53BP1 foci. The data are the mean  $\pm$  SEM from N = 3. The XPC and XPA are N = 2.

(G) Immunostaining for 53BP1 (green) and  $\gamma$ H2AX (red) in U2OS cells transfected with siRNAs. The merged images (foci overlap =

yellow) and DAPI (blue) stained nuclei are shown. The VA13 (WT) and XP-G/CS patient cell line XPCS1R0 were stained as noted for U2OS cells. (H)  $\gamma$ H2AX amounts in U2OS cells depleted of XPG (left) and in primary mouse dermal fibroblasts (MDFs) from two different WT or *Xpg*<sup>-/-</sup> mice (right). The histone H3 was a loading control.

See also Figure S1.

engendered by XPG depletion are due to loss of a function distinct from its NER role.

### XPG Depletion Leads to Genomic Instability

Consistent with induction of DSBs, XPG depletion significantly increased micronuclei in U2OS cells in the absence of any damaging treatment (Figure 2A). In contrast, depletion of XPC or XPA had no effect, thus ruling out a role for NER. We next examined metaphase spreads of HeLa cells and found a significant  $\sim$ 5-fold elevation in chromatid breaks after depletion of XPG (Figure 2B). This result suggests a role for XPG in HRR, since chromatid breaks are a hallmark of defects in this BRCA-mediated pathway (Roy et al., 2012). Supporting this idea, XPG-depleted fibroblasts were sensitive to MMC (Figure S2), which causes DNA crosslinks that are repaired by HRR (Moynahan et al., 2001), and MMC treatment of XPG-depleted HeLa cells further elevated the level of chromatid breaks (Figures 2B and 2D). XPG-depleted cells also had acentric and double-minute chromosomal fragments as well as complex aberrations, not observed in control cells (Figures 2C and 2D). Collectively, these

results establish that XPG functions to maintain genomic integrity in undamaged cells and show that its requirement is even more critical after DNA damaging treatments.

### XPG Mediates Recovery from Replication Stress

Next, we examined the ability of XPG to mitigate replication stress induced by CPT. Compared to siRNA control, CPT treatment of XPG depleted cells led to a significantly greater induction of both ssDNA as marked by pRPA32 (Figures 3A and 3B) and of DSBs as marked by  $\gamma$ H2AX. Consistent with defective repair of DSBs at replication forks,  $\gamma$ H2AX persisted and accumulated for at least 72 hr (Figure 3A). XPG depletion also led to a major delay in cell-cycle reentry after CPT (Figures 3C and 3D) and to CPT hypersensitivity (Figure S3A).

To directly test the possibility that XPG facilitates replication restart after replication stress, we performed DNA fiber labeling to examine replication fork progression in the presence or absence of hydroxyurea (HU). U2OS cells were pulse-labeled with CldU (red), incubated without or with HU to arrest replication forks, and then labeled with IdU (green) (Figures 3E, 3F, S3B,

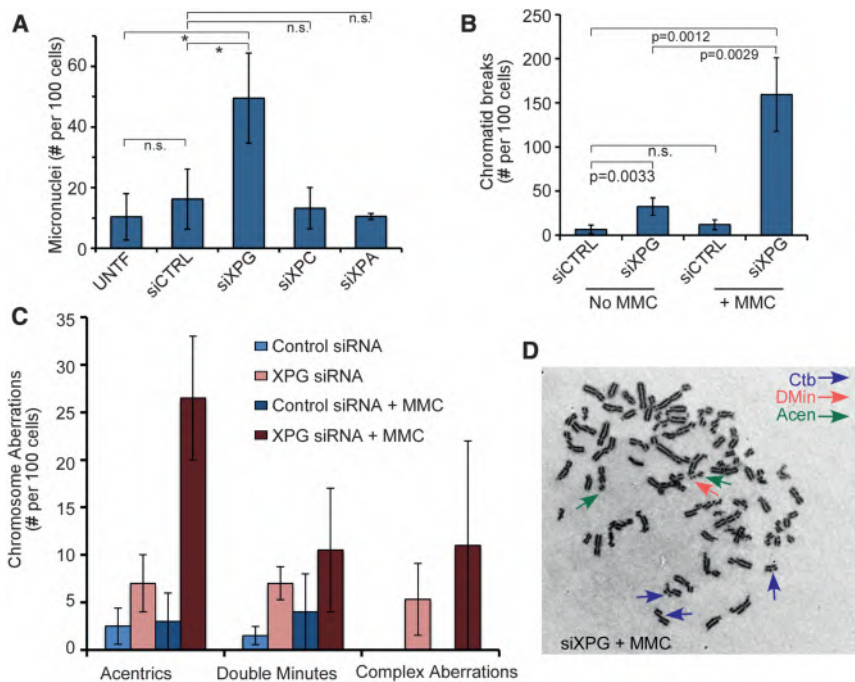


**Figure 2. XPG Is Required for Genome Stability and Cell Survival**

(A) Micronuclei in siRNA transfected U2OS cells. The data represent the mean  $\pm$  SD for N = 2, with XPG depletion significantly higher than control (\* =  $< 0.05$ ; n.s. = not significant).

(B and C) Chromatid breaks (B) and an array of chromosome aberrations (C) in siCTRL or siXPG depleted HeLa cells either mock or MMC-treated (100 nM, 1 hr), scored 24 hr following MMC. The data represent the mean  $\pm$  SD for N = 4 (no MMC) or N = 2 (with MMC).

(D) Giemsa-stained metaphase spread of MMC-treated XPG-depleted HeLa cells. The arrows show examples of chromatid breaks, double-minute, or acentric fragments.

See also Figure S2.

and S3C). Tracts labeled only in red indicate either forks that terminated during the labeling period or forks that stalled or collapsed and were unable to restart. Without HU, the frequency of red-only tracts was not significantly different between control and XPG-depleted cells (Figure 3G legend and Figure S3C). However, after 30 min of HU treatment, the frequency of stalled forks was significantly elevated in XPG-depleted cells (Figures 3F and 3G). Longer HU treatment further increased the frequency of stalled forks in both control and XPG-depleted cells, but the frequency remained significantly higher at every time point when XPG was depleted (Figure 3G). These results establish a previously unsuspected requirement for XPG in recovery from replication stress.

### XPG Protein Is Induced in Response to Replication Stress and Accumulates at Sites of DSBs

During recovery from CPT damage, XPG protein increased approximately 2-fold and remained elevated for at least 72 hr (Figures 3A and 4A). Treatment with the MG132 inhibitor showed that XPG is not regulated by proteasomal degradation (Figure S4A). Rather, quantitative (q)RT-PCR analysis revealed that XPG mRNA levels increased following CPT (Figures 4B and S4B). This upregulation of XPG is surprising, since it does not occur after UV damage (Christmann et al., 2006). It is consistent with the idea that XPG plays an important role in the cellular response to replication stress.

We used immunofluorescence to investigate localization of XPG in normal human fibroblasts and observed distinct nuclear XPG foci in S phase cells marked by staining for Cyclin A (Figure 4C), whereas G1 cells exhibited very few XPG foci (Figure S4C). The XPG foci became noticeably larger and brighter after HU treatment (Figure 4C). We confirmed that the foci reflect localized XPG by their absence in XP-G/CS

whether XPG foci overlap with 53BP1 and  $\gamma$ H2AX foci in cells synchronized into S phase with or without HU treatment (Figure 4D). In contrast to G1 cells, approximately 20% of undamaged S phase cells contained XPG foci that overlapped with 53BP1 and  $\gamma$ H2AX, and this fraction increased to  $\sim$ 70% after HU (Figure 4E). We also observed overlapping XPG and 53BP1 foci in asynchronously growing cells after ionizing radiation treatment (Figure S4E).

### XPG Interacts with HRR Proteins

Consistent with recruitment of XPG to HRR at DSBs caused by collapsed replication forks, XPG foci strongly overlapped with RAD51 foci in mid-S phase cells (Figure 5A). To test the possibility that XPG interacts with HRR proteins, we performed reciprocal co-immunoprecipitations (coIP) from nuclear extracts of U2OS cells. Pull down of XPG, BRCA2, or RAD51 in each case resulted in coIP of the other two and also of PALB2 (Figure 5B). Moreover, XPG foci overlapped with BRCA2 foci in normal human fibroblasts treated with HU (Figure 5C).

We next co-expressed HRR proteins in insect cells to identify direct interactions among them. XPG and RAD51 interacted weakly (Figure S5A), but XPG formed a tight complex with either BRCA2 or PALB2 (Figure 5D, lanes 2 and 4), and the three proteins formed a stable trimeric complex (lane 5). For other co-expression combinations, we first carried out affinity purification of FLAG-tagged BRCA2, elution with FLAG peptide, and IP of another of the co-expressed proteins (Figure 5E) to reveal stable trimeric and tetrameric complexes (Figures S5B and S5D). Since interaction of BRCA2 with the small highly acidic protein DSS1 facilitates HRR (Kristensen et al., 2010), with DSS1 acting as a DNA mimetic to displace RPA and allow RAD51 loading (Zhao et al., 2015), we wondered whether it might also participate in the HRR complex with

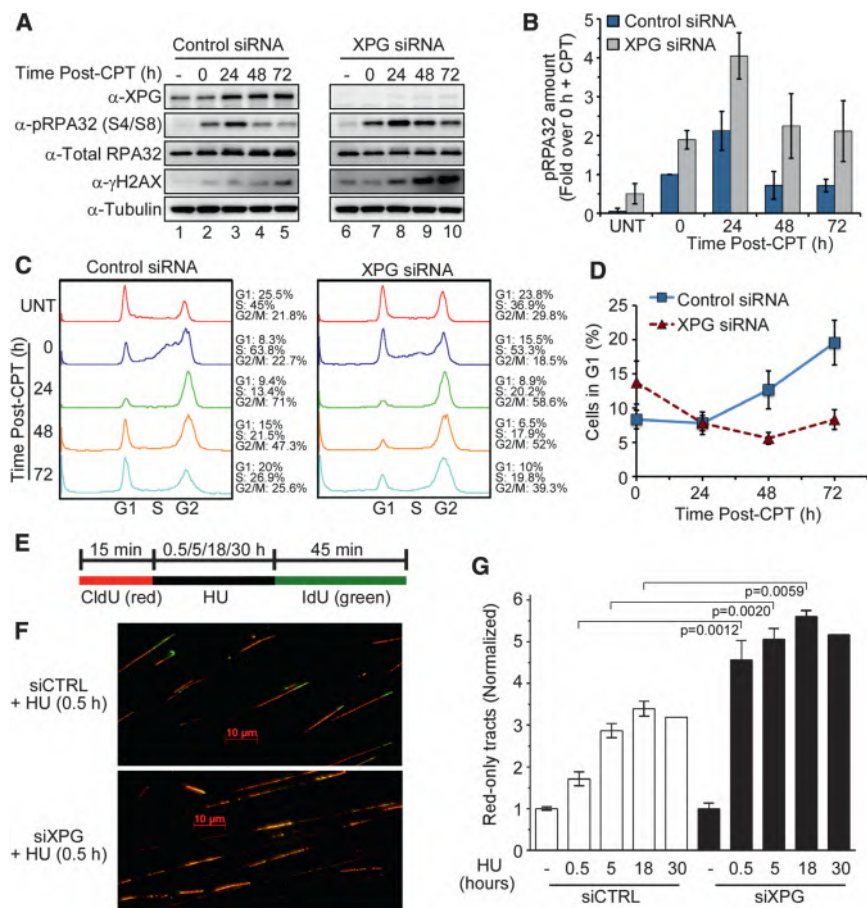


### Figure 3. XPG Mediates Recovery from Replication Stress

(A) pRPA32 (S4/S8) and  $\gamma$ H2AX level in U2OS cells transfected with siRNAs (48 hr), treated with or without CPT (20 nM, 24 hr), followed by CPT removal and harvest at the indicated times. (B) Quantification of pRPA32 (S4/S8) protein from (A). The data represent the mean  $\pm$  SD for N = 3. (C) Cell-cycle progression of U2OS cells treated with CPT (A). (D) G1 cells after CPT treatment (A). The data represent the mean  $\pm$  SD for N = 3. (E) Diagram of the DNA fiber assay showing the addition of nucleotide analog, CldU (red), for 15 min, addition of HU for 0.5, 5, 18, or 30 hr, and then IdU (green) for 45 min. (F) DNA fibers from U2OS cells transfected with siRNAs and treated with HU for 30 min. (G) Relative fraction of red-only DNA fibers in U2OS cells transfected with siRNAs as indicated and treated with HU for various times. The values were normalized to those in the same cells without HU. The percentages of red-only tracts among all the structures assessed were similar and not significantly different ( $p = 0.105$ ) between untreated siCTRL cells ( $18.55\% \pm 0.7621$ ) and untreated XPG-depleted cells ( $14.31\% \pm 1.877$ ). The data represent the mean  $\pm$  SEM for N = 3 (18 hr, N = 2 and 30 hr, N = 1). See also Figure S3.

XPG. Indeed, XPG interacted weakly with DSS1, although much less strongly than the interaction between BRCA2 and DSS1 (Figure S5C). Importantly, XPG formed a stable, five-membered HRR complex with BRCA2, PALB2, RAD51, and DSS1 upon co-expression from five separate baculoviruses. The complex robustly survived affinity purification, release, and re-IP (Figures 5E and 5F). Together, these protein-protein interactions (summarized with relative affinities; Figure 5G) substantiate a role for XPG in HRR and strongly suggest that it functions with BRCA2 to promote presynaptic filament formation.

### XPG Promotes HRR and Loads RAD51, BRCA2, and PALB2 following Replication Stress

We examined whether XPG promotes HRR by measuring gene conversion using a DR-GFP reporter construct (Pierce et al., 1999) integrated into a U2OS cell line (Xia et al., 2006). Depletion of XPG with either of two siRNAs significantly reduced gene conversion to about 50% of control (Figures 6A and S6A). This reduction is comparable to that from loss of RAD51AP1 (Figure 6A) or XRCC3 (Wiese et al., 2007). In contrast, depletion of the NER protein XPC had no effect (Figure 6A), and reduced gene conversion was not due to reduced I-SceI endonuclease expression (Figure S6B). Based on these results, we tested whether XPG depletion sensitizes cells to PARP inhibition, as re-

ported for other HRR proteins (McCabe et al., 2006). We found strong sensitization, comparable to that caused by depletion of BRCA2 itself (Figure 6B).

To understand the mechanism by which XPG promotes HRR, we examined whether loss of XPG affects RAD51 foci formation after CPT. Consistent with slow resolution of pRPA32 (Figure 3), RAD51 foci formation was attenuated (Figures 6C and S6C). This reduction could be due either to overall destabilization of RAD51 protein or its reduced chromatin localization. To distinguish between these, we used biochemical fractionation to examine whole cell extracts (WCE) versus the soluble (S100) or chromatin-bound (P100) fractions from cells treated or not with CPT. Depletion of XPG did not affect the amount of RAD51 in WCE (Figures 6D and S6D), but significantly reduced RAD51 chromatin loading after CPT (Figure 6E). Furthermore, XPG depletion also significantly reduced BRCA2 chromatin loading (Figure 6F) and reduced PALB2 on chromatin (Figure S6E). Conversely, BRCA2 or PALB2 depletion had no effect on XPG loading (Figure S6F).

### XPG Modulates BRCA1 Phosphorylation and Chromatin Loading

If XPG exclusively acts with BRCA2 and PALB2 to promote HRR, then the competing SS annealing (SSA) pathway, which is mediated by RAD52 and repairs DSBs through annealing short homologous sequences on either side of the break (Lok et al., 2013), should increase after XPG depletion, as it does when either BRCA2 or RAD51 is depleted (Stark et al., 2004). However,

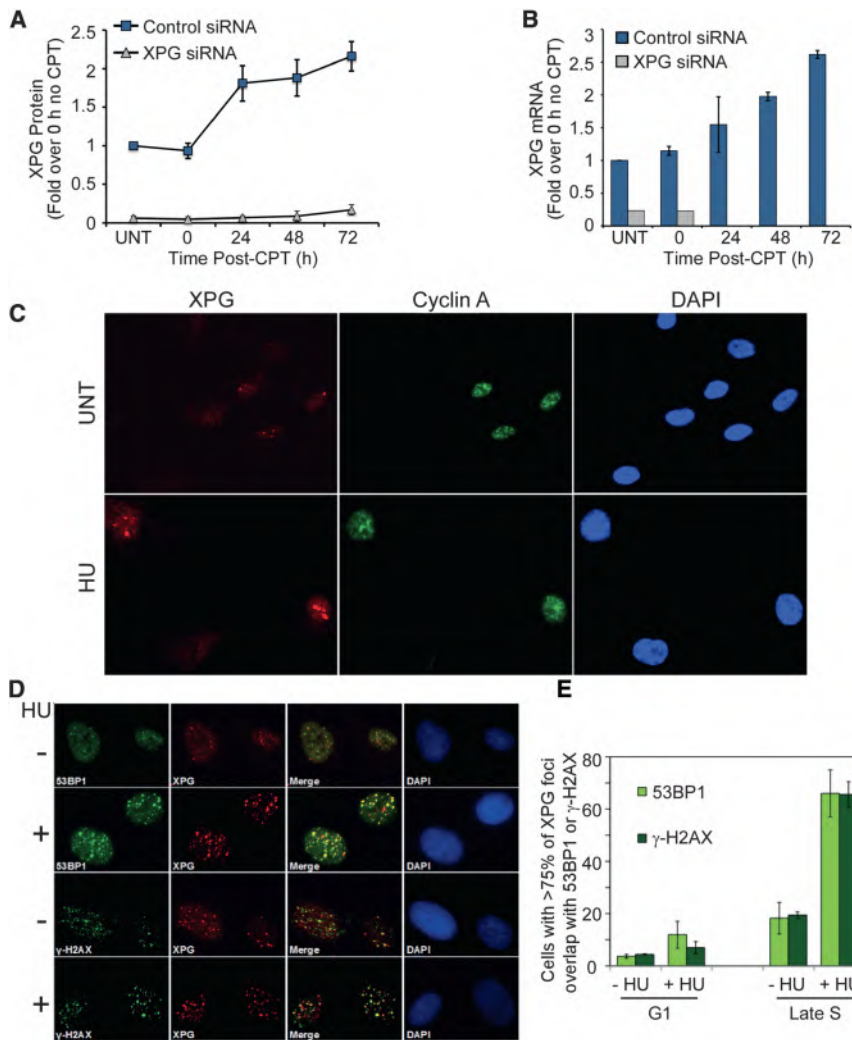


**Figure 4. XPG Increases after Replication Stress and Accumulates at Sites of DSBs**

(A) XPG protein amount (Figure 3A) quantified from U2OS cells after CPT treatment with or without siRNA knockdown, shown with the mean  $\pm$  SD for N = 3.

(B) XPG mRNA quantified by qRT-PCR in U2OS cells treated with CPT (20 nM, 24 hr). The result in cells transfected with XPG siRNA is shown for undamaged cells (UNT) and 0 hr after CPT. The data represent the mean  $\pm$  SD for N = 2 independent experiments run in triplicate.

(C) Immunostaining of XPG (red) and Cyclin A (green) in asynchronous normal human fibroblasts (HCA2) untreated or treated with HU (30 mM, 60 min).

(D) Immunostaining of XPG (red) and either 53BP1 (green) or  $\gamma$ H2AX (green) in hTERT-immortalized HCA2 cells synchronized into late S phase and then mock (-) or HU (+) treated (30 mM, 1 hr). The merged images (foci overlap = yellow) and DAPI (blue) stained nuclei are shown.

(E) Quantification of XPG foci overlap with 53BP1 and  $\gamma$ H2AX in G1 or late S phase. The data represent the mean  $\pm$  SEM for N = 2. See also Figure S4.

in contrast to the dramatic increase in SSA observed upon BRCA2 depletion, depletion of XPG led to a significant decrease in SSA (Figure 7A) as measured in U2OS SA-GFP cells (schematic in Figure S7A) (Gunn and Stark, 2012), while as expected from this pathway's requirement for extensive resection, depletion of the CtIP nuclease virtually eliminated SSA (Figure 7A). We also tested for an effect of XPG on non-homologous end joining (NHEJ), which predominates outside of S/G2 (Escribano-Díaz et al., 2013). Using U2OS EJ5-GFP cells (schematic in Figure S7B) (Gunn and Stark, 2012), we found that depletion of XPG did not alter NHEJ (Figure S7C). We then asked whether XPG was epistatic with RAD52 in SSA, but instead found that simultaneous knock down of both XPG and RAD52 reduced SSA to a level significantly below that from depletion of RAD52 alone (Figure 7A). Since XPG and RAD52 thus are not epistatic in SSA, we hypothesized that XPG may act upstream of both HRR and SSA, perhaps through interaction with BRCA1, which is required for both.

We therefore asked whether XPG depletion affects BRCA1 function. By colP, XPG and BRCA1 are indeed associated in human cell extracts (Figure 7B). We further verified that they

remove and then slowly declined. However, chromatin-bound BRCA1 increased dramatically with time in cells depleted for XPG. These results suggest that XPG is required for BRCA1 release. A possible mechanism is suggested by the fact that, while mobility of BRCA1 is reduced in control cells immediately after removal of CPT and returned to normal with time, the reduced mobility of BRCA1 in XPG-depleted cells was both more pronounced and in fact increased with time (Figures 7D and S7E). The altered mobility was entirely due to hyperphosphorylation, as demonstrated by phosphatase treatment of the modified form (Figure S7G). Inhibiting ATM or ATR did not reduce the interaction between XPG and BRCA1 (Figure S7H).

XPG depleted cells had significantly increased BRCA1 foci both in untreated cells and after CPT (Figures 7F and 7G), consistent with increased chromatin binding. As expected, depletion of BRCA1 resulted in increased DNA damage as marked by 53BP1 foci (Figure S7I). Notably, BRCA1 depletion led to an increase in total XPG protein (Figure S7F), similar to that observed as a result of replication stress (Figure 4A), whereas XPG amounts did not change with PALB2 or BRCA2 depletion (Figure 6D).

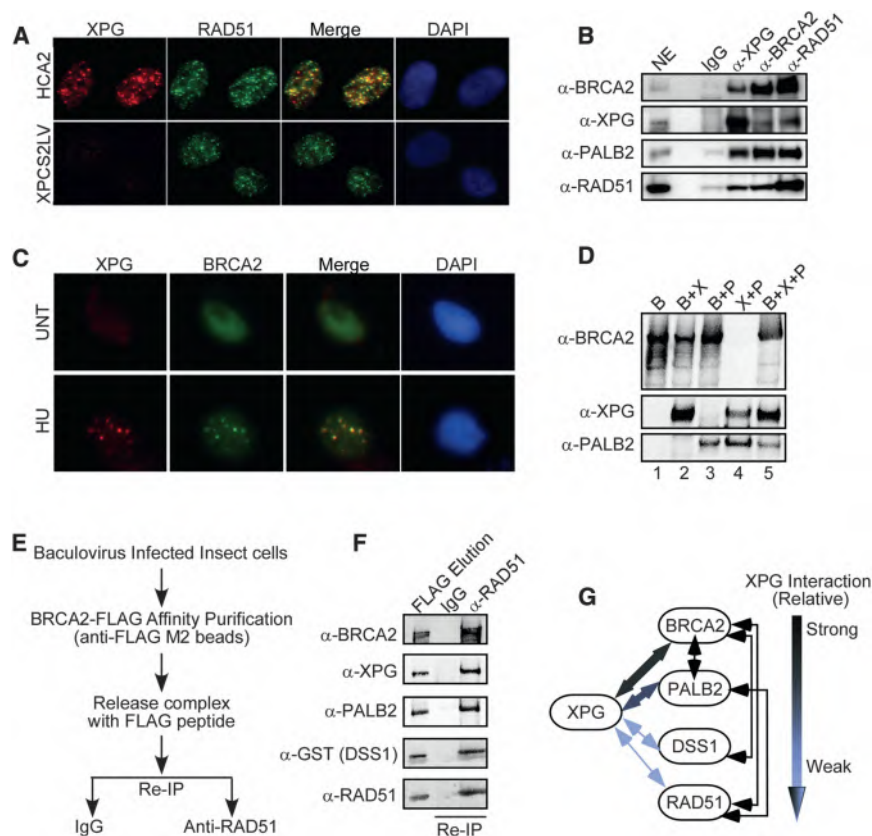


**Figure 5. XPG Interacts with HRR Proteins**

(A) Immunostaining of XPG (red) and RAD51 (green) in HCA2-hTERT (upper) and XPG null cells (XPCS2LV, lower) synchronized in mid-S phase. The merged images (foci overlap = yellow) and DAPI (blue) stained nuclei are shown.

(B) CoIP of XPG, BRCA2, RAD51, and PALB2 from U2OS cell nuclear extracts.

(C) Immunostaining of XPG (red) and BRCA2 (green) foci in asynchronous HCA2-hTERT fibroblasts either untreated or treated with HU (10 mM, 18 hr). The merged image (foci overlap = yellow) and DAPI (blue) stained nuclei are shown.

(D) Affinity purification of FLAG-BRCA2 (B) with either XPG (X) and/or PALB2 (P) proteins from co-infected insect cell extracts. In the X+P co-expression (no BRCA2), XPG was FLAG-tagged.

(E) Schematic of FLAG-affinity purification, followed by elution and IP.

(F) Affinity purification of FLAG-BRCA2, then IP with  $\alpha$ -RAD51 or control IgG from co-infected insect cell extracts reveals stable complex of five HRR proteins.

(G) Schematic of XPG interactions with HRR proteins. See also Figure S5.

Taken together, our findings establish that XPG has an important, complex role in responding to replication stress and maintaining genome stability (Figure 7H) through direct protein-protein interactions with key factors both for initiation of HRR and SSA (BRCA1) and for presynaptic filament formation (BRCA2, PALB2, DSS1, and RAD51).

## DISCUSSION

Our work reveals an unexpected, multi-faceted function for XPG in HRR that is clearly distinct from its role in NER. Specifically, we show that XPG forms a higher-order complex with BRCA2, PALB2, RAD51, and DSS1, that it also interacts with BRCA1, and that loss of XPG leads to a significant reduction of HRR. The reduced HRR reflects decreased RAD51 foci formation caused by decreased chromatin binding of RAD51, BRCA2, and PALB2. The deleterious cellular consequences observed upon XPG depletion are consistent with its requirement in HRR. These include increased pRPA32 signaling, DSB formation, G2/M accumulation, and sensitivity to the crosslinking agent MMC, the topoisomerase I inhibitor CPT, and PARP inhibition. Furthermore, stalled replication forks accumulate dramatically upon XPG depletion, correlating with induction of genomic instability as marked by chromatid breaks and micronuclei even in otherwise undamaged cells.

The observed effects of XPG loss on RAD51, BRCA2, and PALB2, together with its direct interactions with each of these proteins, suggest that XPG functions in HRR as a recombination

mediator to facilitate presynaptic filament formation. It is perhaps important in this context that XPG interacts directly with RPA through an acidic region in the XPG spacer domain (He et al., 1995), and that the spacer also contains a ubiquitin binding motif (UBM) (Hofmann, 2009). The biological relevance of the XPG interaction with RPA has primarily been viewed in the context of NER, where the interaction may assist in coordinating DNA resynthesis with XPG incision (Fagbemi et al., 2011). However, since ubiquitylated RPA is involved in regulating repair at stalled replication forks (Elia et al., 2015b), it is possible that the interaction is also functionally important for localizing XPG to stalled replication forks and/or for coordinating RPA removal in complex with BRCA2/PALB2/DSS1.

The interpretation that XPG functions as an additional recombination mediator, while consistent with most of our observations, would not predict its effects on BRCA1. BRCA1 is phosphorylated by ATM and ATR in response to damage or replication stress respectively, and the phosphorylation is important for BRCA1 focal localization (Cortez et al., 1999; Tibbetts et al., 2000). However, little is known about subsequent regulatory steps, including the mechanism of BRCA1 dephosphorylation or consequences of its failure. XPG involvement in regulating BRCA1 activity, perhaps by promoting phosphatase action, is strongly suggested by the striking hyperphosphorylation, increased foci formation, and persistent chromatin binding of BRCA1 when XPG is lost. It is even possible that the downstream effects of XPG loss on RAD51 foci formation and HRR are simply an indirect consequence of its requirement for regulating BRCA1 function. However, the multiple downstream protein-protein interactions of XPG would be difficult to reconcile with this view. We therefore favor the possibility that XPG has two distinct

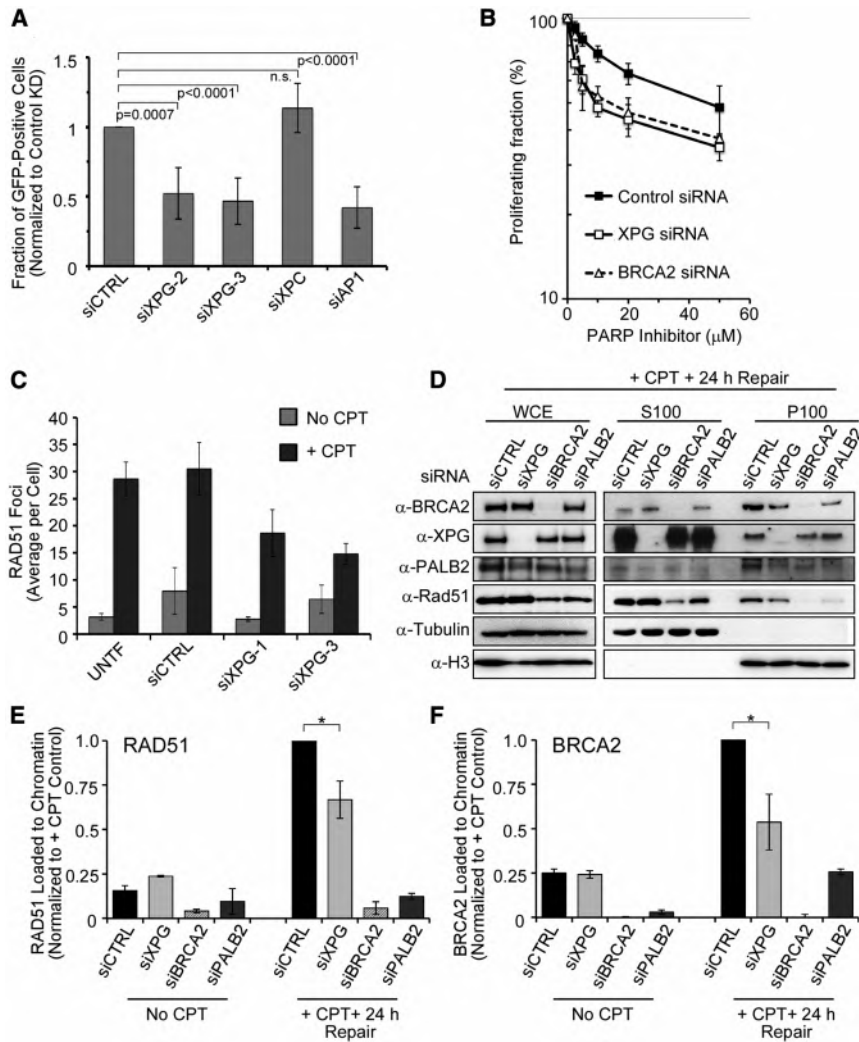


**Figure 6. XPG Promotes HRR and Chromatin Binding of BRCA2, PALB2, and RAD51**

(A) DR-U2OS cells were transfected with siRNAs, followed by transfection with an I-SceI expression plasmid. The data represent the mean ± SD for N = 5–13.

(B) Normal human fibroblasts (HCA2-hTERT) transfected with siRNAs were assayed for survival by BrdU incorporation after PARP inhibition by ABT-888. The data represent the mean ± SEM for N = 3 (siCTRL and siXPG) and N = 2 (siBRCA2).

(C) RAD51 foci formation revealed by immunostaining was quantified in U2OS cells transfected with siRNAs and then treated with or without CPT (20 nM, 24 hr). The data represent the mean ± SEM for N = 3.

(D) U2OS cells were transfected with siRNAs, treated with CPT (20 nM, 24 hr), and harvested for WCE or fractionated into soluble (S100) or chromatin-bound (P100) proteins.

(E and F) Quantification of RAD51 (E) and BRCA2 (F) chromatin loading from (D). The data represent the mean ± SEM for N = 2, with XPG depletion significantly lower than control (\* and <0.05).

See also Figure S6.

functions in HRR, one in the initiation step through regulatory effects on BRCA1 and another through direct participation in RAD51 presynaptic filament formation with BRCA2 and PALB2.

The most well-understood function of XPG is its required role as the 3' endonuclease in NER and transcription-coupled NER (TC-NER). However, several lines of evidence strongly suggest that the dramatic BRCA-like phenotype upon loss of XPG as reported here is separable from this role. In support of this idea, depletion of XPC or XPA, which also block NER or both NER and TC-NER respectively, did not increase DSBs or genomic instability. Furthermore, there are strong biological arguments supporting a critical non-enzymatic role for XPG. Data from both mouse models and human patients establish that while XPG is required for normal postnatal development, its endonuclease activity is not. In both cases, inactivating point mutations cause only UV sensitivity, whereas knockouts (mouse) or truncations (patients) cause the severe CS phenotype and very early death (Barnhoorn et al., 2014).

We suggest that, independently of its catalytic activity, XPG functions as a scaffold protein at multiple steps in HRR. How-

ever, we have been unable to rescue the HRR defect in either XP-G/CS patient cells or siRNA knockdowns by ectopic expression of WT XPG cDNA (e.g., Figure S1F, lanes 3 and 4), despite the fact that the NER defect is complemented (Ellison et al., 1998; Staresinic et al., 2009). There are several possible explanations for this observation. Notably, native XPG expression is apparently tightly regulated and responds to replication stress (Figures 4A and 4B), and it is possible that this regulation is critical for its HRR function. Furthermore, XPG protein is heavily post-translationally modified, including multiple phosphorylations, ubiquitination, and likely sumoylation (Elia et al., 2015a). A lack of UTR sequences in ectopic expression may result in the dysregulation of RNA-mediated co-translational protein modifications (Kramer et al., 2009). In addition, there are at least three protein coding isoforms of XPG/ERCC5 (GENCODE build 19 and later, <http://www.gencodegenes.org>) plus a gene-merge transcript, *BIVM-ERCC5*, of unknown function. Thus, ectopically expressed XPG, although active as an endonuclease, may lack some properties that are critical for its homeostasis and scaffolding functions. Of note, inability to rescue knockdowns by ectopic expression is not without precedent and has recently been observed by us in HRR for the NUCKS1 protein (Parplys et al., 2015). Notwithstanding the failure of ectopically expressed XPG to complement phenotypes other than those related to NER incision, the biology of different classes of XPG mutations (inactivating point mutations versus truncations or deletions) in human patients and in mouse models argues very strongly that XPG has critical functions distinct from its endonuclease activity.

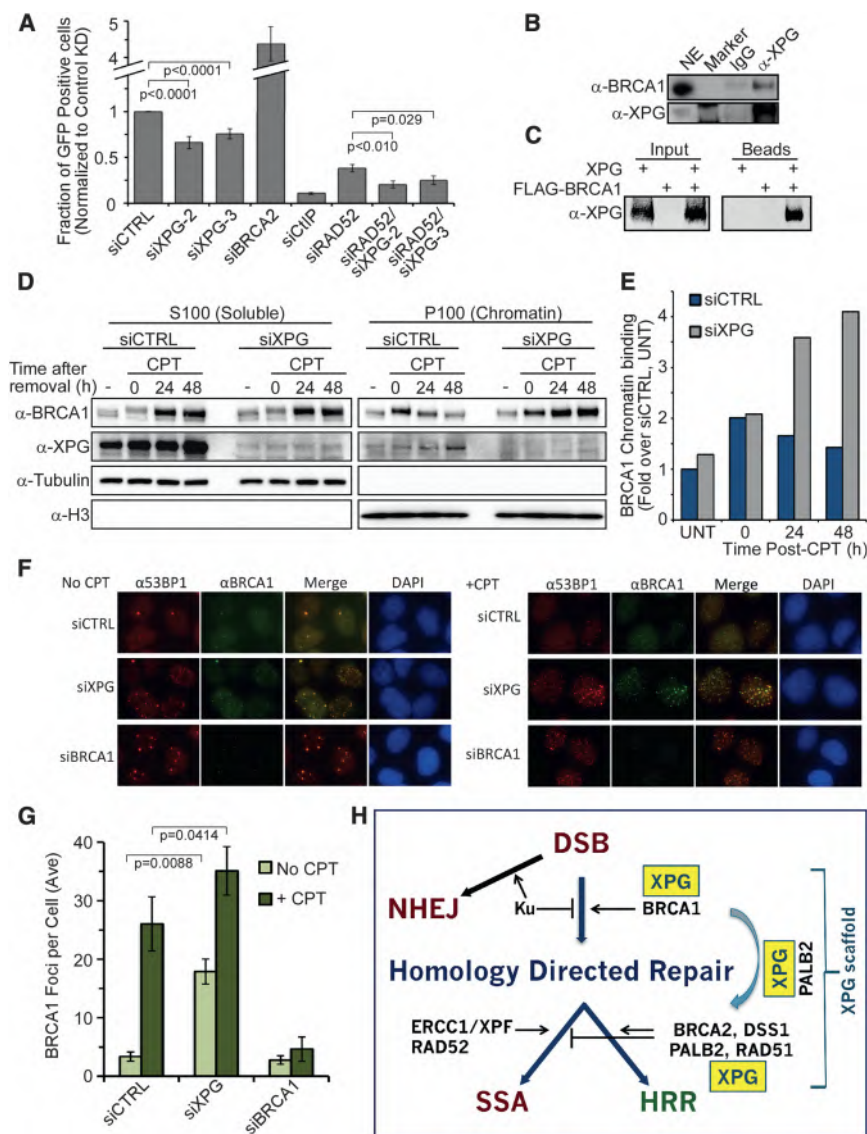


**Figure 7. XPG Promotes SSA and Affects BRCA1 Function**

(A) SA-U2OS cells (carrying an integrated SSA reporter construct as diagrammed in Figure S7A), were transfected with siRNAs, followed by transfection with an I-SceI expression plasmid. The data represent the mean  $\pm$  SEM for N = 6–15.

(B) ColP of BRCA1 with XPG from U2OS cell nuclear extracts.

(C) Affinity purification of FLAG-BRCA1 with XPG from co-infected insect cell extracts.

(D) BRCA1 chromatin loading in U2OS cells transfected with siRNAs, treated with CPT (20 nM, 24 hr), harvested at the indicated times after CPT removal, and fractionated into soluble (S100) or chromatin-bound (P100) proteins.

(E) Quantification of BRCA1 chromatin loading.

(F) Immunofluorescence of BRCA1 (green) and 53BP1 (red) foci in U2OS cells transfected with siRNAs and 48 hr later treated with CPT (20 nM, 24 hr) (right) or mock treated (left). The merged image (overlap = yellow) and DAPI (blue) stained nuclei are shown.

(G) BRCA1 foci (Figure 7F) were quantified and plotted. The data represent the mean  $\pm$  SEM for N = 3.

(H) Model for XPG participation in HRR. XPG regulates BRCA1 action in initiation of homology-directed repair, and depletion of XPG reduces both HRR and SSA. XPG additionally acts in a complex with BRCA2, PALB2, DSS1, and RAD51 as a recombination mediator to promote RAD51 presynaptic filament formation in HRR. See also Figure S7.

(Schlachter et al., 2011, 2012). Replication fork reversal to form a “chicken-foot” structure is also central to avoiding fork breakage and allowing replication restart, and it is mediated by RAD51 in a role outside of its recombinase function (Zellweger et al., 2015). Processing of

Our results as reported here strongly suggest that the XPG role(s) in HRR and in replication fork restart are one such function.

The result of XPG depletion is an approximate 50% reduction in HRR that was consistently observed for several different endpoints. However, the induction of DSBs, genomic instability, and stalled replication forks when XPG is depleted greatly exceeds that expected from a 2-fold decrease in HRR. These discrepancies suggest that other functions of XPG, in addition to the new HRR role(s) described here, likely contribute to genomic stability and replication fork maintenance.

One possibility is that XPG plays an additional role either in replication fork protection or reversal. It is now clear that elaborate mechanisms exist for protecting replication forks that have encountered blocks and for restoring their progress. These mechanisms operate prior to the crisis state of collapse and DSB induction, after which HRR is clearly required. They include protection from excessive resection/degradation, which involves non-HRR functions of both BRCA1 and BRCA2

reversed forks to allow replication restart requires WRN protein (Thangavel et al., 2015), and a non-enzymatic function of WRN has been implicated in protecting nascent DNA upon fork stalling (Su et al., 2014). Since we show that XPG interacts directly with BRCA1, BRCA2, and RAD51, and since it also has a direct, functional interaction with WRN (Trego et al., 2011), one possibility to explain the extreme accumulation of stalled forks when XPG is lost is that it additionally serves as an important co-factor in one or more of these processes.

Another possibility that must be considered relates to the recent demonstration that the presence of XPG endonuclease activity in cells lacking various RNA processing factors causes extensive DSB formation and genomic instability from cleavage of R-loops (Sollier et al., 2014), which are RNA-DNA hybrids with displaced ssDNA that can form behind transcription. However, we show the opposite: DSBs—presumably at stalled replication forks—and genomic instability are caused by loss of XPG. It is presently unclear whether XPG processes R-loops

under normal conditions (i.e., in the presence of RNA processing factors), and if so whether such cleavage is beneficial or deleterious. It is possible that, in the absence of XPG, unprocessed R-loops could lead to DSBs when encountered by replication forks. In this context it is interesting that R-loop cleavage by XPG also requires the TCR protein CSB (Sollier et al., 2014), whose activity is increased by interaction with XPG (Sarker et al., 2005). Loss of either XPG or CSB would therefore both prevent TCR, leading to a dramatic increase in stalled transcription, and increase R-loop formation or persistence. The combined effect could significantly increase replication fork stalling, which would be poorly resolved in the absence of XPG, leading to high levels of replication stress. Thus the relationship between TCR, R-loops, replication fork stalling and collapse, and HRR is evidently complex and certainly poorly understood at present. What is now clear, however, is that XPG occupies a central position in these intertwined processes. Interestingly, CSB has recently been implicated both in recruitment of HRR proteins to oxidative damage at sites of active transcription (Wei et al., 2015) and in the mitotic checkpoint and pathway choice for DSB repair (Batenburg et al., 2015). Although the detailed connection between these findings for CSB and the HRR role of XPG reported here remains to be elucidated, it is increasingly evident that TCR defects in general are likely to have an impact that extends well beyond maintenance of transcription to include effects on genome stability.

In summary, we have demonstrated an unexpected, critical role for XPG in replication fork maintenance and preservation of genomic stability through participation in HRR after replication stress via direct interactions with key HRR proteins. Cell-cycle defects, large numbers of DSBs, HRR defects, and elevated DNA damage response signaling ensue when cells are deprived of XPG. The severe disease presentation that manifests in patients with truncating mutations in *XPG* or in mouse models with deletion of *Xpg* has never been adequately explained and cannot be reconciled with loss of NER alone. Loss of the HRR role for XPG that is described here, and possibly of additional XPG functions in processing of stalled forks, may represent a major contributing factor in the CS phenotype. The assignment of XPG as an important player in BRCA-mediated HRR and the greatly elevated genomic instability that occurs in its absence also raise the possibility that it functions as a previously unrecognized tumor suppressor gene for breast, ovarian, and other BRCA-associated cancers.

## EXPERIMENTAL PROCEDURES

### Cell Culture and siRNA Transfection

Primary and immortalized human cell lines were cultured under ambient oxygen and 10% CO<sub>2</sub> in DMEM. Primary mouse dermal fibroblasts were cultured at 3% oxygen and 5% CO<sub>2</sub> in DMEM/Hams-F12 media. Both were supplemented with fetal calf serum and 1% antibiotic/antimycotic. siRNAs (40 nM) were transiently transfected with LipofectamineRNAiMAX (Invitrogen) on 2 consecutive days, followed by replating and incubation for 24–72 hr prior to experimentation.

### WCE, Cellular Fractionation, and Phosphatase Treatment

Cells were lysed in SDS sample buffer (3% SDS, 10% glycerol, and 100 mM Tris-HCl [pH 6.8]) and heated at 95°C. For experiments with BRCA2, cell lysates were not heated, but were needle sheared in the same buffer. Protein

concentrations were determined by the BCA assay (Pierce). Fractionation into an S100 fraction containing cytoplasmic and nuclear proteins and P100 fraction containing chromatin, nuclear matrix, and insoluble proteins was performed as previously described (Xia et al., 2006). For phosphatase treatment, the P100 pellets were mock or lambda phosphatase treated according to the manufacturer's recommendation (NEB) then needle sheared in SDS buffer.

### Drug Treatments and Cellular Proliferation

Unless otherwise noted, cells were exposed to 20 nM CPT or DMSO for 24 hr in growth medium. After treatment, cultures were washed with PBS and returned to growth medium or harvested. MMC exposure was in growth medium for 1 hr, followed by PBS wash, and incubation for 24 hr prior to analysis. PARP inhibitor ABT-888 treatment was for 1 hr prior to addition of BrdU. HU treatment was for 1 hr at 30 mM or for 16 hr at 5 or 10 mM. To measure proliferation after damage, cells were incubated in the presence of BrdU (20 μM) for 72 hr, harvested, and analyzed by fluorescence-activated cell sorting (FACS) to detect BrdU-positive cells.

### DNA Fiber Assay, Micronuclei, and Chromosome Analysis

The DNA fiber assay, micronuclei assay, and chromosome analysis were performed as described (Parplys et al., 2014; Groesser et al., 2007; Wiese et al., 2007).

### Statistics

Statistical significances were determined using the Student's t test.

### Supplemental Experimental Procedures

Details of cells used, insect cell expression and purification methodologies, reporter assays for gene conversion and SSA, antibodies and protocols used for immunofluorescence and westerns, and other detailed experimental procedures and associated references are found in the Supplemental Information.

## SUPPLEMENTAL INFORMATION

Supplemental Information includes Supplemental Experimental Procedures and seven figures and can be found with this article online at <http://dx.doi.org/10.1016/j.molcel.2015.12.026>.

## AUTHOR CONTRIBUTIONS

K.S.T., T.G., A.R.D., A.C.P., M.S.T., C.W., and P.K.C. designed the studies and analyzed the data. K.S.T., T.G., A.R.D., A.C.P., B.R., A.H., B.S., W.Z., M.R.N., and C.W. performed the experiments and analyzed the data. J.M.P. generated preliminary data that motivated this study. P.S., C.W., J.H.J.H., and J.C. edited the manuscript. K.S.T. and P.K.C. wrote the manuscript.

## ACKNOWLEDGMENTS

We thank Maria Jasin, Jeremy Stark, and Orlando Schärer for cell lines; Ben Brown (ENCODE Consortium) for helpful discussions of *ERCC5* coding potential; David Schild for discussions and comments on the manuscript; Gerald Fontenay for assistance with BioSig3D; Caroline Ho, Stanley Leung, Iris Lee, and Aya Iwamoto for assistance with western blots; and Cliff Ng for major laboratory support. This work was supported by NIH grants R01 ES019935 (P.K.C. and J.C.), P01 CA092584 (P.K.C. and P.S.), R21 CA187765 (P.K.C. and K.S.T.), P01 AG017242 (J.H.J.H., J.C., and P.K.C.), R01 ES015252 (P.S.), and R01 ES021454 (C.W.), and by the DOE Low Dose Radiation Research Program, Contract DE-AC02-05CH11231.

Received: June 8, 2015

Revised: November 13, 2015

Accepted: December 21, 2015

Published: January 28, 2016

## REFERENCES

- Barnhoorn, S., Uittenboogaard, L.M., Jaarsma, D., Vermeij, W.P., Tresini, M., Weymaere, M., Menoni, H., Brandt, R.M., de Waard, M.C., Botter, S.M., et al. (2014). Cell-autonomous progeroid changes in conditional mouse models for repair endonuclease XPG deficiency. *PLoS Genet.* *10*, e1004686.
- Batenburg, N.L., Thompson, E.L., Hendrickson, E.A., and Zhu, X.D. (2015). Cockayne syndrome group B protein regulates DNA double-strand break repair and checkpoint activation. *EMBO J.* *34*, 1399–1416.
- Bermejo, R., Lai, M.S., and Foiani, M. (2012). Preventing replication stress to maintain genome stability: resolving conflicts between replication and transcription. *Mol. Cell* *45*, 710–718.
- Binz, S.K., Sheehan, A.M., and Wold, M.S. (2004). Replication protein A phosphorylation and the cellular response to DNA damage. *DNA Repair (Amst.)* *3*, 1015–1024.
- Buisson, R., Dion-Côté, A.M., Coulombe, Y., Launay, H., Cai, H., Stasiak, A.Z., Stasiak, A., Xia, B., and Masson, J.Y. (2010). Cooperation of breast cancer proteins PALB2 and piccolo BRCA2 in stimulating homologous recombination. *Nat. Struct. Mol. Biol.* *17*, 1247–1254.
- Christmann, M., Tomicic, M.T., Origer, J., Aasland, D., and Kaina, B. (2006). c-Fos is required for excision repair of UV-light induced DNA lesions by triggering the re-synthesis of XPF. *Nucleic Acids Res.* *34*, 6530–6539.
- Chun, J., Buechelmaier, E.S., and Powell, S.N. (2013). Rad51 paralog complexes BCDX2 and CX3 act at different stages in the BRCA1-BRCA2-dependent homologous recombination pathway. *Mol. Cell Biol.* *33*, 387–395.
- Coleman, K.A., and Greenberg, R.A. (2011). The BRCA1-RAP80 complex regulates DNA repair mechanism utilization by restricting end resection. *J. Biol. Chem.* *286*, 13669–13680.
- Cortez, D., Wang, Y., Qin, J., and Elledge, S.J. (1999). Requirement of ATM-dependent phosphorylation of brca1 in the DNA damage response to double-strand breaks. *Science* *286*, 1162–1166.
- Dray, E., Etchin, J., Wiese, C., Saro, D., Williams, G.J., Hammel, M., Yu, X., Galkin, V.E., Liu, D., Tsai, M.S., et al. (2010). Enhancement of RAD51 recombinase activity by the tumor suppressor PALB2. *Nat. Struct. Mol. Biol.* *17*, 1255–1259.
- Elia, A.E., Boardman, A.P., Wang, D.C., Huttlin, E.L., Everley, R.A., Dephoure, N., Zhou, C., Koren, I., Gygi, S.P., and Elledge, S.J. (2015a). Quantitative proteomic atlas of ubiquitination and acetylation in the DNA damage response. *Mol. Cell* *59*, 867–881.
- Elia, A.E., Wang, D.C., Willis, N.A., Boardman, A.P., Hajdu, I., Adeyemi, R.O., Lowry, E., Gygi, S.P., Scully, R., and Elledge, S.J. (2015b). RFW3-dependent ubiquitination of RPA regulates repair at stalled replication forks. *Mol. Cell* *60*, 280–293.
- Ellison, A.R., Nospikel, T., Jaspers, N.G., Clarkson, S.G., and Gruenert, D.C. (1998). Complementation of transformed fibroblasts from patients with combined xeroderma pigmentosum-Cockayne syndrome. *Exp. Cell Res.* *243*, 22–28.
- Emmert, S., Slor, H., Busch, D.B., Batko, S., Albert, R.B., Coleman, D., Khan, S.G., Abu-Libdeh, B., DiGiovanna, J.J., Cunningham, B.B., et al. (2002). Relationship of neurologic degeneration to genotype in three xeroderma pigmentosum group G patients. *J. Invest. Dermatol.* *118*, 972–982.
- Escribano-Díaz, C., Orthwein, A., Fradet-Turcotte, A., Xing, M., Young, J.T., Tkáč, J., Cook, M.A., Rosebrock, A.P., Munro, M., Canny, M.D., et al. (2013). A cell cycle-dependent regulatory circuit composed of 53BP1-RIF1 and BRCA1-CtIP controls DNA repair pathway choice. *Mol. Cell* *49*, 872–883.
- Fagbemi, A.F., Orelli, B., and Schärer, O.D. (2011). Regulation of endonuclease activity in human nucleotide excision repair. *DNA Repair (Amst.)* *10*, 722–729.
- Feng, Z., Scott, S.P., Bussen, W., Sharma, G.G., Guo, G., Pandita, T.K., and Powell, S.N. (2011). Rad52 inactivation is synthetically lethal with BRCA2 deficiency. *Proc. Natl. Acad. Sci. USA* *108*, 686–691.
- Fousteri, M., and Mullenders, L.H. (2008). Transcription-coupled nucleotide excision repair in mammalian cells: molecular mechanisms and biological effects. *Cell Res.* *18*, 73–84.
- Grosser, T., Chun, E., and Rydberg, B. (2007). Relative biological effectiveness of high-energy iron ions for micronucleus formation at low doses. *Radiat. Res.* *168*, 675–682.
- Gunn, A., and Stark, J.M. (2012). I-Scel-based assays to examine distinct repair outcomes of mammalian chromosomal double strand breaks. *Methods Mol. Biol.* *920*, 379–391.
- Harada, Y.N., Shiomi, N., Koike, M., Ikawa, M., Okabe, M., Hirota, S., Kitamura, Y., Kitagawa, M., Matsunaga, T., Nikaido, O., and Shiomi, T. (1999). Postnatal growth failure, short life span, and early onset of cellular senescence and subsequent immortalization in mice lacking the xeroderma pigmentosum group G gene. *Mol. Cell Biol.* *19*, 2366–2372.
- He, Z., Henricksen, L.A., Wold, M.S., and Ingles, C.J. (1995). RPA involvement in the damage-recognition and incision steps of nucleotide excision repair. *Nature* *374*, 566–569.
- Helmrich, A., Ballarino, M., Nudler, E., and Tora, L. (2013). Transcription-replication encounters, consequences and genomic instability. *Nat. Struct. Mol. Biol.* *20*, 412–418.
- Hofmann, K. (2009). Ubiquitin-binding domains and their role in the DNA damage response. *DNA Repair (Amst.)* *8*, 544–556.
- Ito, S., Kuraoka, I., Chymkowitz, P., Compe, E., Takedachi, A., Ishigami, C., Coin, F., Egly, J.M., and Tanaka, K. (2007). XPG stabilizes TFIIH, allowing transactivation of nuclear receptors: implications for Cockayne syndrome in XP-G/CS patients. *Mol. Cell* *26*, 231–243.
- Jensen, R.B., Carreira, A., and Kowalczykowski, S.C. (2010). Purified human BRCA2 stimulates RAD51-mediated recombination. *Nature* *467*, 678–683.
- Klungland, A., Rosewell, I., Hollenbach, S., Larsen, E., Daly, G., Epe, B., Seeberg, E., Lindahl, T., and Barnes, D.E. (1999). Accumulation of premutagenic DNA lesions in mice defective in removal of oxidative base damage. *Proc. Natl. Acad. Sci. USA* *96*, 13300–13305.
- Kramer, G., Boehringer, D., Ban, N., and Bukau, B. (2009). The ribosome as a platform for co-translational processing, folding and targeting of newly synthesized proteins. *Nat. Struct. Mol. Biol.* *16*, 589–597.
- Kristensen, C.N., Bystol, K.M., Li, B., Serrano, L., and Brenneman, M.A. (2010). Depletion of DSS1 protein disables homologous recombinational repair in human cells. *Mutat. Res.* *694*, 60–64.
- Lindenbaum, Y., Dickson, D., Rosenbaum, P., Kraemer, K., Robbins, I., and Rapin, I. (2001). Xeroderma pigmentosum/cockayne syndrome complex: first neuropathological study and review of eight other cases. *Eur. J. Paediatr. Neurol.* *5*, 225–242.
- Liu, J., Doty, T., Gibson, B., and Heyer, W.D. (2010). Human BRCA2 protein promotes RAD51 filament formation on RPA-covered single-stranded DNA. *Nat. Struct. Mol. Biol.* *17*, 1260–1262.
- Lok, B.H., Carley, A.C., Tchang, B., and Powell, S.N. (2013). RAD52 inactivation is synthetically lethal with deficiencies in BRCA1 and PALB2 in addition to BRCA2 through RAD51-mediated homologous recombination. *Oncogene* *32*, 3552–3558.
- Magdalou, I., Lopez, B.S., Pasero, P., and Lambert, S.A. (2014). The causes of replication stress and their consequences on genome stability and cell fate. *Semin. Cell Dev. Biol.* *30*, 154–164.
- Marteijn, J.A., Lans, H., Vermeulen, W., and Hoeijmakers, J.H. (2014). Understanding nucleotide excision repair and its roles in cancer and ageing. *Nat. Rev. Mol. Cell Biol.* *15*, 465–481.
- McCabe, N., Turner, N.C., Lord, C.J., Kluzek, K., Bialkowska, A., Swift, S., Giavara, S., O'Connor, M.J., Tutt, A.N., Zdzienicka, M.Z., et al. (2006). Deficiency in the repair of DNA damage by homologous recombination and sensitivity to poly(ADP-ribose) polymerase inhibition. *Cancer Res.* *66*, 8109–8115.
- Moynahan, M.E., Cui, T.Y., and Jasin, M. (2001). Homology-directed dna repair, mitomycin-c resistance, and chromosome stability is restored with correction of a Brca1 mutation. *Cancer Res.* *61*, 4842–4850.

- Nouspikel, T., Lalle, P., Leadon, S.A., Cooper, P.K., and Clarkson, S.G. (1997). A common mutational pattern in Cockayne syndrome patients from xeroderma pigmentosum group G: implications for a second XPG function. *Proc. Natl. Acad. Sci. USA* *94*, 3116–3121.
- O'Donovan, A., and Wood, R.D. (1993). Identical defects in DNA repair in xeroderma pigmentosum group G and rodent ERCC group 5. *Nature* *363*, 185–188.
- Okinaka, R.T., Perez-Castro, A.V., Sena, A., Laubscher, K., Strniste, G.F., Park, M.S., Hernandez, R., MacInnes, M.A., and Kraemer, K.H. (1997). Heritable genetic alterations in a xeroderma pigmentosum group G/Cockayne syndrome pedigree. *Mutat. Res.* *385*, 107–114.
- Parpys, A.C., Kratz, K., Speed, M.C., Leung, S.G., Schild, D., and Wiese, C. (2014). RAD51AP1-deficiency in vertebrate cells impairs DNA replication. *DNA Repair (Amst.)* *24*, 87–97.
- Parpys, A.C., Zhao, W., Sharma, N., Groesser, T., Liang, F., Maranon, D.G., Leung, S.G., Grundt, K., Dray, E., Idate, R., et al. (2015). NUCKS1 is a novel RAD51AP1 paralog important for homologous recombination and genome stability. *Nucleic Acids Res.* *43*, 9817–9834.
- Pierce, A.J., Johnson, R.D., Thompson, L.H., and Jasin, M. (1999). XRCC3 promotes homology-directed repair of DNA damage in mammalian cells. *Genes Dev.* *13*, 2633–2638.
- Prakash, R., Zhang, Y., Feng, W., and Jasin, M. (2015). Homologous recombination and human health: the roles of BRCA1, BRCA2, and associated proteins. *Cold Spring Harb. Perspect. Biol.* *7*, a016600.
- Roy, R., Chun, J., and Powell, S.N. (2012). BRCA1 and BRCA2: different roles in a common pathway of genome protection. *Nat. Rev. Cancer* *12*, 68–78.
- San Filippo, J., Sung, P., and Klein, H. (2008). Mechanism of eukaryotic homologous recombination. *Annu. Rev. Biochem.* *77*, 229–257.
- Sarker, A.H., Tsutakawa, S.E., Kostek, S., Ng, C., Shin, D.S., Peris, M., Campeau, E., Tainer, J.A., Nogales, E., and Cooper, P.K. (2005). Recognition of RNA polymerase II and transcription bubbles by XPG, CSB, and TFIIH: insights for transcription-coupled repair and Cockayne Syndrome. *Mol. Cell* *20*, 187–198.
- Schärer, O.D. (2008). Hot topics in DNA repair: the molecular basis for different disease states caused by mutations in TFIIH and XPG. *DNA Repair (Amst.)* *7*, 339–344.
- Schlacher, K., Christ, N., Siaud, N., Egashira, A., Wu, H., and Jasin, M. (2011). Double-strand break repair-independent role for BRCA2 in blocking stalled replication fork degradation by MRE11. *Cell* *145*, 529–542.
- Schlacher, K., Wu, H., and Jasin, M. (2012). A distinct replication fork protection pathway connects Fanconi anemia tumor suppressors to RAD51-BRCA1/2. *Cancer Cell* *22*, 106–116.
- Shiomi, N., Kito, S., Oyama, M., Matsunaga, T., Harada, Y.N., Ikawa, M., Okabe, M., and Shiomi, T. (2004). Identification of the XPG region that causes the onset of Cockayne syndrome by using Xpg mutant mice generated by the cDNA-mediated knock-in method. *Mol. Cell. Biol.* *24*, 3712–3719.
- Sollier, J., Stork, C.T., García-Rubio, M.L., Paulsen, R.D., Aguilera, A., and Cimprich, K.A. (2014). Transcription-coupled nucleotide excision repair factors promote R-loop-induced genome instability. *Mol. Cell* *56*, 777–785.
- Sonoda, E., Sasaki, M.S., Buerstedde, J.M., Bezzubova, O., Shinohara, A., Ogawa, H., Takata, M., Yamaguchi-Iwai, Y., and Takeda, S. (1998). Rad51-deficient vertebrate cells accumulate chromosomal breaks prior to cell death. *EMBO J.* *17*, 598–608.
- Staresinic, L., Fagbemi, A.F., Enzlin, J.H., Gourdin, A.M., Wijgers, N., Dunand-Sauthier, I., Giglia-Mari, G., Clarkson, S.G., Vermeulen, W., and Schärer, O.D. (2009). Coordination of dual incision and repair synthesis in human nucleotide excision repair. *EMBO J.* *28*, 1111–1120.
- Stark, J.M., Pierce, A.J., Oh, J., Pastink, A., and Jasin, M. (2004). Genetic steps of mammalian homologous repair with distinct mutagenic consequences. *Mol. Cell. Biol.* *24*, 9305–9316.
- Su, F., Mukherjee, S., Yang, Y., Mori, E., Bhattacharya, S., Kobayashi, J., Yannone, S.M., Chen, D.J., and Asaithamby, A. (2014). Nonenzymatic role for WRN in preserving nascent DNA strands after replication stress. *Cell Rep.* *9*, 1387–1401.
- Sy, S.M., Huen, M.S., and Chen, J. (2009). PALB2 is an integral component of the BRCA complex required for homologous recombination repair. *Proc. Natl. Acad. Sci. USA* *106*, 7155–7160.
- Thangavel, S., Berti, M., Levikova, M., Pinto, C., Gomathinayagam, S., Vujanovic, M., Zellweger, R., Moore, H., Lee, E.H., Hendrickson, E.A., et al. (2015). DNA2 drives processing and restart of reversed replication forks in human cells. *J. Cell Biol.* *208*, 545–562.
- Thorslund, T., McIlwraith, M.J., Compton, S.A., Lekontsev, S., Petronczki, M., Griffith, J.D., and West, S.C. (2010). The breast cancer tumor suppressor BRCA2 promotes the specific targeting of RAD51 to single-stranded DNA. *Nat. Struct. Mol. Biol.* *17*, 1263–1265.
- Tian, M., Jones, D.A., Smith, M., Shinkura, R., and Alt, F.W. (2004). Deficiency in the nuclease activity of xeroderma pigmentosum G in mice leads to hypersensitivity to UV irradiation. *Mol. Cell. Biol.* *24*, 2237–2242.
- Tibbetts, R.S., Cortez, D., Brumbaugh, K.M., Scully, R., Livingston, D., Elledge, S.J., and Abraham, R.T. (2000). Functional interactions between BRCA1 and the checkpoint kinase ATR during genotoxic stress. *Genes Dev.* *14*, 2989–3002.
- Trego, K.S., Chernikova, S.B., Davalos, A.R., Perry, J.J., Finger, L.D., Ng, C., Tsai, M.S., Yannone, S.M., Tainer, J.A., Campisi, J., and Cooper, P.K. (2011). The DNA repair endonuclease XPG interacts directly and functionally with the WRN helicase defective in Werner syndrome. *Cell Cycle* *10*, 1998–2007.
- Vermeulen, W., and Fousteri, M. (2013). Mammalian transcription-coupled excision repair. *Cold Spring Harb. Perspect. Biol.* *5*, a012625.
- Wei, L., Nakajima, S., Böhm, S., Bernstein, K.A., Shen, Z., Tsang, M., Levine, A.S., and Lan, L. (2015). DNA damage during the G0/G1 phase triggers RNA-templated, Cockayne syndrome B-dependent homologous recombination. *Proc. Natl. Acad. Sci. USA* *112*, E3495–E3504.
- Weinfeld, M., Xing, J.Z., Lee, J., Leadon, S.A., Cooper, P.K., and Le, X.C. (2001). Factors influencing the removal of thymine glycol from DNA in gamma-irradiated human cells. *Prog. Nucleic Acid Res. Mol. Biol.* *68*, 139–149.
- Wiese, C., Dray, E., Groesser, T., San Filippo, J., Shi, I., Collins, D.W., Tsai, M.S., Williams, G.J., Rydberg, B., Sung, P., and Schild, D. (2007). Promotion of homologous recombination and genomic stability by RAD51AP1 via RAD51 recombinase enhancement. *Mol. Cell* *28*, 482–490.
- Xia, B., Sheng, Q., Nakanishi, K., Ohashi, A., Wu, J., Christ, N., Liu, X., Jasin, M., Couch, F.J., and Livingston, D.M. (2006). Control of BRCA2 cellular and clinical functions by a nuclear partner, PALB2. *Mol. Cell* *22*, 719–729.
- Zellweger, R., Dalcher, D., Mutreja, K., Berti, M., Schmid, J.A., Herrador, R., Vindigni, A., and Lopes, M. (2015). Rad51-mediated replication fork reversal is a global response to genotoxic treatments in human cells. *J. Cell Biol.* *208*, 563–579.
- Zeman, M.K., and Cimprich, K.A. (2014). Causes and consequences of replication stress. *Nat. Cell Biol.* *16*, 2–9.
- Zhao, W., Vaithiyalingam, S., San Filippo, J., Maranon, D.G., Jimenez-Sainz, J., Fontenay, G.V., Kwon, Y., Leung, S.G., Lu, L., Jensen, R.B., et al. (2015). Promotion of BRCA2-dependent homologous recombination by DSS1 via RPA targeting and DNA mimicry. *Mol. Cell* *59*, 176–187.

# Chromothripsis and Kataegis Induced by Telomere Crisis

John Maciejowski,<sup>1</sup> Yilong Li,<sup>2</sup> Nazario Bosco,<sup>1</sup> Peter J. Campbell,<sup>2,\*</sup> and Titia de Lange<sup>1,\*</sup>

<sup>1</sup>Laboratory for Cell Biology and Genetics, The Rockefeller University, 1230 York Avenue, New York, NY 10065, USA

<sup>2</sup>Wellcome Trust Sanger Institute, Wellcome Trust Genome Campus, Hinxton Cambridge, CB10 1SA, UK

\*Correspondence: delange@mail.rockefeller.edu (T.d.L.), pc8@sanger.ac.uk (P.J.C.)

<http://dx.doi.org/10.1016/j.cell.2015.11.054>

## SUMMARY

Telomere crisis occurs during tumorigenesis when depletion of the telomere reserve leads to frequent telomere fusions. The resulting dicentric chromosomes have been proposed to drive genome instability. Here, we examine the fate of dicentric human chromosomes in telomere crisis. We observed that dicentric chromosomes invariably persisted through mitosis and developed into 50–200  $\mu\text{m}$  chromatin bridges connecting the daughter cells. Before their resolution at 3–20 hr after anaphase, the chromatin bridges induced nuclear envelope rupture in interphase, accumulated the cytoplasmic 3' nuclease TREX1, and developed RPA-coated single stranded (ss) DNA. CRISPR knockouts showed that TREX1 contributed to the generation of the ssDNA and the resolution of the chromatin bridges. Post-crisis clones showed chromothripsis and kataegis, presumably resulting from DNA repair and APOBEC editing of the fragmented chromatin bridge DNA. We propose that chromothripsis in human cancer may arise through TREX1-mediated fragmentation of dicentric chromosomes formed in telomere crisis.

## INTRODUCTION

The view that dicentric chromosomes are broken in mitosis and undergo breakage-fusion-bridge (BFB) cycles originates from McClintock's cytological observation of corn chromosomes (McClintock, 1938; McClintock, 1941). More recently, the fate of dicentric chromosomes has been studied in yeast as well as plants (reviewed in Stimpson et al., 2012). Here, we document the behavior of dicentric chromosomes in human cells.

Dicentric chromosomes can be formed during the early stages of human tumorigenesis when telomere shortening has led to dysfunctional telomeres (reviewed in Artandi and DePinho, 2010). Telomere shortening induces senescence or apoptosis when a few telomeres lose the ability to repress DNA damage signaling pathways. Telomere fusions are infrequent in senescence, most likely because of the low frequency of dysfunctional telomeres. Upon by-pass of senescence due to loss of p53 and Rb, further telomere attrition increases the incidence of telomere dysfunction, eventually leading to a telomere crisis where telo-

meres fuse to form dicentric chromosomes. These dicentrics have been proposed to drive genome instability in cancer. The genomic scars indicative of past telomere crisis have been observed in several types of cancer (Lin et al., 2010; Lin et al., 2014; Roger et al., 2013; Simpson et al., 2015). However, the fate of dicentric chromosomes, including potential BFB cycles, has been elusive.

The genomic footprint of BFB cycles is a “fold-back” inverted rearrangement that demarcates a region of amplification from a terminal chromosomal deletion. Such events have been observed in pancreatic cancer, esophageal cancer, breast cancer, and leukemias, among others (Bignell et al., 2007; Campbell et al., 2010; Waddell et al., 2015; Li et al., 2014; Nones et al., 2014). Interestingly, several of these studies have suggested an association between the rearrangements of BFB cycles and chromothripsis (Nones et al., 2014; Li et al., 2014). Chromothripsis is a mysterious mutational process in which one or more localized chromosomal regions undergo catastrophic shattering, triggering a haphazard repair process of stitching chromosomal fragments together in a random order and orientation (Stephens et al., 2011). Chromothripsis has been observed across many tumor types (Forment et al., 2012), especially those with p53 loss (Rausch et al., 2012), as well as occasional occurrence in the germline (Kloosterman and Cuppen, 2013). Chromothripsis breakpoints often show clusters of base substitutions localized nearby (kataegis), exhibiting the C>T and C>G signature at TpC dinucleotides associated with APOBEC-mediated mutagenesis (Nik-Zainal et al., 2012a; Roberts et al., 2012; Roberts et al., 2013; Chan et al., 2015).

The mechanism of chromosome fragmentation that gives rise to chromothripsis in cancer is not known and it is not clear when, where, and how the DNA fragments are rejoined. A proposed explanation of the localized nature of chromothripsis is the sequestration of a chromosome (fragment) in a micronucleus where it is shattered while the rest of the genome remains intact (Zhang et al., 2015). Micronuclei in cancer cell lines show abnormalities in DNA replication, transcription, and nuclear envelope (NE) structure, and display DNA damage (reviewed in Hatch and Hetzer, 2015). Importantly, micronuclei show frequent nuclear envelope collapse, which could cause the aforementioned abnormalities (Hatch et al., 2013). Chromothripsis was recently shown to arise after rupture of micronuclei containing lagging chromosomes (Zhang et al., 2015). Therefore, a plausible scenario for the origin of chromothripsis involves a lagging chromosome (fragment), formation of a micronucleus that undergoes nuclear envelope collapse, DNA fragmentation due to impaired DNA replication, and random joining of the DNA fragments

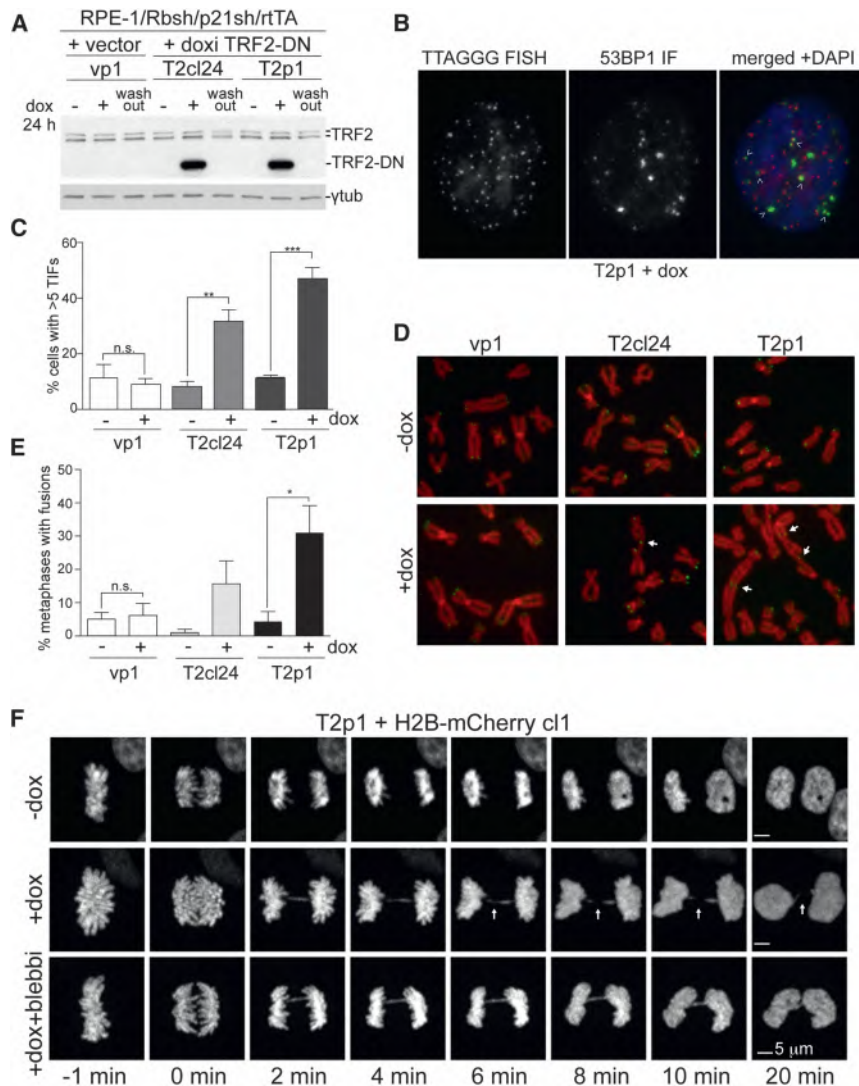


**Figure 1. Dicentric Chromosomes Persist through Anaphase**

(A) Immunoblotting for TRF2 and TRF2-DN 48 hr after dox in the indicated RPE-1 cell lines. Wash-out: 48 hr after removal of dox.

(B) Example of 53BP1 TIFs (arrows) in T2p1 48 hr after dox. Red: telomeric FISH; green: IF for 53BP1; blue: DAPI DNA stain.

(C) Quantification of TIFs as shown in (B). Bar graphs present mean values from three independent experiments (> 49 cells each) and SDs. \*\* $p \leq 0.01$ , \*\*\*;  $p \leq 0.001$  (Student's *t* test).

(D) Metaphases with telomere fusions (arrows) in the indicated cells 48 hr after dox. Red: DAPI DNA stain; green: telomeric FISH.

(E) Quantification of telomere fusions as determined in (D). Data are means and SDs from three independent experiments (> 5600 telomeres per cell line per experiment). n.s., not significant; \* $p \leq 0.05$  (Student's *t* test).

(F) Images of H2B-mCherry marked chromatin at the indicated time points from T2p1 with and without induction (+ and -dox) of telomere fusions with and without blebbistatin. Arrows (+dox images) highlight positions with absent H2B signals. See also related Figure S1 and Movie S1.

upon their incorporation into the primary nucleus (Zhang et al., 2015; Hatch and Hetzer, 2015).

Here, we present data suggesting a telomere-based mechanism for chromothripsis in cancer. Using inducible telomere crisis in vitro, we document chromothripsis and kataegis in half of the descendant clones sequenced. Dicentric chromosomes formed through telomere fusion persisted through mitosis and cytokinesis to form long chromatin bridges between the daughter cells. The DNA in the chromatin bridges became partially single-stranded due to attack by the major cytoplasmic 3' nuclease, TREX1 (DNaseIII) (reviewed in Rice et al., 2015). TREX1 appeared to gain access to the bridge DNA during transient nuclear envelope rupture during interphase (NERDI), and its nucleolytic activity was required for the timely resolution of the chromatin bridges. After bridge resolution, the partially ssDNA generated by TREX1 rejoined the primary nuclei. We infer from sequence analysis of clones emerging from telomere crisis that the ssDNA is processed by APOBEC3A/B-mediated cytosine deamination (reviewed in Roberts and Gordenin, 2014),

(see Table S1). To induce the telomere fusions typical of telomere crisis, we used a dox-inducible dominant negative allele of TRF2 (TRF2-DN), which deprotects telomeres and induces telomere fusions (van Steensel et al., 1998). As expected, doxycycline induced the 53BP1-containing telomere dysfunction-induced foci (TIFs; Takai et al., 2003), which are indicative of TRF2-DN-induced ATM kinase signaling (Karlseder et al., 1999); impaired proliferation; and generated metaphases with telomere fusions (Figures 1A–1E, S1A, and S1B). Whereas the dox-inducible clone T2cl24 showed infrequent fusions, a pool of TRF2-DN expressing cells (T2p1) showed telomere fusions in a large fraction of the metaphases, allowing cell biological experiments (Figures 1A–1E, S1B). Despite the frequent telomere fusions, the induced T2p1 cells formed micronuclei infrequently (Figure S1C).

### Dicentric Chromosomes Persist through Mitosis and Cytokinesis

The behavior of dicentric chromosomes in mitosis was examined using spinning-disk confocal imaging of H2B-mCherry-marked

leading to kataegis, and that the DNA fragments are joined randomly to generate the hallmarks of chromothripsis.

## RESULTS

### An In Vitro Model for Telomere Crisis

To approximate telomere crisis in vitro, we generated a derivative of the hTERT expressing RPE-1 retinal pigment epithelial cell line in which the Rb and p53 pathways were disabled with shRNAs to Rb and p21

chromatin in induced T2p1 cells, which developed anaphase bridges in the majority of mitosis (Figure 2B) as expected since ~1% of the 92 telomeres in these cells undergo fusion (Figure S1B). The images obtained with these cells were similar to those described by McClintock (McClintock, 1938), showing apparent cleavage of the chromatin bridges immediately before or during cytokinesis (Figure 1F, S1D and S1E, Movie S1, panel 1). Imaging with myrPALM-mTurquoise2 to mark the plasma membrane (Zacharias et al., 2002) showed that the H2B signal was diminished only at the site of ingression (Figure S1D and S1E, Movie S1, panel 2), indicating that the disappearance of the H2B signal was likely due to the cleavage furrow pinching the chromatin. Indeed, when ingression was blocked with the actomyosin inhibitor blebbistatin (Straight et al., 2003), the dicentric chromosomes clearly remained intact (0/24 resolution events) (Figure 1F, Movie S1, panel 1). Thus, as is the case in budding yeast (Haber et al., 1984; Lopez et al., 2015; Hill and Bloom, 1989), mammalian dicentric chromosomes can withstand the forces of the mitotic spindle and do not break before cytokinesis. This result is not unexpected given that the spindle force (0.5–1.5 nN) is insufficient to break a mitotic chromosome, which can withstand at least 100 nN (Houchmandzadeh et al., 1997). Cells with dicentrics did not show a delay in their progression through mitosis (Figure S1F) although tubulin remained associated with the midbody slightly longer (Figures S1G and S1H, Movie S1, panel 3).

### Dicentric Chromosomes Develop into Long Chromatin Bridges

To monitor the fate of the dicentric chromosomes after cytokinesis, we captured 108 adjacent fields by spinning-disk confocal imaging at 10 min intervals for 24–48 hr (Figures S2A and S2B). Computational joining of the fields (Preibisch et al., 2009) allowed ~1,000 cells to be followed for 2 days (Movie S2). This “stitching” microscopy of H2B-mCherry labeled cells showed that daughter cells migrated away from each other despite their connecting chromatin bridge (Figures 2A–2D, Movie S3). The chromatin bridges, which were detectable with YOYO-1 in fixed samples (Figure 2C), developed with high frequency and measured 50–200  $\mu\text{m}$  before breaking (Figures 2B and 2D). The H2B-mCherry intensity on the bridges appeared diminished and the IF signals for histones H2A, H2B, and H4 were low (Figure S2C), suggesting the loss of nucleosomes, perhaps due to the stretching of the chromatin bridge (Bennink et al., 2001).

The chromatin bridges remained intact for 3–20 hr with a median persistence time of ~9.3 hr (Figure 2E). Bridge resolution was apparent from a sudden change in morphology, the rapid movement of bridge remnants toward the primary nuclei, and the rapid movement of the daughter cells away from each other (Movie S3). The primary nuclei were often heart-shaped with invaginations opposite from the chromatin bridge, suggesting that the fused chromosome(s) were pulling at the nuclear envelope (Figures 2A and 2C; S2D, Movie S3). After bridge resolution, a small tail of chromatin was observed that shortened and eventually disappeared, most likely because the nuclear envelope regained its rounded state (Figure S2E). In some cases the bridge remnant persisted until the next mitosis (see below). The chromatin bridges did not appear to give rise to micronuclei (0 out of >100 events scored).

To determine the timing of bridge resolution relative to the cell cycle stage of the connected cells, we examined mTurquoise2-RPA70 patterns in the primary nuclei. At the time of bridge rupture, most primary nuclei had diffusely distributed RPA, indicating that they were not yet in S phase. When >90% of the bridges were resolved at 20 hr, fewer than 20% of the primary nuclei showed the punctate RPA pattern indicative of S phase (Figure 2E and S3A–S3C). Therefore, most chromatin bridges were resolved before DNA replication in the primary nuclei. EdU labeling showed no signal on the bridge DNA, suggesting that the chromatin bridges did not undergo aberrant premature DNA replication (Figure 2F).

### Chromatin Bridges Accumulate RPA-Coated ssDNA

Although the chromatin bridges resolved before the primary nuclei entered S phase, ~80% of the bridges contained RPA before and/or at the time of their resolution (Figures 2G, 2H, and S3A–S3F). IF for endogenous RPA32 and imaging of mTurquoise2-RPA70 showed a punctate pattern on the bridges that developed into bright domains just before resolution (Figures 2G, 2H, S3A, and S3B, Movie S3, panel 2).

After bridge resolution, the RPA-coated domains became embedded in the primary nucleus or persisted as short connected tails before joining a daughter nucleus after the next mitosis (Figures S3C–S3F). Once resolved, the bridge remnants showed the presence of  $\gamma\text{H2AX}$ , 53BP1, and Mre11 (Figures S3G–S3I), indicating chromatinization of the DNA and activation of the DNA damage response.

RPA-coated chromatin bridges were also observed after deletion of the shelterin protein TIN2 from mouse cells (Takai et al., 2011). Furthermore, RPA accumulated on chromatin bridges induced by TRF2-DN in the HTC75-T4 cell line, which is derived from the human HT1080 fibrosarcoma cell line (Figures S4A–S4C) (van Steensel et al., 1998). Finally, RPA was present on chromatin bridges resulting from lagging chromosomes induced by either inhibition of the Mps1 kinase (Santaguida et al., 2010) or treatment with nocodazole (Figures S4D–S4G), suggesting that the formation of ssDNA is not a peculiarity of chromatin bridges formed by dicentrics resulting from telomere fusions.

### Chromatin Bridges Have an Altered Nuclear Envelope

IF for the transmembrane nuclear envelope protein LAP2 showed that the chromatin bridges were surrounded by NE (Figures 3A and B). Similarly, BAF1, which binds chromatin and helps assemble the nuclear lamina, was detectable on the chromatin bridges (Figure S4F). In contrast, IF for Lamins A/C and B1; nuclear pore complexes (NPCs) (detected by mAb414 and  $\alpha\text{-TPR}$ ); and the NE proteins SUN1, SUN2, and MAD1 suggested that while the chromatin bridges contained an NE, its composition was altered (Figures 3C–3F and S4F). Specifically, the intensity of Lamin A/C and Lamin B1 staining gradually diminished as the bridges extended and several NE components (e.g., NPCs, SUN1/2, and MAD1) were not detectable (Figures 3C–3F and S4F). Interestingly, Lamin B1 was also depleted from the NE of the primary nuclei (Figure 3E).

### Cells with Chromatin Bridges Undergo NERDI

Some of the cells with chromatin bridges appeared to transiently lose RPA from one of the primary nuclei with a concomitant

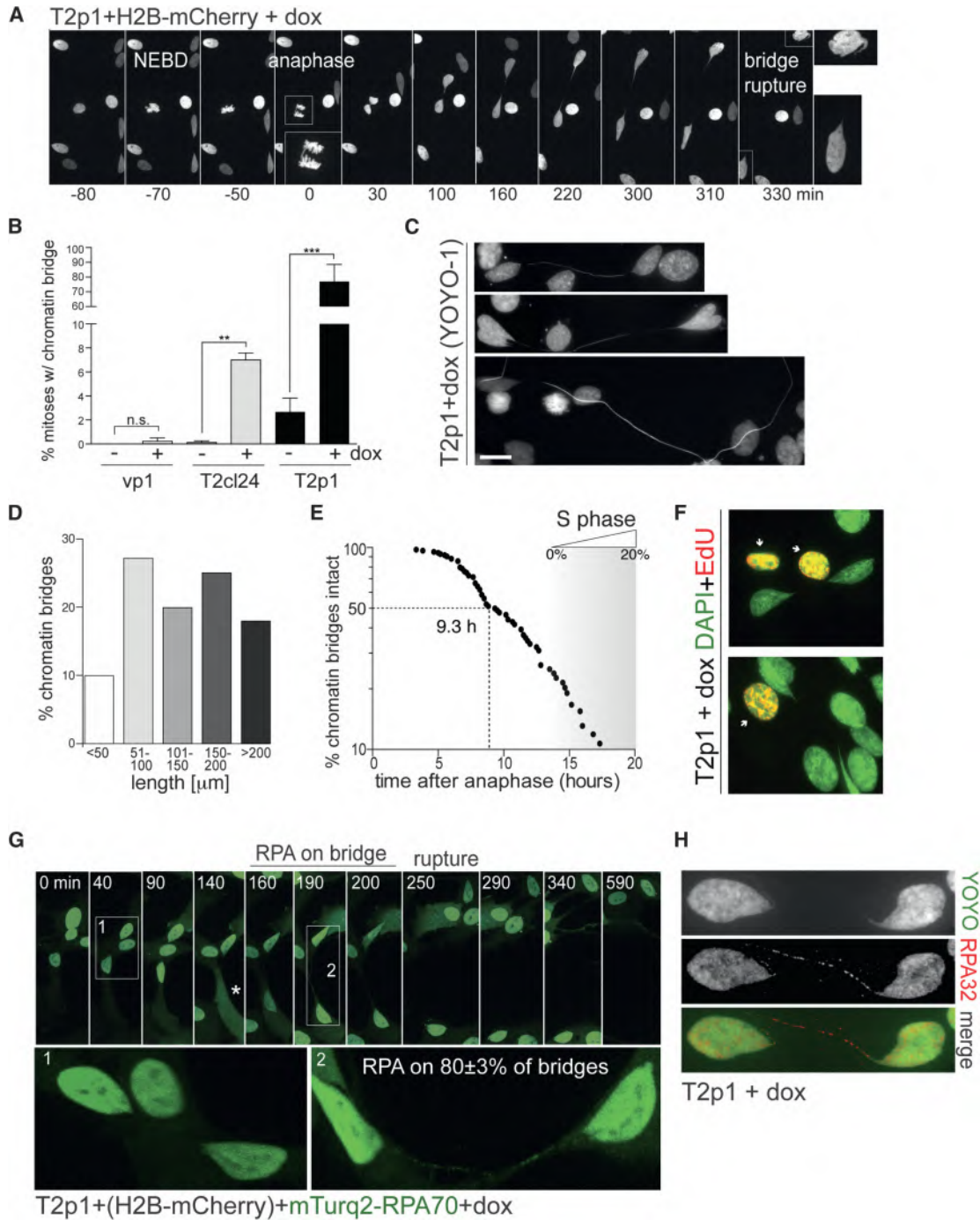


**Figure 2. Dicentric Chromosomes form RPA-Containing Chromatin Bridges**

(A) Images of chromatin from live-cell imaging of T2p1+H2B-mCherry treated with dox. Time points as indicated. NEBD: Nuclear envelope breakdown. Anaphase is shown in enlarged inset. The bridge resolves  $\sim$ 5.5 hr after anaphase. The images of the two daughter nuclei are enlarged on the right.

(B) Quantification of chromatin bridge induction derived from movies as in (A). Bar graphs represent the means and SDs of three independent experiments ( $>$  50 cell divisions per experiment). n.s., not significant;  $**p \leq 0.01$  (Student's *t* test).

(C) Chromatin bridges with YOYO-1 DNA stain. Scale bar, 10  $\mu$ m.

(D) Quantification of chromatin bridge length at resolution. Data derived from movies as in (A).

(E) Measurements of the timing of chromatin bridge resolution in h after anaphase. Data obtained from movies as in (A) ( $n = 84$  from three independent experiments). Entry into S phase was based on RPA patterns. At 20 hr,  $\sim$ 20% of the cells are in S phase.

(F) Two examples of EdU staining (30 min pulse; red) and DAPI stain (green). Note the lack of EdU signal on the chromatin bridges and connected nuclei.

(legend continued on next page)

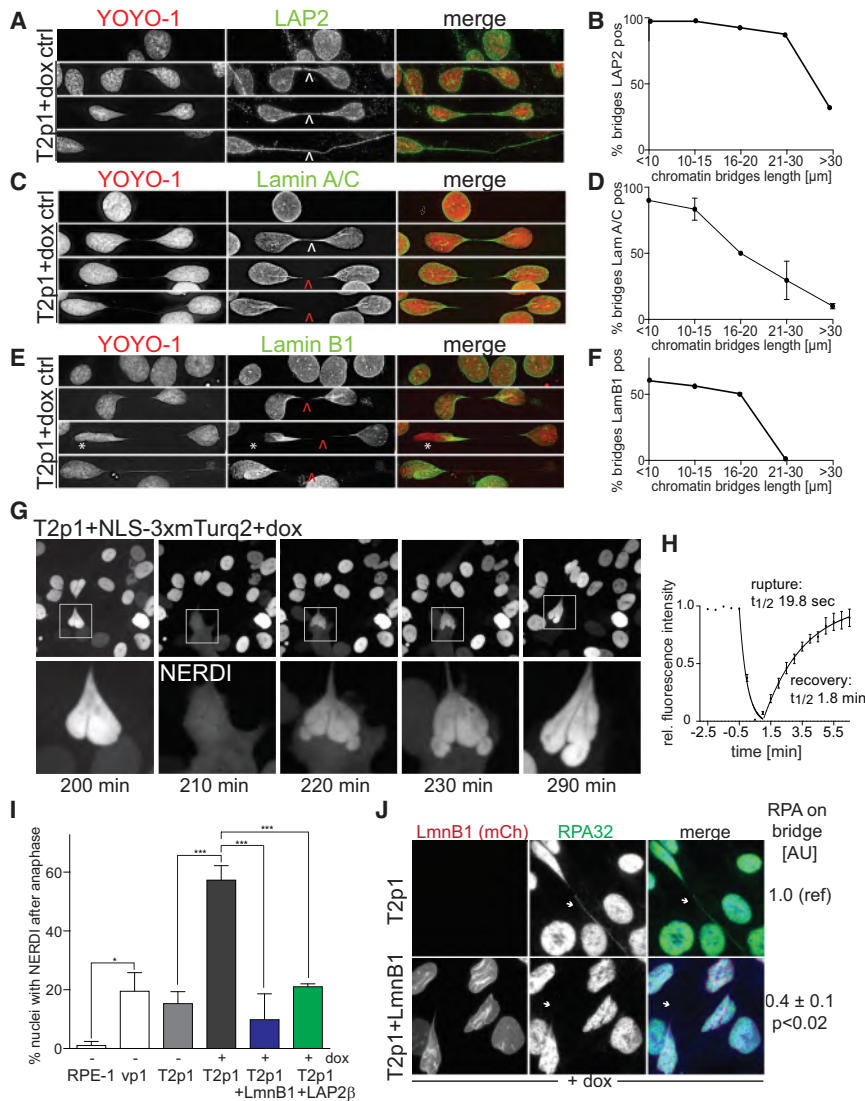


### Figure 3. Transient NERDI Is Frequently Associated with Chromatin Bridges

(A, C, and E) IF for LAP2, Lamin A/C, or Lamin B1 (green) in T2p1 before and 48 hr after induction with dox. DNA stained with YOYO-1 (red). Arrows: white, signals present; red, signals undetectable. Asterisk: loss of Lamin B1 from NE of primary nucleus.

(B, D, and F) Quantification of LAP2, Lamin A/C, and Lamin B1 signals on chromatin bridges of the indicated length classes. Chromatin bridges were classified as positive if the IF signal was contiguous across the entire length of the bridge. Data from > 100 chromatin bridges in two independent experiments. Error bars: SEMs.

(G) Example of transient NERDI in cells with a chromatin bridge. NLS-3xmTurq2 images at the indicated time points from Movie S4. Bottom: enlargements of the transient NERDI.

(H) Duration of NERDI. Data obtained with 30 s interval imaging on 10 cells as in (G). Error bars, SEMs.

(I) Quantification of the frequency of NERDI events occurring in at least one of the two daughter cells within 6 hr of anaphase before and after induction with dox. NERDI was assessed as in (G) but at 5 min intervals over 8 hr after anaphase. For the +dox samples, only cells with chromatin bridges were scored. Data from at least two experiments with > 40 anaphases each. \* $p \leq 0.05$ ; \*\*\* $p \leq 0.001$  (one-way ANOVA with Tukey's correction for multiple comparisons). Error bars, SEMs.

(J) IF of RPA32 (green) with mCherry-Lamin B1 (red) and YOYO-1 stained DNA (blue) in cells with and without Lamin B1 overexpression. Arrows mark chromatin bridges. Note absence of RPA32 on the chromatin bridge in mCherry-Lamin B1 expressing cells. Numbers to the right show quantification (means  $\pm$  SEMs) from > 40 chromatin bridges from two independent experiments.  $p$  value from Student's  $t$  test. See also Figure S4 and Movie S4.

increase of the RPA signal in the cytoplasm (Figure 2G, asterisk). This mis-localization of RPA70 could be explained if the cells experienced NERDI. In micronuclei, NE collapse drives an irreversible loss of compartmentalization (Hatch et al., 2013), whereas in several cancer cell lines, NERDI of the main nucleus is transient (Vargas et al., 2012). Relevant to the anomalous Lamin B1 staining observed in nuclei connected by chromatin bridges (Figure 3E), Lamin B1 depletion exacerbates NERDI (Vargas et al., 2012).

To assay for NERDI, we used a fusion of three tandem copies of mTurquoise2 and the nuclear localization signal (NLS) of SV40

large T, which is confined to the nucleus when the NE is intact. Time-lapse imaging showed that cells with chromatin bridges had frequent and short-lived ( $\sim 5$  min) NERDI as evidenced by the appearance of cytoplasmic NLS-3xmTurq2 and its diminished intensity in the nucleus (Figures 3G and 3H; Movie S4). After NERDI, the nuclear envelope regained its integrity and retained the NLS-3xmTurq2 marker. Cells that did not contain TRF2-DN (vp1; Table S1) and non-induced T2p1 cells exhibited at least one NERDI event in 20% of daughter cell pairs within 6 hr of anaphase (Figure 3I). This high baseline rate of NERDI is likely due to p21 and/or Rb inactivation since NERDI was infrequent

(G) Accumulation of RPA on chromatin bridges before their resolution. T2p1+H2B-mCherry+mTurquoise2-RPA70 cells were examined by live-cell imaging. Stills showing the mTurquoise-RPA70 signal on one chromatin bridge are shown. Enlargements: bridge without and later with RPA70.  $80\% \pm 3\%$  of bridges (mean  $\pm$  SD; 102 bridges from 3 independent experiments) contained RPA. Asterisk: apparent NERDI.

(H) IF for RPA32 (red) on fixed cells with a chromatin bridge. DNA stained with YOYO-1 (green). See also Figure S2, S3, and S4, and Movies S2 and S3.

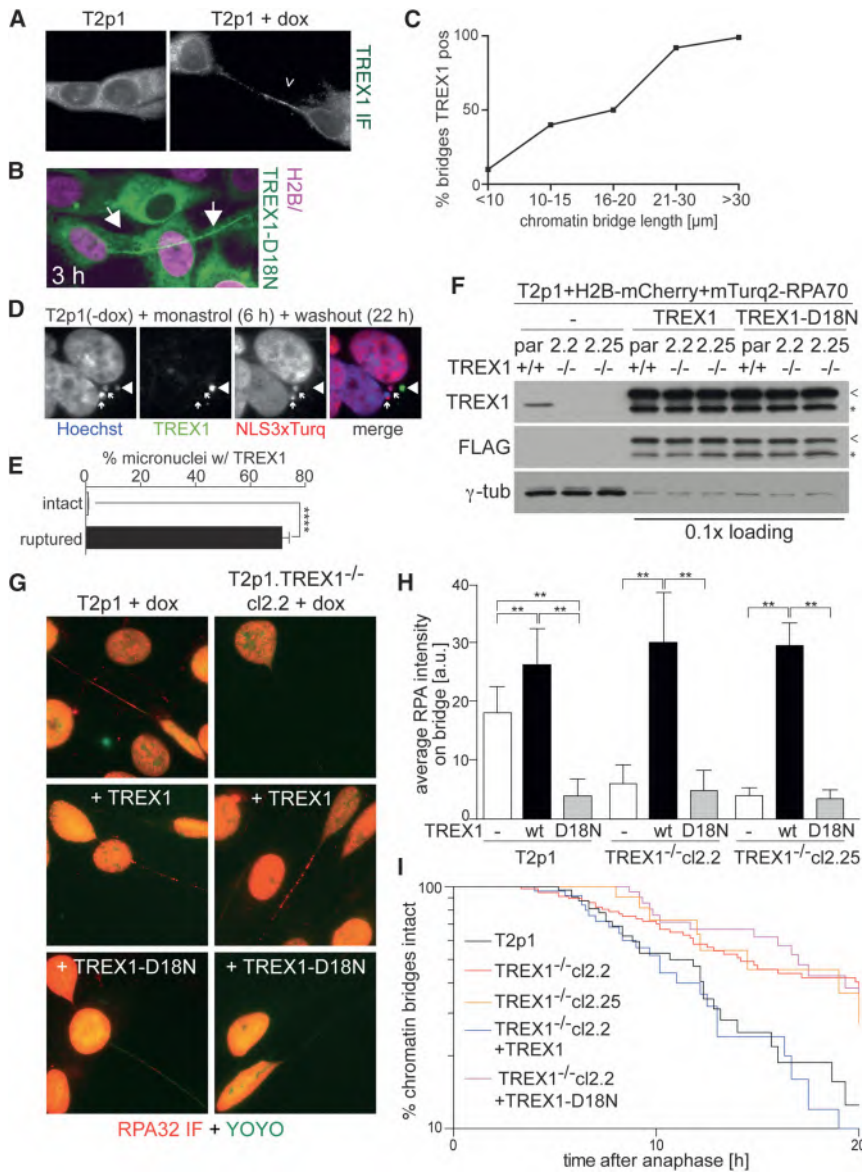


**Figure 4. TREX1 Generates ssDNA in Chromatin Bridges and Promotes Resolution**

(A) IF for TREX1 (white) on T2p1 cells with and without dox.  
 (B) Images from live-cell imaging of mTurq2-TREX1-D18N on a chromatin bridge (Movie S5).  
 (C) Quantification of TREX1 positive chromatin bridges of the indicated length classes. Positively scored chromatin bridges had at least five TREX1 foci. Data from three independent experiments with 100 chromatin bridges each.  
 (D) IF for TREX1 (green) in T2p1 cells with intact (NLS-3xTurq+; arrows) and disrupted (NLS-3xTurq-; arrowhead) micronuclei induced with monastrol.  
 (E) Quantification of TREX1 positive micronuclei as in (D). Over 300 micronuclei were analyzed from three independent experiments. \*\*\*\*p ≤ 0.0001 (Student's t test). Error bars, SEMs.  
 (F) Immunoblotting for endogenous TREX1 and exogenous wild-type and mutant TREX1 (FLAG) in the indicated cell lines. Par: parental T2p1+H2B-mCherry+mTurq2-RPA70 cells. Cl.2.2 and cl.2.25: TREX1 CRISPR KO clones. Arrowheads: full-length FLAG-TREX1. Asterisks: degradation products.  
 (G) Examples of the RPA32 IF in cells as in (F).  
 (H) Quantification of the RPA32 IF intensity on chromatin bridges in cells as in (F). Data were obtained from 55 chromatin bridges from three independent experiments. Bars indicate SDs. \*\*p ≤ 0.01 (Student's t test).  
 (I) Timing of chromatin bridge resolution after anaphase in the indicated cell lines. See legend to Figure 2E.  
 See also related Figure S4 and S5 and Movie S5.

**Chromatin Bridge DNA Is Processed by the Cytoplasmic 3' Exonuclease TREX1**

Although we initially queried nuclear nucleases, the frequent NERDI suggested that a cytoplasmic nuclease might attack the chromatin bridges to generate ssDNA. IF showed that the major cytoplasmic 3' exonuclease TREX1 was present on the chromatin bridges in cells undergoing telomere crisis, whereas TREX1 was only observed in the cytoplasm of control cells (Figure 4A). TREX1 also localized to chromatin bridges induced by telomere dysfunction in the HTC75-T4 cell line and to chromatin bridges formed by lagging chromosomes induced by nocodazole (Figures S4A and S4G). IF analysis and imaging of the inactive mTurq2-tagged TREX1-D18N (Lehtinen et al., 2008) indicated that this nuclease often appears on the chromatin bridges before their rupture (Figures 4B and 4C, Movie S5). IF for TREX1 in micronuclei induced by monastrol also showed TREX1 accumulation specifically in micronuclei that had undergone NE rupture (Figures 4D and 4E).

To test the role of TREX1 in the generation of ssDNA, we used CRISPR/Cas9 to derive TREX1 KO subclones from the T2p1 telomere crisis cell line (Figures S5A and S5B). Loss of TREX1

in the parental RPE1-hTERT cells (Figure 3I). Importantly, NERDI frequency increased to nearly 60% in dox-induced T2p1 daughter cells with chromatin bridges (Figure 3I). NERDI usually occurred in one of the two connected nuclei. Because NERDI can be induced by Lamin B1 depletion (Vargas et al., 2012), we tested whether Lamin B1 or LAP2β overexpression could repress the nuclear envelope rupture in induced T2p1 cells (Figure 3I). Overexpression of both proteins diminished the frequency of NERDI (Figure 3I). Lamin B1 overexpression strongly diminished RPA accumulation on chromatin bridges suggesting that the formation of ssDNA on chromatin bridges depended on NERDI (Figure 3J). We conclude that telomere dysfunction in this cell system induces a significant increase in NERDI. As a result, at least one of the two cells connected by a chromatin bridge is likely to experience a NERDI event within the time period preceding bridge resolution.

was demonstrated by immunoblotting and IF (Figure 4F, S5C, and S5D), and sequence analysis revealed bi-allelic CRISPR gene editing (Figure S5E). The TREX1 KO cell lines showed normal proliferation and, after induction of TRF2-DN, displayed the expected reduced proliferation and chromatin bridges (Figures S5F and S5G). Importantly, IF showed a nearly complete abrogation of the accumulation of RPA on the chromatin bridges in the TREX1 KO cells (Figures 4G and 4H). This absence of RPA accumulation could be reversed by reintroduction of wild-type TREX1, whereas the inactive TREX1-D18N did not have this effect (Figures 4F–4H). Consistent with a previous report (Lehtinen et al., 2008), TREX1-D18N had a dominant-negative effect in the TREX1-proficient parental cell line, significantly reducing the appearance of RPA on the chromatin bridges (Figures 4F–4H). In contrast, overexpression of the wild-type allele in the parental Tp21 cell line slightly increased the accumulation of RPA on the chromatin bridges. As a control, we confirmed that TREX1 deficiency did not diminish RPA foci formed during replication stress (Figures S5H and S5I).

TREX1 deletion from the HTC75-T4 cell line also strongly diminished RPA accumulation on chromatin bridges (Figures S4B and S4C). Furthermore, chromatin bridges resulting from lagging chromosomes induced by Mps1 kinase inhibition failed to accumulate RPA when TREX1 was absent (Figures S4D–S4F). Thus, TREX1 deficiency generally affects the formation of RPA-containing ssDNA in chromatin bridges.

Cells lacking TREX1 showed a significant delay in the resolution of chromatin bridges (Figure 4I). At 20 hr post-anaphase, only 15% of the chromatin bridges in the TREX1-proficient cells remained, whereas more than 40% of the bridges of the TREX1 KO cell line were still intact. The timing of bridge resolution was restored by wild-type TREX1, but not by TREX1-D18N. TREX1-independent mechanisms also contribute to the resolution of the chromatin bridges, since resolution was not abrogated by TREX1 deficiency.

### Frequent Chromothripsis in Post-crisis Clones

To determine the genetic alterations induced by telomere crisis, we isolated post-crisis subclones of T2p1 and T2cl24. Clones were karyotyped to exclude those that had escaped the telomere dysfunction (Figure S6 and Table S2). Clones with aneuploidy and/or marker chromosomes were analyzed by telomere fusion PCR to confirm the presence of telomere fusion (Figure S6C). Ten such post-crisis clones were selected for sequence analysis, as were the parental T2p1, one post-crisis subclone with the parental karyotype (24.2), and seven control subclones derived from uninduced T2p1 cells. We performed whole-genome sequencing on all 19 lines, comparing post-crisis whole-genome sequencing data with that from the parental lines, in order to identify mutations acquired during telomere crisis. None of the subclones derived from the uninduced T2p1 cells showed genomic alterations.

Strikingly, five of ten post-telomere crisis lines showed clusters of genomic rearrangements affecting one or more chromosomes (Figures 5 and S7A). These rearrangements exhibited the hallmarks of chromothripsis, including spatial clustering, randomness of fragment orientation and oscillating copy-number states (Figures 5A, 5B, and S7A) (Korbel and Campbell,

2013). In several examples, the rearrangements were near telomeres and associated with terminal deletions of the chromosome, consistent with products of telomere fusion. Chromothripsis events that are more internal in the chromosomes can also result from telomere fusions since the genomic region in the bridge could be far from the telomere depending on the structure of the dicentric. Sometimes the clustered rearrangements affected one chromosome, sometimes two or three, as has been observed in cancers (Stephens et al., 2011). Importantly, chromothripsis never involved whole chromosomes but rather was localized to specific regions that presumably resided in the chromatin bridge. Consistent with these results, chromothripsis was recently reported in cells that were subjected to TRF2 inhibition and an Mps1 kinase inhibitor (Mardin et al., 2015).

The oscillations of copy number in regions of apparent chromothripsis often sampled three copy-number states. Such a scenario can arise either from a chromothripsis event simultaneously affecting two copies of the same genomic region or from a subsequent duplication of part of a chromothripsis chromosome. These two possibilities can be distinguished by the patterns of copy-number changes across breakpoints in the region (Li et al., 2014). In all examples observed here, the patterns of copy number and rearrangements implied that two copies of the affected genomic regions were simultaneously subjected to the catastrophic shattering and repair of chromothripsis (Figures 5 and S7). Two copies could derive from the end-to-end fusion of sister chromatids that form the chromatin bridge.

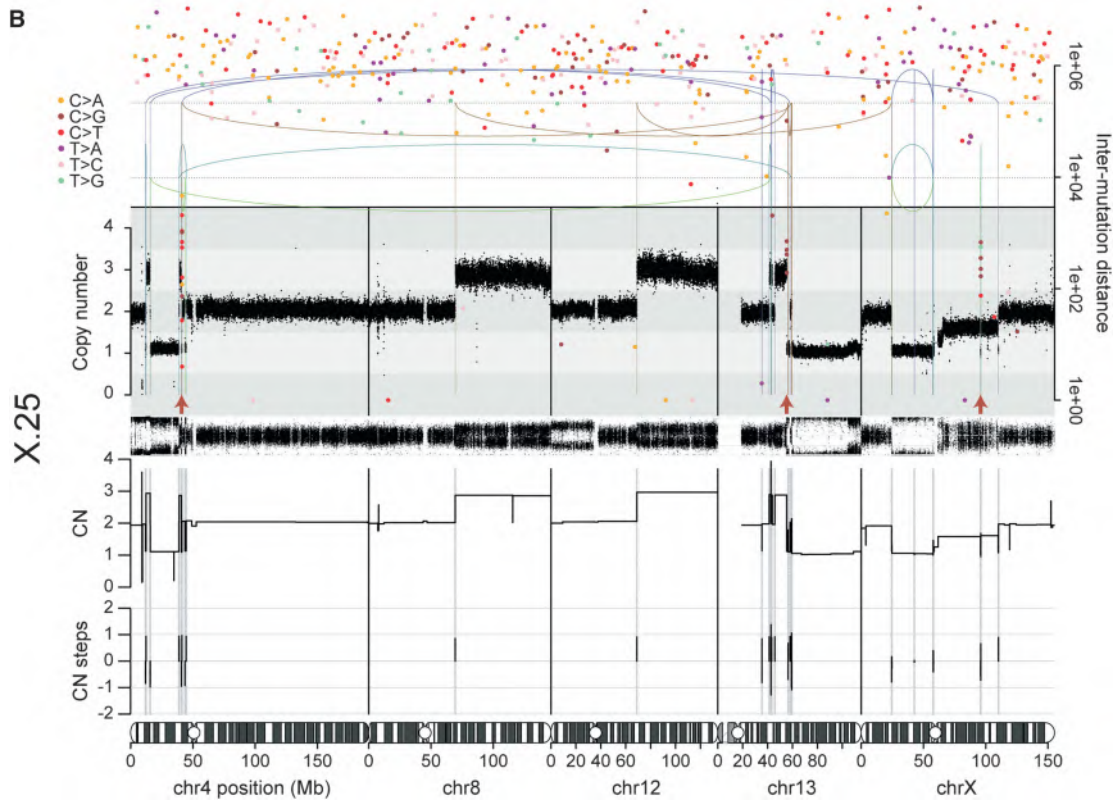
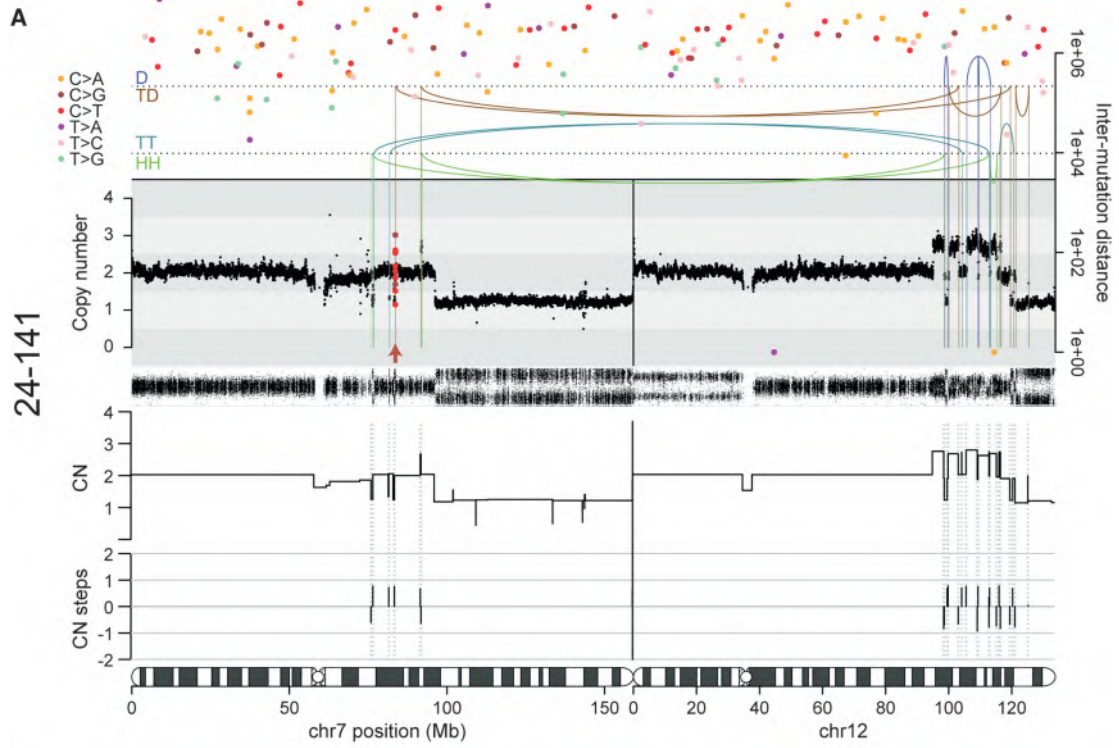
### Kataegis Accompanies Chromothripsis

The recruitment of RPA suggested that chromatin bridges contain extensive ssDNA. As ssDNA represents one of the target substrates for APOBEC enzymes, we hypothesized that the regions caught up in the chromatin bridge would show clusters of point mutations, known as kataegis, analogous to those seen in cancers (Nik-Zainal et al., 2012a; Nik-Zainal et al., 2012b; Roberts et al., 2012).

We observed 29 clusters of point mutations from seven of the ten post-crisis samples sequenced here that were absent from the parental cell lines. These clusters exhibited the cardinal features of kataegis observed in human cancers. First, clusters were often found within a kilobase or two of genomic breakpoints (Figures 6A–6D). These were predominantly in association with chromothripsis rearrangements, although occasional clusters were also found near simpler structural variants (Figure 6C). Second, the clusters exhibited a pronounced preference for C>T and C>G mutations occurring in a TpC context (Figures 6E and 6F), the classic signature of APOBEC3A/B activity (Roberts et al., 2013; Burns et al., 2013a; Burns et al., 2013b; reviewed in Roberts and Gordenin, 2014). Third, the mutation clusters were processive, indicative of the damage occurring on a single strand of DNA (Figures 6A and 6B).

### DISCUSSION

The findings reported here suggest that chromothripsis and kataegis can arise as a consequence of telomere crisis in the early stages of human tumorigenesis (Figure 7). The dicentric



(legend on next page)

chromosomes formed in telomere crisis developed into long chromatin bridges that connect the two primary nuclei until the bridge breaks. Three important events in cells with chromatin bridges can explain the observed chromothripsis and kataegis. First, one of the connected primary nuclei undergoes NERDI that allows entry of the cytoplasmic 3' exonuclease TREX1. Second, TREX1 generates extensive ssDNA in the chromatin bridges. Third, TREX1-mediated processing contributes to the resolution of the bridge, leaving two bridge DNA remnants that each join their primary nucleus. Subsequent repair of the bridge remnant DNA results in random joining of DNA segments typical of chromothripsis. In addition, APOBEC-derived hypermutation is prominent at the boundaries of the rearranged sequences. Since APOBEC enzymes act on ssDNA, the observed kataegis is consistent with the extensive single-stranded nature of the bridge remnants.

Complex clusters of structural variants have been observed in many cancer genomes. Chromothripsis is an extreme example of such clusters, with tens to hundreds of genomic rearrangements affecting one or a few chromosomes or chromosome regions. Especially high rates have been observed in sarcomas, esophageal cancers, and neuroblastomas (Nones et al., 2014; Stephens et al., 2011; Garsed et al., 2014; Mehine et al., 2013), and there appears to be an association with telomere crisis, especially BFB cycles (Li et al., 2014). Our study strengthens this association, suggesting that one of the routes to the chromosome damage that precipitates chromothripsis could be chromatin bridges formed by dicentric chromosomes.

While this study suggests that telomere crisis can precipitate chromothripsis events in cancer, many mechanistic questions remain. These issues are briefly discussed below.

### Formation of Extended Chromatin Bridges

Chromatin bridges have been documented and observed numerous times upon induction of telomere fusions in a wide variety of cell lines, but their significance, duration, and eventual fate had not been determined. In all cases, the chromatin bridges were observed in adherent tissue culture cells. We do not know whether chromatin bridges also develop if cells are grown in soft agar or indeed if such bridges would occur when incipient cancer cells undergo telomere crisis *in vivo*. Presumably, cell migration is not limited to tissue culture settings and takes place in the mass of cells that eventually gives rise to overt cancer. Cell motility is well documented in wound healing and is promoted by the epithelial-mesenchymal transition (EMT) in cancers of epithelial origin (Scheel and Weinberg, 2012). Furthermore, modeling suggests that cell migration is an important contributor to cancer development (Waclaw et al., 2015).

### NERDI in Cells with Chromatin Bridges

In cells with chromatin bridges, NERDI is more frequent and occurs sooner after anaphase. What is the mechanism by which chromatin bridges induce NERDI? One possibility is that the long bridges simply deplete critical NE components (e.g., Lamin B1, Lamin A/C) from the primary nuclei, thus inducing the transient failure in compartmentalization. A second possibility is that the stretching of the bridge exerts mechanical forces on the primary nuclei that overwhelm the resilience of the NE. Indeed, the shape of many of the primary nuclei suggests that considerable pulling forces are exerted by the chromosome(s) in the bridge, but further work is required to understand the exact mechanism by which NERDI occurs. The attachment of human chromosomes to the nuclear lamins (Guelen et al., 2008) could play a role in generating the observed distortions and contribute to NERDI induction.

### Preferential TREX1 Action on Bridge DNA

Why does TREX1 accumulate on the bridge and attack the bridge DNA rather than affecting the chromatin of the primary nucleus undergoing NERDI? One explanation could be that the bridge DNA is in a non-canonical chromatin state. It is possible that the pulling force of the migrating daughter cells results in loss of nucleosomes from the chromatin in the bridge (reviewed in Chien and van Noort, 2009). This mechanical nucleosome removal is consistent with the diminished staining for histones on the chromatin bridges. If TREX1 preferentially binds naked dsDNA, it would be expected to accumulate more on the non-nucleosomal bridge DNA than on the chromatin in the primary nucleus. Indeed, TREX1 degrades naked DNA much faster than nucleosomal DNA (Chowdhury et al., 2006), but whether this effect is due a higher affinity for naked DNA is not known.

Since TREX1 is a 3' exonuclease, it will require nicked DNA substrates for the generation of ssDNA. Indeed, TUNEL staining has previously shown free 3' ends on a chromatin bridge (Gisselsson et al., 2001). The nicks in the bridge DNA could originate from RNaseH2-mediated removal of misincorporated ribonucleotides (Reijns et al., 2012). Another possibility is that the TREX1-associated endonuclease NM23-H1 generates the 3' ends used by the exonuclease (Chowdhury et al., 2006). So far, we have failed to detect NM23-H1 on the chromatin bridges but its abundance there may simply be too low for detection.

### Bridge Resolution

Bridge resolution is strongly correlated with a sudden increase in RPA staining, suggesting that the formation of ssDNA is a critical step. In the absence of TREX1, no or very low amounts of RPA

### Figure 5. Chromothripsis and Kataegis in Post-Crisis Clones 24-141 and X-25

(A) Chromothripsis and rainfall plot of sample 24-141 involving chromosomes 7 and 12.

(B) Chromothripsis and rainfall plot of sample X-25 involving chromosomes 4, 13 and X. The unbalanced rearrangements involving chromosomes 8 and 12 may have taken place together with the chromothripsis event. In (A) and (B), top: the arcs represent the two ends of rearrangements. Arcs are grouped from top to bottom by the type of rearrangement orientation as follows: deletion (D; +-); tandem duplication (TD; -+); tail-tail (TT; ++); head-head (HH;-). Middle: estimated copy number over genomic windows. The variant allele frequency (VAF) track is shown below the copy-number track. Inferred copy-number segments are shown below the VAF track. Bottom: amount of copy-number change between copy-number segments. Chromothripsis after a duplication will yield three copy-number states with copy-number steps of +1 or -1. Duplication after chromothripsis will yield some copy-number steps of +2 or -2. Filled circles: positions of point mutations colored by mutation type. The y axis shows the distance of each mutation to the next on the same chromosome, with the respective axis on the right-hand side of the graph. Red arrows: kataegis clusters.

See also related Figure S6 and S7.

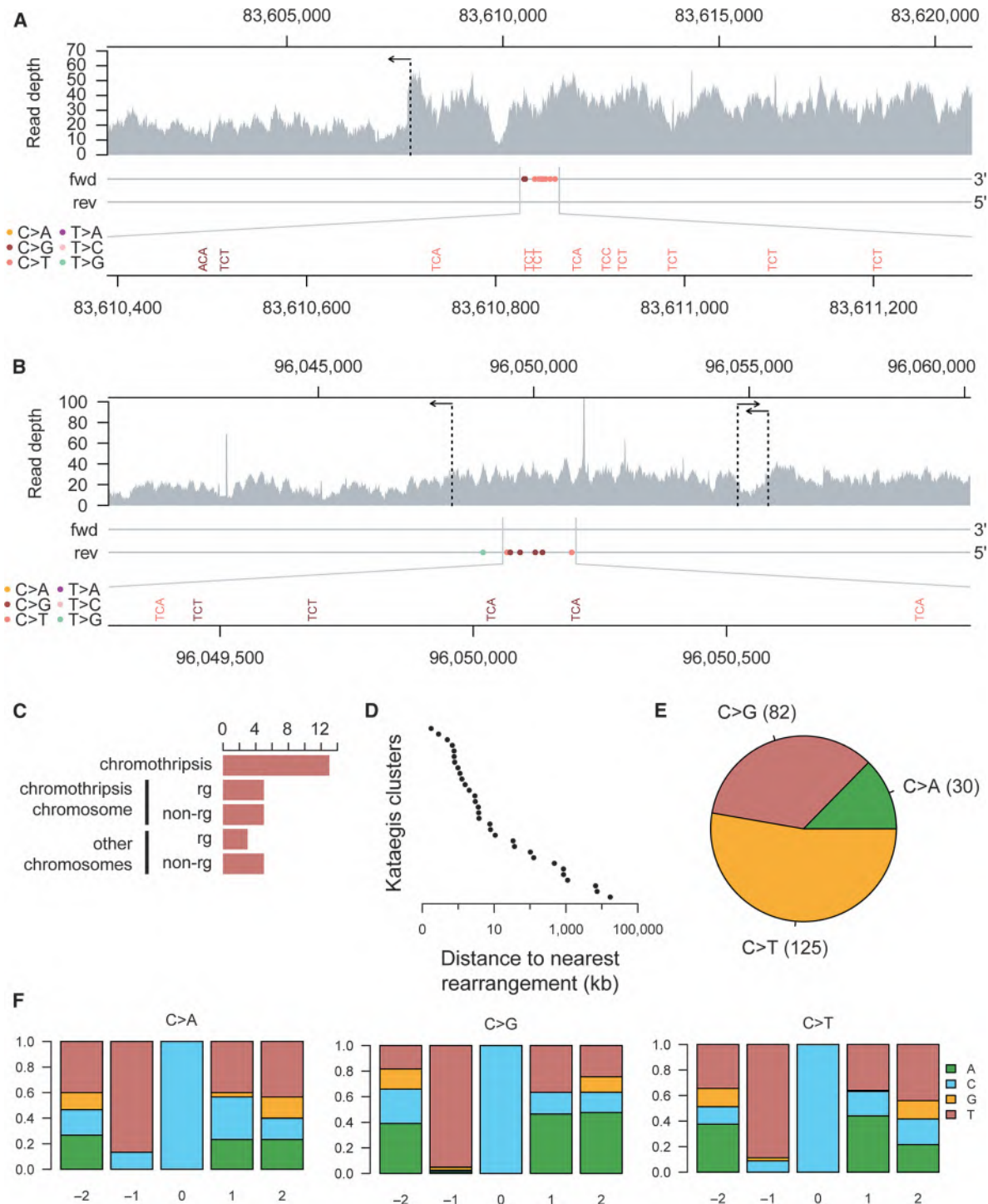


**Figure 6. Mutational Patterns of Kataegis in Post-Crisis Clones**

(A) A chromothripsis-associated kataegis in sample 24-141 on chromosome 7.

(B) A kataegis event in sample X-25 on chromosome X. This kataegis event took place on a chromosome with evidence for chromothripsis, but the rearrangements associated with the kataegis event do not appear to be part of the chromothripsis (Figure 5B). For both (A) and (B), the top panel shows raw read coverage of the region. The horizontal arrows indicate the positions of rearrangements. The two horizontal lines in the middle panel represent the forward and reverse strands. The pyrimidine strands of the mutations called are indicated by their placement on one of the two strands. Mutations are colored by mutation type. The bottom panel magnifies the mutation cluster regions and shows mutation contexts.

(C) The number of kataegis events grouped by their association with rearrangements as follows. From top to bottom: kataegis events within 10 kb of a chromothripsis rearrangement; kataegis events on a chromothripsis chromosome within 10 kb of a non-chromothripsis rearrangement; kataegis events on a

(legend continued on next page)

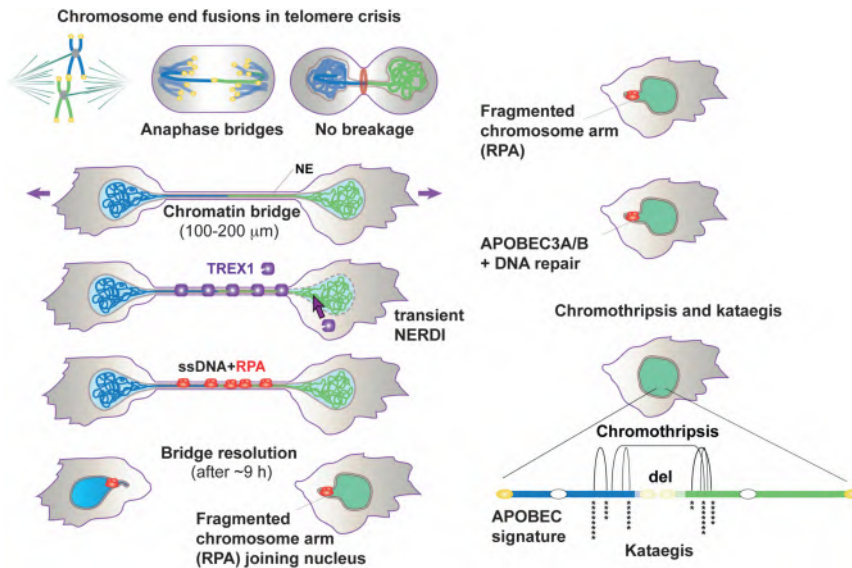


**Figure 7. The Fate of Dicentric Chromosomes Formed in Telomere Crisis**

Telomere fusions in telomere crisis give rise to anaphase bridges that persist and develop into chromatin bridges. Cells with chromatin bridges undergo frequent NERDI and TREX1 accumulates on the chromatin bridge. TREX1 generates RPA-marked ssDNA in the chromatin bridge before their resolution. The RPA marked bridge remnants eventually join the primary nucleus where DNA repair and APOBEC3A/B editing are inferred to take place. Clonal descendants derived from telomere crisis cells show chromothripsis and kataegis.

are detected on the chromatin bridges. The residual RPA staining could be due to another nuclease or could be due to the over-stretching of the DNA, which can lead to RPA-coated denatured DNA in vitro (van Mameren et al., 2009). Although TREX1 is not solely responsible for bridge resolution, it significantly enhances the resolution of the bridges. We imagine that resolution occurs when two TREX1 3' exonucleases acting on the Watson and Crick strands meet.

## CONCLUSIONS

Telomere crisis has previously been shown to give rise to aneuploidy, non-reciprocal translocations, and whole-genome reduplication (Artandi et al., 2000; Davoli and de Lange, 2012; Davoli et al., 2010). The data presented here suggest that chromothripsis and kataegis can be added to the list of cancer-relevant genome alterations that could be the consequence of telomere crisis. It will therefore be of interest to develop better tools to detect telomere crisis in the early stages of cancer. Methods to detect telomere crisis in pre-cancerous lesions may have predictive power with regard to disease progression and outcome.

## EXPERIMENTAL PROCEDURES

Additional experimental procedures are available in Supplemental Information.

### Cell Culture Procedures and Plasmids

RPE1-hTERT and Phoenix cells from the American Type Culture Collection (ATCC) were cultured as described by the ATCC. Drug treatments, retroviral

transduction, and cell cloning were performed using standard conditions (see Supplemental Experimental Procedures). CRISPR/Cas9 knock-outs were generated with sgTREX1-2, 5'-GAGC CCCCCACCTCTC-(PAM)-3' using the gRNA cloning vector (Addgene) and co-transfection with an hCas9 plasmid (Addgene) by nucleofection

(Lonza apparatus). Clones were isolated by limiting dilution, screened for TREX1 deletion by immunoblotting, and sequenced.

### Immunoblotting and Immunofluorescence

Immunoblotting and IF were performed using standard protocols. Cells were incubated with EdU for 30 min prior to PFA fixation and EdU detection with a Click-iT EdU Alexa Fluor 647 imaging kit (Life Technologies).

### Live-Cell Imaging

Cells were plated onto 35 mm glass bottom dishes (MatTek) 48 hr before imaging. One hour before imaging, the media was replaced with phenol red-free DMEM/F12 medium. Live-cell imaging was performed at 37°C and 5% CO<sub>2</sub> using a CellVoyager CV1000 spinning-disk confocal system (Yokogawa, Olympus) equipped with 445, 488, and 561 nm lasers, a Hamamatsu 512 × 512 EMCCD camera, and pinhole size of 50 μm. Details of image acquisition, processing, and quantification are given in the Supplemental Information.

### Telomere Fusion PCR and Karyotypic Analysis

PCR for telomeric fusions and metaphase telomere fusion assays were performed essentially as described (Letsolo et al., 2010; Capper et al., 2007). Karyotypes were determined using standard protocols.

### X-ten Sequencing and Mapping

Genomic DNA sequencing libraries were synthesized on robots and cluster generation and sequencing were performed using the manufacturer pipelines. Average sequence coverage across the samples was 33.3x (range, 27.4–35.9x). Mapping to genome build hs37d5 was performed using the BWA algorithm (BWA mem 0.7.8 (Li and Durbin, 2010)).

### Copy-Number Analysis

The reference genome divided into windows of equivalent read numbers (Campbell et al., 2008; Li et al., 2009) was used to extract reads with a mapping quality of at least 35 and the following flags: Properly paired; non-secondary;

chromothripsis chromosome with no rearrangements within 10 kb; kataegis events on a non-chromothripsis chromosome within 10 kb of a rearrangement; and kataegis events on non-chromothripsis chromosome with no rearrangements within 10 kb.

(D) The distance of each of the 31 detected kataegis events to their nearest respective rearrangement breakpoint.

(E) The frequency distribution of mutation types in the detected kataegis clusters.

(F) The nucleotide context around the mutated cytosine grouped by cytosine mutation type. The relative positions shown are on the pyrimidine (cytosine) strand. The Y-axes show the fraction of each nucleotide on the pyrimidine strand.

See also related Figure S7.

QC-pass; non-duplicate; non-supplementary. Reads overlapping with each window were counted using BEDTools (Quinlan, 2014) and copy numbers were inferred from read depth data (Li et al., 2014).

### Rearrangement Calling and Chromothripsis

Clusters of abnormally paired read pairs were identified from the merged sequence data using an in-house algorithm “Brass.” Raw rearrangement calls supported by clusters of abnormally mapped read pairs were called if the clusters were formed of at least four read pairs all from the same sample. For X-37, which yielded noisier data, at least six read pairs were required. The raw rearrangements were filtered as described previously (Li et al., 2014).

### Mutation Calling and Kataegis

Point mutations were called using an in-house algorithm “Caveman” as before (Nik-Zainal et al., 2012a) with RPE-1/Rbsh/p21sh/rtTA (Table S1) as reference. Raw mutations filtering is described in the Supplemental Information. Kataegis mutation clusters were detected using visual inspection based on the criteria of short inter-mutation distance (generally <2 kb) between cytosine mutations that were processive and enriched with TpC context.

### ACCESSION NUMBERS

The accession number for the genome sequence data reported in this paper is European Genome-Phenome Archive (<http://www.ebi.ac.uk/ega/>, hosted by the EBI): EGAD00001001629 (<https://www.ebi.ac.uk/ega/datasets/EGAD00001001629>).

### SUPPLEMENTAL INFORMATION

Supplemental Information includes Supplemental Experimental Procedures, seven figures, two tables, and five movies and can be found with this article online at <http://dx.doi.org/10.1016/j.cell.2015.11.054>.

### AUTHOR CONTRIBUTIONS

J.M. and T.d.L. designed the experiments. J.M. performed all the cell biological experiments with the help of N.B. Y.L. and P.J.C. performed the genomic analysis on clones derived by J.M. and N.B. T.d.L. and P.J.C. wrote the paper with the help of the other authors.

### ACKNOWLEDGMENTS

We thank Prasad Jallepalli for reagents, Martin Hetzer for discussion, and Zhe Yang for performing PCR validation of chromothriptic breakpoints. We thank S. Yu and the de Lange lab for discussion and help with this manuscript. P. Ariel, T. Tong, and A. North of the RU Bio-imaging Core Facility provided expert assistance with microscopy. The MSKCC Cytogenetics Core acknowledges NIH Cancer Center grant P30 CA008748. J.M. is a Merck Fellow of The Jane Coffin Childs Memorial Fund for Medical Research. Work in P.J.C.’s lab was supported by the Wellcome Trust (077012/Z/05/Z), and P.J.C. holds a Wellcome Trust Senior Clinical Fellowship (WT088340MA). This work was supported by grants from the NCI (5R01CA181090) and the Breast Cancer Research Foundation to T.d.L. T.d.L. is an American Cancer Society Research Professor.

Received: August 18, 2015

Revised: November 3, 2015

Accepted: November 20, 2015

Published: December 17, 2015

### REFERENCES

Artandi, S.E., and DePinho, R.A. (2010). Telomeres and telomerase in cancer. *Carcinogenesis* 31, 9–18.

Artandi, S.E., Chang, S., Lee, S.L., Alson, S., Gottlieb, G.J., Chin, L., and DePinho, R.A. (2000). Telomere dysfunction promotes non-reciprocal translocations and epithelial cancers in mice. *Nature* 406, 641–645.

Bennink, M.L., Leuba, S.H., Leno, G.H., Zlatanova, J., de Groot, B.G., and Greve, J. (2001). Unfolding individual nucleosomes by stretching single chromatin fibers with optical tweezers. *Nat. Struct. Biol.* 8, 606–610.

Bignell, G.R., Santarius, T., Pole, J.C., Butler, A.P., Perry, J., Pleasance, E., Greenman, C., Menzies, A., Taylor, S., Edkins, S., et al. (2007). Architectures of somatic genomic rearrangement in human cancer amplicons at sequence-level resolution. *Genome Res.* 17, 1296–1303.

Burns, M.B., Lackey, L., Carpenter, M.A., Rathore, A., Land, A.M., Leonard, B., Refsland, E.W., Kotandeniya, D., Tretyakova, N., Nikas, J.B., et al. (2013a). APOBEC3B is an enzymatic source of mutation in breast cancer. *Nature* 494, 366–370.

Burns, M.B., Temiz, N.A., and Harris, R.S. (2013b). Evidence for APOBEC3B mutagenesis in multiple human cancers. *Nat. Genet.* 45, 977–983.

Campbell, P.J., Stephens, P.J., Pleasance, E.D., O’Meara, S., Li, H., Santarius, T., Stebbings, L.A., Leroy, C., Edkins, S., Hardy, C., et al. (2008). Identification of somatically acquired rearrangements in cancer using genome-wide massively parallel paired-end sequencing. *Nat. Genet.* 40, 722–729.

Campbell, P.J., Yachida, S., Mudie, L.J., Stephens, P.J., Pleasance, E.D., Stebbings, L.A., Morsberger, L.A., Latimer, C., McLaren, S., Lin, M.L., et al. (2010). The patterns and dynamics of genomic instability in metastatic pancreatic cancer. *Nature* 467, 1109–1113.

Capper, R., Britt-Compton, B., Tankimanova, M., Rowson, J., Letsolo, B., Man, S., Houghton, M., and Baird, D.M. (2007). The nature of telomere fusion and a definition of the critical telomere length in human cells. *Genes Dev.* 21, 2495–2508.

Chan, K., Roberts, S.A., Klimczak, L.J., Sterling, J.F., Saini, N., Malc, E.P., Kim, J., Kwiatkowski, D.J., Fargo, D.C., Mieczkowski, P.A., et al. (2015). An APOBEC3A hypermutation signature is distinguishable from the signature of background mutagenesis by APOBEC3B in human cancers. *Nat. Genet.* 47, 1067–1072.

Chien, F.T., and van Noort, J. (2009). 10 years of tension on chromatin: results from single molecule force spectroscopy. *Curr. Pharm. Biotechnol.* 10, 474–485.

Chowdhury, D., Beresford, P.J., Zhu, P., Zhang, D., Sung, J.S., Demple, B., Perrino, F.W., and Lieberman, J. (2006). The exonuclease TREX1 is in the SET complex and acts in concert with NM23-H1 to degrade DNA during granzyme A-mediated cell death. *Mol. Cell* 23, 133–142.

Davoli, T., and de Lange, T. (2012). Telomere-driven tetraploidization occurs in human cells undergoing crisis and promotes transformation of mouse cells. *Cancer Cell* 21, 765–776.

Davoli, T., Denchi, E.L., and de Lange, T. (2010). Persistent telomere damage induces bypass of mitosis and tetraploidy. *Cell* 141, 81–93.

Forment, J.V., Kaidi, A., and Jackson, S.P. (2012). Chromothripsis and cancer: causes and consequences of chromosome shattering. *Nat. Rev. Cancer* 12, 663–670.

Garsed, D.W., Marshall, O.J., Corbin, V.D., Hsu, A., Di Stefano, L., Schröder, J., Li, J., Feng, Z.P., Kim, B.W., Kowarsky, M., et al. (2014). The architecture and evolution of cancer neochromosomes. *Cancer Cell* 26, 653–667.

Gisselsson, D., Jonson, T., Petersén, A., Strömbeck, B., Dal Cin, P., Höglund, M., Mitelman, F., Mertens, F., and Mandahl, N. (2001). Telomere dysfunction triggers extensive DNA fragmentation and evolution of complex chromosome abnormalities in human malignant tumors. *Proc. Natl. Acad. Sci. USA* 98, 12683–12688.

Guelen, L., Pagie, L., Brasset, E., Meuleman, W., Faza, M.B., Talhout, W., Eussen, B.H., de Klein, A., Wessels, L., de Laat, W., and van Steensel, B. (2008). Domain organization of human chromosomes revealed by mapping of nuclear lamina interactions. *Nature* 453, 948–951.

Haber, J.E., Thorburn, P.C., and Rogers, D. (1984). Meiotic and mitotic behavior of dicentric chromosomes in *Saccharomyces cerevisiae*. *Genetics* 106, 185–205.

- Hatch, E.M., and Hetzer, M.W. (2015). Linking Micronuclei to Chromosome Fragmentation. *Cell* 161, 1502–1504.
- Hatch, E.M., Fischer, A.H., Deerinck, T.J., and Hetzer, M.W. (2013). Catastrophic nuclear envelope collapse in cancer cell micronuclei. *Cell* 154, 47–60.
- Hill, A., and Bloom, K. (1989). Acquisition and processing of a conditional dicentric chromosome in *Saccharomyces cerevisiae*. *Mol. Cell. Biol.* 9, 1368–1370.
- Houchmandzadeh, B., Marko, J.F., Chatenay, D., and Libchaber, A. (1997). Elasticity and structure of eukaryote chromosomes studied by micromanipulation and micropipette aspiration. *J. Cell Biol.* 139, 1–12.
- Karlseder, J., Broccoli, D., Dai, Y., Hardy, S., and de Lange, T. (1999). p53- and ATM-dependent apoptosis induced by telomeres lacking TRF2. *Science* 283, 1321–1325.
- Kloosterman, W.P., and Cuppen, E. (2013). Chromothripsis in congenital disorders and cancer: similarities and differences. *Curr. Opin. Cell Biol.* 25, 341–348.
- Korbel, J.O., and Campbell, P.J. (2013). Criteria for inference of chromothripsis in cancer genomes. *Cell* 152, 1226–1236.
- Lehtinen, D.A., Harvey, S., Mulcahy, M.J., Hollis, T., and Perrino, F.W. (2008). The TREX1 double-stranded DNA degradation activity is defective in dominant mutations associated with autoimmune disease. *J. Biol. Chem.* 283, 31649–31656.
- Letsolo, B.T., Rowson, J., and Baird, D.M. (2010). Fusion of short telomeres in human cells is characterized by extensive deletion and microhomology, and can result in complex rearrangements. *Nucleic Acids Res.* 38, 1841–1852.
- Li, H., and Durbin, R. (2010). Fast and accurate long-read alignment with Burrows-Wheeler transform. *Bioinformatics* 26, 589–595.
- Li, H., Handsaker, B., Wysoker, A., Fennell, T., Ruan, J., Homer, N., Marth, G., Abecasis, G., and Durbin, R.; 1000 Genome Project Data Processing Subgroup (2009). The Sequence Alignment/Map format and SAMtools. *Bioinformatics* 25, 2078–2079.
- Li, Y., Schwab, C., Ryan, S.L., Papaemmanuil, E., Robinson, H.M., Jacobs, P., Moorman, A.V., Dyer, S., Borrow, J., Griffiths, M., et al. (2014). Constitutional and somatic rearrangement of chromosome 21 in acute lymphoblastic leukaemia. *Nature* 508, 98–102.
- Lin, T.T., Letsolo, B.T., Jones, R.E., Rowson, J., Pratt, G., Hewamana, S., Feigan, C., Pepper, C., and Baird, D.M. (2010). Telomere dysfunction and fusion during the progression of chronic lymphocytic leukemia: evidence for a telomere crisis. *Blood* 116, 1899–1907.
- Lin, T.T., Norris, K., Heppel, N.H., Pratt, G., Allan, J.M., Allsup, D.J., Bailey, J., Cawkwell, L., Hills, R., Grimstead, J.W., et al. (2014). Telomere dysfunction accurately predicts clinical outcome in chronic lymphocytic leukaemia, even in patients with early stage disease. *Br. J. Haematol.* 167, 214–223.
- Lopez, V., Barinova, N., Onishi, M., Pobięga, S., Pringle, J.R., Dubrana, K., and Marcand, S. (2015). Cytokinesis breaks dicentric chromosomes preferentially at pericentromeric regions and telomere fusions. *Genes Dev.* 29, 322–336.
- Mardin, B.R., Drinas, A.P., Waszak, S.M., Weischenfeldt, J., Isokane, M., Stütz, A.M., Raeder, B., Efthymiopoulos, T., Buccitelli, C., Segura-Wang, M., et al. (2015). A cell-based model system links chromothripsis with hyperploidy. *Mol. Syst. Biol.* 11, 828.
- McClintock, B. (1938). The Production of Homozygous Deficient Tissues with Mutant Characteristics by Means of the Aberrant Mitotic Behavior of Ring-Shaped Chromosomes. *Genetics* 23, 315–376.
- McClintock, B. (1941). The stability of broken ends of chromosomes in *Zea mays*. *Genetics* 26, 234–282.
- Mehine, M., Kaasinen, E., Mäkinen, N., Katainen, R., Kämpjärvi, K., Pitkänen, E., Heinonen, H.R., Bützow, R., Kilpivaara, O., Kuosmanen, A., et al. (2013). Characterization of uterine leiomyomas by whole-genome sequencing. *N. Engl. J. Med.* 369, 43–53.
- Nik-Zainal, S., Alexandrov, L.B., Wedge, D.C., Van Loo, P., Greenman, C.D., Raine, K., Jones, D., Hinton, J., Marshall, J., Stebbings, L.A., et al.; Breast Cancer Working Group of the International Cancer Genome Consortium (2012a). Mutational processes molding the genomes of 21 breast cancers. *Cell* 149, 979–993.
- Nik-Zainal, S., Van Loo, P., Wedge, D.C., Alexandrov, L.B., Greenman, C.D., Lau, K.W., Raine, K., Jones, D., Marshall, J., Ramakrishna, M., et al.; Breast Cancer Working Group of the International Cancer Genome Consortium (2012b). The life history of 21 breast cancers. *Cell* 149, 994–1007.
- Nones, K., Waddell, N., Wayte, N., Patch, A.M., Bailey, P., Newell, F., Holmes, O., Fink, J.L., Quinn, M.C., Tang, Y.H., et al. (2014). Genomic catastrophes frequently arise in esophageal adenocarcinoma and drive tumorigenesis. *Nat. Commun.* 5, 5224.
- Preibisch, S., Saalfeld, S., and Tomancak, P. (2009). Globally optimal stitching of tiled 3D microscopic image acquisitions. *Bioinformatics* 25, 1463–1465.
- Quinlan, A.R. (2014). BEDTools: The Swiss-Army Tool for Genome Feature Analysis. *Curr. Protoc. Bioinformatics* 47, 1–34.
- Rausch, T., Jones, D.T., Zapatka, M., Stütz, A.M., Zichner, T., Weischenfeldt, J., Jäger, N., Remke, M., Shih, D., Northcott, P.A., et al. (2012). Genome sequencing of pediatric medulloblastoma links catastrophic DNA rearrangements with TP53 mutations. *Cell* 148, 59–71.
- Reijns, M.A., Rabe, B., Rigby, R.E., Mill, P., Astell, K.R., Lettice, L.A., Boyle, S., Leitch, A., Keighren, M., Kilanowski, F., et al. (2012). Enzymatic removal of ribonucleotides from DNA is essential for mammalian genome integrity and development. *Cell* 149, 1008–1022.
- Rice, G.I., Rodero, M.P., and Crow, Y.J. (2015). Human disease phenotypes associated with mutations in TREX1. *J. Clin. Immunol.* 35, 235–243.
- Roberts, S.A., and Gordenin, D.A. (2014). Hypermutation in human cancer genomes: footprints and mechanisms. *Nat. Rev. Cancer* 14, 786–800.
- Roberts, S.A., Sterling, J., Thompson, C., Harris, S., Mav, D., Shah, R., Klimczak, L.J., Kryukov, G.V., Malc, E., Mieczkowski, P.A., et al. (2012). Clustered mutations in yeast and in human cancers can arise from damaged long single-strand DNA regions. *Mol. Cell* 46, 424–435.
- Roberts, S.A., Lawrence, M.S., Klimczak, L.J., Grimm, S.A., Fargo, D., Stojanov, P., Kiezun, A., Kryukov, G.V., Carter, S.L., Saksena, G., et al. (2013). An APOBEC cytidine deaminase mutagenesis pattern is widespread in human cancers. *Nat. Genet.* 45, 970–976.
- Roger, L., Jones, R.E., Heppel, N.H., Williams, G.T., Sampson, J.R., and Baird, D.M. (2013). Extensive telomere erosion in the initiation of colorectal adenomas and its association with chromosomal instability. *J. Natl. Cancer Inst.* 105, 1202–1211.
- Santaguida, S., Tighe, A., D'Alise, A.M., Taylor, S.S., and Musacchio, A. (2010). Dissecting the role of MPS1 in chromosome biorientation and the spindle checkpoint through the small molecule inhibitor reversine. *J. Cell Biol.* 190, 73–87.
- Scheel, C., and Weinberg, R.A. (2012). Cancer stem cells and epithelial-mesenchymal transition: concepts and molecular links. *Semin. Cancer Biol.* 22, 396–403.
- Simpson, K., Jones, R.E., Grimstead, J.W., Hills, R., Pepper, C., and Baird, D.M. (2015). Telomere fusion threshold identifies a poor prognostic subset of breast cancer patients. *Mol. Oncol.* 9, 1186–1193.
- Stephens, P.J., Greenman, C.D., Fu, B., Yang, F., Bignell, G.R., Mudie, L.J., Pleasance, E.D., Lau, K.W., Beare, D., Stebbings, L.A., et al. (2011). Massive genomic rearrangement acquired in a single catastrophic event during cancer development. *Cell* 144, 27–40.
- Stimpson, K.M., Matheny, J.E., and Sullivan, B.A. (2012). Dicentric chromosomes: unique models to study centromere function and inactivation. *Chromosome Res.* 20, 595–605.
- Straight, A.F., Cheung, A., Limouze, J., Chen, I., Westwood, N.J., Sellers, J.R., and Mitchison, T.J. (2003). Dissecting temporal and spatial control of cytokinesis with a myosin II inhibitor. *Science* 299, 1743–1747.
- Takai, K.K., Kibe, T., Donigian, J.R., Frescas, D., and de Lange, T. (2011). Telomere protection by TPP1/POT1 requires tethering to TIN2. *Mol. Cell* 44, 647–659.
- Takai, H., Smogorzewska, A., and de Lange, T. (2003). DNA damage foci at dysfunctional telomeres. *Curr. Biol.* 13, 1549–1556.

- van Mameren, J., Gross, P., Farge, G., Hooijman, P., Modesti, M., Falkenberg, M., Wuite, G.J., and Peterman, E.J. (2009). Unraveling the structure of DNA during overstretching by using multicolor, single-molecule fluorescence imaging. *Proc. Natl. Acad. Sci. USA* 106, 18231–18236.
- van Steensel, B., Smogorzewska, A., and de Lange, T. (1998). TRF2 protects human telomeres from end-to-end fusions. *Cell* 92, 401–413.
- Vargas, J.D., Hatch, E.M., Anderson, D.J., and Hetzer, M.W. (2012). Transient nuclear envelope rupturing during interphase in human cancer cells. *Nucleus* 3, 88–100.
- Waclaw, B., Bozic, I., Pittman, M.E., Hruban, R.H., Vogelstein, B., and Nowak, M.A. (2015). A spatial model predicts that dispersal and cell turnover limit intratumour heterogeneity. *Nature* 525, 261–264.
- Waddell, N., Pajic, M., Patch, A.M., Chang, D.K., Kassahn, K.S., Bailey, P., Johns, A.L., Miller, D., Nones, K., Quek, K., et al.; Australian Pancreatic Cancer Genome Initiative (2015). Whole genomes redefine the mutational landscape of pancreatic cancer. *Nature* 518, 495–501.
- Zacharias, D.A., Violin, J.D., Newton, A.C., and Tsien, R.Y. (2002). Partitioning of lipid-modified monomeric GFPs into membrane microdomains of live cells. *Science* 296, 913–916.
- Zhang, C.Z., Spektor, A., Cornils, H., Francis, J.M., Jackson, E.K., Liu, S., Meyerson, M., and Pellman, D. (2015). Chromothripsis from DNA damage in micronuclei. *Nature* 522, 179–184.

# HELB Is a Feedback Inhibitor of DNA End Resection

Ján Tkáč,<sup>1,2,9</sup> Guotai Xu,<sup>3,9</sup> Hemanta Adhikary,<sup>4,5</sup> Jordan T.F. Young,<sup>1,2</sup> David Gallo,<sup>6</sup> Cristina Escribano-Díaz,<sup>1</sup> Jana Krietsch,<sup>4,5</sup> Alexandre Orthwein,<sup>1</sup> Meagan Munro,<sup>1</sup> Wendy Sol,<sup>3</sup> Abdallah Al-Hakim,<sup>1</sup> Zhen-Yuan Lin,<sup>1</sup> Jos Jonkers,<sup>7</sup> Piet Borst,<sup>3</sup> Grant W. Brown,<sup>6</sup> Anne-Claude Gingras,<sup>1,2</sup> Sven Rottenberg,<sup>3,8</sup> Jean-Yves Masson,<sup>4,5</sup> and Daniel Durocher<sup>1,2,\*</sup>

<sup>1</sup>Lunenfeld-Tanenbaum Research Institute, Mount Sinai Hospital, 600 University Avenue, Toronto, ON M5G 1X5, Canada

<sup>2</sup>Department of Molecular Genetics, University of Toronto, ON M5S 1A8, Canada

<sup>3</sup>Division of Molecular Oncology, Netherlands Cancer Institute, Plesmanlaan 121, 1066 CX Amsterdam, the Netherlands

<sup>4</sup>Genome Stability Laboratory, CHU de Québec Research Center, HDQ Pavilion, Oncology Axis, 9 McMahan, Québec City, QC G1R 2J6, Canada

<sup>5</sup>Department of Molecular Biology, Medical Biochemistry and Pathology, Laval University, Québec City, QC G1V 0A6, Canada

<sup>6</sup>Department of Biochemistry and Donnelly Centre for Cellular and Biomolecular Research, University of Toronto, ON M5S 3E1, Canada

<sup>7</sup>Division of Molecular Pathology, Netherlands Cancer Institute, Plesmanlaan 121, 1066 CX Amsterdam, the Netherlands

<sup>8</sup>Institute of Animal Pathology, Vetsuisse Faculty, University of Bern, Laenggassstrasse 122, 3012 Bern, Switzerland

<sup>9</sup>Co-first author

\*Correspondence: durocher@lunenfeld.ca

<http://dx.doi.org/10.1016/j.molcel.2015.12.013>

## SUMMARY

DNA double-strand break repair by homologous recombination is initiated by the formation of 3' single-stranded DNA (ssDNA) overhangs by a process termed end resection. Although much focus has been given to the decision to initiate resection, little is known of the mechanisms that regulate the ongoing formation of ssDNA tails. Here we report that DNA helicase B (HELB) underpins a feedback inhibition mechanism that curtails resection. HELB is recruited to ssDNA by interacting with RPA and uses its 5'-3' ssDNA translocase activity to inhibit EXO1 and BLM-DNA2, the nucleases catalyzing resection. HELB acts independently of 53BP1 and is exported from the nucleus as cells approach S phase, concomitant with the upregulation of resection. Consistent with its role as a resection antagonist, loss of HELB results in PARP inhibitor resistance in BRCA1-deficient tumor cells. We conclude that mammalian DNA end resection triggers its own inhibition via the recruitment of HELB.

## INTRODUCTION

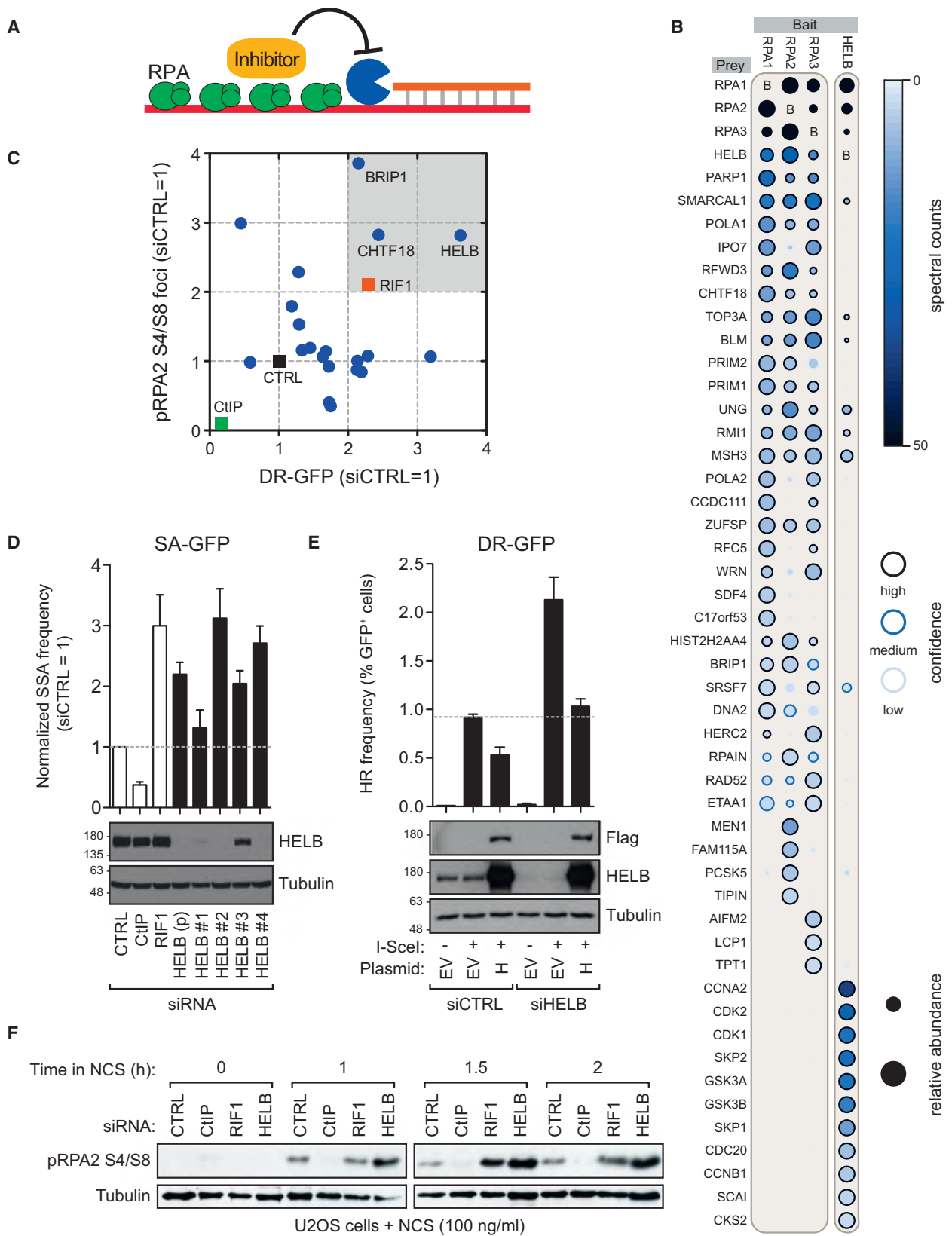
The maintenance of genomic integrity necessitates a profound integration of DNA repair with the cell division cycle (Chapman et al., 2012; Symington and Gautier, 2011). In particular, the fidelity of DNA double-strand break (DSB) repair by homologous recombination (HR) depends on the presence of a sister chromatid produced by DNA replication, as it provides an ideal template for the HR reaction (Jasin and Rothstein, 2013). HR is thus suppressed during G1 and is activated as cells enter S phase (Orthwein et al., 2015). Cells remain HR competent until they enter mitosis, a period during which DSB repair

is suppressed for the benefit of accurate chromosome segregation (Orthwein et al., 2014).

The regulation of HR by the cell cycle depends in large part on the regulation of DNA end resection, as it is the initiating step in HR (Ferretti et al., 2013). Cyclin-dependent kinases (CDKs), which drive cell-cycle progression, provide a “go” signal for resection through the activation of various DNA end resection factors such as CtIP (Huertas and Jackson, 2009; Polato et al., 2014; Yun and Hiom, 2009), Dna2 (in yeast) (Chen et al., 2011), EXO1 (Tomimatsu et al., 2014), and NBS1 (Falck et al., 2012; Ferretti et al., 2013).

CDKs must also provide a one-two punch in favor of end resection by simultaneously relieving the inhibitory mechanisms that actively suppress resection in G1. One mechanism antagonized by CDKs is the end protection pathway controlled by 53BP1 and its interacting proteins RIF1 and PTIP (Bothmer et al., 2010; Callen et al., 2013; Chapman et al., 2013; Di Virgilio et al., 2013; Escribano-Díaz et al., 2013; Feng et al., 2013; Zimmermann et al., 2013). REV7 (also known as MAD2L2) is also a participant in this pathway, acting downstream of RIF1 (Boersma et al., 2015; Xu et al., 2015). In G1, 53BP1 accumulates on the chromatin surrounding DSB sites, where it recruits RIF1 to block the accumulation of BRCA1, a positive regulator of resection (Chapman et al., 2012; Panier and Durocher, 2013). As cells enter S phase, CDKs promote the interaction of CtIP with BRCA1, resulting in the inhibition of RIF1 accumulation at DSB sites (Chapman et al., 2013; Escribano-Díaz et al., 2013).

It seems unlikely that the antagonism of end protection by CDKs is the only inhibitory mechanism that must be relieved to trigger long-range end resection. One under-explored avenue is the process of resection itself. As noted by Symington and Gautier (2011), it is unknown whether mechanisms exist to curtail end resection after it is launched, but we surmised that such processes would represent an effective way to modulate resection. We reasoned that a negative-feedback pathway underpinned by RPA would be an especially attractive means to control the formation of single-stranded DNA (ssDNA), because the accumulation of RPA at resected DSB sites correlates with end resection



(legend on next page)

(Figure 1A). Here we report that the ATP-dependent motor HELB is recruited to resected DNA ends by RPA to inhibit EXO1- and BLM-DNA2-dependent end resection in human and mouse cells. This mechanism operates independently of 53BP1 and is influenced by the rise of CDK activity as cells approach S phase. Indeed, HELB is exported from the nucleus in a CDK2-dependent manner as cells approach and progress through S phase, causing a drop in the nuclear concentration of HELB that we propose stimulates long-range resection. In line with a role as an inhibitor of resection, loss of HELB partially restores HR in BRCA1-deficient mammary tumor cells and causes resistance to poly(ADP-ribose) polymerase (PARP) inhibition in cell and allograft models.

## RESULTS

### HELB Is an RPA-Interacting Protein that Limits Resection in Human Cells

To identify RPA-dependent resection inhibitors, we sought to identify RPA-interacting proteins and then mine them for negative regulators of end resection. We carried out immunoprecipitations (IPs) of all three RPA subunits, followed by mass spectrometry (MS). Briefly, each RPA subunit was tagged with the Flag epitope, and stable human embryonic kidney 293 (HEK293)-derived cell lines were generated using the Flp-In/T-REX system. Twelve IP-MS experiments were carried out (three biological replicates for each RPA subunit and control cell lines) using extracts of cells treated with neocarzinostatin (NCS), a radiomimetic drug. The proteins were identified by MASCOT and then subjected to SAINT analysis (Choi et al., 2011) to identify high-confidence interactors (Figure 1B). Twenty-six proteins were found to interact with two or all three RPA subunits (Table S4), and this list comprised known RPA interactors such as DNA polymerase  $\alpha$  (POLA1/2, PRIM1/2), the Werner syndrome helicase, and the UNG glycosylase. We also identified previously unrecognized RPA interactors such as ETAA1 and ZUFSP (Figure 1B).

Next, small interfering RNA (siRNA) pools targeting 20 of the 26 RPA interactors (Table S1) were screened in two orthogonal assays that are responsive to changes in end resection. First, we monitored the formation of pRPA2 S4/S8 foci following NCS treatment, using high-content microscopy (Figure S1A). RPA2 S4/S8 phosphorylation occurs when RPA is bound to ssDNA at DSB sites (Marechal and Zou, 2014). RPA phosphory-

lation was assessed in a U2OS cell line carrying the FUCCI cell-cycle reporter (Sakae-Sawano et al., 2008), which enabled us to restrict our analysis to S/G2-phase cells. In a second assay, we assessed DSB repair by HR using the direct repeat (DR)-GFP reporter (Pierce et al., 1999). As controls, along with a non-targeting siRNA, we used siRNAs against CtIP and RIF1 whose knock-down cause lower and higher levels of resection, respectively. When the average of two biological replicates was analyzed, three siRNA pools led to increases in both assays that were equal or superior to those seen with the depletion of RIF1 (Figure 1C; Table S1). Those three siRNA pools targeted BRIP1, CHTF18, and HELB.

Since BRIP1 promotes HR (Litman et al., 2005), the phenotype observed was likely due to an siRNA off-target effect, and BRIP1 was not pursued further. Of the remaining two candidates, we focused on HELB because its function in genome maintenance is poorly understood. As a third assay, we assessed whether HELB depletion affected DSB repair by single-strand annealing (SSA) using the strand annealing (SA)-GFP reporter (Stark et al., 2004). SSA occurs when end resection reveals complementary DNA sequences that are annealed and processed to generate interstitial deletions. Because it is a RAD51-independent process, conditions that increase both SSA and gene conversion (as in the DR-GFP assay) are indicative of increased resection (Stark et al., 2004). We found that the siRNA pool and two of four individual siRNAs targeting HELB efficiently depleted the protein and resulted in increased SSA by 2-fold or more (Figures 1D and S1B). We then generated a HELB expression vector that produces an mRNA resistant to siRNA #2 and confirmed that the increase in gene conversion imparted by HELB depletion could be rescued by reintroduction of HELB (Figure 1E). Together, these results suggest that HELB depletion causes an increase in resection. In support of this possibility, RPA2 S4/S8 phosphorylation by immunoblotting (Figures 1F and S1D) and RPA focus formation in response to NCS treatment (Figure S1C) were both increased by HELB depletion, consistent with increased resection.

### RPA Recruits HELB to DSB Sites

HELB, schematically depicted in Figure 2A, is a helicase of the SF1b family that translocates on ssDNA in the 5'-3' direction (Singleton et al., 2007; Taneja et al., 2002). HELB binds to RPA directly (Guler et al., 2012) but a clear biological function for HELB remains unknown, although it has been proposed to

#### Figure 1. HELB Restricts End Resection in Human Cells

(A) Model of a putative RPA-dependent negative-feedback mechanism that restrains resection.

(B) Visualization of the interactions of each of the RPA subunits and HELB. The interaction list for each of the baits is displayed as a dot plot summarizing the data. The relative abundance is determined by the size of the circle and the spectral counts by the shade of purple within the circle, and the outer line represents the false discovery rate (FDR) (high confidence is  $FDR \leq 1\%$ , medium confidence is  $FDR \leq 5\%$ , low confidence is  $FDR > 5\%$ ).

(C) High-confidence RPA interactors found by IP-MS (Table S1) were screened in assays that monitored pRPA2 S4/S8 foci (y axis) and HR via the DR-GFP assay (x axis). The results of each assay were normalized to the non-targeting siRNA (siCTRL). Each point represents the mean of two replicates for each assay.

(D) SSA frequency, as determined by the SA-GFP assay in U2OS cells transfected with a non-targeting siRNA (CTRL) or siRNAs targeting the indicated proteins. Data are presented as mean  $\pm$  SEM,  $n = 3$ . (p), pooled HELB siRNAs. See also Figure S1B.

(E) HR frequency, as determined by the DR-GFP assay in HeLa cells transfected with non-targeting (siCTRL) or HELB-targeting (siHELB) siRNAs in combination with empty vector (EV) or siRNA-resistant Flag-HELB (H) vector. Data are presented as mean  $\pm$  SEM,  $n = 3$ . Immunoblots of a representative experiment are shown under the graph.

(F) U2OS cells were transfected with the indicated siRNAs and treated with NCS (100 ng/ml). At the indicated time points, cells were harvested and extracts were analyzed by immunoblotting with antibodies against pRPA2 S4/S8 and tubulin. See also Figure S1D.

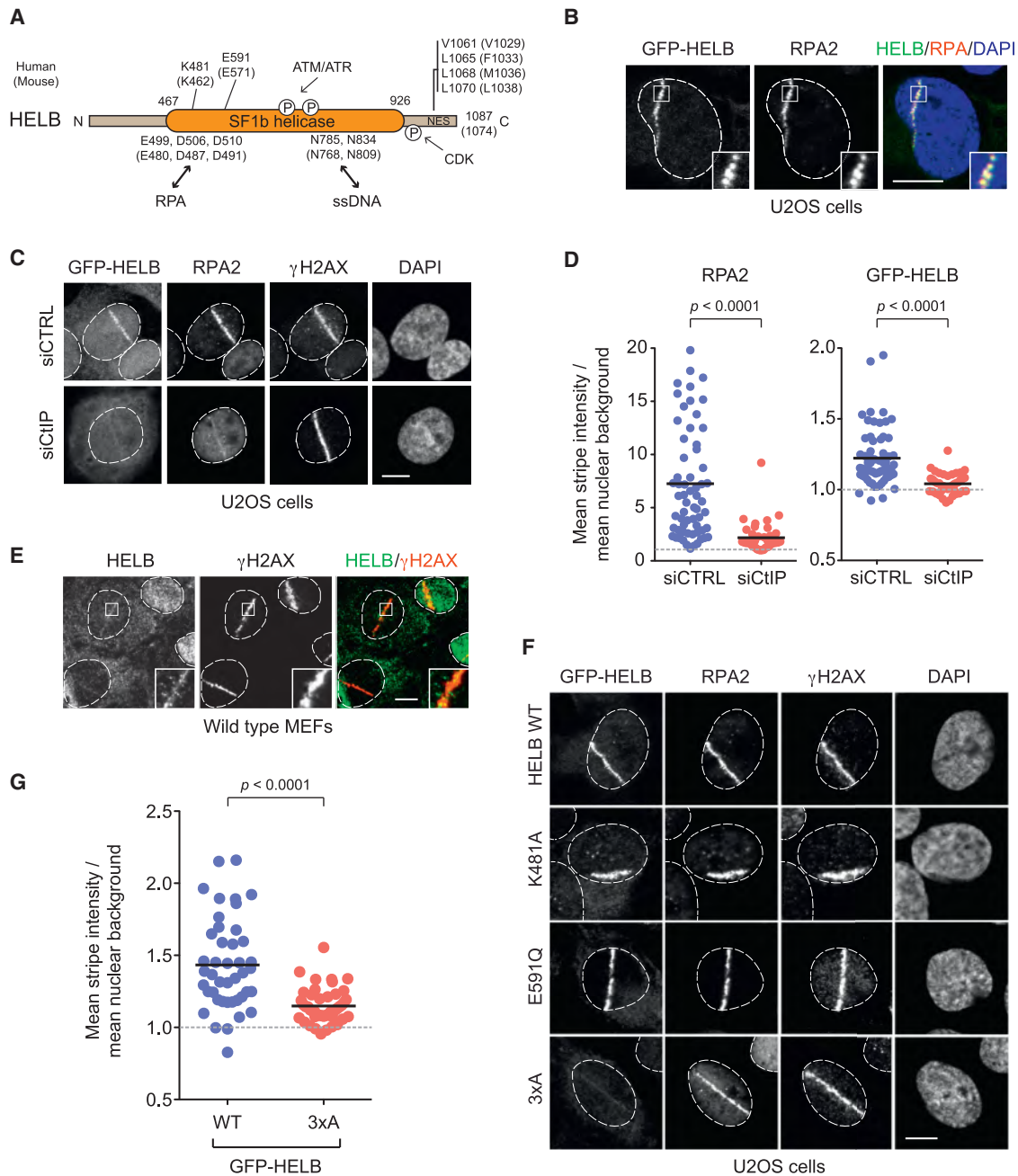


**Figure 2. RPA Recruits HELB to Sites of DNA Damage**

(A) HELB domain organization with important residues indicated for the human protein (equivalent residues in mouse HELB are in brackets). (B) U2OS cells expressing GFP-HELB were microirradiated with a UVA laser. Four hours after irradiation, cells were fixed and processed for RPA2 immunofluorescence. The outline of the nucleus is also shown. The scale bar represents 10  $\mu$ m. (C) U2OS cells expressing GFP-HELB were transfected with non-targeting (siCTRL) or CtIP-targeting (siCtIP) siRNA. Seventy-two hours after transfection, the cells were laser microirradiated as in (B) and processed for immunofluorescence. The scale bar represents 10  $\mu$ m. See also Figure S2A. (D) Quantitation of the fluorescence intensities of RPA2 (left) and GFP-HELB (right) stripes in U2OS cells transfected with the indicated siRNA. Each dot represents a nucleus analyzed. Stripe intensity was normalized to the mean nuclear background intensity in each cell (represented by the dashed gray line). The distributions were compared using the Mann-Whitney U test. (E) MEFs were laser microirradiated as in (B). Four hours after irradiation, cells were fixed and processed for endogenous HELB and  $\gamma$ -H2AX immunofluorescence. The scale bar represents 10  $\mu$ m.

(legend continued on next page)

promote DNA replication (Gerhardt et al., 2015; Taneja et al., 2002) or recovery from DNA replication stress (Guler et al., 2012). HELB is an ATM/ATR target (Matsuoka et al., 2007) along with being a CDK substrate (Gu et al., 2004; Spencer et al., 2013). The identification of HELB-interacting proteins confirmed its interaction with RPA, RPA-interacting proteins, and CDK complexes (Figure 1B).

HELB accumulates on chromatin in response to genotoxic stress (Guler et al., 2012). This observation, coupled with the finding that HELB interacts with RPA, suggests that HELB may localize to DSB sites by contacting the RPA-ssDNA filament. Indeed, we observed that GFP-tagged HELB accumulates at laser microirradiation-induced DSBs in U2OS cells, with a staining pattern that is coincident with that of RPA and that is dependent on CtIP (Figures 2B–2D and S2A). Endogenous HELB also accumulates at microirradiation sites in a portion of primary murine embryonic fibroblasts (MEFs) (Figures 2E and S2B). We tested whether the recruitment of HELB to DSB sites required its ATP-dependent motor activity using GFP-HELB harboring the K481A or E591Q mutations that disrupt the Walker A or B motif, respectively (Taneja et al., 2002), or its interaction with RPA using the 3xA (E499A/D506A/D510A) mutant (Guler et al., 2012). We found that HELB recruitment to DSB sites was dependent on its interaction with RPA but independent of its catalytic activity (Figures 2F, 2G, S2F, and S2G).

### HELB Limits BLM-DNA2- and EXO1-Dependent End Resection

To further analyze the role of HELB in end resection, we derived primary and 3T3-immortalized MEFs from mice carrying a homozygous *Helb* deletion (*Helb*<sup>tm1(KOMP)Vlcg</sup>, which is referred to as *Helb*<sup>-/-</sup>; Figure S3A). *Helb*<sup>-/-</sup> mice are born at a normal Mendelian ratio (Figures S3B and S3C; Table S2), and are fertile and phenotypically normal under unchallenged conditions. Immunoblotting of MEF cell extracts from a *Helb*<sup>+/-</sup> × *Helb*<sup>+/-</sup> cross confirmed that the knockout allele leads to a complete loss of HELB (Figure 3A).

Analysis of SSA in wild-type (WT), *Helb*<sup>-/-</sup>, and HELB-complemented *Helb*<sup>-/-</sup> MEFs using the traffic light reporter (TLR) system (Kuhar et al., 2014) indicated that HELB is also an SSA antagonist in mouse cells, consistent with a role as an inhibitor of DNA end resection (Figures 3B and S3D). However, we did not observe an increase in RPA phosphorylation following NCS treatment in *Helb*<sup>-/-</sup> MEFs, despite its being detectably increased in *53bp1*<sup>-/-</sup> cells (Figure S3E). Because this result was at odds with our SSA data and our results in human cells, we monitored the formation of ssDNA by quantitating 5-bromo-2'-deoxyuridine (BrdU) levels under native conditions (Figure 3C) to have a more definitive view of resection in HELB-deficient animals. Using this direct readout of ssDNA formation, we detected a robust increase in resection after NCS treatment in *Helb*<sup>-/-</sup> cells that was similar to that observed in *53bp1*<sup>-/-</sup> cells (Figure 3DE). This increase was not caused by

higher BrdU incorporation in the knockout MEFs (Figure 3D), nor was it due to a greater induction of DNA damage as assessed by the neutral comet assay (Figure S3F) or an altered cell-cycle distribution (Figure S3G). The increase in ssDNA observed in *Helb*<sup>-/-</sup> cells was dependent entirely on CtIP, indicating that the ssDNA signal detected was due to end resection (Figure 3F).

Next, we reintroduced untagged mouse HELB in *Helb*<sup>-/-</sup> MEFs using retroviral transduction. The WT protein restored end resection to the levels seen in *Helb*<sup>+/+</sup> cells, confirming that loss of HELB increases resection (Figure 3G). We also transduced viruses expressing the catalytically inactive K462A and E571Q mutants (equivalent to human K481A and E591Q, respectively), the RPA binding-defective 3xA mutant, and a mutant based on the structure of RecD2 (Saikrishnan et al., 2009) that impairs ssDNA binding and helicase activities (N768A/N809A or 2NA; Figures S3H and S3I). Each mutant was expressed (Figure S3J), and when assessed for ssDNA formation, we observed that HELB requires RPA and ssDNA binding as well as its catalytic activity to suppress end resection (Figures 3G and S3K).

Long-range resection is catalyzed by two redundant nucleases: EXO1 and BLM-DNA2 (Gravel et al., 2008; Nimonkar et al., 2011). We therefore tested whether the increased resection observed in *Helb*<sup>-/-</sup> MEFs was due to the action of these nucleases. We depleted EXO1 and BLM in *Helb*<sup>-/-</sup> cells alone or in combination (Figure S3L) and measured resection using the native BrdU assay. We found that the depletion of EXO1 and BLM in *Helb*<sup>-/-</sup> cells partially decreased resection, but the combined depletion of EXO1 and BLM suppressed resection completely (Figure 3H). These results suggest that HELB antagonizes, directly or indirectly, the activity of EXO1 and BLM-DNA2.

### HELB Inhibits End Resection In Vitro

The above data suggest that HELB may be able to suppress resection irrespective of the nature of the nuclease. Helicases can act as molecular “cowcatchers” that displace DNA-bound proteins using their ATP-dependent motor activity. The prototypical cowcatcher helicase is Dda from T4 bacteriophage, which like HELB is a member of the SF1b family (Byrd and Raney, 2004). HELB displays cowcatcher activity, as detected by its ability to displace streptavidin from a 3'-biotinylated ssDNA oligonucleotide (Figure S4A). This result suggested that HELB might antagonize resection enzymes by translocating on ssDNA in the 5'-3' direction. To test this possibility directly, we assessed whether HELB could limit DNA end resection of a radiolabeled 2.7 kb substrate in vitro. We observed that HELB limits resection by the MRN-BLM-EXO1 and MRN-BLM-DNA2 machineries in a manner that required the inclusion of RPA in the reaction (Figures 4A, 4B, and S4B–S4E). EXO1 could also be inhibited by HELB using a minimal system in which this nuclease alone was added to a 2.7 kb substrate, indicating that the HELB-RPA interaction might be particularly important to limit resection in the context of BLM-containing nuclease complexes (Figures S4F and

(F) U2OS cells expressing the indicated GFP-HELB derivatives were laser microirradiated as in (B) and processed for RPA2 and  $\gamma$ -H2AX immunofluorescence. The scale bar represents 10  $\mu$ m. See also Figure S2G.

(G) Fluorescence intensities of GFP-HELB stripes in U2OS cells were quantitated as in (D). The dashed gray line represents the background nuclear fluorescence. The distributions were compared using the Mann-Whitney U test.

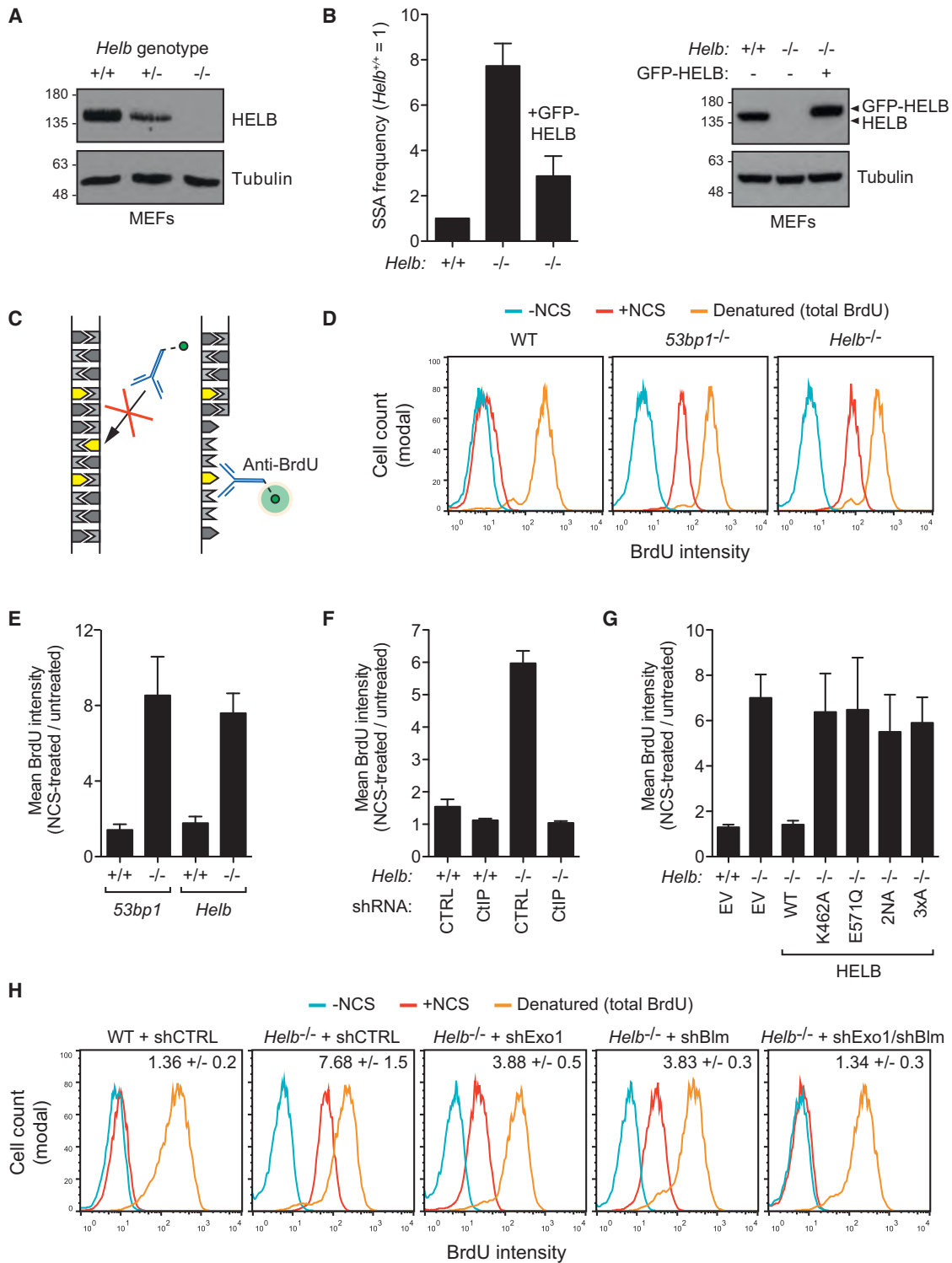


**Figure 3. HELB Limits Resection by Inhibiting EXO1 and BLM-DNA2**

(A) Extracts from *Helb*<sup>+/+</sup>, *Helb*<sup>+/-</sup>, and *Helb*<sup>-/-</sup> MEFs were immunoblotted with antibodies against HELB and tubulin. (B) SSA frequency in *Helb*<sup>+/+</sup>, *Helb*<sup>-/-</sup>, and GFP-HELB-complemented *Helb*<sup>-/-</sup> MEFs was quantitated using the TLR (left). Data are presented as mean ± SEM, n = 3. In parallel, extracts from these cells were analyzed by immunoblotting with antibodies against HELB and tubulin (right). See also Figure S3D. (C) Schematic depicting the native BrdU assay to detect ssDNA.

(legend continued on next page)

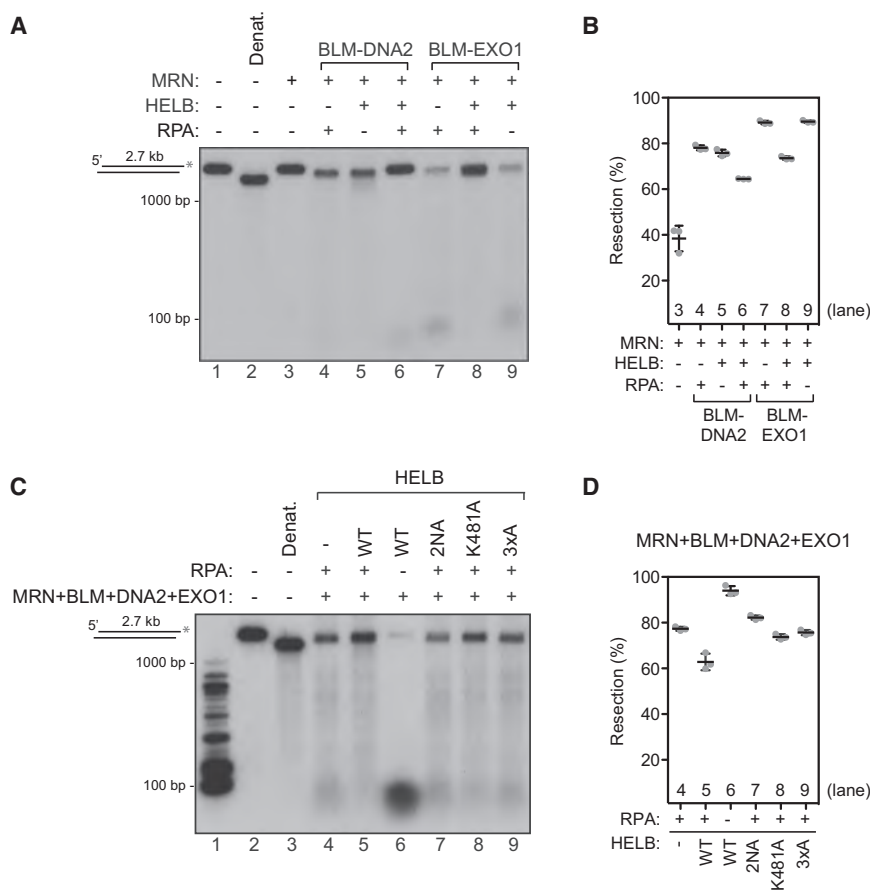


**Figure 4. HELB Inhibits Resection In Vitro**

(A) The indicated combinations of purified recombinant proteins were incubated with a [<sup>32</sup>P]-labeled linear 2.7 kb dsDNA substrate. The resection products were detected by autoradiography after agarose gel electrophoresis. See also Figures S2C–S2E and S4B–S4E.

(B) Densitometric quantitation of the autoradiography signals shown in (A). The data represent the percentage of intact DNA substrate in the reaction mixtures divided by the percentage of intact DNA substrate in the no-enzyme control (lane 1). The bars indicate the mean ± SD, n = 3.

(C) WT or the indicated mutant versions of purified recombinant HELB protein were incubated with MRN-BLM-DNA2-EXO1 and with a [<sup>32</sup>P]-labeled linear 2.7 kb dsDNA substrate in the presence or absence of RPA. The resection products were detected by autoradiography after agarose gel electrophoresis.

(D) Densitometric quantitation of the autoradiography signals shown in (C). The bars indicate the mean ± SD, n = 3.

### HELB Does Not Regulate DSB Repair Pathway Choice

The inhibition of end resection by 53BP1, RIF1, and Ku is linked to their ability to promote NHEJ (Chapman et al., 2012). We therefore assessed whether loss of HELB similarly affects NHEJ. First, we tested whether *Helb*<sup>-/-</sup> B cells undergo class switch recombination (CSR), the

S4G). Next, we assessed the ability of HELB to limit resection under conditions in which the MRN, BLM-DNA2, and EXO1 nucleases were added together and found that HELB could suppress resection under those conditions in an RPA-dependent manner and in a manner that depended on its ability to bind ssDNA, hydrolyze ATP, and bind to RPA, the activities needed to inhibit resection in vivo (Figures 4C, 4D, and S2C). However, we note that in the absence of BLM, HELB was unable to inhibit the flap endonuclease activity of DNA2, suggesting that it inhibits the BLM-DNA2 machine specifically (Figure S4H). Interestingly, end resection was never entirely inhibited by HELB under the conditions used. This suggests that HELB modulates the efficiency of resection, or it may reflect the requirement for RPA binding prior to the action of HELB on partially resected DNA.

process by which the constant region of the immunoglobulin (Ig) gene is rearranged to switch antibody isotype. Splenic B cells were isolated from isogenic WT, *Helb*<sup>-/-</sup>, and *53bp1*<sup>-/-</sup> mice and stimulated with interleukin-4 (IL-4) and lipopolysaccharide (LPS), and the IgM-to-IgG<sub>1</sub> switching was determined by flow cytometry. We found that contrary to the case of cells isolated from *53bp1*<sup>-/-</sup> animals, which are severely impaired in CSR, loss of HELB did not result in a significant change in CSR (Figure 5A), suggesting that HELB may not influence the choice between NHEJ and HR. *Helb*<sup>-/-</sup> MEFs can form normal levels of ionizing radiation (IR)-induced RIF1 foci (Figures 5B and S4I), further indicating that HELB loss does not influence NHEJ. We directly assessed NHEJ by assaying the ability of cells to recircularize exogenous linear substrates (Waters et al., 2014). *Helb*<sup>-/-</sup> cells

(D) MEFs of the indicated genotypes were grown in the presence of BrdU for 24 hr prior to incubation in the absence (-NCS) or presence (+NCS) of 200 ng/mL NCS for 3 hr. Cells were fixed and processed for detection of BrdU by flow cytometry without denaturation. A sample was also denatured to detect total BrdU incorporation. Shown are representative histogram plots of 10,000 cells analyzed for each condition.

(E) Quantitation of the flow cytometry data shown in (D), presented as the mean BrdU fluorescence intensity following NCS treatment normalized to the untreated control cells for each sample (±SEM, n = 5). WT MEFs corresponding to each mutant were derived from their respective littermates.

(F) Quantitation of resection by the native BrdU assay of *Helb*<sup>+/+</sup> and *Helb*<sup>-/-</sup> MEFs transduced with lentiviruses expressing non-targeting (CTRL) or *CtIP*-targeting shRNAs and treated with NCS. Data were normalized as in (E) and are presented as mean ± SEM, n = 3.

(G) Quantitation of resection by the native BrdU assay of *Helb*<sup>+/+</sup> or *Helb*<sup>-/-</sup> MEFs transduced with either a control retrovirus (EV) or viruses expressing the indicated HELB proteins and treated with NCS. Data were normalized as in (E) and are presented as mean ± SEM, n ≥ 4. See also Figures S3J and S3K.

(H) WT or *Helb*<sup>-/-</sup> MEFs transduced with retroviruses expressing non-targeting (shCTRL) or *Exo1*-targeting (shExo1) or *Blm*-targeting (shBlm) shRNAs were processed for detection of BrdU as described in (D). Shown are representative histogram plots of 10,000 cells analyzed for each condition and the mean fold increase in BrdU fluorescence intensity after NCS treatment (±SEM, n = 4).

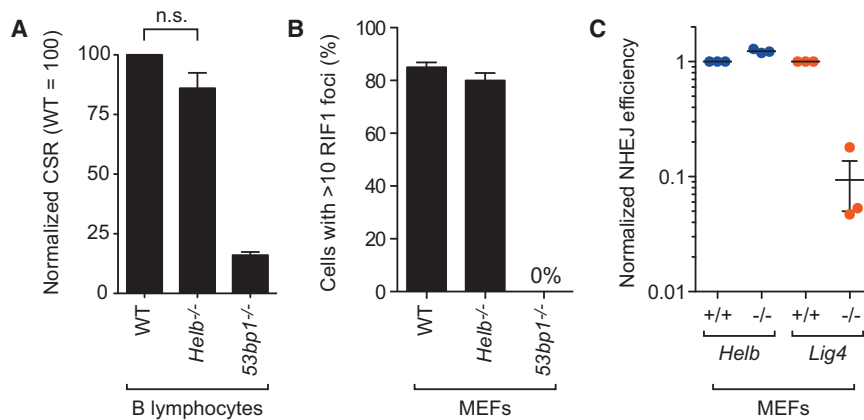


**Figure 5. HELB Is Not Involved in DSB Repair Pathway Choice**

(A) B lymphocytes were isolated from the spleens of adult WT, *Helb*<sup>-/-</sup>, and *53bp1*<sup>-/-</sup> mice and treated with LPS and IL-4 to induce switching from IgM to IgG<sub>1</sub>. Cells were analyzed 4 days later by flow cytometry using an anti-IgG<sub>1</sub> antibody. Data are presented as mean ± SEM, n = 3. Significance was determined using the Mann-Whitney U test (n.s., not significant).

(B) Quantitation of RIF1 IR-induced foci in WT, *Helb*<sup>-/-</sup>, and *53bp1*<sup>-/-</sup> MEFs fixed 1 hr after a 3 Gy dose of IR. Data are presented as mean ± SEM, n = 3. See also Figure S4I.

(C) Quantitation of extrachromosomal NHEJ in *Helb*<sup>-/-</sup> (blue) and *Lig4*<sup>-/-</sup> (red) MEFs and their WT counterparts. Data are presented as mean ± SEM, n = 3.

were as competent as their parental counterparts in this assay, whereas *Lig4*<sup>-/-</sup> cells showed a markedly reduced efficiency (Figure 5C). We conclude that HELB does not promote NHEJ.

### HELB Mediates the Cell-Cycle Regulation of End Resection

The subcellular localization of HELB is controlled by the cell cycle (Gu et al., 2004; Spencer et al., 2013). In early G1 cells, HELB is predominantly nuclear. As cells approach the G1/S transition, HELB is phosphorylated at its C terminus by CDK2, which results in its nuclear export, leaving only a fraction of HELB in the nucleus as S phase progresses (Gu et al., 2004). We observed this phenomenon by immunofluorescence of endogenous HELB in MEFs, where HELB loses its nuclear enrichment in cells that are undergoing DNA replication (Figures 6A and S5A). The cell cycle-dependent subcellular shuttling of HELB was puzzling at first because DNA end resection is restricted to the S/G2 phase of the cell cycle, that is, at a time when HELB becomes predominantly cytoplasmic. We therefore tested whether forcing HELB to localize to the nucleus in S/G2 phase could restore normal resection levels in *Helb*<sup>-/-</sup> cells. We found that introduction of mutations that disrupt the HELB nuclear export signal (NES) (V1029A/F1033A/M1036A/L1038A or NESm) resulted in a partial nuclear enrichment in S/G2 phase cells (Figures 6B and S5B) that can potentially suppress DNA end resection (Figure 6C) despite the NESm mutant's being expressed at lower levels than the WT protein (Figure S3J). Together, these data indicate that HELB acts in the nucleus to limit resection.

These results further suggest that the nuclear export of HELB may be critical for the upregulation of DNA end resection seen in S phase cells. If this model is correct, expression of the HELB-NESm protein should curtail the normal upregulation of resection upon S phase entry. Because the dynamic range of the native BrdU resection assay in WT MEFs is small (Figure 3D), we assessed whether expression of HELB-NESm in *53bp1*<sup>-/-</sup> cells suppressed its associated hyper-resection phenotype. Indeed, the HELB-NESm protein, but not its catalytically inactive K462A mutant, potently blocks the formation of ssDNA in *53bp1*<sup>-/-</sup> cells following NCS treatment (Figure 6D). Overexpression of the WT protein could also dominantly suppress end resection in S/G2 cells (Figure 6D), suggesting that resection is sensitive to nuclear

HELB dosage. These results also suggest that HELB and 53BP1 act in distinct pathways to curtail resection. To test this possibility directly, we generated *Helb*<sup>-/-</sup> *53bp1*<sup>-/-</sup> MEFs and assessed resection following NCS treatment. We observed that the combined loss of HELB and 53BP1 results in an additive increase in DNA end resection (Figures 6E, S5C, and S5D). Together, these results indicate that HELB acts independently of 53BP1 to suppress resection and suggest that the reduction in the nuclear abundance of HELB prior to S phase entry is critical for the activation of end resection during this stage of the cell cycle.

### Loss of HELB Results in PARP Inhibitor Resistance in BRCA1-Deficient Cells

Loss of 53BP1 rescues the lethality of BRCA1 deficiency and leads to PARP inhibitor (PARPi) resistance in cell and animal models, through the restoration of end resection and HR in those cells (Bouwman et al., 2010; Bunting et al., 2010; Cao et al., 2009; Jaspers et al., 2013). REV7 has also recently been shown to be required for PARPi sensitivity in BRCA1-deficient cells (Xu et al., 2015). In a screen to identify other factors that promote PARPi sensitivity in BRCA1-deficient cells, the Amsterdam-based authors independently identified murine HELB as a mediator of the cytotoxic effects of PARPi in BRCA1-deficient mammary tumors. Indeed, in confirmation studies, HELB depletion by two short hairpin RNAs (shRNAs) in two independent *Brca1*<sup>-/-</sup> *p53*<sup>-/-</sup> mouse mammary tumor cell lines (G3 and B11) (Jaspers et al., 2013) resulted in resistance to the PARP inhibitors olaparib and AZD2461 at two different concentrations (Figures S6A–S6C). Because hairpin #2 targeted the 3' UTR of murine *Helb*, we reintroduced HELB (as a fusion protein with GFP) in *Brca1*<sup>-/-</sup> *p53*<sup>-/-</sup> cells depleted of the endogenous HELB protein (Figure 7A). When these cells were subjected to clonogenic survival assays with olaparib and AZD2461, we observed that the reintroduction of WT HELB nearly completely restored the sensitivity of *Brca1*<sup>-/-</sup> *p53*<sup>-/-</sup> cells to PARP inhibition (Figure 7BC). The ability of HELB to re-sensitize cells to PARPi was dependent on its catalytic, ssDNA- and RPA-binding activities (Figure 7BC), closely mirroring its requirements in suppressing end resection (compare Figures 7C and 3G). Furthermore, expression of the NESm mutant, which potently suppresses end resection, hyper-sensitized cells to PARPi treatment (Figure 7BC).

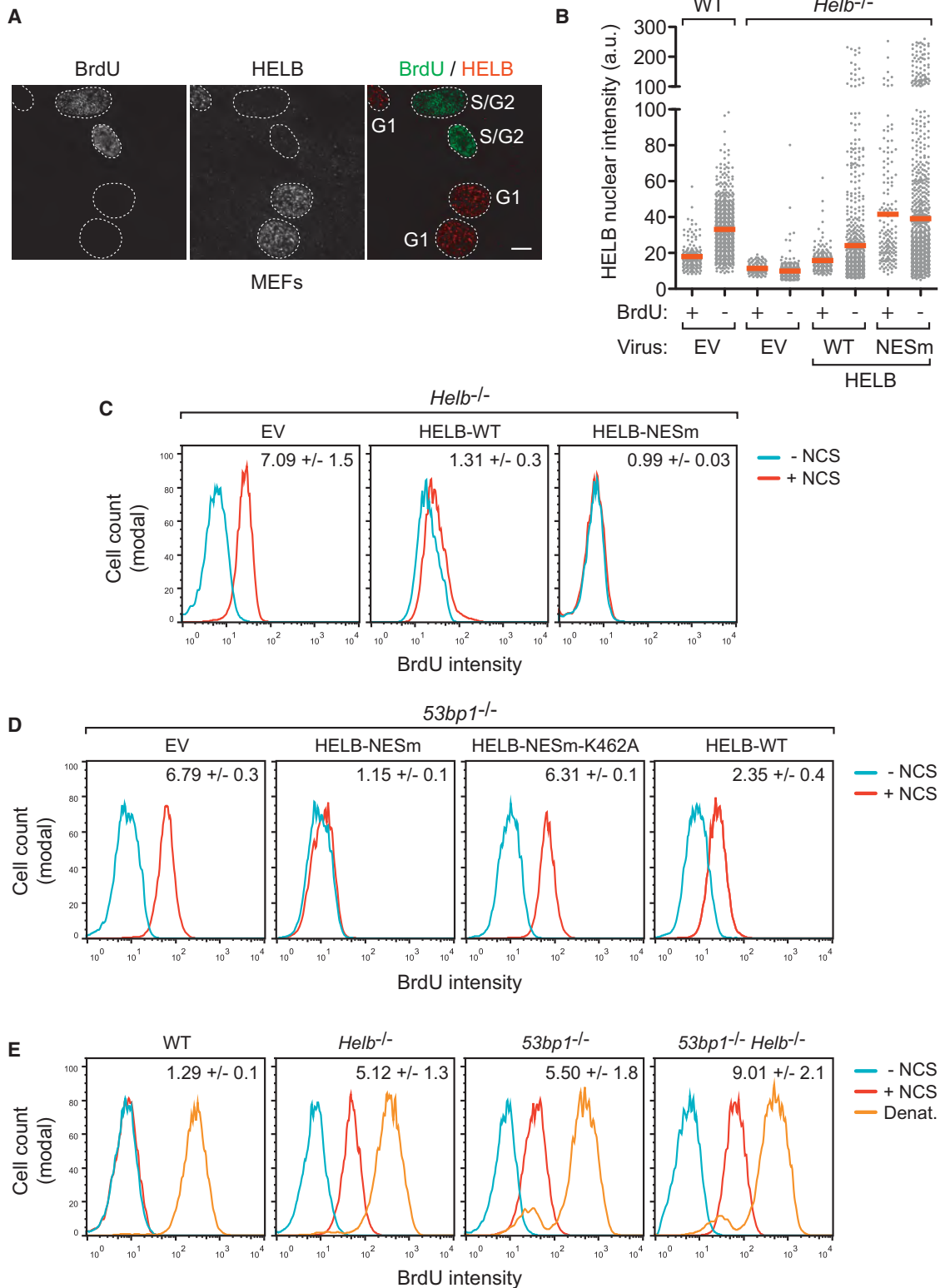


**Figure 6. The Nuclear Export of HELB Promotes End Resection**

(A) WT MEFs were pulsed with BrdU for 3 hr prior to fixation and processing for HELB and BrdU immunofluorescence after denaturation. The scale bar represents 10  $\mu$ m.

(legend continued on next page)

ATM activity is critical for the suppression of PARPi sensitivity in *Brca1* <sup>$\Delta 11/\Delta 11$</sup>  *53bp1*<sup>-/-</sup> cells (Bunting et al., 2010) and for the unscheduled resection observed in H2AX- and 53BP1-deficient cells. Strikingly, treatment of HELB-depleted *Brca1*<sup>-/-</sup> *p53*<sup>-/-</sup> cell lines with two ATM inhibitors, KU55933 and KU60019, reversed the resistance of these cells to PARPi (Figure S6D), reflecting the reduction in resection observed in *Helb*<sup>-/-</sup> MEFs treated with KU55933 (Figure S6E). Furthermore, ectopic expression of GFP-HELB in PARPi-resistant *Brca1*<sup>-/-</sup> *p53*<sup>-/-</sup> cells stably depleted of 53BP1 or REV7 restored their PARPi sensitivity (Figures 7A, 7D, and S6F). Collectively, our results suggest that the regulation of resection by HELB modulates the cellular sensitivity of BRCA1-deficient cells to PARPi.

In parallel to these studies, the *Brca1*<sup>-/-</sup> *p53*<sup>-/-</sup> tumor cell lines that carried either the control shRNA vector or a vector expressing an shRNA against HELB (shHelb-2) were injected into the fat pads of female mice. When tumors reached a volume of 200 mm<sup>3</sup>, mice were either left untreated or were treated with olaparib for 28 days, after which the mice were followed until the tumor relapsed to a volume of about 1,500 mm<sup>3</sup>. Tumor growth and animal survival were monitored. In the absence of olaparib treatment, tumor growth (Figure 7E, left) and median time of survival was similar for control and HELB-depleted cells (7.5 versus 11.5 days, respectively) (Figure 7E, right). However, in mice grafted with HELB-depleted *Brca1*-null tumor cells, olaparib treatment resulted in only a minor reduction in tumor growth (Figure 7E, left) causing a striking decrease in the median survival time (28 versus 49 days for control; Figure 7E, right).

These results suggest that mechanistically, the increased resection caused by HELB depletion might restore HR in *Brca1*-null cells. Consistent with this possibility, loss of HELB restored RAD51 focus formation in *Brca1*<sup>-/-</sup> *p53*<sup>-/-</sup> cells (Figures 7F and S7A) to a magnitude that was similar to that seen with REV7 depletion (Xu et al., 2015). This phenotype was recapitulated in human cells using siRNA-mediated depletion of BRCA1 and HELB (Figures S7B and S7C). Together, these data indicate that the ability of HELB to block resection modifies the response of BRCA1-deficient cells to PARPi in vitro and in vivo. However, introduction of the *Helb*<sup>-/-</sup> mutation in the *Brca1* <sup>$\Delta 11/\Delta 11$</sup>  mouse background did not rescue the embryonic lethality of BRCA1 deficiency (Table S3), indicating that the reactivation of HR in BRCA1-deficient cells that have lost HELB activity is not as complete as what is observed following 53BP1 deletion.

## DISCUSSION

We propose that HELB mediates a negative feedback loop initiated by RPA-coated ssDNA that antagonizes the activity of the EXO1 and BLM-DNA2 nucleases. Interestingly, this feedback mechanism is itself finely tuned by CDK activity through the modulation of HELB concentration within the nucleus, such that resection is suppressed in G1 and activated as cells enter and progress through S phase. As this pathway operates independently of the known end protection systems that target the initiation of resection, mammalian cells may have evolved at least two distinct regulatory systems that limit ssDNA overhang formation: the first system is embodied by the Ku heterodimer and the 53BP1 pathway, which are critical for DSB repair pathway choice, and the second, reported here and mediated by HELB, which limits end resection in an RPA-dependent manner.

Retention of HELB in the nucleus during S phase, either by impairing its nuclear export or through overexpression, results in inhibition of resection that can even overcome the hyper-resection phenotype of *53bp1*<sup>-/-</sup> cells. As cells enter S phase, the decrease in nuclear HELB may be an important feature in activating resection. Although nuclear export is clearly an important mechanism of regulation, we noted that even in the NESm mutant, there was still some cell-cycle regulation of HELB. This may be due to the modulation of nuclear import or may be an entirely different mode of regulation. For example, the interaction of HELB with SKP2 hints that nuclear HELB levels may be additionally modulated through ubiquitin-mediated proteolysis.

Our genetic and biochemical dissection of HELB suggests that it is an ATP-driven motor that translocates on ssDNA in the 5'-3' direction to inhibit the action of the BLM-DNA2 and EXO1 nucleases. The exact mechanism by which HELB acts remains to be determined and will likely require single-molecule studies that track resection enzymes as well as HELB. Elegant studies with fission yeast Pfh1, another SF1b family helicase, have indicated that Pfh1 is anchored at 3'-tailed ssDNA-double-stranded DNA (dsDNA) junctions and uses the energy of ATP to periodically "reel" in the DNA tail to displace telomerase from telomeric overhangs (Zhou et al., 2014). An analogous patrolling activity could endow HELB with the ability to remove proteins selectively at the site of resection and represents an attractive model for HELB action. However, we have so far failed to gain support for this model when monitoring the accumulation of EXO1 or BLM at laser microirradiation sites in the presence or absence of HELB (not shown), and thus this model should be considered speculative.

(B) WT or *Helb*<sup>-/-</sup> MEFs transduced with the indicated retrovirus were processed for HELB and BrdU immunofluorescence as in (A). The nuclear intensity of the HELB signal in G1 (BrdU<sup>-</sup>) and S/G2 (BrdU<sup>+</sup>) cells was determined and plotted. Each point represents a nucleus analyzed and bar represents the mean. See also Figure S5B.

(C) *Helb*<sup>-/-</sup> MEFs transduced with either an empty retrovirus (EV) or a retrovirus expressing the indicated HELB variants were grown in the presence of BrdU for 24 hr prior to the addition of 200 ng/mL of NCS for 3 hr. Cells were fixed and processed for the native BrdU assay. Shown are representative histogram plots of 10,000 cells analyzed for each condition and the mean fold increase in BrdU fluorescence intensity after NCS treatment ( $\pm$ SEM, n = 3).

(D) *53bp1*<sup>-/-</sup> MEFs transduced with either an empty retrovirus (EV) or a retrovirus expressing the indicated HELB variants were processed for native BrdU detection as in (C). Shown are representative histogram plots of 10,000 cells analyzed for each condition and the mean fold increase in BrdU fluorescence intensity after NCS treatment ( $\pm$ SEM, n = 3).

(E) WT, *Helb*<sup>-/-</sup>, *53bp1*<sup>-/-</sup>, and *53bp1*<sup>-/-</sup> *Helb*<sup>-/-</sup> MEFs were processed for native BrdU detection as in (C). Shown are representative histogram plots of 10,000 cells analyzed for each condition and the mean fold increase in BrdU fluorescence intensity after NCS treatment ( $\pm$ SEM, n = 3). See also Figures S5C and S5D.

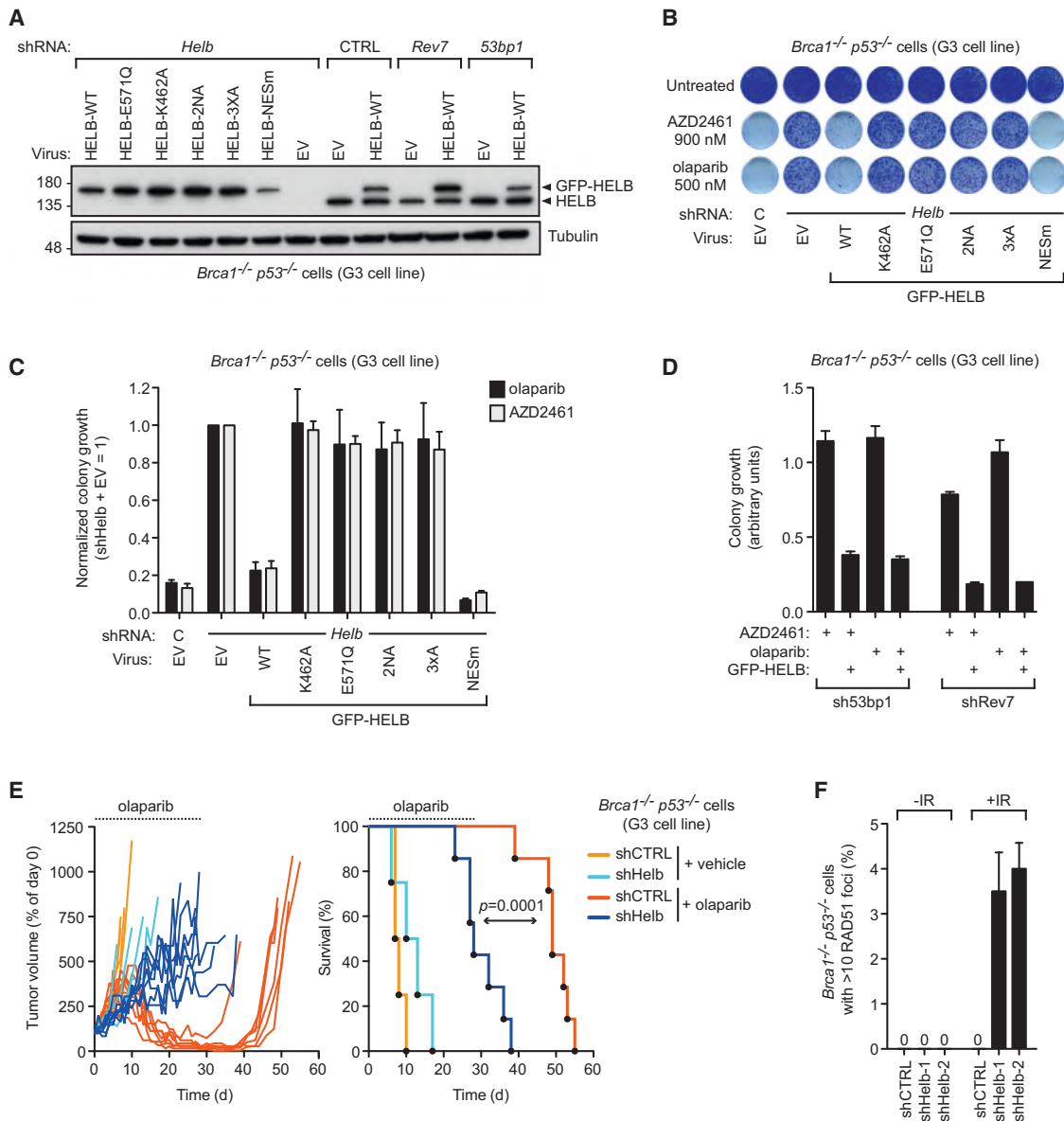


### Figure 7. Loss of HELB Leads to PARPi Resistance in BRCA1-Deficient Cells

(A) Extracts from *Brca1*<sup>-/-</sup> *p53*<sup>-/-</sup> mouse mammary tumor cells (G3 cell line) expressing a non-targeting shRNA (CTRL) or shRNAs against *Helb*, *53bp1*, or *Rev7* and stably transduced with an empty retrovirus (EV) or a virus expressing the indicated GFP-HELB protein were analyzed by immunoblotting with antibodies against HELB and tubulin.

(B) Clonogenic assay using the G3 cell line transduced with the indicated shRNA and GFP-HELB expression constructs and treated with the indicated concentration of olaparib or AZD2461 or left untreated. Shown are representative images of the culture dishes after staining with crystal violet.

(C) Quantitation of the clonogenic assay shown in (B). Data were normalized to the sh*Helb* + EV sample and are presented as the mean  $\pm$  SD,  $n = 3$ .

(D) Quantitation of clonogenic assays of G3 cells expressing shRNAs against *53bp1* or *Rev7* and stably transduced with a retroviral GFP-HELB expression construct or empty vector before treatment with olaparib or AZD2461. Data are presented as mean  $\pm$  SD,  $n = 3$ . See also Figure S6F.

(E) Relative tumor volume (left) and survival (right) in mice allografted with *Brca1*<sup>-/-</sup> *p53*<sup>-/-</sup> (G3) cells expressing the indicated shRNA and treated with one regimen of 50 mg olaparib per kilogram daily for 28 d or treated with vehicle. The indicated  $p$  value was calculated using the log rank test.

(F) Quantitation of RAD51 foci in *Brca1*<sup>-/-</sup> *p53*<sup>-/-</sup> cells expressing a non-targeting shRNA (shCTRL) or one of two different shRNAs targeting *Helb*. Cells were fixed 5 hr after a 10 Gy dose of IR. Data are presented as mean  $\pm$  SD,  $n = 3$ . See also Figure S7A.

HELB could alternatively modulate the RPA-ssDNA filament in a manner that inhibits resection and that confounded our attempts to monitor resection by assaying RPA phosphorylation in MEFs.

In addition to its role in resection, HELB will likely play a role in other processes by virtue of its strong interaction with RPA. In particular, HELB has been proposed to participate in various

aspects of DNA replication (Gerhardt et al., 2015; Guler et al., 2012; Taneja et al., 2002). DNA replication in *Helb*<sup>-/-</sup> MEFs is normal, as measured by molecular combing of nascent DNA fibers (Figures S7D and S7E). However, we detected a mild decrease in replication fork rate during recovery from hydroxyurea treatment (Figure S7D). The nature of this slowdown is intriguing because fork asymmetry (an indicator of fork stalling) is not affected in *Helb*<sup>-/-</sup> cells (Figure S7E), perhaps suggesting that the role for HELB in the recovery from DNA replication stress is indirect.

Finally, our observation that HELB depletion causes PARPi resistance in BRCA1-deficient cells has implications for our understanding of HR and the development of PARPi. First, as 53BP1 promotes both NHEJ and end protection, it had been difficult to untangle which activity of 53BP1 is required to promote PARPi sensitivity in BRCA1-deficient cells. Because HELB is not involved in DSB repair pathway choice but rather limits ATM-dependent end resection, our finding that HELB depletion promotes resistance of *Brca1*<sup>-/-</sup> *p53*<sup>-/-</sup> cells to PARPi suggests that increasing the extent of resection alone, without affecting NHEJ, is sufficient to activate BRCA1-independent HR. However, as the PARPi resistance in HELB-depleted cells is not as pronounced as that in *53bp1*<sup>-/-</sup> or REV7-depleted cells, our results also indicate that the proportion of ends engaging in long-range resection may be another important factor in the ability of cells to survive PARPi treatment.

## EXPERIMENTAL PROCEDURES

### HR and SSA DNA Repair Assays

The DR-GFP assay to measure the frequency of HR and the SA-GFP assay to measure the frequency of SSA were performed as previously described (Stark et al., 2004). Briefly, HeLa DR-GFP or U2OS SA-GFP cells were transfected with 10 nM siRNA (Dharmacon) using Lipofectamine RNAiMAX (Invitrogen). Twenty-four hours later, the cells were transfected with the pCBAScel plasmid (Addgene #26477) using polyethylenimine. Forty-eight hours after plasmid transfection, the cells were trypsinized, and the percentage of GFP-expressing cells was analyzed using the BD FACSCalibur flow cytometer. Mouse experiments in Toronto were approved by the Toronto Centre for Phenogenomics Animal Care Committee. Mouse experiments in Amsterdam were approved by the Animal Experiments Review Board of the Netherlands Cancer Institute.

### Laser Microirradiation

Cells were sensitized to UV radiation by incubation with Hoechst 33342 for 30 min at 37°C. The samples were irradiated using a 355 nm (UVA) laser source (Coherent) with 8 mW power, then incubated for 4 hr at 37°C before fixation with 2% paraformaldehyde (human cells) or 95% ethanol/5% acetic acid (MEFs). Fluorescence intensities were quantitated using ImageJ software. To control for intercellular variability of GFP-HELB expression in U2OS cells, the mean laser microirradiation stripe intensity was normalized to the mean nuclear background intensity in each cell.

### Native BrdU Resection Assay

Analysis of end resection using BrdU detection under native conditions was carried out as previously described (Nishi et al., 2014), with some modifications. Briefly, MEFs were incubated with 30 μM BrdU for 24 hr, followed by treatment with 200 ng/mL NCS for 3 hr. For experiments examining the ATM dependence of end resection, the ATM inhibitor KU55933 (Selleck Chemicals #S1092) was added to the growth medium 1 hr prior to the addition of NCS and kept in the medium during the NCS incubation. Cells were trypsinized, washed with PBS, and fixed with 75% ethanol in PBS for 16 hr at -20°C. Cells were washed with 0.1% Tween 20 in PBS following fixation

and each subsequent incubation. One half of each sample of cells was denatured using 2 N HCl for 30 min at 22°C, in order to assess total BrdU incorporation. Blocking was performed in 5% fetal bovine serum (FBS) in PBS for 30 min at 22°C. BrdU in resected ssDNA was detected under native conditions by incubation with mouse anti-BrdU antibody in 5% FBS in PBS for 2 hr at 22°C. The cells were then incubated with a fluorescent anti-mouse IgG antibody in 5% FBS in PBS for 1 hr at 22°C. Subsequently, BrdU fluorescence intensity was analyzed using the BD FACSCalibur flow cytometer and FlowJo software.

## ACCESSION NUMBERS

The accession numbers for the MS data reported in this paper are MassIVE: MSV000079395 and ProteomeXchange: PXD003259.

## SUPPLEMENTAL INFORMATION

Supplemental Information includes Supplemental Experimental Procedures, seven figures, and four tables and can be found with this article online at <http://dx.doi.org/10.1016/j.molcel.2015.12.013>.

## AUTHOR CONTRIBUTIONS

J.T. and D.D. conceived the study. G.X., W.S., J.J., P.B., and S.R. conceived and designed and G.X. carried out the PARPi clonogenic and tumor growth assays. H.A., J.K., and J.-Y.M. designed and carried out the HELB biochemical assays. J.T., M.M., A.A.-H., and Z.-Y.L. carried out the mass spectrometry; A.-C.G. and D.D. analyzed the data. J.T. carried out the HR, SSA, laser microirradiation, and native BrdU assays. J.T.F.Y. carried out the high-content microscopy and immunofluorescence assays. C.E.-D. carried out the NHEJ and immunofluorescence assays. A.O. carried out the neutral comet and CSR assays. D.G. and G.W.B. designed and carried out the DNA combing assays. D.D. and J.T. wrote the manuscript with input from the other authors.

## ACKNOWLEDGMENTS

We are grateful to R. Szilard and M. Zimmermann for critical reading of the manuscript, S. Weller for discussions, and S. Landry, R. Szilard, and C. Hu for experimental help. We thank the Centre for Modeling Human Disease Pathology Core and the Princess Margaret Hospital Flow Cytometry Facility for their services. We thank J. Stark for the U2OS SA-GFP cells, R. Greenberg for the HeLa DR-GFP cells, A. Nussenzweig for vectors, T. de Lange for *53bp1*<sup>-/-</sup> cells and shRNA vectors, and D. Ramsden and R. Woods for advice on the NHEJ assay. A.-C.G. is a Canada Research Chair (Tier II) in Functional Proteomics. S.R. is supported by a personal project grant of the Netherlands Organization for Scientific Research. J.-Y.M. is a FRQS Chercheur National investigator. D.D. is the Thomas Kierans Chair in Mechanisms of Cancer Development and a Canada Research Chair (Tier I) in the Molecular Mechanisms of Genome Integrity. This work was supported by the Dutch Cancer Society (grant NKI 2011-5220) and the Swiss National Science Foundation (grant 310030-156869 to S.R.); Canadian Cancer Society Research Institute Impact grant 702310 (to G.W.B.); a Canadian Institutes of Health Research (CIHR) grant (to J.-Y.M.); CIHR Foundation grants FDN143343 (to D.D.) and FDN143301 (to A.-C.G.); the Genome Canada Genomics Innovation Network (through the Ontario Genomics Institute, to A.-C.G.), and a Grant-in-Aid from the Krembil Foundation (to D.D.).

Received: January 9, 2015

Revised: November 4, 2015

Accepted: December 3, 2015

Published: January 7, 2016

## REFERENCES

Boersma, V., Moatti, N., Segura-Bayona, S., Peuscher, M.H., van der Torre, J., Wevers, B.A., Orthwein, A., Durocher, D., and Jacobs, J.J. (2015). MAD2L2

- controls DNA repair at telomeres and DNA breaks by inhibiting 5' end resection. *Nature* 521, 537–540.
- Bothmer, A., Robbiani, D.F., Feldhahn, N., Gazumyan, A., Nussenzweig, A., and Nussenzweig, M.C. (2010). 53BP1 regulates DNA resection and the choice between classical and alternative end joining during class switch recombination. *J. Exp. Med.* 207, 855–865.
- Bouwman, P., Aly, A., Escandell, J.M., Pieterse, M., Bartkova, J., van der Gulden, H., Hiddingh, S., Thanasoula, M., Kulkarni, A., Yang, Q., et al. (2010). 53BP1 loss rescues BRCA1 deficiency and is associated with triple-negative and BRCA-mutated breast cancers. *Nat. Struct. Mol. Biol.* 17, 688–695.
- Bunting, S.F., Callén, E., Wong, N., Chen, H.T., Polato, F., Gunn, A., Bothmer, A., Feldhahn, N., Fernandez-Capetillo, O., Cao, L., et al. (2010). 53BP1 inhibits homologous recombination in Brca1-deficient cells by blocking resection of DNA breaks. *Cell* 141, 243–254.
- Byrd, A.K., and Raney, K.D. (2004). Protein displacement by an assembly of helicase molecules aligned along single-stranded DNA. *Nat. Struct. Mol. Biol.* 11, 531–538.
- Callen, E., Di Virgilio, M., Kruhlak, M.J., Nieto-Soler, M., Wong, N., Chen, H.T., Faryabi, R.B., Polato, F., Santos, M., Starnes, L.M., et al. (2013). 53BP1 mediates productive and mutagenic DNA repair through distinct phosphoprotein interactions. *Cell* 153, 1266–1280.
- Cao, L., Xu, X., Bunting, S.F., Liu, J., Wang, R.H., Cao, L.L., Wu, J.J., Peng, T.N., Chen, J., Nussenzweig, A., et al. (2009). A selective requirement for 53BP1 in the biological response to genomic instability induced by Brca1 deficiency. *Mol. Cell* 35, 534–541.
- Chapman, J.R., Taylor, M.R., and Boulton, S.J. (2012). Playing the end game: DNA double-strand break repair pathway choice. *Mol. Cell* 47, 497–510.
- Chapman, J.R., Barral, P., Vannier, J.B., Borel, V., Steger, M., Tomas-Loba, A., Sartori, A.A., Adams, I.R., Batista, F.D., and Boulton, S.J. (2013). RIF1 is essential for 53BP1-dependent nonhomologous end joining and suppression of DNA double-strand break resection. *Mol. Cell* 49, 858–871.
- Chen, X., Niu, H., Chung, W.H., Zhu, Z., Papusha, A., Shim, E.Y., Lee, S.E., Sung, P., and Ira, G. (2011). Cell cycle regulation of DNA double-strand break end resection by Cdk1-dependent Dna2 phosphorylation. *Nat. Struct. Mol. Biol.* 18, 1015–1019.
- Choi, H., Larsen, B., Lin, Z.Y., Breitkreutz, A., Mellacheruvu, D., Fermin, D., Qin, Z.S., Tyers, M., Gingras, A.C., and Nesvizhskii, A.I. (2011). SAINT: probabilistic scoring of affinity purification-mass spectrometry data. *Nat. Methods* 8, 70–73.
- Di Virgilio, M., Callen, E., Yamane, A., Zhang, W., Jankovic, M., Gitlin, A.D., Feldhahn, N., Resch, W., Oliveira, T.Y., Chait, B.T., et al. (2013). Rif1 prevents resection of DNA breaks and promotes immunoglobulin class switching. *Science* 339, 711–715.
- Escribano-Díaz, C., Orthwein, A., Fradet-Turcotte, A., Xing, M., Young, J.T., Tkáč, J., Cook, M.A., Rosebrock, A.P., Munro, M., Canny, M.D., et al. (2013). A cell cycle-dependent regulatory circuit composed of 53BP1-RIF1 and BRCA1-CtIP controls DNA repair pathway choice. *Mol. Cell* 49, 872–883.
- Falck, J., Forment, J.V., Coates, J., Mistrik, M., Lukas, J., Bartek, J., and Jackson, S.P. (2012). CDK targeting of NBS1 promotes DNA-end resection, replication restart and homologous recombination. *EMBO Rep.* 13, 561–568.
- Feng, L., Fong, K.W., Wang, J., Wang, W., and Chen, J. (2013). RIF1 counteracts BRCA1-mediated end resection during DNA repair. *J. Biol. Chem.* 288, 11135–11143.
- Ferretti, L.P., Lafranchi, L., and Sartori, A.A. (2013). Controlling DNA-end resection: a new task for CDKs. *Front. Genet.* 4, 99.
- Gerhardt, J., Guler, G.D., and Fanning, E. (2015). Human DNA helicase B interacts with the replication initiation protein Cdc45 and facilitates Cdc45 binding onto chromatin. *Exp. Cell Res.* 334, 283–293.
- Gravel, S., Chapman, J.R., Magill, C., and Jackson, S.P. (2008). DNA helicases Sgs1 and BLM promote DNA double-strand break resection. *Genes Dev.* 22, 2767–2772.
- Gu, J., Xia, X., Yan, P., Liu, H., Podust, V.N., Reynolds, A.B., and Fanning, E. (2004). Cell cycle-dependent regulation of a human DNA helicase that localizes in DNA damage foci. *Mol. Biol. Cell* 15, 3320–3332.
- Guler, G.D., Liu, H., Vaithiyalingam, S., Arnett, D.R., Kremmer, E., Chazin, W.J., and Fanning, E. (2012). Human DNA helicase B (HDHB) binds to replication protein A and facilitates cellular recovery from replication stress. *J. Biol. Chem.* 287, 6469–6481.
- Huertas, P., and Jackson, S.P. (2009). Human CtIP mediates cell cycle control of DNA end resection and double strand break repair. *J. Biol. Chem.* 284, 9558–9565.
- Jasin, M., and Rothstein, R. (2013). Repair of strand breaks by homologous recombination. *Cold Spring Harb. Perspect. Biol.* 5, a012740.
- Jaspers, J.E., Kersbergen, A., Boon, U., Sol, W., van Deemter, L., Zander, S.A., Drost, R., Wientjens, E., Ji, J., Aly, A., et al. (2013). Loss of 53BP1 causes PARP inhibitor resistance in Brca1-mutated mouse mammary tumors. *Cancer Discov.* 3, 68–81.
- Kuhar, R., Gwiazda, K.S., Humbert, O., Mandt, T., Pangallo, J., Brault, M., Khan, I., Maizels, N., Rawlings, D.J., Scharenberg, A.M., and Certo, M.T. (2014). Novel fluorescent genome editing reporters for monitoring DNA repair pathway utilization at endonuclease-induced breaks. *Nucleic Acids Res.* 42, e4.
- Litman, R., Peng, M., Jin, Z., Zhang, F., Zhang, J., Powell, S., Andreassen, P.R., and Cantor, S.B. (2005). BACH1 is critical for homologous recombination and appears to be the Fanconi anemia gene product FANCF. *Cancer Cell* 8, 255–265.
- Marechal, A., and Zou, L. (2014). RPA-coated single-stranded DNA as a platform for post-translational modifications in the DNA damage response. *Cell Res.* 25, 9–23.
- Matsuoka, S., Ballif, B.A., Smogorzewska, A., McDonald, E.R., 3rd, Hurov, K.E., Luo, J., Bakalarski, C.E., Zhao, Z., Solimini, N., Lerenthal, Y., et al. (2007). ATM and ATR substrate analysis reveals extensive protein networks responsive to DNA damage. *Science* 316, 1160–1166.
- Nimonkar, A.V., Genschel, J., Kinoshita, E., Polaczek, P., Campbell, J.L., Wyman, C., Modrich, P., and Kowalczykowski, S.C. (2011). BLM-DNA2-RPA-MRN and EXO1-BLM-RPA-MRN constitute two DNA end resection machineries for human DNA break repair. *Genes Dev.* 25, 350–362.
- Nishi, R., Wijnhoven, P., le Sage, C., Tjeertes, J., Galanty, Y., Forment, J.V., Clague, M.J., Urbé, S., and Jackson, S.P. (2014). Systematic characterization of deubiquitylating enzymes for roles in maintaining genome integrity. *Nat. Cell Biol.* 16, 1016–1026, 1–8.
- Orthwein, A., Fradet-Turcotte, A., Noordermeer, S.M., Canny, M.D., Brun, C.M., Strecker, J., Escribano-Díaz, C., and Durocher, D. (2014). Mitosis inhibits DNA double-strand break repair to guard against telomere fusions. *Science* 344, 189–193.
- Orthwein, A., Noordermeer, S.M., Wilson, M.D., Landry, S., Enchev, R.I., Sherker, A., Munro, M., Pinder, J., Salsman, J., Delliare, G., et al. (2015). A mechanism for the suppression of homologous recombination in G1 cells. *Nature* 528, 422–426.
- Panier, S., and Durocher, D. (2013). Push back to respond better: regulatory inhibition of the DNA double-strand break response. *Nat. Rev. Mol. Cell Biol.* 14, 661–672.
- Pierce, A.J., Johnson, R.D., Thompson, L.H., and Jasin, M. (1999). XRCC3 promotes homology-directed repair of DNA damage in mammalian cells. *Genes Dev.* 13, 2633–2638.
- Polato, F., Callen, E., Wong, N., Faryabi, R., Bunting, S., Chen, H.T., Kozak, M., Kruhlak, M.J., Reczek, C.R., Lee, W.H., et al. (2014). CtIP-mediated resection is essential for viability and can operate independently of BRCA1. *J. Exp. Med.* 211, 1027–1036.
- Saikhshnan, K., Powell, B., Cook, N.J., Webb, M.R., and Wigley, D.B. (2009). Mechanistic basis of 5'-3' translocation in SF1B helicases. *Cell* 137, 849–859.
- Sakaue-Sawano, A., Kurokawa, H., Morimura, T., Hanyu, A., Hama, H., Osawa, H., Kashiwagi, S., Fukami, K., Miyata, T., Miyoshi, H., et al. (2008).

- Visualizing spatiotemporal dynamics of multicellular cell-cycle progression. *Cell* 132, 487–498.
- Singleton, M.R., Dillingham, M.S., and Wigley, D.B. (2007). Structure and mechanism of helicases and nucleic acid translocases. *Annu. Rev. Biochem.* 76, 23–50.
- Spencer, S.L., Cappell, S.D., Tsai, F.C., Overton, K.W., Wang, C.L., and Meyer, T. (2013). The proliferation-quiescence decision is controlled by a bifurcation in CDK2 activity at mitotic exit. *Cell* 155, 369–383.
- Stark, J.M., Pierce, A.J., Oh, J., Pastink, A., and Jasin, M. (2004). Genetic steps of mammalian homologous repair with distinct mutagenic consequences. *Mol. Cell. Biol.* 24, 9305–9316.
- Symington, L.S., and Gautier, J. (2011). Double-strand break end resection and repair pathway choice. *Annu. Rev. Genet.* 45, 247–271.
- Taneja, P., Gu, J., Peng, R., Carrick, R., Uchiumi, F., Ott, R.D., Gustafson, E., Podust, V.N., and Fanning, E. (2002). A dominant-negative mutant of human DNA helicase B blocks the onset of chromosomal DNA replication. *J. Biol. Chem.* 277, 40853–40861.
- Tomimatsu, N., Mukherjee, B., Catherine Hardebeck, M., Ilcheva, M., Vanessa Camacho, C., Louise Harris, J., Porteus, M., Llorente, B., Khanna, K.K., and Burma, S. (2014). Phosphorylation of EXO1 by CDKs 1 and 2 regulates DNA end resection and repair pathway choice. *Nat. Commun.* 5, 3561.
- Waters, C.A., Strande, N.T., Pryor, J.M., Strom, C.N., Mieczkowski, P., Burkhalter, M.D., Oh, S., Qaqish, B.F., Moore, D.T., Hendrickson, E.A., and Ramsden, D.A. (2014). The fidelity of the ligation step determines how ends are resolved during nonhomologous end joining. *Nat. Commun.* 5, 4286.
- Xu, G., Chapman, J.R., Brandsma, I., Yuan, J., Mistrik, M., Bouwman, P., Bartkova, J., Gogola, E., Warmerdam, D., Barazas, M., et al. (2015). REV7 counteracts DNA double-strand break resection and affects PARP inhibition. *Nature* 521, 541–544.
- Yun, M.H., and Hiom, K. (2009). CtIP-BRCA1 modulates the choice of DNA double-strand-break repair pathway throughout the cell cycle. *Nature* 459, 460–463.
- Zhou, R., Zhang, J., Bochman, M.L., Zakian, V.A., and Ha, T. (2014). Periodic DNA patrolling underlies diverse functions of Pif1 on R-loops and G-rich DNA. *eLife* 3, e02190.
- Zimmermann, M., Lottersberger, F., Buonomo, S.B., Sfeir, A., and de Lange, T. (2013). 53BP1 regulates DSB repair using Rif1 to control 5' end resection. *Science* 339, 700–704.

# Targeting BRCA1 and BRCA2 Deficiencies with G-Quadruplex-Interacting Compounds

Jutta Zimmer,<sup>1</sup> Eliana M.C. Tacconi,<sup>1</sup> Cecilia Folio,<sup>1</sup> Sophie Badie,<sup>1</sup> Manuela Porru,<sup>2</sup> Kerstin Klare,<sup>1,10</sup> Manuela Tumiaty,<sup>3</sup> Enni Markkanen,<sup>4,11</sup> Swagata Halder,<sup>5</sup> Anderson Ryan,<sup>6</sup> Stephen P. Jackson,<sup>7,8</sup> Kristijan Ramadan,<sup>5</sup> Sergey G. Kuznetsov,<sup>3</sup> Annamaria Biroccio,<sup>2</sup> Julian E. Sale,<sup>9</sup> and Madalena Tarsounas<sup>1,\*</sup>

<sup>1</sup>Genome Stability and Tumorigenesis Group, CRUK/MRC Oxford Institute for Radiation Oncology, Department of Oncology, University of Oxford, Old Road Campus Research Building, Oxford OX3 7DQ, UK

<sup>2</sup>Area of Translational Research, Regina Elena National Cancer Institute, 00144 Rome, Italy

<sup>3</sup>Institute for Molecular Medicine Finland (FIMM), University of Helsinki, P.O. Box 20, FIN-00014 Helsinki, Finland

<sup>4</sup>Biochemistry and Regulation of DNA Repair Group, CRUK/MRC Oxford Institute for Radiation Oncology, Department of Oncology, University of Oxford, Old Road Campus Research Building, Oxford OX3 7DQ, UK

<sup>5</sup>DNA Damage and Repair Group, CRUK/MRC Oxford Institute for Radiation Oncology, Department of Oncology, University of Oxford, Old Road Campus Research Building, Oxford OX3 7DQ, UK

<sup>6</sup>Lung Cancer Translational Science Research Group, CRUK/MRC Oxford Institute for Radiation Oncology, Department of Oncology, University of Oxford, Old Road Campus Research Building, Oxford OX3 7DQ, UK

<sup>7</sup>The Gurdon Institute, CRUK Laboratories, University of Cambridge, Tennis Court Road, Cambridge CB2 1QN, UK

<sup>8</sup>The Sanger Institute, Hinxton, Cambridge CB10 1SA, UK

<sup>9</sup>Medical Research Council Laboratory of Molecular Biology, Francis Crick Avenue, Cambridge CB2 0QH, UK

<sup>10</sup>Present address: Department of Mechanistic Cell Biology, Max Planck Institute of Molecular Physiology, 44227 Dortmund, Germany

<sup>11</sup>Present address: Institute of Pharmacology and Toxicology, Vetsuisse Faculty, University of Zürich, 8006 Zürich, Switzerland

\*Correspondence: madalena.tarsounas@oncology.ox.ac.uk

<http://dx.doi.org/10.1016/j.molcel.2015.12.004>

This is an open access article under the CC BY license (<http://creativecommons.org/licenses/by/4.0/>).

## SUMMARY

G-quadruplex (G4)-forming genomic sequences, including telomeres, represent natural replication fork barriers. Stalled replication forks can be stabilized and restarted by homologous recombination (HR), which also repairs DNA double-strand breaks (DSBs) arising at collapsed forks. We have previously shown that HR facilitates telomere replication. Here, we demonstrate that the replication efficiency of guanine-rich (G-rich) telomeric repeats is decreased significantly in cells lacking HR. Treatment with the G4-stabilizing compound pyridostatin (PDS) increases telomere fragility in BRCA2-deficient cells, suggesting that G4 formation drives telomere instability. Remarkably, PDS reduces proliferation of HR-defective cells by inducing DSB accumulation, checkpoint activation, and deregulated G2/M progression and by enhancing the replication defect intrinsic to HR deficiency. PDS toxicity extends to HR-defective cells that have acquired olaparib resistance through loss of 53BP1 or REV7. Altogether, these results highlight the therapeutic potential of G4-stabilizing drugs to selectively eliminate HR-compromised cells and tumors, including those resistant to PARP inhibition.

## INTRODUCTION

Genomic instability is a hallmark of cancer caused by failure of normal DNA replication and/or repair mechanisms (Halazonetis

et al., 2008; Negrini et al., 2010). During replication, the enzymatic activities of DNA polymerases, helicases, and nucleases act in concert to assemble the active replication fork and to achieve high-fidelity duplication of the genome. Damaged DNA, secondary DNA structures, and DNA-protein complexes obstruct progression of replication forks, leading to fork stalling or, in more severe cases, to irreversible fork collapse and DNA breakage. Several mechanisms have evolved to overcome barriers to replication-fork movement, one of which exploits the HR DNA repair machinery. HR factors act to stabilize stalled replication forks by preventing their nucleolytic degradation (Hashimoto et al., 2010; Schlacher et al., 2011) to restart arrested forks (Lambert et al., 2010) and to repair double-strand breaks (DSBs) arising from disintegrated forks (Aze et al., 2013).

The tumor suppressor BRCA2 is a key component of the HR pathway of DSB repair. BRCA2 promotes recombination reactions by loading the RAD51 recombinase onto single-stranded DNA (ssDNA) in concert with the family of proteins known as the RAD51 paralogs, of which RAD51C is a member (Suwaki et al., 2011). RAD51-coated ssDNA invades an intact, homologous duplex DNA molecule, most commonly a sister chromatid, which becomes the template for accurate DSB repair.

In vitro, G-rich ssDNA can adopt secondary structures known as G4s under physiological-like conditions (Lipps and Rhodes, 2009). G4s consist of stacks of two or more G-quartets formed by four guanines via Hoogsteen base pairing stabilized by a monovalent cation. While in silico analyses have identified more than 300,000 sites with G4-forming potential in the human genome (Huppert and Balasubramanian, 2005), more recent G4-seq approaches enabled detection of more than 700,000 G4 structures genome-wide (Chambers et al., 2015). The first in vitro visualization of a G4 structure was based on diffraction

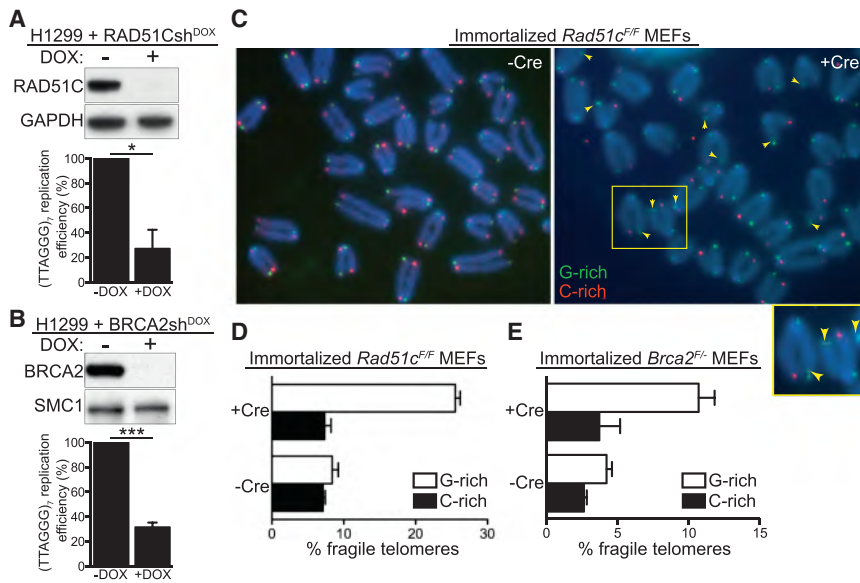


**Figure 1. RAD51C and BRCA2 Prevent Lagging-Strand Telomere Fragility**

(A and B) Replication efficiency of a plasmid containing (TTAGGG)<sub>7</sub> in H1299 cells expressing doxycycline (DOX)-inducible RAD51C (A) or BRCA2 (B) shRNAs is shown relative to the replication efficiency of the empty vector (n = 3 for RAD51Csh<sup>DOX</sup>; n = 4 for BRCA2sh<sup>DOX</sup>; error bars, SEM). p values were calculated using a one-sample t test (\*p ≤ 0.05 and \*\*\*p ≤ 0.001). Cell extracts prepared at the time of plasmid transfection were immunoblotted as indicated. GAPDH and SMC1 were used as loading controls.

(C) CO-FISH detection of lagging (G-rich, green) and leading (C-rich, red) telomeric strands in immortalized *Rad51c<sup>F/F</sup>* MEFs treated with Cre (+Cre) and control (–Cre) retroviruses. Enlarged inset shows the area marked with the yellow rectangle. Arrows mark lagging-strand fragile telomeres.

(D and E) Quantification of fragile telomeres in immortalized *Rad51c<sup>F/F</sup>* (D) and *Brca2<sup>F/F</sup>* (E) MEFs. Approximately 1,000 telomeres were scored per condition per replica (n = 2; error bars, SD). See also Figure S1.

patterns of a guanylic acid solution (Gellert et al., 1962), while evidence that G4s assemble *in vivo* initially came from immunostaining of *Stylonychia* macronuclei with antibodies raised against G4 structures with telomere sequences (Schaffitzel et al., 2001). This study demonstrated that telomeres adopt a G4 configuration *in vivo*. G4 structures have been subsequently detected with several other structure-specific antibodies (Biffi et al., 2013; Henderson et al., 2014; Schaffitzel et al., 2001) and interacting small molecules (Lam et al., 2013; Müller et al., 2010; Rodriguez et al., 2012). Importantly, telomeric G-rich DNA sequences have a high propensity to adopt G4 configurations (Parkinson et al., 2002). Telomeres, repetitive DNA sequences bound by the protein complex shelterin, protect chromosome ends from degradation and fusion. Telomeric G4s can interfere with telomere replication, leading to fragile, shorter telomeres. Supporting this concept, treatment with G4-stabilizing compounds induces telomere dysfunction (Gomez et al., 2006; Rodriguez et al., 2008; Salvati et al., 2007; Tahara et al., 2006).

During DNA replication, G4s are thought to assemble spontaneously on G-rich ssDNA displaced during fork movement. Due to their thermodynamic stability, G4s cause uncoupling of replisome components and fork stalling, which have the potential to trigger genomic instability. Helicases such as FANCD1, PIF1, RECQ, BLM, and WRN, the chromatin remodeler ATRX, and the REV1 translesion polymerase act to dismantle G4s *in vitro*. Several lines of evidence support a similar function *in vivo* for these factors, essential to preserve genome stability during DNA replication (Murat and Balasubramanian, 2014). Conversely, G4 configurations can be stabilized by specific ligands that exhibit higher binding specificity for G4s over duplex DNA, with the G4-interacting compound PDS being one example (Chambers et al., 2015). In mammalian cells, G4 stabilization by PDS results in dissociation of shelterin components from telomeres (Rodriguez et al., 2008). More recently, PDS was demonstrated to trigger replication- and transcription-associated DNA

damage at genomic sites with predicted G4-forming potential (Lam et al., 2013; Rodriguez et al., 2012). These findings highlight the deleterious consequences of persistent G4s for telomere and genome integrity.

HR factors, including BRCA2 and RAD51, are required to facilitate telomere replication and to prevent telomere shortening (Badie et al., 2010). It remained unclear, however, whether assembly of telomeric G4s could contribute to the telomere replication defect of HR-deficient cells. In this work, we demonstrate that telomere fragility in cells lacking HR repair is enhanced by PDS treatment. Importantly, G4-stabilizing compounds, including PDS, decrease the viability of BRCA1-, BRCA2-, or RAD51-deficient cells, which is associated with elevated levels of DNA damage and replication stress. We suggest that in the context of HR deficiency, persistent G4 structures exacerbate the cell-intrinsic challenges that arise during replication of regions with G4-forming potential, thus eliciting checkpoint activation, G2/M cell-cycle arrest, and cell death. This work is therefore highly relevant to the search for treatments that selectively kill tumor cells whose capacity for HR-mediated repair has been compromised.

## RESULTS

### BRCA2 and RAD51C Are Required for G-Rich Strand Telomere Replication

Abrogation of key HR activities elicits telomere fragility (Badie et al., 2010) suggestive of a role for HR in telomere replication. To further investigate this concept, we used a plasmid-based replication assay (Szüts et al., 2008) in H1299 cells harboring inducible small hairpin RNA (shRNA) against RAD51C or BRCA2. Doxycycline addition induced efficient depletion of both proteins, as determined by western blotting (Figures 1A and 1B). The replication efficiency of a plasmid containing an array of seven telomeric repeats (TTAGGG)<sub>7</sub> was significantly lower in RAD51C- or BRCA2-deficient cells compared to control

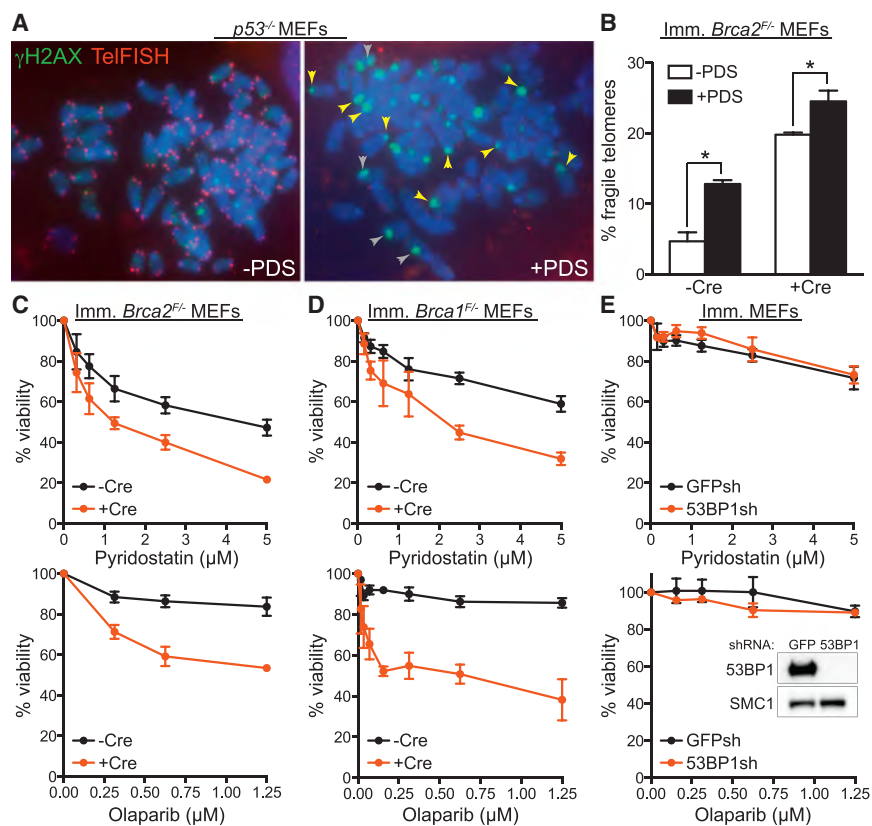


**Figure 2. Effect of the G4-Interacting Compound PDS on Telomere Fragility and Viability of *Brca*-Deficient MEFs**

(A) Mitotic chromosome spreads of  $p53^{-/-}$  MEFs grown in the presence (+PDS) or absence (–PDS) of 5  $\mu$ M PDS for 48 hr. Preparations were fixed and stained with anti- $\gamma$ H2AX monoclonal antibody (green). Telomeres were visualized with a Cy3-conjugated (CCCTAA)<sub>6</sub>-PNA probe (red), using identical exposure conditions for untreated and PDS-treated cells. DNA was counterstained with DAPI (blue).

(B) Quantification of fragile telomeres visualized by FISH on metaphase chromosomes from *Brca2*<sup>F/F</sup> MEFs treated with Cre (+Cre) and control (–Cre) retroviruses incubated with 5  $\mu$ M PDS for 40 hr ( $n = 2$ ; > 1,500 long-arm telomeres were scored per condition per replica; error bars, SD).  $p$  values were calculated using an unpaired two-tailed  $t$  test (\* $p \leq 0.05$ ).

(C) Dose-dependent viability assays of *Brca2*<sup>F/F</sup> MEFs treated with Cre (+Cre) and control (–Cre) retroviruses exposed to PDS or olaparib at the indicated concentrations.

(D) Dose-dependent viability assays of *Brca1*<sup>F/F</sup> MEFs treated as in (C).

(E) Dose-dependent viability assays of immortalized (imm.) MEFs treated as in (C) with retroviruses encoding shRNA against GFP or 53BP1 (Bouman et al., 2010). Cell extracts were immunoblotted as indicated. SMC1 was used as a loading control. See also Figures S1 and S2. Graphs shown are representative of at least two independent experiments, each performed in triplicate. Error bars represent SD of triplicate values obtained from a single experiment.

cells (Figures 1A and 1B). RAD51C inhibition did not affect cell proliferation rate (Figure S1A, available online). Full-length human RAD51C rescued the telomere replication defect completely, indicating specificity of the shRNA for its target (Figure S1B). Importantly, replication of a plasmid containing a (TTACGC)<sub>7</sub> sequence, with two G-to-C substitutions in the telomere repeat, which abrogated the G4-forming potential of the sequence, was not affected by loss of RAD51C expression (Figure S1C). Collectively, these data suggest that assembly of G4 secondary structures on the telomere-containing plasmid underlines its inefficient replication in BRCA2- or RAD51C-depleted cells.

We previously reported that *Brca2* or *Rad51c* deletion in mouse embryonic fibroblasts (MEFs) leads to increased levels of multiple telomeric fluorescence in situ hybridization (FISH) signals (Badie et al., 2010), indicative of telomere fragility. To examine the specificity of the fragile telomere phenotype to the leading or lagging-strand template, chromosome orientation FISH (CO-FISH) assays were performed in immortalized *Brca2*<sup>F/F</sup> or *Rad51c*<sup>F/F</sup> MEFs, in which gene deletion was induced with “hit-and-run” Cre recombinase. The telomeric G-rich strand showed a clear propensity for FISH signal fragmentation (Figure 1C, green). Quantification of fragmented telomeric CO-FISH signals further demonstrated the bias toward fragility of the G-rich telomeric strand in Cre-treated *Brca2*<sup>F/F</sup> and

*Rad51c*<sup>F/F</sup> MEFs (Figures 1D and 1E) as well as in a *Brca2*<sup>–/–</sup> mouse mammary tumor-derived cell line (Evers et al., 2010; Figure S1D).

### G4 Structure Stabilization Exacerbates the Telomere Fragility in *Brca2*-Deleted MEFs

Telomere fragility indicates a telomere replication defect (Martinez et al., 2009; Sfeir et al., 2009), which is thought to stem from the potential of telomere DNA sequences to adopt G4 secondary structures known to obstruct replication fork progression. To test whether telomere fragility in HR-deficient cells was linked to G4 formation, we used the G4 ligand PDS (Rodriguez et al., 2008, 2012) to treat  $p53^{-/-}$  MEFs, which are known to proliferate in the presence of DNA damage, followed by immunofluorescence combined with telomere FISH (IF-FISH) detection. Exposure to PDS led to accumulation of nuclear foci of the Ser139-phosphorylated form of histone H2AX ( $\gamma$ H2AX, Figure 2A), a well-established DSB marker. A subset of these foci colocalized with chromosome ends (Figure 2A, yellow arrowheads), while others localized intrachromosomally (Figure 2A, gray arrowheads). A similar PDS effect has been reported in human cells (Rodriguez et al., 2012). In addition, PDS triggered a dramatic reduction in the intensity of telomere FISH signals corresponding to the G-rich telomere strand (Figures 2A and S1E). In these images, the same exposure time was used for image

acquisition of untreated and PDS-treated cells, to enable comparison of the telomeric signal intensity between the two samples. In contrast, in Figure 2B the exposure time was increased when acquiring images of PDS-treated samples (but not in untreated controls) in order to compensate for the reduced telomeric FISH signal and to enable quantification of fragile telomeres. G4 stabilization significantly enhanced the telomere fragility characteristic of *Brca2*-deleted MEFs (Figure 2B), suggesting that persistent G4 structures contribute to the telomere replication defect intrinsic to cells lacking BRCA2.

We next monitored the viability of *Brca2*-deleted MEFs grown in the presence of PDS or poly (ADP-ribose) polymerase 1 (PARP1) inhibitor olaparib. Even though PDS was moderately toxic to BRCA2-proficient MEFs, we detected a more prominent dose-dependent reduction in the viability of Cre-treated *Brca2*<sup>F/-</sup> MEFs exposed to this compound or olaparib (Figure 2C). The same specific elimination by PDS was observed for BRCA2-deficient V-C8 hamster cells (Kraakman-van der Zwet et al., 2002; Figure S2A) and *Brca2*<sup>-/-</sup> mouse mammary tumor-derived cells (Figure S2B).

The tumor suppressor BRCA1 plays a key role in HR by promoting end resection, which enables loading of the RAD51 recombinase and initiation of HR-mediated repair. This activity of BRCA1 is antagonized by 53BP1, which protects broken DNA ends and channels their repair into non-homologous end joining (NHEJ) (Bouwman et al., 2010; Bunting et al., 2010). To address whether NHEJ deficiency also sensitizes cells to G4 stabilizing agents, similarly to HR ablation, we tested whether *Brca1* or 53BP1 loss confers sensitivity to PDS. Only viability of *Brca1*-deleted cells was affected by exposure to PDS (Figures 2D and 2E), suggesting that G4 stabilization is specifically toxic to HR-, but not to NHEJ-compromised cells. A similar HR-specific effect was observed in response to olaparib (Figures 2D and 2E).

### G4-Interacting Compounds Specifically Kill HR-Deficient Human Cells

To investigate whether PDS-induced G4 stabilization affects viability of human cells lacking BRCA2, we used a matched pair of BRCA2-proficient and deficient DLD1 colorectal adenocarcinoma cell lines (Hucl et al., 2008). Exposure of BRCA2-deficient DLD1 cells to PDS led to a marked decrease in viability compared to BRCA2-proficient cells within 3 days (Figure S2C), which became more pronounced after six days of treatment (Figure 3A). The PARP1 inhibitor olaparib was used as a control in these experiments based on its ability to preferentially kill BRCA2-deficient cells (Figure 3B). Importantly, PDS toxicity to cells lacking BRCA2 was recapitulated in clonogenic assays in which cells were exposed to the drug for only 24 hr (Figure S2D).

BRCA2 plays a central role in HR repair by recruiting RAD51 to the sites of DSBs ssDNA present at stalled replication forks to initiate strand-invasion reactions. We therefore investigated whether RAD51 deficiency sensitized cells to G4-interacting compounds, similarly to loss of BRCA2. Indeed, exposure to PDS caused a substantial drop in cell viability of HEK293T cells lacking RAD51 compared to control cells (Figures 3C and S2C). Olaparib reduced the viability of RAD51-depleted cells; however,

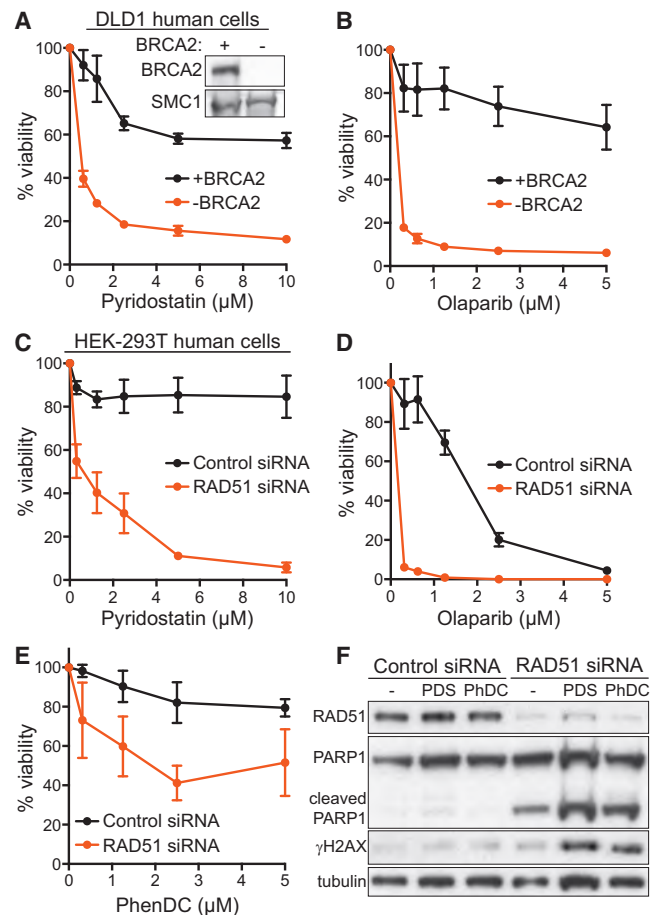


**Figure 3. Effect of PDS on BRCA2- or RAD51-Deficient Human Cell Viability**

(A and B) Dose-dependent viability assays of DLD1 cells, BRCA2 proficient (+BRCA2) or deficient (-BRCA2), treated with indicated concentrations of PDS (A) or olaparib (B).

(C-E) Dose-dependent viability assays of HEK293T cells transfected with control or RAD51 siRNA treated with indicated concentrations of PDS (C), olaparib (D), or PhenDC (E). Graphs shown are representative of at least two independent experiments, each performed in triplicate. Error bars represent SD of triplicate values obtained from a single experiment.

(F) Whole-cell extracts prepared after 4 days of treatment with 2 μM PDS or PhenDC (PhDC) were immunoblotted as indicated. Tubulin was used as a loading control. See also Figure S2.

it also exhibited toxicity against control cells (Figure 3D). Moreover, RAD51 depletion sensitized HEK293T cells to the G4 ligand PhenDC (Figure 3E; Piazza et al., 2010). In western blot analyses (Figure 3F), PDS and PhenDC both induced apoptosis specifically in RAD51-deficient cells, detected by cleaved PARP1 and γH2AX expression, a well-established marker for DNA damage that is also induced by apoptosis (Rogakou et al., 2000). Thus, treatment with G4-interacting agents elicits DNA damage leading to specific killing of cells lacking BRCA2 or RAD51. While PhenDC drastically reduced viability of *Brca1*<sup>-/-</sup> mouse tumor-derived cells (Figure S2E), its toxicity against BRCA2-deficient V-C8 cells was rather modest (Figure S2A).

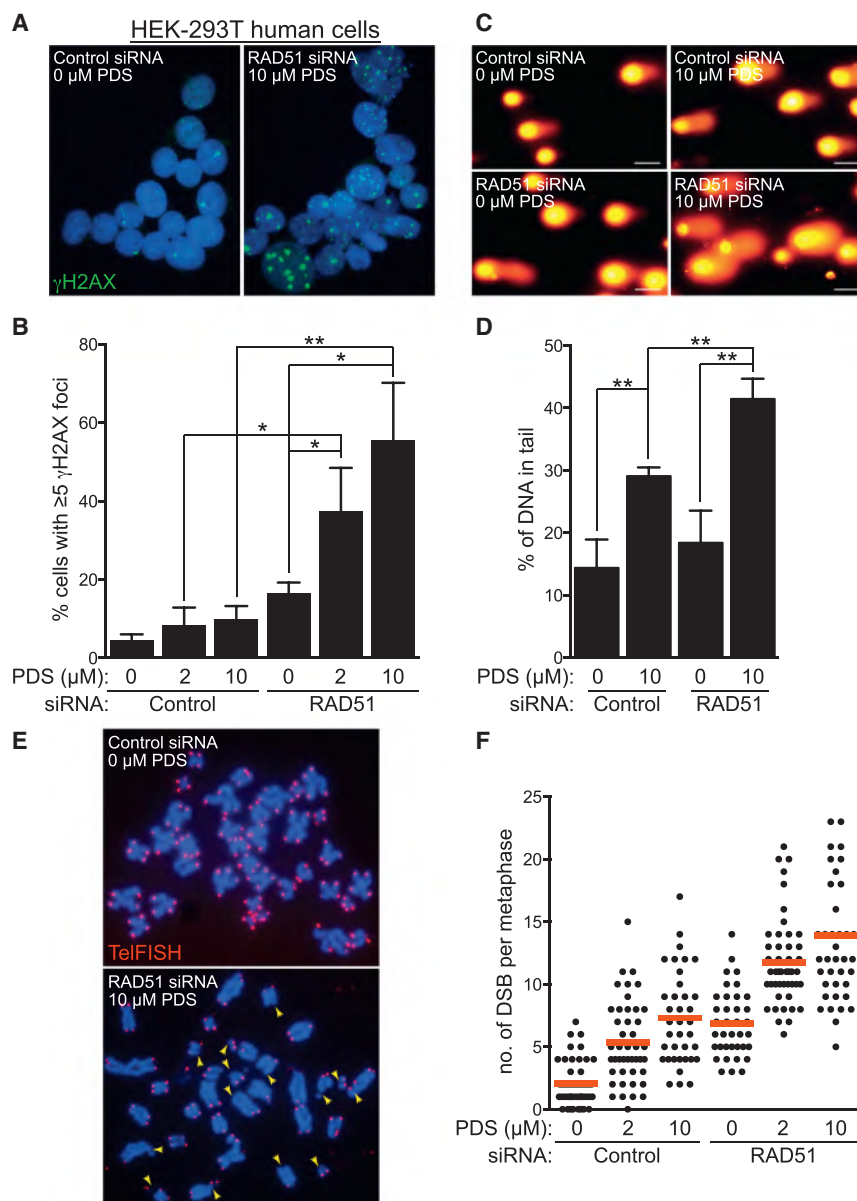


**Figure 4. Elevated Levels of DNA Damage in RAD51-Deficient Human Cells Treated with PDS**

(A) Representative images of HEK293T cells transfected with control or RAD51 siRNA and treated with PDS for 4 days before processing for immunofluorescence staining with anti-γH2AX antibody (green). DNA was counterstained with DAPI (blue).

(B) Quantification of the frequency of cells with  $\geq 5$  γH2AX foci treated as in (A);  $n = 3$ ; error bars, SD.  $p$  values were calculated using an unpaired two-tailed  $t$  test ( $*p \leq 0.05$ ;  $**p \leq 0.01$ ).

(C) Representative images of cells treated as in (A) processed for comet assays. Scale bar, 50 μm.

(D) Quantification of tail moment using comet assays of cells treated as in (A);  $n = 3$ ; error bars, SD.  $p$  values were calculated using an unpaired two-tailed  $t$  test ( $*p \leq 0.05$ ).

(E) Representative images of FISH analysis of metaphase chromosome spreads of cells treated as in (A) with a Cy3-conjugated telomeric probe (red). DNA was counterstained with DAPI (blue). Arrowheads point to chromatid/chromosome breaks.

(F) Quantification of mean DSB frequencies (red bars) in cells treated as in (A). Approximately 40 metaphases were analyzed for each sample. See also Figure S3.

### PDS Enhances DNA Damage Levels in HR-Compromised Cells

We next focused on understanding the mechanism underlying the impaired viability of RAD51-deficient cells in the presence of PDS. Quantification of γH2AX foci as detected by immunofluorescence staining (Figures 4A and S3A) revealed a significant increase in the frequency of HR-deficient cells containing γH2AX foci in response to PDS (Figure 4B). On average, 16.5% of untreated RAD51-depleted cells exhibited five or more γH2AX foci, which escalated to 37.3% and 55.4% following treatment with 2 or 10 μM PDS, respectively. In control cells, the focal γH2AX accumulation upon PDS treatment was not statistically significant (from 4.5% to 8.2% and 9.7%). Alkaline comet assays, in which the percentage of tail DNA was indicative of the levels of DNA damage present in

an individual cell (Figure 4C), confirmed that PDS-triggered DNA damage was significantly augmented in HR-deficient compared to HR-proficient cells (Figure 4D). In agreement with this, PDS elicited increased numbers of DBSs per metaphase in control cells, and RAD51 depletion further enhanced this effect (Figures 4E, 4F, and S3B). In these images we used telomeric FISH probes that helped define individual chromosomes. Given the reduced intensity of the FISH signal for the telomeric G-rich strand in PDS-treated samples, we increased acquisition time for these images, as described for Figure 2B. The average number of breaks detected in this assay reflects break accumulation in mitosis, while cells with higher levels of DNA damage most likely arrest during G2/M transition. Consistently, PDS treatment and RAD51 depletion caused a decrease in the mitotic index (Figure S3C). Taken together, these data supported the concept that G4 stabilization triggers DNA damage, with lethal consequences in cells with compromised capacity for HR-mediated repair.

### Acute Replication Stress Induced by PDS in Cells Lacking RAD51 or BRCA2

PDS has been proposed to induce replication-dependent DNA damage (Rodriguez et al., 2012). This prompted us to monitor the assembly of replication protein A (RPA) subnuclear foci

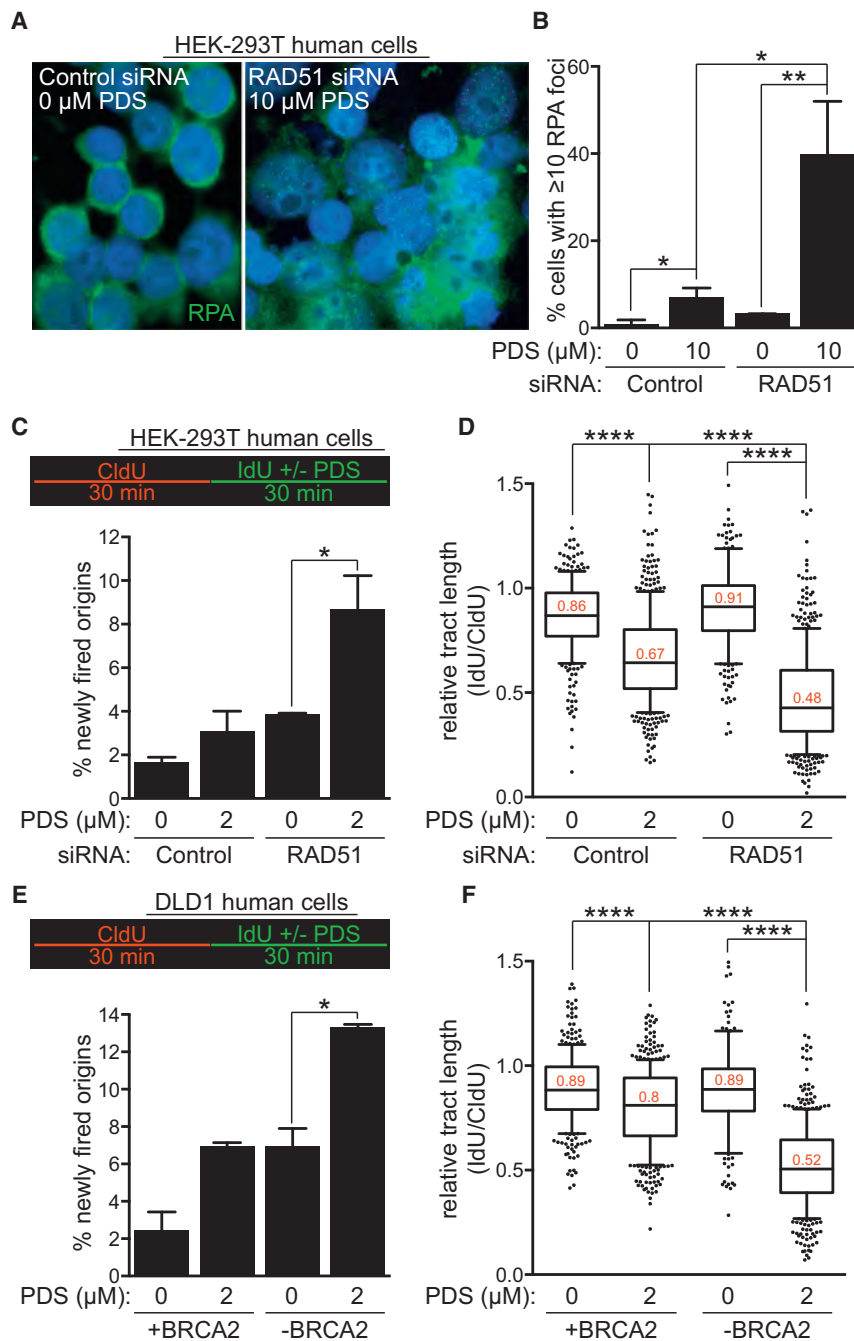


**Figure 5. PDS Exacerbates the Replication Defect of RAD51- and BRCA2-Deficient Human Cells.**

(A) Representative images of HEK293T cells transfected with PDS for 4 days before processing for immunofluorescence staining with anti-RPA antibody (green). DNA was counterstained with DAPI (blue).

(B) Quantification of the frequency of cells with  $\geq 10$  RPA foci treated as in (A);  $n = 3$ ; error bars, SD.  $p$  values were calculated using an unpaired two-tailed  $t$  test (\* $p \leq 0.05$ ; \*\* $p \leq 0.01$ ).

(C) HEK293T cells transfected with control or RAD51 esiRNA were processed for DNA fiber analysis as outlined in the inset, followed by quantification of the frequency of newly fired origins ( $n = 2$ ; error bars, SD).  $p$  values were calculated using an unpaired two-tailed  $t$  test (\* $p \leq 0.05$ ).

(D) Quantification of the relative replication tract length (IdU/CldU) in cells treated as in (C). Middle line represents median, and the box extends from the 25<sup>th</sup> to 75<sup>th</sup> percentiles. The whiskers mark the 10<sup>th</sup> and 90<sup>th</sup> percentiles.  $p$  values were calculated using a Mann-Whitney test ( $n = 2$ ; \*\*\*\* $p < 0.0001$ ).

(E) DLD1 cells, BRCA2 proficient (+BRCA2) or deficient (–BRCA2), were processed for DNA fiber analysis as outlined in the inset, followed by quantification of the frequency of newly fired origins ( $n = 2$ ; error bars, SD).  $p$  values were calculated using an unpaired two-tailed  $t$  test (\* $p \leq 0.05$ ).

(F) Quantification of the relative replication tract length (IdU/CldU) in cells treated as in (E). Middle line represents median, and the box extends from the 25<sup>th</sup> to 75<sup>th</sup> percentiles. The whiskers mark the 10<sup>th</sup> and 90<sup>th</sup> percentiles.  $p$  values were calculated using a Mann-Whitney test ( $n = 2$ ; \*\*\*\* $p < 0.0001$ ). See also Figure S4.

(Figures 5A and S4A) as a readout for genome-wide ssDNA accumulation. PDS induced an approximately 6-fold increase in the levels of RPA foci in control cells and approximately 12-fold increase in RAD51-deficient cells (Figure 5B). RPA accumulation on the chromatin, together with elevated frequency of origin firing and reduced replication rates, represents signatures of replicative stress (Zeman and Cimprich, 2014). To define the nature of this replication defect, we performed DNA fiber analyses in which replication tracks were labeled with consecutive 30 min pulses of CldU and IdU. Addition of PDS during the

second pulse enabled us to evaluate the immediate effect of G4 stabilization on replication. Relative tract length was decreased significantly in PDS-treated cells compared to untreated cells, an effect that was more prominent in cells lacking RAD51 or BRCA2 expression (Figures 5D, 5F, S4B, and S4C). PDS may induce persistent G4s that reduce replication rate or cause DNA breakage that obstructs replication fork progression. Possibly as a compensatory mechanism, PDS treatment significantly increased the number of newly fired origins, detected as green tract only, specifically in RAD51- (Figure 5C) or BRCA2-deficient cells (Figure 5E). Notably, elevated origin firing was also detected in untreated HR-deficient cells. Thus, the replication stress endogenous to HR-compromised cells may be potentiated by chemical G4 stabilization to levels that become lethal. To test this possibility, we used aphidicolin as an alternative means to elicit replication stress (Figure S4D). Treatment with a nontoxic

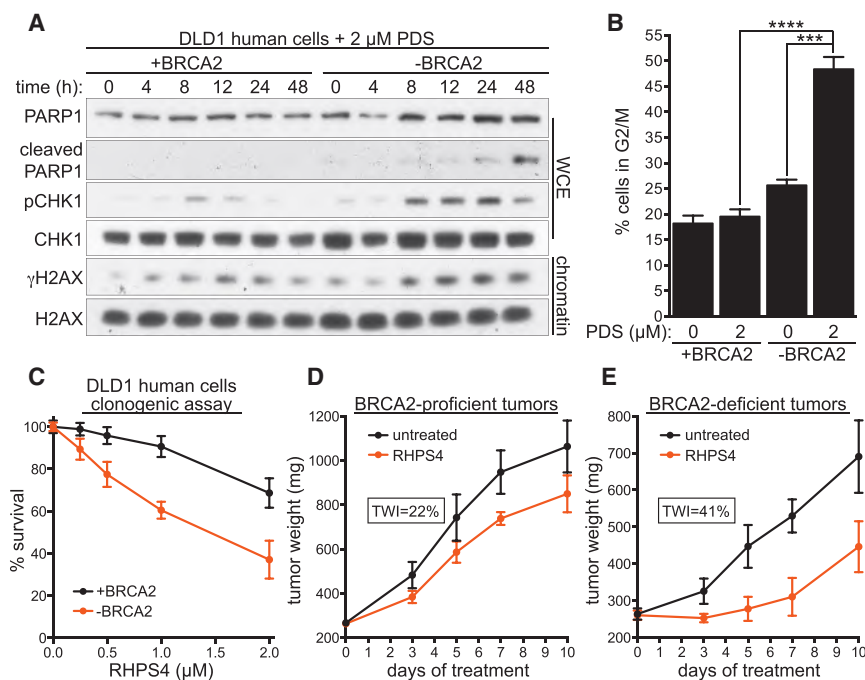


**Figure 6. Effect of PDS on Viability of BRCA2-Deficient Cells and Tumors**

(A) DLD1 cells, BRCA2 proficient (+BRCA2) or deficient (-BRCA2), were incubated with 2  $\mu$ M PDS. Whole-cell extracts (WCE) or chromatin fractions prepared at indicated time points were immunoblotted as shown.

(B) Cells treated as in (A) were processed for FACS analyses of DNA content after 48 hr. Quantification of the percentage of cells in G2/M is shown (n = 3; error bars, SD). p values were calculated using an unpaired two-tailed t test (\*\*\*p  $\leq$  0.001; \*\*\*\*p  $\leq$  0.0001).

(C) Clonogenic survival assays of DLD1 cells, BRCA2 proficient (+BRCA2) or deficient (-BRCA2), exposed to the indicated concentrations of RHPS4 for 24 hr. Error bars represent SD of triplicate values obtained from a single experiment. (D and E) Mean tumor weights in untreated and RHPS4-treated mice injected with BRCA2-proficient (+BRCA2; D) or deficient (-BRCA2; E) DLD1 cells (n = 8; error bars, SD). Tumor weight inhibition (TWI) was calculated at the time point of maximum effect. See also Figures S5 and S6.

dose of aphidicolin led to sensitization of BRCA2-proficient cells to PDS. The synergy between the two compounds was not observed in BRCA2-deficient cells. This suggested that BRCA2 abrogation and aphidicolin treatment cause equivalent levels of replication stress and DNA damage, leading to comparable outcomes in the context of G4 stabilization by PDS.

### PDS Triggers Checkpoint Activation and G2/M Arrest in HR-Defective Cells

Given the profound antiproliferative effect of PDS in BRCA2- or RAD51-deficient cells, we examined its impact on the DNA damage response (DDR). In cells lacking BRCA2 or RAD51 expression, continuous PDS treatment for 4 days elicited a robust phosphorylation of KAP1 (Ser824), CHK1 (Ser314/345), and RPA (Ser4/8), indicative of ATM/ATR checkpoint activation, as well as PARP1 cleavage, a marker for apoptosis (Figures S5A and S5B). To establish whether DDR preceded apoptosis onset, we monitored the response to PDS over a 48 hr interval. In BRCA2-deficient cells, PDS triggered H2AX and CHK1 phosphorylation after 8 hr of treatment, whereas PARP1 cleavage was initiated between 24 hr and 48 hr (Figure 6A). RAD51-depleted HEK293T cells similarly exhibited  $\gamma$ H2AX activation prior to PARP1 cleavage (Figure S5C). These results indicate that PDS-induced DDRs are provoked prior to apoptosis in cells lacking BRCA2 or RAD51. Accordingly, BRCA2- and RAD51-deficient cells accumulated in G2/M after PDS treatment (Figures 6B and S6A). A decrease in S-phase cells further reflected the effect of PDS on cell-cycle progression and checkpoint activation specifically in HR-deficient cells (Figures S6A and S6B). PDS induces replication-associated DSBs, although transcription-related DNA damage may accumulate in stages of the cell cycle other than S phase (Rodriguez et al., 2012). To address whether PDS causes damage in noncycling cells, G0/G1 arrest

was induced by serum starvation in the presence or absence of PDS. Arrested cells lacked the ability to incorporate the thymidine analog EdU, in contrast to cells released into the cell cycle by serum addition to the media (Figure S6C). Quantification of  $\gamma$ H2AX-positive cells demonstrated that PDS treatment for 48 hr did not induce DNA damage in noncycling cells, while a marked increase in the percentage of cells expressing  $\gamma$ H2AX was detected in the subset of cycling cells treated with PDS (Figure S6C).

### In Vivo Responses of BRCA2-Deficient Tumors to G4 Ligands

Regardless of the effective suppression of HR-deficient cell viability and survival by PDS-mediated G4 stabilization (Figures 3A and S2D), the efficacy of PDS could not be established in vivo due to its toxicity predicted by in vitro studies (Rodriguez et al., 2012). Instead, we tested in our cellular models a previously reported G4-stabilizing drug, RHPS4 (Gavathiotis et al., 2003; Gowan et al., 2001; Heald et al., 2002), with well-characterized pharmacological features (Leonetti et al., 2008; Salvati et al., 2007). RHPS4 markedly diminished survival of BRCA2-deficient DLD1 cells relative to BRCA2-proficient cells (Figure 6C). To test its efficacy in vivo, DLD1 cells were injected into mice and allowed to form palpable tumors. In line with previous publications reporting the antitumor effect of RHPS4 (Leonetti et al., 2008; Salvati et al., 2007), this drug repressed growth of BRCA2-proficient tumors as assessed by tumor weight inhibition (TWI) (22%, Figure 6D). Importantly, the growth inhibitory effect of RHPS4 was almost twice as pronounced in BRCA2-deficient tumors (TWI = 41%, Figure 6E). RHPS4 treatment elicited a marked delay in tumor regrowth (approximately 7 days in BRCA2-deficient compared to 4 days in BRCA2-proficient tumors). Thus, our conclusions based on cellular models can be translated

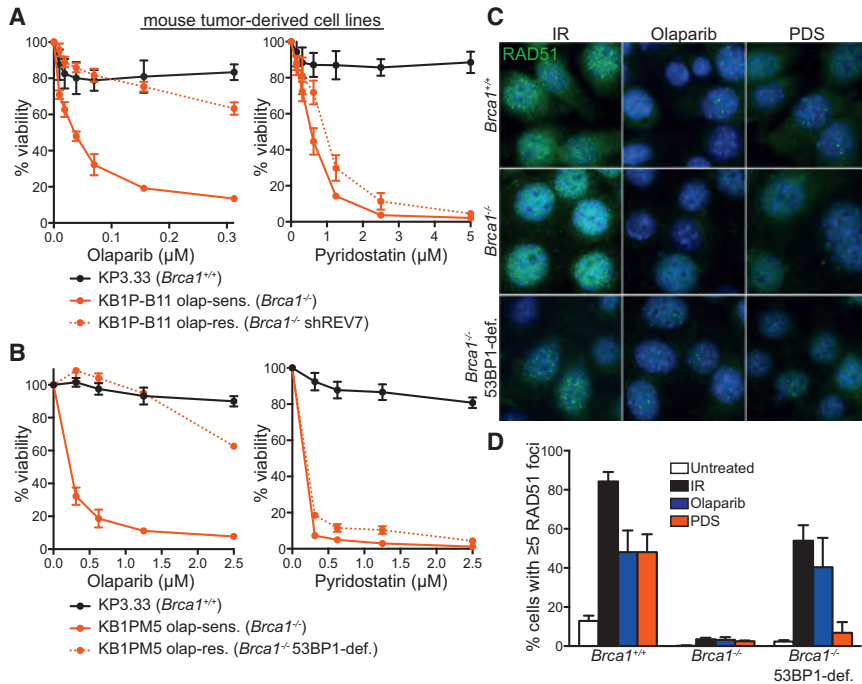


**Figure 7. Olaparib-Resistant *Brca1*-Deleted Tumor Cells Exhibit PDS Sensitivity**

(A and B) Dose-dependent viability assays of mouse mammary tumor-derived cell lines deficient in REV7 (A) or 53BP1 (B) treated with indicated concentrations of PDS or olaparib. Graphs shown are representative of at least two independent experiments, each performed in triplicate. Error bars represent SD of triplicate values obtained from a single experiment.

(C) Representative images of cells described in (A) incubated with 0.5  $\mu$ M olaparib (OLAP), PDS for 40 hr, or irradiated with 10 Gy of IR followed by 1 hr recovery and processed for immunofluorescence staining with anti-RAD51 antibody (green). DNA was counterstained with DAPI (blue).

(D) Quantification of the frequency of cells with  $\geq 5$  RAD51 foci in cells treated as in (C);  $n = 2$ ; error bars, SD;  $>200$  nuclei were analyzed for each condition per replica. See also Figure S7.

in vivo and support the concept that G4-stabilizing compounds identify a class of drugs, which may facilitate future development of novel therapeutic strategies for targeting BRCA2-deficient tumors.

### PDS Kills Olaparib-Resistant Tumor-Derived Cells

Treatment of BRCA-deficient tumors poses a major challenge in the clinic due to the rapid emergence of drug resistance. To test the potential of PDS to eliminate *Brca1*-deficient mouse tumor-derived cells refractory to olaparib, we used two *Brca1*<sup>-/-</sup> cellular mouse models, in which olaparib resistance was mediated by concomitant loss of REV7 (Figure 7A; Xu et al., 2015) or 53BP1 (Figure 7B; Jaspers et al., 2013). Cells carrying intact *Brca1* (*Brca1*<sup>+/+</sup>) showed no sensitivity to PDS or olaparib, while cells established from a *Brca1*<sup>-/-</sup> tumor were sensitive to both drugs, as determined in viability and clonogenic assays (Figures 7A, 7B, S7A, and S7B). Strikingly, olaparib-resistant *Brca1*-deficient cells lacking REV7 or 53BP1 expression (*Brca1*<sup>-/-</sup> shREV7; *Brca1*<sup>-/-</sup> 53BP1-deficient) were hypersensitive to PDS (Figures 7A, 7B, S7A, and S7B). These effects were recapitulated in human cells, in which 53BP1 and BRCA1 were depleted using siRNA (Figure S7C). Our results, therefore, strongly suggest that BRCA1-deficient cells, including those resistant to PARP inhibitors, can be targeted by treatment with G4-stabilizing compounds.

HR restoration in *Brca1*-deleted cells and tumors is driven by 53BP1 loss, which enables survival (Bouwman et al., 2010; Bunting et al., 2010). Moreover, ionizing radiation (IR)-induced RAD51 foci assemble in olaparib-resistant *Brca1*<sup>-/-</sup>, 53BP1-deficient cells (albeit not at the same level as in *Brca1*<sup>+/+</sup> cells), but not in olaparib-sensitive *Brca1*<sup>-/-</sup> tumor-derived cells (Jaspers et al., 2013). Our data (Figures 7C and 7D) demonstrate

that olaparib treatment itself triggers RAD51 foci in wild-type and olaparib-resistant, but not olaparib-sensitive, cells, thereby providing a direct correlation between olaparib-induced HR reactivation and its impact on cell survival. PDS treatment induced RAD51 foci in *Brca1*<sup>+/+</sup> cells, similarly to olaparib (Figures 7C and 7D). However, RAD51 foci were absent in both olaparib-sensitive and olaparib-resistant cells upon treatment with PDS (Figures 7C and 7D), suggesting that failure to reactivate HR repair contributes to the toxicity of this compound in *Brca1*<sup>-/-</sup>, 53BP1-deficient cells. To gain further insight into the mechanism of RAD51 foci suppression, we evaluated the levels of chromatin-associated RPA, indicative of end resection activity. In the chromatin fraction of PDS-treated cells, less RPA was detected than in cells exposed to olaparib or IR (Figure S7D). Thus, impaired HR reactivation upon PDS treatment in a *Brca1*<sup>-/-</sup>, 53BP1-deficient background is likely caused by defects in end resection.

### DISCUSSION

The ability of G-rich DNA to adopt G4 secondary structures in vitro was reported over 50 years ago (Gellert et al., 1962). Although G4s are thought to positively regulate key cellular processes, they can also obstruct replication-fork progression, leading to genomic instability (Tarsounas and Tijsterman, 2013). In this study, we establish that effective replication of G4 structures requires HR activities. G4s represent potent replication barriers, and HR provides a well-characterized mechanism for replication-fork restart and repair of replication-associated DSBs. Yet, the potential requirement for HR in G4 stability has not been investigated, with the notable exception of *Saccharomyces cerevisiae pif1* mutants, in which attempts to restart forks stalled in the vicinity of G4 structures generated recombination intermediates. This suggested a role for HR in fork restart when Pif1 activity is abrogated (Ribeyre et al., 2009).

### HR Is Required for Effective Replication of Genomic Regions with G4-Forming Potential

HR factors have previously been implicated in telomere maintenance (Tacconi and Tarsounas, 2015). In the present work, we used a plasmid-based replication assay in human cells to show that replication of telomeric repeats is ineffective when key HR activities are abrogated. Two lines of evidence established the HR requirement for replication of the G-rich telomeric strand. First, telomere fragility triggered by HR gene deletion was specific to the G-rich telomeric strand, which possesses G4-forming potential. Second, disruption of the G4-forming telomeric repeats through G-to-C substitutions rescued its replication defect in HR-deficient cells.

We propose that HR promotes replication in the presence of obstructive G4 structures by restarting stalled forks and/or by repairing replication-associated DSBs within telomeres, rather than contributing to telomeric G4 dissolution per se. The latter process is likely mediated by the shelterin component TRF1, which recruits BLM helicase to telomeres to unwind G4 structures (Zimmermann et al., 2014). The concept that HR and shelterin provide distinct mechanisms for telomere replication is supported by the synthetic lethality observed between *Brca2* and *Trf1* gene deletions in immortalized MEFs, accompanied by additive levels of telomere fragility (Badie et al., 2010). Inhibition of BLM expression with shRNA in *Brca2*-deleted cells similarly induced cell-cycle arrest (J.Z. and M.T., unpublished data), further arguing that independent mechanisms act during telomere replication to dismantle G4s and to repair the DNA damage induced by persistent G4 structures.

Importantly, G4 stabilization by PDS reduced viability of mouse, human, and hamster cells lacking BRCA1, BRCA2, or RAD51. It exacerbated telomere fragility and DNA damage levels in HR-deficient cells. Conceivably, unresolved G4s presenting intrachromosomally or within telomeres are converted to DSBs, eliciting in turn checkpoint activation, cell-cycle arrest, and/or specific elimination of HR-compromised cells by apoptotic mechanisms.

The efficacy of PDS in cell killing was previously attributed to its genome-wide toxicity, suggested by the accumulation of DNA damage marker  $\gamma$ H2AX at genomic sites with computationally inferred G4-forming sequences (Rodriguez et al., 2012). It is conceivable that the same sites may be prone to breakage in HR-deficient cells treated with PDS. Our mitotic DSB quantification illustrates the additive effect of PDS on the levels of DNA damage triggered by HR abrogation itself. A conundrum posed by this quantification was that PDS induced approximately fifteen DSBs per metaphase in cells lacking RAD51, yet in silico predictions suggested that more than 300,000 genomic sites can adopt G4 configurations (Huppert and Balasubramanian, 2005). This discrepancy could be explained by the multitude of mechanisms known to maintain genome integrity by dismantling G4s formed during genome replication (Tarsounas and Tijsterman, 2013). While most genomic G4s are dissolved by alternative mechanisms, our data suggest that a subset triggers fork stalling and DSBs, which are particularly toxic in HR-deficient cells lacking a key pathway of fork restart and break repair. G4-induced DNA damage may be repaired by error-prone mechanisms in the absence of HR, which seems insufficient for the survival of

these cells. Moreover, checkpoint activation prevented entry of cells with elevated DSB levels into mitosis, which further justifies the lower number of mitotic DSBs detected in our assay.

### Implications for Cancer Therapies

The work presented here demonstrates that the G4-stabilizing drug RHPS4 limits the growth of BRCA2-deficient tumors grafted in mice. The well-characterized ability of RHPS4 to trigger telomere dysfunction may contribute to its toxicity to BRCA2-deficient cells (Salvati et al., 2007). Therefore, we propose that the anticancer potential of the G4-stabilizing drug RHPS4 can be exploited in the clinic for specific targeting of BRCA2-deficient tumors. This tumor subset is likely to benefit most from this novel class of anticancer drugs. Furthermore, these results open a favorable prospective for future clinical development of PDS into a drug-like compound, with a more robust anticipated antitumor activity than RHPS4 in models for BRCA2 inactivation.

Mutations in HR genes such as *BRCA1*, *BRCA2*, or *RAD51C* predispose individuals to breast and ovarian cancers. Tumors carrying HR gene deletions are vulnerable to drugs that either introduce replication-associated DNA damage (e.g., platinum drugs) or inhibit DNA repair pathways other than HR (e.g., PARP1 inhibitors, such as olaparib). In both cases, excessive DNA-damage accumulation triggers cell death. Here, we propose that G4-binding compounds identify a novel class of molecules that can be used to target BRCA deficiency. They act by stabilizing secondary structures in genomic regions with high G-rich content, thus reducing replication fork speed and inducing RPA foci indicative of ssDNA accumulation. *BRCA* gene abrogation is associated with the same responses (Carlos et al., 2013). In the absence of HR, G4-interacting compounds are likely to elevate the endogenous replication stress to levels that become lethal due to excessive DNA-damage accumulation.

One well-documented caveat of targeted drug treatments, such as olaparib, is that tumors rapidly acquire resistance through mechanisms that include activation of P-glycoprotein drug efflux transporter, genetic *Brca1/2* re-activation, and loss of 53BP1/REV7 (Bouwman and Jonkers, 2014; Jaspers et al., 2013; Xu et al., 2015). In this work, we establish that G4-stabilizing compounds are profoundly toxic to BRCA-defective cells, including those resistant to PARP inhibitors. In particular, the striking cytotoxicity of PDS is due to the combined replication failure induced by this drug and the DNA repair defect associated with HR abrogation. Therefore, pharmacological G4 stabilization could be exploited in future therapeutic modalities targeting this difficult to treat tumor subset. Olaparib-resistant cells fail to reactivate HR in response to PDS, which may account for the lethality induced by this G4-stabilizing compound. We therefore anticipate that further clinical development of G4-stabilizing compounds will enhance their ability to selectively eliminate HR-compromised tumors, including those that have acquired resistance to existing therapies.

### EXPERIMENTAL PROCEDURES

For detailed descriptions of these and additional procedures, see Supplemental Experimental Procedures.

### Cell Lines, Culture Conditions, and In Vivo Experiments

HEK293T, H1299, and DLD1 cells were cultured under conventional growth conditions. In vivo experiments were performed as previously described (Salvati et al., 2007). All animal procedures were in compliance with the national and international directives (D.L. March 4, 2014, no. 26; directive 2010/63/EU of the European Parliament and of the council; Guide for the Care and Use of Laboratory Animals, United States National Research Council, 2011).

### Plasmid-Based Replication Assay

Plasmid-based replication assays were performed as previously described (Sarkies et al., 2010; Szüts et al., 2008) with modifications listed in Supplemental Experimental Procedures.

### RNAi

DLD1 and HEK293T cells were transfected with 40 nM siRNA using Dharmafect 1 (Dharmacon) according to manufacturer's instructions.

### Cell Viability Assays

Cell viability was determined by incubation with 10  $\mu$ g/ml of resazurin for 2 hr. Fluorescence was measured at 590 nm using a plate reader (POLARstar, Omega one). Cell viability was expressed relative to untreated cells of the same cell line, thus accounting for any differences in viability caused by HR deficiency. Graphs shown are representative of at least two independent experiments, each performed in triplicate. Error bars represent SD of triplicate values obtained from a single experiment.

### FACS Analysis

Cells were harvested by trypsinization, washed in cold PBS, and fixed in ice-cold 70% ethanol overnight at 4°C. Following two washes in PBS, cells were incubated with 20  $\mu$ g/ml propidium iodide and 10  $\mu$ g/ml RNase A (Sigma) in PBS. At least 10,000 cells were analyzed by flow cytometry (Becton Dickinson). Data were processed using CellQuest (Becton Dickinson) and ModFit LT software.

### Alkaline Single-Cell Gel Electrophoresis Comet Assay

The comet assay was performed as previously described (Singh et al., 1988). Tail measurement was performed using the Komet 5.5 image analysis software.

### Immunofluorescence

Cells were subjected to immunofluorescence staining as described (Tarsounas et al., 2004).

### Preparation of Metaphase Spreads and Telomere FISH

Metaphase spread preparation and telomeric FISH were performed as previously described (Badie et al., 2015).

### Chromosome Orientation FISH and IF-FISH

For CO-FISH, cells were plated at 50%–60% confluency and treated with 10  $\mu$ M bromodeoxyuridine (BrdU) for 20 hr. Colcemid (0.2  $\mu$ g/ml) was added to the cells 4–6 hr before metaphases were processed for CO-FISH as previously described (Bailey et al., 2001).

For IF-FISH, metaphases were spun onto coverslips using a cytospin apparatus (Cytospin 4, Fisher) and subjected to immunofluorescence staining as described (Tarsounas et al., 2004). Samples were fixed again in 4% paraformaldehyde in PBS, and FISH was performed as described (Tarsounas et al., 2004) using 15  $\mu$ g/ml Cy3-conjugated (CCCTAA)<sub>6</sub>-PNA telomeric probe (Applied Biosystems).

### DNA Fiber Assay

DNA fiber assays were performed as described previously (Jackson and Pombo, 1998).

### Immunoblotting

SDS-PAGE and immunoblotting were performed as previously described (Badie et al., 2015). See Supplemental Experimental Procedures for antibodies used in this study.

### SUPPLEMENTAL INFORMATION

Supplemental Information includes Supplemental Experimental Procedures and seven figures and can be found with this article online at <http://dx.doi.org/10.1016/j.molcel.2015.12.004>.

### ACKNOWLEDGMENTS

E.M.C.T. and C.F. contributed equally to this work. We are grateful to Peter Bouwman and Alexandra Duarte (NKI, Amsterdam), Sven Rottenberg (Vet-suisse, University of Bern), Marie-Paule Teulade-Fichou (Curie Institute, Paris), Steve West (CRUK Clare Hall Laboratories), Hyunsook Lee (Seoul National University), and Carmen D'Angelo (Regina Elena Cancer Institute, Italy) for valuable reagents and/or technical suggestions. Research in the S.P.J. lab is funded by Cancer Research UK program grant C6/A11224, the European Research Council, and the European Community Seventh Framework Program grant agreement number HEALTH-F2-2010-259893 (DDRResponse). Core infrastructure funding was provided by Cancer Research UK grant C6946/A14492 and Wellcome Trust grant WT092096. S.P.J. receives salary from the University of Cambridge, supplemented by Cancer Research UK. Research in the K.R. lab is supported by Medical Research Council (MC\_PC\_12001/1), University of Oxford, and Swiss National Science Foundation (31003A\_141197). Work in the A.B. lab is supported by Italian Association for Cancer Research (AIRC # #11567). Work in the J.E.S. lab is supported by a central grant to the Laboratory of Molecular Biology, Cambridge from the Medical Research Council (U105178808). J.Z. is supported by a Cancer Research UK D.Phil. Studentship and E.M.C.T. by a Medical Research Council D.Phil. Studentship. Work in the M.T. lab is supported by Cancer Research UK, Medical Research Council, University of Oxford, and EMBO Young Investigator Program.

Received: March 27, 2015

Revised: September 17, 2015

Accepted: November 2, 2015

Published: December 31, 2015

### REFERENCES

- Aze, A., Zhou, J.C., Costa, A., and Costanzo, V. (2013). DNA replication and homologous recombination factors: acting together to maintain genome stability. *Chromosoma* 122, 401–413.
- Badie, S., Escandell, J.M., Bouwman, P., Carlos, A.R., Thanasoula, M., Gallardo, M.M., Suram, A., Jaco, I., Benitez, J., Herbig, U., et al. (2010). BRCA2 acts as a RAD51 loader to facilitate telomere replication and capping. *Nat. Struct. Mol. Biol.* 17, 1461–1469.
- Badie, S., Carlos, A.R., Folio, C., Okamoto, K., Bouwman, P., Jonkers, J., and Tarsounas, M. (2015). BRCA1 and CtIP promote alternative non-homologous end-joining at uncapped telomeres. *EMBO J.* 34, 828.
- Bailey, S.M., Cornforth, M.N., Kurimasa, A., Chen, D.J., and Goodwin, E.H. (2001). Strand-specific postreplicative processing of mammalian telomeres. *Science* 293, 2462–2465.
- Biffi, G., Tannahill, D., McCafferty, J., and Balasubramanian, S. (2013). Quantitative visualization of DNA G-quadruplex structures in human cells. *Nat. Chem.* 5, 182–186.
- Bouwman, P., and Jonkers, J. (2014). Molecular pathways: how can BRCA-mutated tumors become resistant to PARP inhibitors? *Clin. Cancer Res.* 20, 540–547.
- Bouwman, P., Aly, A., Escandell, J.M., Pieterse, M., Bartkova, J., van der Gulden, H., Hiddingh, S., Thanasoula, M., Kulkarni, A., Yang, Q., et al. (2010). 53BP1 loss rescues BRCA1 deficiency and is associated with triple-negative and BRCA-mutated breast cancers. *Nat. Struct. Mol. Biol.* 17, 688–695.
- Bunting, S.F., Callén, E., Wong, N., Chen, H.T., Polato, F., Gunn, A., Bothmer, A., Feldhahn, N., Fernandez-Capetillo, O., Cao, L., et al. (2010). 53BP1 inhibits

- homologous recombination in Brca1-deficient cells by blocking resection of DNA breaks. *Cell* 141, 243–254.
- Carlos, A.R., Escandell, J.M., Kotsantis, P., Suwaki, N., Bouwman, P., Badie, S., Folio, C., Benitez, J., Gomez-Lopez, G., Pisano, D.G., et al. (2013). ARF triggers senescence in Brca2-deficient cells by altering the spectrum of p53 transcriptional targets. *Nat. Commun.* 4, 2697.
- Chambers, V.S., Marsico, G., Boutell, J.M., Di Antonio, M., Smith, G.P., and Balasubramanian, S. (2015). High-throughput sequencing of DNA G-quadruplex structures in the human genome. *Nat. Biotechnol.* 33, 877–881.
- Evers, B., Schut, E., van der Burg, E., Braumuller, T.M., Egan, D.A., Holstege, H., Edser, P., Adams, D.J., Wade-Martins, R., Bouwman, P., and Jonkers, J. (2010). A high-throughput pharmaceutical screen identifies compounds with specific toxicity against BRCA2-deficient tumors. *Clin. Cancer Res.* 16, 99–108.
- Gavathiotis, E., Heald, R.A., Stevens, M.F., and Searle, M.S. (2003). Drug recognition and stabilisation of the parallel-stranded DNA quadruplex d(TTAGGGT)<sub>4</sub> containing the human telomeric repeat. *J. Mol. Biol.* 334, 25–36.
- Gellert, M., Lipsett, M.N., and Davies, D.R. (1962). Helix formation by guanylic acid. *Proc. Natl. Acad. Sci. USA* 48, 2013–2018.
- Gomez, D., Wenner, T., Brassart, B., Douarre, C., O'Donohue, M.F., El Khoury, V., Shin-Ya, K., Morjani, H., Trentesaux, C., and Riou, J.F. (2006). Telomestatin-induced telomere uncapping is modulated by POT1 through G-overhang extension in HT1080 human tumor cells. *J. Biol. Chem.* 281, 38721–38729.
- Gowan, S.M., Heald, R., Stevens, M.F., and Kelland, L.R. (2001). Potent inhibition of telomerase by small-molecule pentacyclic acridines capable of interacting with G-quadruplexes. *Mol. Pharmacol.* 60, 981–988.
- Halazonetis, T.D., Gorgoulis, V.G., and Bartek, J. (2008). An oncogene-induced DNA damage model for cancer development. *Science* 319, 1352–1355.
- Hashimoto, Y., Ray Chaudhuri, A., Lopes, M., and Costanzo, V. (2010). Rad51 protects nascent DNA from Mre11-dependent degradation and promotes continuous DNA synthesis. *Nat. Struct. Mol. Biol.* 17, 1305–1311.
- Heald, R.A., Modi, C., Cookson, J.C., Hutchinson, I., Laughton, C.A., Gowan, S.M., Kelland, L.R., and Stevens, M.F. (2002). Antitumor polycyclic acridines. 8.(1) Synthesis and telomerase-inhibitory activity of methylated pentacyclic acridinium salts. *J. Med. Chem.* 45, 590–597.
- Henderson, A., Wu, Y., Huang, Y.C., Chavez, E.A., Platt, J., Johnson, F.B., Brosh, R.M.J., Jr., Sen, D., and Lansdorp, P.M. (2014). Detection of G-quadruplex DNA in mammalian cells. *Nucleic Acids Res.* 42, 860–869.
- Hucl, T., Rago, C., Gallmeier, E., Brody, J.R., Gorospe, M., and Kern, S.E. (2008). A syngeneic variance library for functional annotation of human variation: application to BRCA2. *Cancer Res.* 68, 5023–5030.
- Huppert, J.L., and Balasubramanian, S. (2005). Prevalence of quadruplexes in the human genome. *Nucleic Acids Res.* 33, 2908–2916.
- Jackson, D.A., and Pombo, A. (1998). Replicon clusters are stable units of chromosome structure: evidence that nuclear organization contributes to the efficient activation and propagation of S phase in human cells. *J. Cell Biol.* 140, 1285–1295.
- Jaspers, J.E., Kersbergen, A., Boon, U., Sol, W., van Deemter, L., Zander, S.A., Drost, R., Wientjens, E., Ji, J., Aly, A., et al. (2013). Loss of 53BP1 causes PARP inhibitor resistance in Brca1-mutated mouse mammary tumors. *Cancer Discov.* 3, 68–81.
- Kraakman-van der Zwet, M., Overkamp, W.J.I., van Lange, R.E.E., Essers, J., van Duijn-Goedhart, A., Wiggers, I., Swaminathan, S., van Buul, P.P.W., Errami, A., Tan, R.T.L., et al. (2002). Brca2 (XRCC11) deficiency results in radioresistant DNA synthesis and a higher frequency of spontaneous deletions. *Mol. Cell Biol.* 22, 669–679.
- Lam, E.Y., Beraldi, D., Tannahill, D., and Balasubramanian, S. (2013). G-quadruplex structures are stable and detectable in human genomic DNA. *Nat. Commun.* 4, 1796.
- Lambert, S., Mizuno, K., Blaisonneau, J., Martineau, S., Chanut, R., Fréon, K., Murray, J.M., Carr, A.M., and Baldacci, G. (2010). Homologous recombination restarts blocked replication forks at the expense of genome rearrangements by template exchange. *Mol. Cell* 39, 346–359.
- Leonetti, C., Scarsella, M., Riggio, G., Rizzo, A., Salvati, E., D'Incalci, M., Staszewsky, L., Frapolli, R., Stevens, M.F., Stoppacciaro, A., et al. (2008). G-quadruplex ligand RHPS4 potentiates the antitumor activity of camptothecins in preclinical models of solid tumors. *Clin. Cancer Res.* 14, 7284–7291.
- Lipps, H.J., and Rhodes, D. (2009). G-quadruplex structures: in vivo evidence and function. *Trends Cell Biol.* 19, 414–422.
- Martínez, P., Thanasoula, M., Muñoz, P., Liao, C., Tejera, A., McNeese, C., Flores, J.M., Fernández-Capetillo, O., Tarsounas, M., and Blasco, M.A. (2009). Increased telomere fragility and fusions resulting from TRF1 deficiency lead to degenerative pathologies and increased cancer in mice. *Genes Dev.* 23, 2060–2075.
- Müller, S., Kumari, S., Rodriguez, R., and Balasubramanian, S. (2010). Small-molecule-mediated G-quadruplex isolation from human cells. *Nat. Chem.* 2, 1095–1098.
- Murat, P., and Balasubramanian, S. (2014). Existence and consequences of G-quadruplex structures in DNA. *Curr. Opin. Genet. Dev.* 25, 22–29.
- Negrini, S., Gorgoulis, V.G., and Halazonetis, T.D. (2010). Genomic instability—an evolving hallmark of cancer. *Nat. Rev. Mol. Cell Biol.* 11, 220–228.
- Parkinson, G.N., Lee, M.P., and Neidle, S. (2002). Crystal structure of parallel quadruplexes from human telomeric DNA. *Nature* 417, 876–880.
- Piazza, A., Boulé, J.B., Lopes, J., Mingo, K., Largy, E., Teulade-Fichou, M.P., and Nicolas, A. (2010). Genetic instability triggered by G-quadruplex interacting Phen-DC compounds in *Saccharomyces cerevisiae*. *Nucleic Acids Res.* 38, 4337–4348.
- Ribeyre, C., Lopes, J., Boulé, J.B., Piazza, A., Guédin, A., Zakian, V.A., Mergny, J.L., and Nicolas, A. (2009). The yeast Pif1 helicase prevents genomic instability caused by G-quadruplex-forming CEB1 sequences in vivo. *PLoS Genet.* 5, e1000475.
- Rodriguez, R., Müller, S., Yeoman, J.A., Trentesaux, C., Riou, J.F., and Balasubramanian, S. (2008). A novel small molecule that alters shelterin integrity and triggers a DNA-damage response at telomeres. *J. Am. Chem. Soc.* 130, 15758–15759.
- Rodriguez, R., Miller, K.M., Forment, J.V., Bradshaw, C.R., Nikan, M., Britton, S., Oelschlaegel, T., Xhemalce, B., Balasubramanian, S., and Jackson, S.P. (2012). Small-molecule-induced DNA damage identifies alternative DNA structures in human genes. *Nat. Chem. Biol.* 8, 301–310.
- Rogakou, E.P., Nieves-Neira, W., Boon, C., Pommier, Y., and Bonner, W.M. (2000). Initiation of DNA fragmentation during apoptosis induces phosphorylation of H2AX histone at serine 139. *J. Biol. Chem.* 275, 9390–9395.
- Salvati, E., Leonetti, C., Rizzo, A., Scarsella, M., Mottolose, M., Galati, R., Sperduti, I., Stevens, M.F., D'Incalci, M., Blasco, M., et al. (2007). Telomere damage induced by the G-quadruplex ligand RHPS4 has an antitumor effect. *J. Clin. Invest.* 117, 3236–3247.
- Sarkies, P., Reams, C., Simpson, L.J., and Sale, J.E. (2010). Epigenetic instability due to defective replication of structured DNA. *Mol. Cell* 40, 703–713.
- Schaffitzel, C., Berger, I., Postberg, J., Hanes, J., Lipps, H.J., and Plüchthun, A. (2001). In vitro generated antibodies specific for telomeric guanine-quadruplex DNA react with *Styloynchia lemnae* macronuclei. *Proc. Natl. Acad. Sci. USA* 98, 8572–8577.
- Schlacher, K., Christ, N., Sliad, N., Egashira, A., Wu, H., and Jasin, M. (2011). Double-strand break repair-independent role for BRCA2 in blocking stalled replication fork degradation by MRE11. *Cell* 145, 529–542.
- Sfeir, A., Kosiyatrakul, S.T., Hockemeyer, D., MacRae, S.L., Karlseder, J., Schildkraut, C.L., and de Lange, T. (2009). Mammalian telomeres resemble fragile sites and require TRF1 for efficient replication. *Cell* 138, 90–103.
- Singh, N.P., McCoy, M.T., Tice, R.R., and Schneider, E.L. (1988). A simple technique for quantitation of low levels of DNA damage in individual cells. *Exp. Cell Res.* 175, 184–191.
- Suwaki, N., Klare, K., and Tarsounas, M. (2011). RAD51 paralogs: roles in DNA damage signalling, recombinational repair and tumorigenesis. *Semin. Cell Dev. Biol.* 22, 898–905.

- Szűts, D., Marcus, A.P., Himoto, M., Iwai, S., and Sale, J.E. (2008). REV1 restrains DNA polymerase zeta to ensure frame fidelity during translesion synthesis of UV photoproducts in vivo. *Nucleic Acids Res.* **36**, 6767–6780.
- Tacconi, E.M., and Tarsounas, M. (2015). How homologous recombination maintains telomere integrity. *Chromosoma* **124**, 119–130.
- Tahara, H., Shin-Ya, K., Seimiya, H., Yamada, H., Tsuruo, T., and Ide, T. (2006). G-Quadruplex stabilization by telomestatin induces TRF2 protein dissociation from telomeres and anaphase bridge formation accompanied by loss of the 3' telomeric overhang in cancer cells. *Oncogene* **25**, 1955–1966.
- Tarsounas, M., and Tijsterman, M. (2013). Genomes and G-quadruplexes: for better or for worse. *J. Mol. Biol.* **425**, 4782–4789.
- Tarsounas, M., Muñoz, P., Claas, A., Smiraldi, P.G., Pittman, D.L., Blasco, M.A., and West, S.C. (2004). Telomere maintenance requires the RAD51D recombination/repair protein. *Cell* **117**, 337–347.
- Xu, G., Chapman, J.R., Brandsma, I., Yuan, J., Mistrik, M., Bouwman, P., Bartkova, J., Gogola, E., Warmerdam, D., Barazas, M., et al. (2015). REV7 counteracts DNA double-strand break resection and affects PARP inhibition. *Nature* **521**, 541–544.
- Zeman, M.K., and Cimprich, K.A. (2014). Causes and consequences of replication stress. *Nat. Cell Biol.* **16**, 2–9.
- Zimmermann, M., Kibe, T., Kabir, S., and de Lange, T. (2014). TRF1 negotiates TTAGGG repeat-associated replication problems by recruiting the BLM helicase and the TPP1/POT1 repressor of ATR signaling. *Genes Dev.* **28**, 2477–2491.

# The Fanconi Anemia Pathway Maintains Genome Stability by Coordinating Replication and Transcription

Rebekka A. Schwab,<sup>1</sup> Jadwiga Nieminuszczy,<sup>1</sup> Fenil Shah,<sup>2</sup> Jamie Langton,<sup>1</sup> David Lopez Martinez,<sup>3</sup> Chih-Chao Liang,<sup>3</sup> Martin A. Cohn,<sup>3</sup> Richard J. Gibbons,<sup>4</sup> Andrew J. Deans,<sup>2</sup> and Wojciech Niedzwiedz<sup>1,\*</sup>

<sup>1</sup>Department of Oncology, Weatherall Institute of Molecular Medicine, University of Oxford, John Radcliffe Hospital, Oxford OX3 9DS, UK

<sup>2</sup>Genome Stability Unit, St. Vincent's Institute, Fitzroy, VIC 3065, Australia

<sup>3</sup>Department of Biochemistry, University of Oxford, Oxford OX1 3QU, UK

<sup>4</sup>Medical Research Council Molecular Haematology Unit, Weatherall Institute of Molecular Medicine, University of Oxford, John Radcliffe Hospital, Oxford OX3 9DS, UK

\*Correspondence: wojciech.niedzwiedz@imm.ox.ac.uk

<http://dx.doi.org/10.1016/j.molcel.2015.09.012>

## SUMMARY

DNA replication stress can cause chromosomal instability and tumor progression. One key pathway that counteracts replication stress and promotes faithful DNA replication consists of the Fanconi anemia (FA) proteins. However, how these proteins limit replication stress remains largely elusive. Here we show that conflicts between replication and transcription activate the FA pathway. Inhibition of transcription or enzymatic degradation of transcription-associated R-loops (DNA:RNA hybrids) suppresses replication fork arrest and DNA damage occurring in the absence of a functional FA pathway. Furthermore, we show that simple aldehydes, known to cause leukemia in FA-deficient mice, induce DNA:RNA hybrids in FA-depleted cells. Finally, we demonstrate that the molecular mechanism by which the FA pathway limits R-loop accumulation requires FANCM translocase activity. Failure to activate a response to physiologically occurring DNA:RNA hybrids may critically contribute to the heightened cancer predisposition and bone marrow failure of individuals with mutated FA proteins.

## INTRODUCTION

Replication of the human genome is a complex process requiring orchestrated activation and maintenance of replication forks emanating from thousands of origins of replication during S-phase. Replication forks stall when they encounter obstacles on the DNA, upon which they require swift processing to prevent their disassembly, resulting in DNA damage. Such collapsed replication forks can contribute to spontaneous recombination events and genomic instability, a hallmark of cancer (Aguilera and Gómez-González, 2008). Faithful DNA replication requires several factors, including proteins of the Fanconi anemia (FA) pathway. To date, 18 FA genes (FANCA-T) have been identified,

and homozygous inactivation of any FA gene product leads to the pediatric syndrome Fanconi anemia, characterized by progressive bone marrow failure, spontaneous chromosomal instability, and high cancer predisposition. Functionally, the FA pathway can be divided into at least three different sub-complexes, the largest of which is the core complex consisting of the FANCA, FANCB, FANCC, FANCE, FANCF, FANCG, FANCL, and FANCM gene products. The core complex, together with the E2 ubiquitin-conjugating enzyme FANCT/UBE2T, have a critical role in activating the FA pathway through monoubiquitination of the FANCD2 and FANCI proteins. This, in turn, promotes DNA repair through the specialized downstream Fanconi proteins FANCD1/BRCA2, FANCN/PALB2, FANCI/BRIP1, FANCO/RAD51C, FANCP/SLX4, FANCF/XPF/ERCC4, and FANCS/BRCA1 (Hira et al., 2015; Kee and D'Andrea, 2012; Kottemann and Smogorzewska, 2013; Rickman et al., 2015; Walden and Deans, 2014; Wang, 2007). Cells from FA patients are hypersensitive to DNA interstrand crosslinking (ICL) agents, potent inhibitors of both DNA replication and transcription. Accordingly, it has been proposed that the FA pathway has a major role in responding to replication stress by facilitating the resolution of DNA lesions arising during DNA replication (Constantinou, 2012; Knipscheer et al., 2009; Kottemann and Smogorzewska, 2013). Recently, work from the Patel group (Langevin et al., 2011) has identified simple aldehydes that can arise endogenously from processes of cellular metabolism as a potent source of DNA damage that requires action of the FA proteins. Mice with combined deficiency for FANCD2 or FANCA and the aldehyde-catabolizing enzyme Aldh2 show developmental defects and early onset of acute leukemia (Langevin et al., 2011; Oberbeck et al., 2014). However, it is unclear how aldehydes confer their toxicity because mice mutually deficient for Aldh2 and the DNA translesion synthesis polymerase Rev1, which cooperates with FA proteins in the same pathway for ICL repair (Niedzwiedz et al., 2004), do not develop any of the phenotypes observed in FANCA/Aldh2-deficient mice (Oberbeck et al., 2014). Therefore, identifying the endogenous substrate that activates the FA pathway under normal growth conditions remains one of the key questions critical for the understanding of this devastating disease.

During transcription, nascent RNA can form hydrogen bonds with one strand of the DNA double helix, leading to the formation

of DNA:RNA hybrids (R-loops). R-loop formation has been described *in vivo*, and its physiological functions include class switch recombination, bacterial and mitochondrial replication, and protection against DNA methylation at CpG island promoters (Aguilera and Garcia-Muse, 2012; Skourti-Stathaki and Proudfoot, 2014). Persistent R-loops could stall replication forks driving genome instability, which is fundamental to cancer and other diseases (Bhatia et al., 2014; Lecona and Fernández-Capetillo, 2014). Here we show that conflicts between replication and transcription and also transcription-associated DNA:RNA hybrids are crucial endogenous DNA lesions that require action of the FA proteins. In particular, we provide evidence that a functional FA pathway protects cells from unscheduled accumulation of such hybrids and that its loss results in an increased level of DNA damage and spontaneous chromosomal instability, both hallmarks of FA patients. Accordingly, inhibition of transcription or removal of excess DNA:RNA hybrids by expression of RNase H1 suppresses increased replication fork stalling and DNA damage occurring in FA-depleted cells. At the mechanistic level, we show that FANCM, the most highly conserved protein in the FA pathway, resolves DNA:RNA hybrids via its intrinsic translocase activity. Unexpectedly, we also found that aldehydes induce DNA:RNA hybrid formation in FANCD2-depleted cells, suggesting a mechanism by which by-products of cellular metabolism, such as simple aldehydes, could exert their toxic effect on our genome. Therefore, we propose that DNA:RNA hybrids are endogenous and physiological substrates of the FA pathway and that, by suppressing excessive DNA:RNA hybrid formation, the FA pathway ensures faithful genome duplication.

## RESULTS

### The FA Pathway Facilitates Accurate Replication under Normal Growth Conditions

Hypersensitivity to agents that impede the progression of replisomes is a hallmark of FA, and, consequently, we and others have found that the FA pathway plays a role in the response to replicative stress (Knipscheer et al., 2009; Lossaint et al., 2013; Schlacher et al., 2012; Schwab et al., 2010). Accordingly, upon treatment with replication inhibitors, a central component of the FA pathway, FANCD2, is activated by monoubiquitination in an ATR-dependent manner (Andreassen et al., 2004). Subsequently, FANCD2 is targeted to damaged replication forks (Lossaint et al., 2013) and forms foci colocalizing with the DNA repair proteins  $\gamma$ H2AX, BRCA1, and RAD51 (Montes de Oca et al., 2005; Taniguchi et al., 2002). Interestingly, FANCD2 is also monoubiquitinated and forms foci that colocalize with  $\gamma$ H2AX in unchallenged cells (Taniguchi et al., 2002; Figure S1A). This suggests that FANCD2 is also required for dealing with replicative stress that arises in cells undergoing normal cell cycle progression. To test this, we analyzed DNA replication in control and FANCD2-depleted cells under normal growth conditions using the DNA fiber technique (Blackford et al., 2012; Schwab and Niedzwiedz, 2011). To determine the impact of FANCD2 depletion on global replication fork dynamics, we measured the lengths of sister fork tracts. Sister forks emanating from the same origin of replication and traveling in opposite directions typically display similar replication rates (Conti et al., 2007).

Consequently, differences in tract lengths indicate that individual forks are more prone to stalling. We noticed a significant increase in asymmetric sister forks in FANCD2-downregulated cells compared with control cells (Figure 1A), suggesting a widespread perturbation of the normal replication program. In support of this notion, we also found increased phosphorylation of MCM2 on Ser-108 and RPA on Ser-33 (Figure 1B) in FANCD2 knockdown cells, both markers of replicative stress (Cortez et al., 2004; Sirbu et al., 2011). Failure to restart stalled forks is a strong signal for DNA damage (Schlacher et al., 2012), and, accordingly, western blot analysis showed increased  $\gamma$ H2AX and phosphorylation of RPA2 at Ser-4/Ser-8 in FANCD2 knockdown cells (Figure 1C). These modifications are associated with DNA double-strand breaks (Sartori et al., 2007), and, therefore, we examined DNA integrity by single-cell gel electrophoresis. Cells with FANCD2 knockdown showed a significant increase in DNA breaks compared with control cells (Figure 1D). DNA damage is a precursor of genomic instability, and, in line with this, we found a greater number of cells with micronuclei in FANCD2-depleted cells (Figure 1E), a phenotype also observed in FA patient cells (Heddle et al., 1978). Moreover, *FANCC*<sup>-/-</sup> mouse embryonic fibroblasts (MEFs) as well as *FANCA*<sup>-/-</sup> mouse hematopoietic stem cells also display signs of replisome instability and activation of the DNA damage response (DDR) in unchallenged cells (Luebben et al., 2014; Walter et al., 2015). Taken together, these findings underscore the FA pathway's general role in facilitating replication under normal growth conditions.

### The Fanconi Anemia Pathway Protects Replication Forks against Transcription-Induced Fork Collapse

Replication of actively transcribed genes induces local replication stress, and, hence, compromises genome stability (Helmrich et al., 2011; Tuduri et al., 2009). We wondered whether the defects we observed in FANCD2-deficient cells could stem from transcription impeding replisome progression. Using proximity ligation assays (PLAs), we observed that FANCD2 colocalizes with total as well as elongating RNA polymerase II (Figure 2A). This colocalization is decreased upon transcription inhibition, with the majority of the PLA-positive cells being confined to the S-phase of the cell cycle (Figures S1B and S1C). Next, we addressed whether transcription contributes to the FA pathway activation and genome instability seen in FANCD2-depleted cells by inhibiting transcription with cordycepin, a potent inhibitor of RNA chain elongation (Rose et al., 1977). Cordycepin treatment significantly decreased FA pathway activation, as measured by the frequency of FANCD2 focus-positive cells as well as FANCD2 monoubiquitination (Figure 2B; Figure S1D). The dose of cordycepin used extensively inhibited transcription without appreciably altering the cell cycle profile (Figures S3E–S3G). Importantly, treatment with two additional transcription inhibitors, 5,6-dichloro-1- $\beta$ -D-ribofuranosyl-benzimidazole (DRB) and flavopiridol, also greatly decreased the number of FANCD2 focus-positive cells (Figure 2C). Strikingly, inhibition of transcription restored sister fork symmetry in FANCD2-depleted cells to the level observed in the control (Figures 2D and 2E), and this correlated with a reduction in the DNA damage response (Figures 2F and 2G).

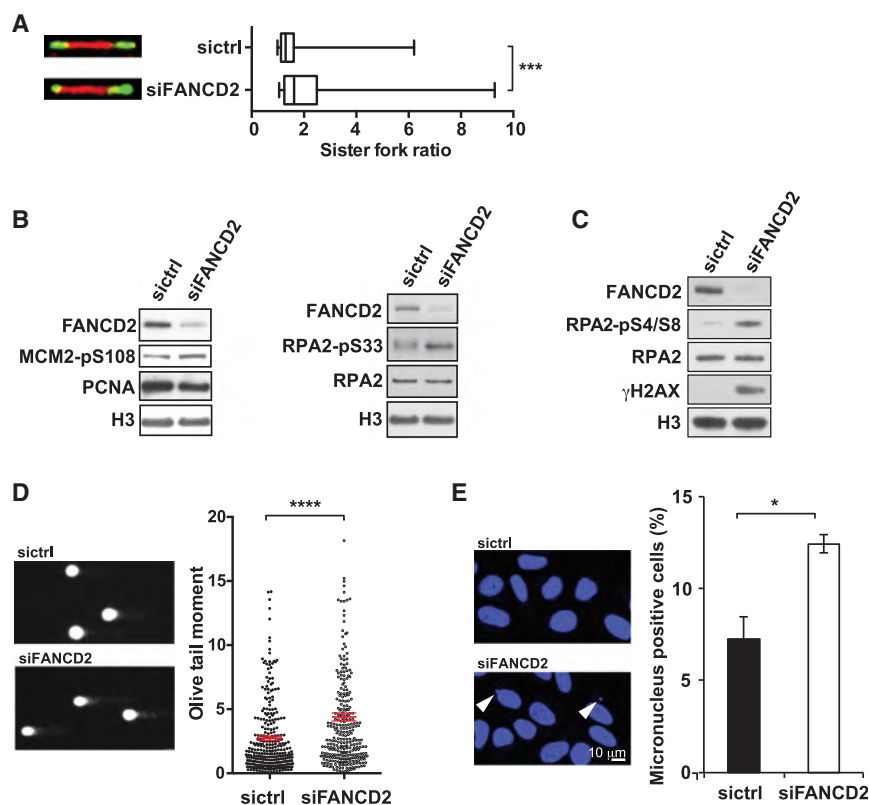


**Figure 1. FANCD2 Protects Cells from Replication Stress and Preserves Genomic Integrity**

(A) DNA fiber analysis comparing sister fork symmetry. Shown are typical sister forks of U2OS cells treated with control (sictrl) or FANCD2 siRNA (siFANCD2). The ratios of the lengths of two corresponding sister replication forks are plotted. The middle line represents the median and the boxes the 25<sup>th</sup> and 75<sup>th</sup> percentiles. The whiskers mark the smallest and largest values. Mann-Whitney test was used to determine statistical significance (n = 3). \*\*\*p ≤ 0.001.

(B) Western blots of whole-cell lysates of control and FANCD2 siRNA-treated U2OS cells probed for phosphorylation of MCM2 on Ser-108 (MCM2-pS108) and RPA2 on Ser-33 (RPA2-pS33). Histone H3, PCNA, and RPA2 served as loading controls. (C) Western blot showing activation of the DDR upon depletion of FANCD2, including phosphorylation of histone H2AX on Ser-139 (γH2AX) and of RPA2 on Ser-4 and Ser-8 (RPA2-pS4/S8). RPA2 and histone H3 were used as loading controls.

(D) Comet assays of RNAi-treated U2OS cells. Individual data points of olive tail moment are plotted, showing mean ±SEM in red (n = 3, two-tailed Mann-Whitney test). \*\*\*\*p ≤ 0.0001.

(E) DAPI-stained nuclei and micronuclei (arrowheads) of RNAi-treated U2OS cells. Mean ±SEM of micronucleus-positive cells are plotted (n = 3; unpaired, two-tailed Student's t test). \*p ≤ 0.05.

Depletion of RNA biogenesis factors such as ASF/SF2 compromises transcription and results in genome instability (Li and Manley, 2005; Luna et al., 2005). Therefore, we hypothesized that ASF/SF2 knockdown should increase the likelihood of replication forks colliding with stalled transcription complexes and, as such, further compromise genome stability in FANCD2-depleted cells. Accordingly, we found that ASF/FANCD2 double-depleted cells grew significantly slower (Figure 3A; Figure S2A) and showed increased genome instability, as indicated by an elevated frequency of micronuclei and chromosomal aberrations compared with any of the single depletions (Figures 3B and 3C). These results provide further support to the notion that the defective DNA replication and genome instability observed in FANCD2 knockdown cells are associated with transcription complexes acting as promiscuous replication fork barriers.

### The FA Pathway Suppresses Genomic Instability Associated with Unscheduled Accumulation of DNA:RNA Hybrids

Perturbation of transcription is associated with excessive R-loop formation and has recently been linked to genome instability (Aguilera and García-Muse, 2012; Gan et al., 2011; Skourti-Stathaki and Proudfoot, 2014; Tuduri et al., 2009). To determine whether the FA pathway is required to limit such structures, we blotted genomic DNA from control and FANCD2-depleted cells onto a membrane and probed it with the S9.6 antibody, which specifically recognizes DNA:RNA hybrids (Boguslawski et al.,

1986). The intensity of the DNA:RNA hybrid signal was increased in FANCD2-depleted cells (Figure 4A). We confirmed this finding by performing immunostaining experiments with the S9.6 antibody and also noticed a marked increase in the nuclear fluorescence intensity in cells depleted of FANCD2 (Figure 4B). We also found increased nuclear DNA:RNA levels when excluding nucleolar signals from the analysis (Figure S2B), indicating that RNA:DNA hybrids are elevated both in the nucleoli and the nucleus.

To understand whether suppression of DNA:RNA hybrids is a general function of the FA pathway, we analyzed additional FA mutants. To this end, we depleted FANCA, which is required for FANCD2 monoubiquitination, and we found significantly increased DNA:RNA hybrid formation in these cells (Figure 4C; Figures S2C and S2D). To verify and extend this observation, we also analyzed the level of DNA:RNA hybrids in avian *FANCD2*<sup>-/-</sup> and *FANCL*<sup>-/-</sup> DT40 mutants. The levels of DNA:RNA hybrids were increased in these mutants compared with wild-type cells (Figure 4D), suggesting that accumulation of DNA:RNA hybrids is a general phenomenon associated with FA deficiency. The presence of increased levels of DNA:RNA hybrids in *FANCL*<sup>-/-</sup> knockout cells suggests that monoubiquitination of FANCD2 is required to suppress their formation because FANCL is the E3 ligase that carries out FANCD2 activation by monoubiquitination (Alpi et al., 2008; Meetei et al., 2003). Therefore, it was not surprising that avian FANCD2 knockin cells expressing endogenous levels of the monoubiquitination-defective FANCD2 K563R mutant protein (Seki et al., 2007) showed higher

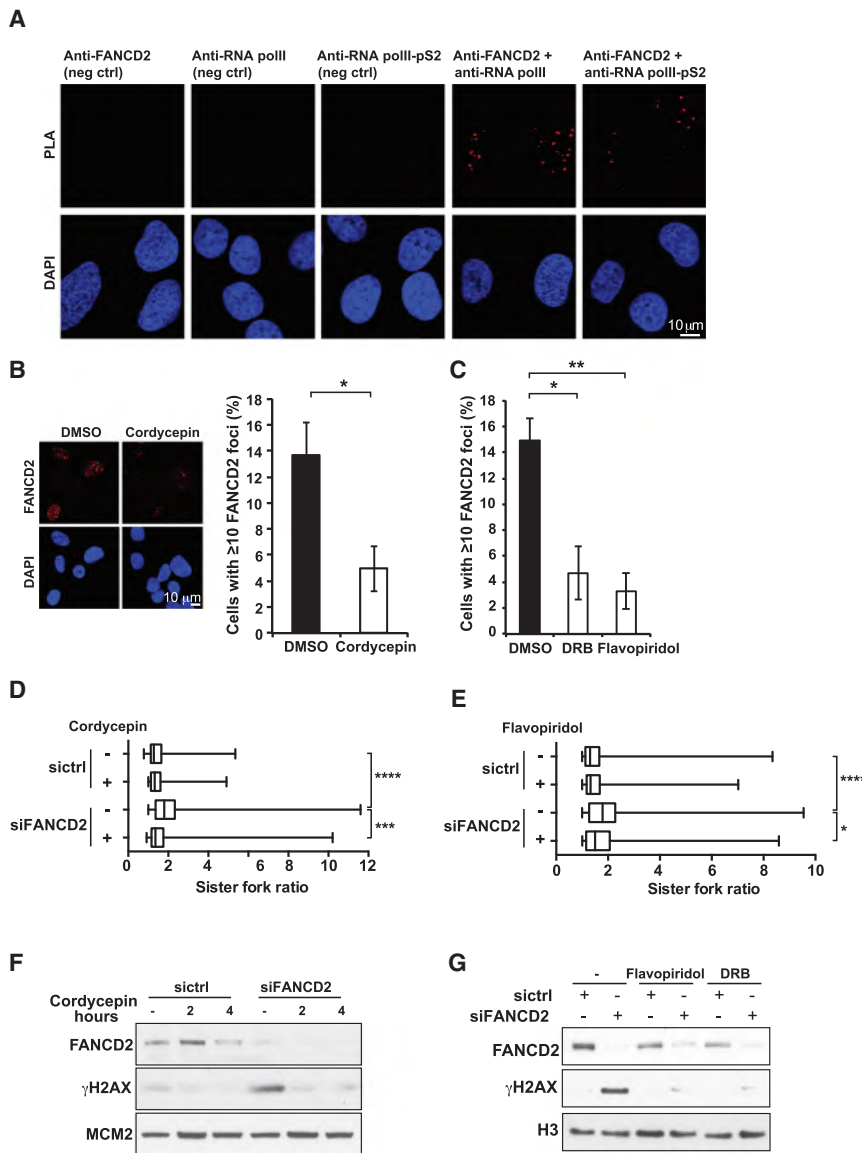


**Figure 2. FANCD2 Colocalizes with Sites of Transcription and Prevents Transcription-Induced Replication Stress**

(A) Proximity ligation assay showing that FANCD2 colocalizes with total and transcriptionally elongating (phospho-S2) RNA polymerase II. neg. ctrl., negative control.

(B) Treatment with 50  $\mu$ M of the transcription inhibitor cordycepin for 3 hr decreases the number of FANCD2 focus-positive cells. Means  $\pm$ SEM are displayed (n = 4; unpaired, two-tailed Student's t test). \*p  $\leq$  0.05.

(C) Treatment with either 100  $\mu$ M DRB or 0.8  $\mu$ M flavopiridol for 2 hr decreases the number of FANCD2 focus-positive cells. Means  $\pm$ SEM are shown (n = 3; unpaired, two-tailed Student's t test). \*p  $\leq$  0.05, \*\*p  $\leq$  0.01.

(D) DNA fiber analysis comparing sister fork symmetry in control or FANCD2-depleted U2OS cells treated with DMSO or cordycepin. The ratios of the lengths of two corresponding sister replication forks are plotted. The middle line represents the median and the boxes the 25<sup>th</sup> and 75<sup>th</sup> percentiles. The whiskers mark the smallest and largest values. Mann-Whitney test was used to determine statistical significance (n = 3). \*\*\*p  $\leq$  0.001, \*\*\*\*p  $\leq$  0.0001.

(E) Flavopiridol treatment reduces replication fork asymmetry. The experiments were plotted and statistical analysis was performed as in(D). \*p  $\leq$  0.05, \*\*\*\*p  $\leq$  0.0001.

(F) Western blot of whole-cell lysates from cordycepin- and siRNA-treated U2OS cells. Cordycepin abolishes the activation of  $\gamma$ H2AX occurring in the absence of FANCD2. MCM2 was the loading control.

(G) Western blot of whole-cell lysates from control and FANCD2-depleted cells treated with the transcription inhibitor DRB or flavopiridol. H3 served as the loading control.

levels of DNA:RNA hybrids compared with the level observed in wild-type cells (Figure 4D). Taken together, our findings indicate that FA pathway activation and FANCD2 monoubiquitination are required to limit DNA:RNA hybrid formation.

Next, we tested whether DNA:RNA hybrids contribute to the genome instability associated with FA deficiency. To this end, we made use of RNase H1, a nuclease that specifically removes such hybrids. First, we verified that overexpression of RNase H1 reduces the elevated DNA:RNA hybrid load observed in FANCD2 knockdown cells (Figure 5A). We confirmed this observation by incubating genomic DNA purified from control and FANCD2 knockdown cells with RNase H1. As expected, this treatment abolished the DNA:RNA hybrid signal in both samples (Figure S3A). Importantly, RNase H1 overexpression attenuated activation of the FA pathway in cells undergoing normal cell cycle progression, as judged by the significantly diminished formation of FANCD2 focus-positive cells as well as FANCD2 monoubiquitina-

tion (Figure 5B; Figure S3B), while not considerably altering the cell cycle profile (Figure S3C). Furthermore, it also rescued impaired the replication fork progression seen in FANCD2 knockdown cells (Figure 5C). This was accompanied by a significant reduction in DNA breaks as well as diminished activation of the DDR response (Figures 5D and 5E). Replicative stress has recently been linked to progressive elimination of hematopoietic stem and progenitor cells in FA patients because of constitutive activation of the p53/p21 response (Ceccaldi et al., 2012). We found that FANCD2-depleted U2OS cells also show a similar response, which was decreased upon overexpression of RNase H1 (Figure 5E). This indicates that physiologically occurring DNA:RNA hybrids induce FA pathway activation and, in its absence, contribute to the constitutive activation of the p53/p21 axis as well as genome instability associated with this disease.

Recently, it has been shown that DNA:RNA hybrid-associated DSB formation is dependent on XPF (Sollier et al., 2014). Therefore, we knocked down XPF in FANCD2-deficient cells to test the contribution of this structure-specific nuclease to the DNA

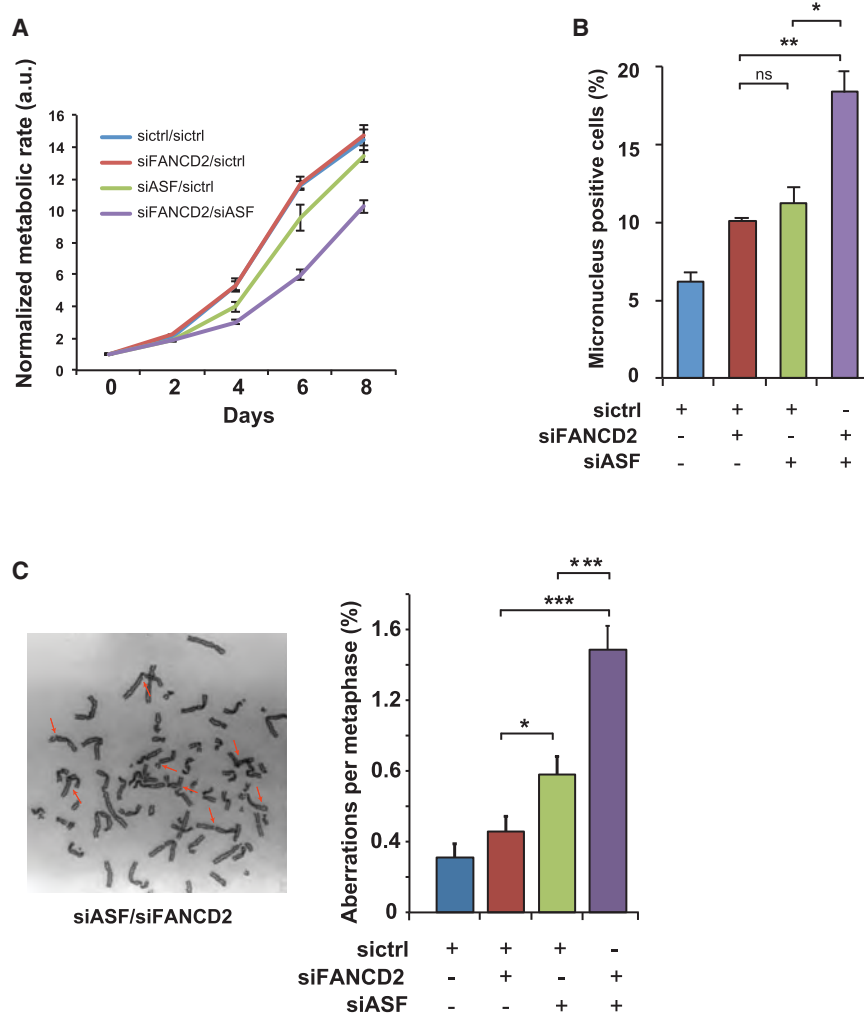


**Figure 3. Transcription-Associated Stress Exacerbates the Phenotype of FANCD2-Depleted Cells**

(A) Representative alamar blue assay showing that mutual downregulation of ASF and FANCD2 decreases cell proliferation compared with control or single knockdown cells. Error bars show SD from triplicates. a.u., arbitrary unit.

(B) Quantification of micronuclei in U2OS cells showing mean  $\pm$ SEM of three independent assays. Student's t test was used for statistical analysis. \* $p \leq 0.05$ ; \*\* $p \leq 0.01$ ; ns, not significant.

(C) Typical example of a metaphase spread of cells treated with siRNA against ASF and FANCD2. Arrows point to aberrations. The graph displays the frequency of chromosomal aberrations in U2OS cells after treatment with the indicated siRNAs (SEM of three independent experiments; Student's t test was used for statistical analysis). \* $p \leq 0.05$ , \*\*\* $p \leq 0.001$ .

*FANCD2*<sup>-/-</sup> clones displayed increased DNA breaks, genome instability, and DNA:RNA hybrid formation under normal growth conditions (Figures S4D–S4F).

Given that DNA-damaging agents, such as camptothecin (CPT) and UV light, induce DNA:RNA hybrid formation (Sollier et al., 2014; Tresini et al., 2015), we analyzed whether aldehydes, which have recently been implicated in the pathology of FA (Langevin et al., 2011), could also promote the formation of such structures. First, we assessed the effect of low, non-toxic doses of formaldehyde on transcription and cell cycle progression. Treatment with 5  $\mu$ M formaldehyde for 2 hr did not

markedly reduce overall transcription efficiency and cell cycle progression (Figures S5A and S5B). However, we found that formaldehyde treatment resulted in a further increase in DNA:RNA hybrids in FANCD2-deficient cells (Figure 5F). In line with the putative role for formaldehyde in DNA:RNA induction in FANCD2-deficient cells, inhibition of transcription with flavopiridol decreased the level of DNA:RNA hybrids in these cells (Figure S5C). Therefore, formaldehyde toxicity in FA-deficient cells could be, at least partially, related to its ability to induce DNA:RNA hybrids, thereby impacting replisome stability in the absence of FA. Taken together, these data suggest that the FA pathway prevents the deleterious effects associated with DNA:RNA hybrid accumulation and that such structures could be the cause of genome instability in FA-defective cells.

damage load observed in these cells. As shown previously, knockdown of XPF decreased the overall level of DNA breaks, as measured by comet assay (Sollier et al., 2014; Figures S3D and S3E). Concomitant depletion of both XPF and FANCD2 resulted in a slightly decreased level of DNA breaks compared with the siFANCD2 sample. However, the level of damage seen in the double knockdown was still significantly higher than in XPF-depleted cells (Figure S3D). Therefore, we conclude that FANCD2 is required to suppress DNA breaks associated with the presence of DNA:RNA hybrids in a manner that is partially independent of the role of XPF in this process, perhaps specifically during the S-phase of the cell cycle. Finally, to verify our small interfering RNA (siRNA) data, we used clustered regularly interspaced short palindromic repeats (CRISPR)/Cas9 nickase-based gene editing (Hsu et al., 2014) in U2OS cells to generate *FANCD2*<sup>-/-</sup> clones (Figures S4A and S4B). The use of Cas9 nickase has been shown recently to minimize any off-target effects (Shen et al., 2014). As expected, deletion of FANCD2 in the analyzed clones rendered the cells hypersensitive to the crosslinking agent cisplatin (Figure S4C). Similar to what we observed in siRNA-treated U2OS cells, both

markedly reduce overall transcription efficiency and cell cycle progression (Figures S5A and S5B). However, we found that formaldehyde treatment resulted in a further increase in DNA:RNA hybrids in FANCD2-deficient cells (Figure 5F). In line with the putative role for formaldehyde in DNA:RNA induction in FANCD2-deficient cells, inhibition of transcription with flavopiridol decreased the level of DNA:RNA hybrids in these cells (Figure S5C). Therefore, formaldehyde toxicity in FA-deficient cells could be, at least partially, related to its ability to induce DNA:RNA hybrids, thereby impacting replisome stability in the absence of FA. Taken together, these data suggest that the FA pathway prevents the deleterious effects associated with DNA:RNA hybrid accumulation and that such structures could be the cause of genome instability in FA-defective cells.

### The Fanconi Anemia Pathway Promotes Genome Stability through FANCM-Coupled Resolution of DNA:RNA Hybrids

Next, we asked whether the FA pathway could provide enzymatic activity to resolve DNA:RNA hybrids directly. A likely member of the FA pathway with such a putative function is FANCM. It

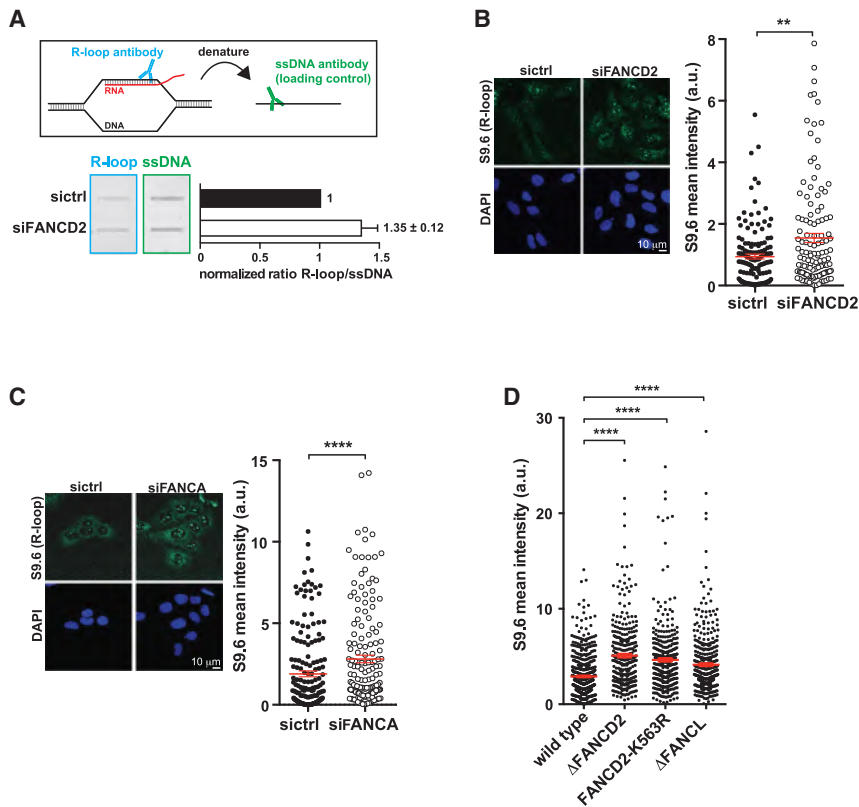


**Figure 4. The FA Pathway Prevents the Accumulation of DNA:RNA Hybrids**

(A) Experimental overview. Quantitative infrared (IR) fluorescence of genomic DNA of control and FANCD2-depleted cells using S9.6 antibody. Denatured DNA was probed with an antibody against single-stranded DNA (ssDNA) to determine DNA loading. The graph shows the ratio of DNA:RNA hybrid IR fluorescence intensity divided by single-stranded DNA IR fluorescence intensity from four independent experiments.

(B) Assembled z stacks of immunofluorescence staining with S9.6 antibody of FANCD2-depleted or control U2OS cells. Shown is the distribution of mean fluorescence intensity of individual nuclei in arbitrary units, with mean ± SEM in shown red (two-tailed Mann-Whitney test,  $n = 3$ ).  $**p \leq 0.01$ .

(C) The same as in (B) but with cells incubated with sictrl or siFANCA.  $****p \leq 0.0001$ .

(D) Quantified immunofluorescence intensity with the DNA:RNA hybrid-specific antibody S9.6 of wild-type (WT) DT40,  $FANCD2^{-/-}$ , FANCD2 K563R mutant, and  $FANCL^{-/-}$  cells. The dot plot represents the mean fluorescence intensity of individual nuclei from three independent experiments, with the middle line representing the mean and whiskers the SEM (two-tailed Mann-Whitney test).  $****p \leq 0.0001$ .

possesses double-stranded DNA translocase activity implicated in the processing of Holliday junction intermediates and replication fork reversal in vitro (Gari et al., 2008). In vivo, the protein has been shown to rescue stalled forks (Blackford et al., 2012; Schwab et al., 2010). Studies using recombinant FANCM have tested its activity only with DNA:DNA substrates (Gari et al., 2008). However, the protein is, in fact, classified to belong to the DEAD/DEAH family of DNA:RNA helicases. Therefore, we considered the possibility that FANCM could directly remove DNA:RNA hybrids through its translocase activity. In line with this notion, we observed a significant increase in DNA:RNA hybrid formation in FANCM-depleted cells (Figure 6A; Figure S6A). Importantly, purified FANCM was not only able to unwind replication fork structures, as shown previously (Gari et al., 2008; Figure S6B), but it efficiently unwound DNA:RNA hybrids in vitro (Figures 6B and 6C) despite such substrates being more stable than DNA:DNA hybrids found at a replication fork (Chien and Davidson, 1978). The branch-migratable structures were designed to mimic both the 5' and 3' ends of a DNA:RNA hybrid, and our biochemical analyses have shown that FANCM can translocate along either the Watson or Crick strand in a 3'-5' direction and disrupt DNA:RNA base pairing (Figures 6B and 6C). As expected, the resolution of DNA:RNA hybrids requires FANCM's translocase activity because the translocase-dead mutant protein was unable to unwind these substrates. Similarly, addition of non-hydrolysable ATP (ATP- $\gamma$ -S) blocked the reaction (Figures 6B and 6C; Figure S6B). Finally, knockin DT40 cells expressing the translocase-dead variant of FANCM (Rosado

et al., 2009) also displayed elevated levels of DNA:RNA hybrids (Figure 6D). This suggests a mechanism by which FANCM directly promotes DNA:RNA hybrid resolution, replication fork restart, and, consequently, faithful genome duplication. Because we observed no unwinding activity when the RNA sequence and flap sequence were heterologous (Figure S6C), we conclude that DNA:RNA hybrid resolution is carried out via its branch migration activity.

## DISCUSSION

Although DNA:RNA hybrids form naturally and have an important role in various biological processes, such as class-switch recombination or transcription termination (Skourti-Stathaki et al., 2011; Yu et al., 2003), it has recently become apparent that their persistent presence can drive genomic instability (Aguilera and García-Muse, 2012; Skourti-Stathaki and Proudfoot, 2014). Consequently, their formation and removal must be controlled and balanced carefully to prevent a detrimental effect on genome stability, cell survival, and organismal development. Our data suggest that the FA pathway is an important player in controlling DNA:RNA hybrid-associated defects. Accordingly, we show that, under normal growth conditions and in the absence of a functional FA pathway, cells display signs of replicative stress because of replication forks being stalled by transcription complexes, which subsequently leads to replisome collapse, DNA breaks and genome instability. These phenotypes are suppressed by inhibition of transcription or removal

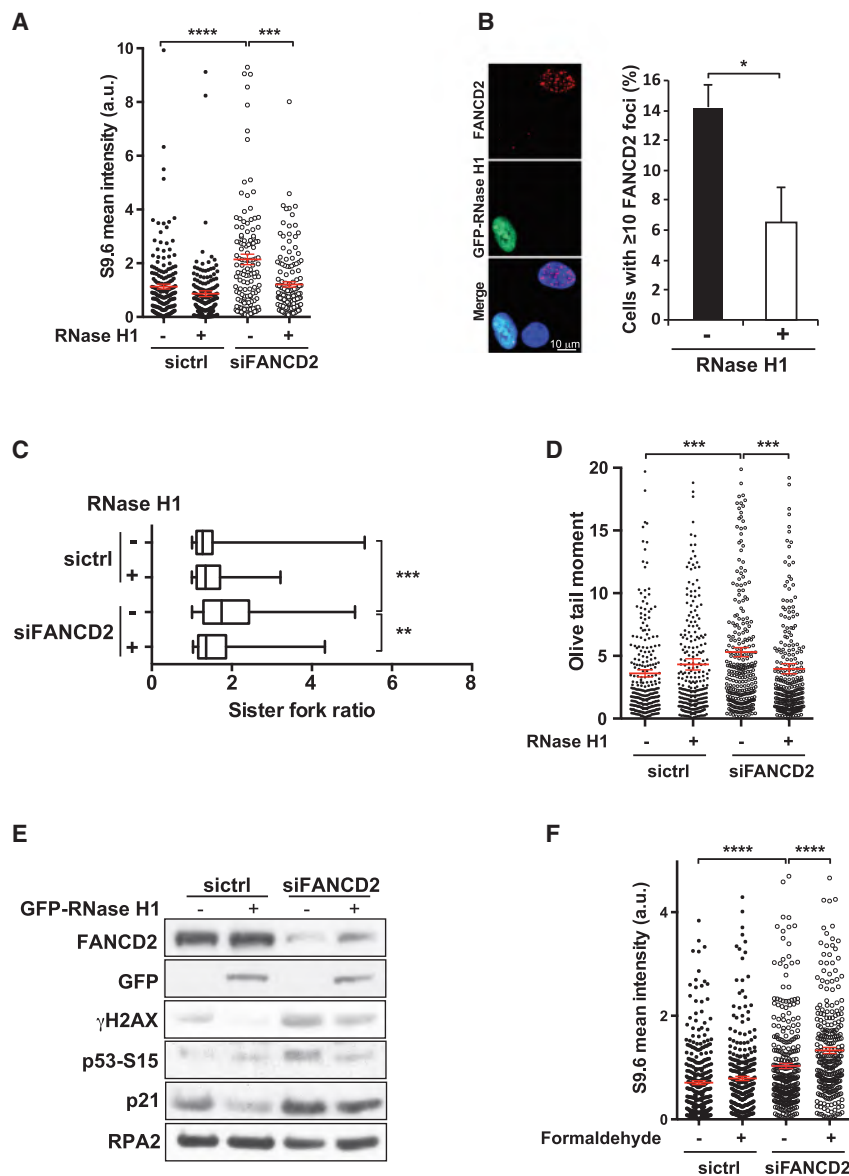


**Figure 5. Removal of DNA:RNA Hybrids Prevents Transcription-Induced Replication Stress in FANCD2-Depleted Cells**

(A) Mean nuclear DNA:RNA hybrid fluorescence intensity of RNaseH1-overexpressing sictrl or siFANCD2-treated cells ( $n = 3$ , mean  $\pm$  SEM, two-tailed Mann-Whitney test). \*\*\*\* $p \leq 0.001$ , \*\*\*\* $p \leq 0.0001$ .

(B) Frequency of cells with more than ten FANCD2 foci in control or GFP-RNaseH1-transfected U2OS cells. Mean  $\pm$  SEM are plotted (two-tailed Student's t test,  $n = 5$ ). \* $p \leq 0.05$ .

(C) Sister fork ratio with or without RNaseH1 overexpression. Box and whiskers are as in Figure 1A ( $n = 3$ , two-tailed Mann-Whitney test). \*\* $p \leq 0.01$ , \*\*\* $p \leq 0.001$ .

(D) Comet assay with sictrl and siFANCD2-treated cells overexpressing RNaseH1. Mean  $\pm$  SEM is shown in red (two-tailed Mann-Whitney test,  $n = 3$ ). \*\*\* $p \leq 0.001$ .

(E) Western blot showing decreased activation of  $\gamma$ H2AX, p53 (S-15) and p21 in FANCD2-depleted cells overexpressing RNaseH1. RPA2 served as a loading control.

(F) Distribution of mean fluorescence intensity of individual nuclei from control and FANCD2-depleted cells in the presence or absence of formaldehyde, with mean  $\pm$  SEM shown in red (two-tailed Mann-Whitney test,  $n = 3$ ). \*\*\*\* $p \leq 0.0001$ .

of DNA:RNA hybrids through overexpression of RNase H1. Mechanistically, the FA pathway not only suppresses the formation of R-loops but also actively resolves such structures utilizing FANCM's translocase activity. Based on these observations, we propose that the FA pathway plays a dual role in suppressing genome instability associated with conflicts between replication and transcription machineries. On one hand, it contributes to the stabilization of stalled replication forks until DNA:RNA hybrids are removed, and, on the other hand, it provides enzymatic activity to directly dismantle them. Consequently, this allows arrested replisomes to restart and faithfully complete genome duplication (Figure 6E).

Mutations in proteins controlling DNA:RNA hybrid levels have been identified in various tumors and are also highly prevalent in leukemias (Groh and Gromak, 2014), occurring at a high rate in FA patients (Kee and D'Andrea, 2012). Therefore, it is conceiv-

able that the FA pathway suppresses tumorigenesis by promoting the resolution of transcription-dependent replication blockades that could otherwise initiate the collapse of replication forks. This hypothesis could also explain the characteristic stem cell defects and heightened risk of tumorigenesis of FA patients because increased fork collapse might affect specific cellular compartments harboring cells that are particularly sensitive to DNA damage, such as hematopoietic precursors. In support of this, constitutive activation of the p53/p21 axis because of physiologically occurring replicative stress has recently been proposed as a central mechanism for progressive elimination of hematopoietic stem cells in FA patients (Ceccaldi et al., 2012). Accordingly, FANCA-deficient mouse hematopoietic stem cells show high levels of DNA damage during progression through S-phase (Walter et al., 2015).

Recently, seminal work from the Patel laboratory has suggested naturally derived aldehydes as drivers of bone marrow failure in FA-deficient mice (Langevin et al., 2011). Because aldehydes generate a plethora of DNA adducts, it is still impossible to precisely pinpoint the nature of the endogenous DNA lesion induced by aldehydes upon which the FA proteins act. Interestingly, our data show that treatment with formaldehyde results in increased DNA:RNA hybrid formation, suggesting a mechanism by which these compounds could contribute to genome instability, in particular in the absence of FA. Notably, treatment

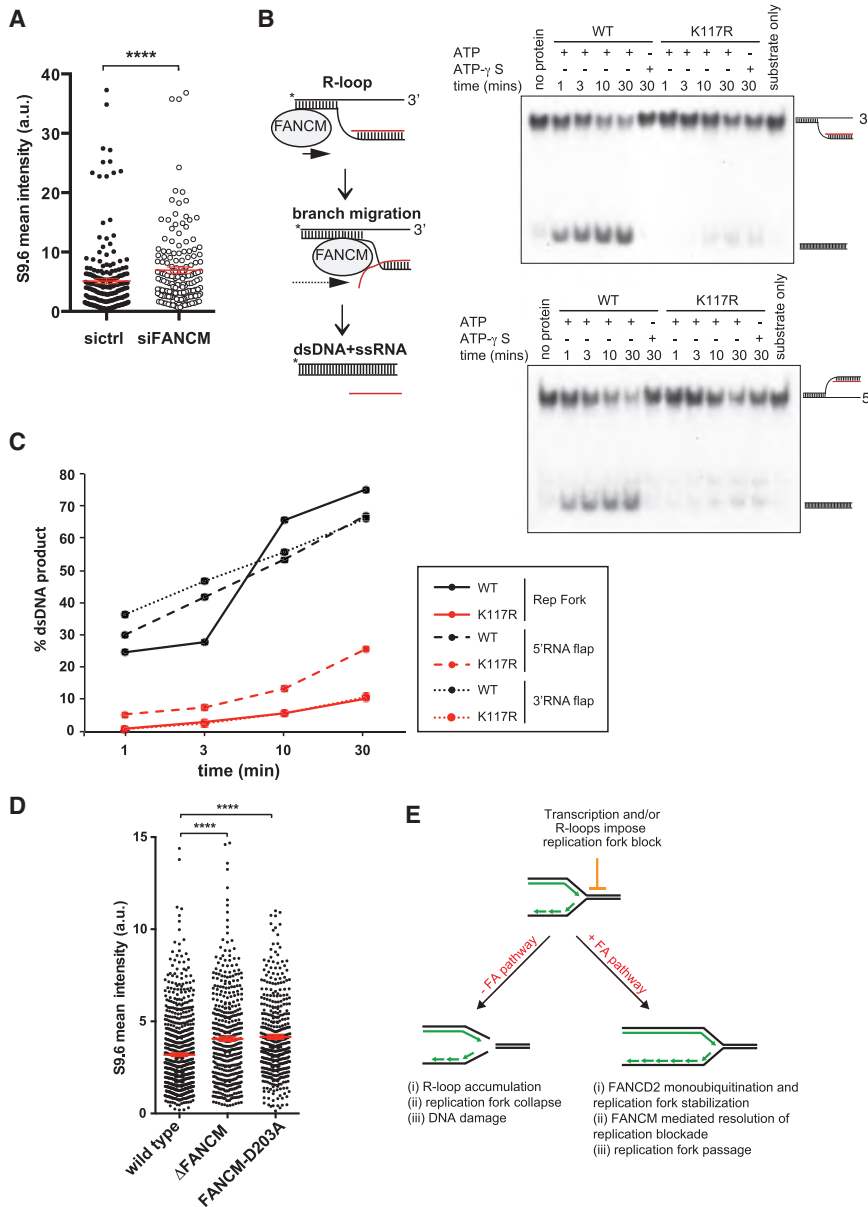


**Figure 6. The FA Pathway Prevents DNA:RNA Hybrid Accumulation via the DNA:RNA Branch Migration Activity of FANCM**

(A) Quantified immunofluorescence intensity with the DNA:RNA hybrid-specific antibody S9.6 of sic1r1 or siFANCM-treated cells. The dot plot represents the mean fluorescence intensity of individual nuclei from three experiments, with the middle line representing the mean and whiskers the SEM (two-tailed Mann-Whitney test). \*\*\*\*p ≤ 0.0001.

(B) Model of branch migration activity of FANCM, leading to the resolution of DNA:RNA hybrids, and in vitro unwinding assays with purified FANCM or FANCM K117R mutant and FAAP24 on migratable 3' and 5' DNA:RNA flap structures.

(C) Quantification of DNA:RNA hybrid resolution using a migratable replication (Rep) fork substrate as a positive control.

(D) Quantified immunofluorescence intensity with the DNA:RNA hybrid-specific antibody S9.6 of WT DT40, FANCM<sup>-/-</sup> cells, and DT40 cells expressing FANCM D203A translocase-dead mutant protein. The dot plot represents mean fluorescence intensity of individual nuclei from three independent experiments, with the middle line representing the mean and whiskers the SEM (two-tailed Mann-Whitney test). \*\*\*\*p ≤ 0.0001.

(E) Model explaining how the FA pathway prevents conflicts between replication and transcription. In the absence of the FA pathway, conflicts between replication and transcription result in activation of the DDR, DNA:RNA hybrid accumulation, defects in replication fork progression, DNA lesions, and genomic instability. In the presence of a functional FA pathway, transcription-induced replication fork stalling leads to monoubiquitination of FANCD2 by the FA core complex proteins and, therefore, activation of the FA pathway, resulting in stabilization of stalled replication forks. Subsequently, FANCM resolves replication blocks consisting of DNA:RNA hybrids via its translocase activity, and replication can resume normally.

with other DNA-damaging agents, such as CPT or UV light, has recently been shown to also induce R-loop formation (Sollier et al., 2014; Tresini et al., 2015). Therefore, toxicity associated with aldehydes could, at least partially, arise from altered transcription and/or transcript splicing, which can induce DNA:RNA hybrid formation (Huertas and Aguilera, 2003; González-Aguilera et al., 2008; Tresini et al., 2015). Alternatively, DNA nicks generated during the repair of aldehyde adducts could drive the formation of such hybrids. Indeed, it has been reported recently that nicks in the DNA template serve as strong DNA:RNA hybrid-initiating sites (Roy et al., 2010). Furthermore, it is possible that multiple compounds that arise endogenously from cellular metabolism could directly or indirectly induce DNA:RNA hybrid formation. Accordingly, DNA damage arises spontaneously in FA-deficient cells, including hematopoietic stem cells (Walter

et al., 2015), which are still proficient for aldehyde-detoxifying enzymes. Therefore, we propose that the FA pathway counteracts physiologically arising replicative stress associated with transcription complexes and/or unresolved DNA:RNA hybrids acting as potent replication barriers.

## EXPERIMENTAL PROCEDURES

### Cell Culture and Transfection with siRNA and DNA

U2OS and HeLa cells were maintained in DMEM and 10% fetal bovine serum (FBS). Chicken DT40 cells were cultured as described before (Schwab et al., 2010). siRNAs from Invitrogen were used for all knockdowns, with the following sequences: FANCA, AAGGGUCAAGAGGGAAAAUA (Sato et al., 2012); FANCD2, GGUCAGAGCUGUAUUUUUUC (Wagner and Karnitz, 2009); FANCM, AGACUAGCUGAAUUUUAAA (Xue et al., 2008); siASF, GUUUGACCUUUAUCUAAA (Tuduri et al., 2009); sic1r1, CGUACGCGAAUACUUCGA

(Tuschl, 2006); and siXPF, UUAACGUGGUGCAUCAAGG. Cells were transfected twice with 24 nM siRNA oligonucleotides using HiPerFect (QIAGEN). Cells were harvested 48 hr after the second siRNA administration. For experiments with RNase H1, transfections were performed 24 hr after the second siRNA pulse, and cells were harvested 36 hr later. 0.8 ng/ $\mu$ l GFP-RNase H1 plasmid DNA was used for experiments analyzing FANCD2 ubiquitylation status, and 0.3 ng/ $\mu$ l was transfected for all other experiments. Transfections were performed with Lipofectamine 2000 (Invitrogen). The GFP-RNase H1 plasmid was a gift from N. Proudfoot.

### Chromosomal Aberrations

Cells were prepared for analysis of chromosomal aberrations as described previously (Blackford et al., 2015).

### Generation of FANCD2 by CRISPR/Cas9

The following guide RNA (gRNA) sequences targeting the fourth exon of FANCD2 were selected using the optimized CRISPR Design tool (<http://crispr.mit.edu>; Hsu et al., 2013; gRNA1, TTTGTCTTGAGCGTCTGC; gRNA2, GGAGTCTTACATTGAGGATG). DNA oligonucleotides were purchased from Integrated DNA Technologies and cloned into the pX335-GFP vector (Cong et al., 2013) to generate targeting constructs that were subsequently co-transfected in an equimolar ratio into U2OS cells using Lipofectamine 2000. 24 hr after transfection, cells were sorted using a MoFlo cell sorter (Beckman Coulter) for cells expressing Cas9 nickase (GFP-positive cells) and left to recover for 6 days before sorting for single cells and allowing colonies to form. FANCD2 expression was analyzed by western blotting. Two clones showing loss of all detectable FANCD2 were selected for subsequent analysis.

### Immunofluorescence Microscopy

U2OS cells were grown overnight on coverslips. DT40 cells were allowed to set on Polysine slides (Thermo Scientific) for 10 min before fixation. Blocking was performed with 10% FBS in PBS for 1 hr. All antibodies were diluted in 0.1% FBS in PBS, and washes were performed with PBS unless stated otherwise. Alexa Fluor 488 or Alexa Fluor 555 secondary antibodies (Molecular Probes) were diluted 1:500. For quantification of micronuclei, cells were fixed and permeabilized in 100% methanol at  $-20^{\circ}\text{C}$  for 20 min, blocked, and then incubated with anti- $\alpha$ -tubulin (1:1,000). The coverslips were mounted onto a microscope slide with Vectashield containing DAPI (Vector Laboratories). To visualize GFP-RNase H1 and FANCD2 foci, cells were fixed with 4% paraformaldehyde for 10 min and permeabilized with 0.5% Triton X-100 for 5 min. After blocking, cells were incubated with anti-FANCD2 (1:750) or anti- $\gamma$ H2AX (1:750), followed by incubation with the secondary antibody. Finally, coverslips were incubated with GFP booster (1:200, Atto488, Chromotek) and then mounted. For quantification of the S9.6 mean fluorescence intensity, cells were fixed with 4% paraformaldehyde for 10 min, extracted with 100% methanol at  $-20^{\circ}\text{C}$  for 5 min, and then blocked with 5% BSA and 0.2% milk in PBS for 1 hr. S9.6 (1:60) was incubated in blocking buffer for 3 hr, and washes were performed with PBS containing 0.1% Tween 20. Images were acquired with a Zeiss 510 Meta laser-scanning confocal microscope at  $\times 63$  magnification. ImageJ was used for picture processing, assembly of z stacks, and quantification of S9.6 mean intensity.

### DNA Slot Blot Analysis

$3\text{--}5 \times 10^6$  cells were washed in PBS and lysed overnight in DNA lysis buffer (100 mM Tris-HCl [pH 8.5], 5 mM EDTA, 0.2% SDS, and 100 mM NaCl) containing 0.5 mg/ml proteinase K at  $55^{\circ}\text{C}$ . Genomic DNA was precipitated with isopropanol, spooled onto a rod, washed with 70% ethanol, air-dried, and resuspended in Tris-EDTA (TE) buffer. Equal amounts of DNA were blotted onto a nitrocellulose membrane (Amersham Biosciences) using a slot blot apparatus (Bio-Rad) and subsequently baked at  $80^{\circ}\text{C}$  for 2 hr. The membrane was blocked with 5% skimmed milk in PBS and incubated with S9.6 antibody, followed by incubation with an infrared dye secondary antibody (LI-COR Biosciences). The membrane was scanned using a quantitative fluorescence imaging system (Odyssey, LI-COR Biosciences). Subsequently, the membrane was incubated in denaturing buffer (0.4 M NaOH and 0.6 M NaCl), followed by neutralizing buffer (1.5 M NaCl and 0.5 M Tris [pH 7.4]) and an anti-single-strand DNA antibody to detect total DNA.

### DNA Fiber Assay

The assay was performed as described elsewhere in detail (Schwab and Niedzwiedz, 2011).

### Antibodies, Western Blotting, Cell Cycle Analysis, Transcription Inhibition, and PLA

See Supplemental Experimental Procedures for details.

### Biochemical Analysis

Purification of FANCM:FAAP24 was performed as described previously (Coulthard et al., 2013). DNA:RNA hybrids that mimic the 5' or 3' region of the transcription bubble were generated using 30-base pair (bp) and 60-bp DNA and RNA oligonucleotides (Table S1). 5 pmol 5'- $[\gamma\text{-}^{32}\text{P}]$ -labeled XOrig1 and 15 pmol cold oligos were annealed in 50  $\mu$ l annealing buffer (5 mM Tris-HCl [pH 7.5], 10 mM NaCl, 1 mM MgCl<sub>2</sub>, and 0.1 mM DTT) using a two-step assembly method according to Table S2 and purified as described previously (Rass and West, 2006). For branch migration assays, 15- $\mu$ l reactions contained 0.5 nM protein and 0.25 nM DNA substrate in reaction buffer (6 mM Tris [pH 7.5], 5% glycerol, 0.1 mM EDTA, 1 mM DTT, and 0.5 mM MgCl<sub>2</sub>) and 1 mM ATP or ATP- $\gamma$ -S. Reactions were carried out at  $30^{\circ}\text{C}$  for the indicated periods, deproteinized, and separated by 12% PAGE in Tris-borate-EDTA (TBE). Quantification was performed using ImageJ after subtracting the background level of double-stranded DNA (dsDNA) in the input. See Tables S1 and S2 for oligo sequences.

### Statistics

Statistical analysis was performed using GraphPad Prism 6.0e software and the tests described in the figure legends.

### SUPPLEMENTAL INFORMATION

Supplemental Information includes Supplemental Experimental Procedures, six figures, and two tables and can be found with this article online at <http://dx.doi.org/10.1016/j.molcel.2015.09.012>.

### AUTHOR CONTRIBUTIONS

R.A.S. carried out the majority of experimental work with contributions from J.N., W.N., J.L., D.L.M., C.C.L., and M.A.C. F.S. and A.J.D. performed the biochemical analysis. R.J.G. contributed to the DNA:RNA hybrid experiments. W.N. and R.A.S. conceived the project and wrote and edited the manuscript.

### ACKNOWLEDGMENTS

We thank Profs. K.J. Patel and M. Takata and Dr. G. Stewart for cell lines and Profs. A. Harris, K.J. Patel, P. McHugh, and N.J. Proudfoot for plasmids, antibodies, and siRNA. We thank Dr. D. Waithe (Wolfson Imaging Centre, Oxford) for his help with analysis of fluorescence immunostainings. We also thank Profs. K.J. Patel and J. Walter for helpful comments on the manuscript. This work was funded by a Worldwide Cancer Research International Fellowship and a WIMM/Medical Research Council Senior Non-Clinical Fellowship (to W.N.), Royal Society Grant UF100717 (to M.A.C.), a Goodger scholarship (to C.C.L.), and MRC and Clarendon scholarships (to D.L.M.). R.J.G.'s research is supported by the Medical Research Council (grant H4R00121-H40D). A.J.D. is a National Breast Cancer Foundation fellow supported by funding from NHMRC, the Fanconi Anemia Research Fund, and the Victorian Government IOS program.

Received: April 22, 2015

Revised: June 20, 2015

Accepted: September 16, 2015

Published: October 22, 2015

### REFERENCES

Aguilera, A., and García-Muse, T. (2012). R loops: from transcription byproducts to threats to genome stability. *Mol. Cell* 46, 115–124.

- Aguilera, A., and Gómez-González, B. (2008). Genome instability: a mechanistic view of its causes and consequences. *Nat. Rev. Genet.* 9, 204–217.
- Alpi, A.F., Pace, P.E., Babu, M.M., and Patel, K.J. (2008). Mechanistic insight into site-restricted monoubiquitination of FANCD2 by Ube2t, FANCL, and FANCI. *Mol. Cell* 32, 767–777.
- Andreassen, P.R., D'Andrea, A.D., and Taniguchi, T. (2004). ATR couples FANCD2 monoubiquitination to the DNA-damage response. *Genes Dev.* 18, 1958–1963.
- Bhatia, V., Barroso, S.I., García-Rubio, M.L., Tumini, E., Herrera-Moyano, E., and Aguilera, A. (2014). BRCA2 prevents R-loop accumulation and associates with TREX-2 mRNA export factor PCID2. *Nature* 511, 362–365.
- Blackford, A.N., Schwab, R.A., Nieminuszczy, J., Deans, A.J., West, S.C., and Niedzwiedz, W. (2012). The DNA translocase activity of FANCM protects stalled replication forks. *Hum. Mol. Genet.* 21, 2005–2016.
- Blackford, A.N., Nieminuszczy, J., Schwab, R.A., Galanty, Y., Jackson, S.P., and Niedzwiedz, W. (2015). TopBP1 interacts with BLM to maintain genome stability but is dispensable for preventing BLM degradation. *Mol. Cell* 57, 1133–1141.
- Boguslawski, S.J., Smith, D.E., Michalak, M.A., Mickelson, K.E., Yehle, C.O., Patterson, W.L., and Carrico, R.J. (1986). Characterization of monoclonal antibody to DNA:RNA and its application to immunodetection of hybrids. *J. Immunol. Methods* 89, 123–130.
- Ceccaldi, R., Parmar, K., Mouly, E., Delord, M., Kim, J.M., Regairaz, M., Pla, M., Vasquez, N., Zhang, Q.S., Pondarre, C., et al. (2012). Bone marrow failure in Fanconi anemia is triggered by an exacerbated p53/p21 DNA damage response that impairs hematopoietic stem and progenitor cells. *Cell Stem Cell* 11, 36–49.
- Chien, Y.H., and Davidson, N. (1978). RNA:DNA hybrids are more stable than DNA:DNA duplexes in concentrated perchlorate and trichloroacetate solutions. *Nucleic Acids Res.* 5, 1627–1637.
- Cong, L., Ran, F.A., Cox, D., Lin, S., Barretto, R., Habib, N., Hsu, P.D., Wu, X., Jiang, W., Marraffini, L.A., and Zhang, F. (2013). Multiplex genome engineering using CRISPR/Cas systems. *Science* 339, 819–823.
- Constantinou, A. (2012). Rescue of replication failure by Fanconi anaemia proteins. *Chromosoma* 121, 21–36.
- Conti, C., Saccà, B., Herrick, J., Lalou, C., Pommier, Y., and Bensimon, A. (2007). Replication fork velocities at adjacent replication origins are coordinately modified during DNA replication in human cells. *Mol. Biol. Cell* 18, 3059–3067.
- Cortez, D., Glick, G., and Elledge, S.J. (2004). Minichromosome maintenance proteins are direct targets of the ATM and ATR checkpoint kinases. *Proc. Natl. Acad. Sci. USA* 101, 10078–10083.
- Coulthard, R., Deans, A.J., Swuec, P., Bowles, M., Costa, A., West, S.C., and McDonald, N.Q. (2013). Architecture and DNA recognition elements of the Fanconi anemia FANCM-FAAP24 complex. *Structure* 21, 1648–1658.
- Gan, W., Guan, Z., Liu, J., Gui, T., Shen, K., Manley, J.L., and Li, X. (2011). R-loop-mediated genomic instability is caused by impairment of replication fork progression. *Genes Dev.* 25, 2041–2056.
- Gari, K., Décaillot, C., Stasiak, A.Z., Stasiak, A., and Constantinou, A. (2008). The Fanconi anemia protein FANCM can promote branch migration of Holliday junctions and replication forks. *Mol. Cell* 29, 141–148.
- González-Aguilera, C., Tous, C., Gómez-González, B., Huertas, P., Luna, R., and Aguilera, A. (2008). The THP1-SAC3-SUS1-CDC31 complex works in transcription elongation-mRNA export preventing RNA-mediated genome instability. *Mol. Biol. Cell* 19, 4310–4318.
- Groh, M., and Gromak, N. (2014). Out of balance: R-loops in human disease. *PLoS Genet.* 10, e1004630.
- Heddle, J.A., Lue, C.B., Saunders, E.F., and Benz, R.D. (1978). Sensitivity to five mutagens in Fanconi's anemia as measured by the micronucleus method. *Cancer Res.* 38, 2983–2988.
- Helmrich, A., Ballarino, M., and Tora, L. (2011). Collisions between replication and transcription complexes cause common fragile site instability at the longest human genes. *Mol. Cell* 44, 966–977.
- Hira, A., Yoshida, K., Sato, K., Okuno, Y., Shiraishi, Y., Chiba, K., Tanaka, H., Miyano, S., Shimamoto, A., Tahara, H., et al. (2015). Mutations in the gene encoding the E2 conjugating enzyme UBE2T cause Fanconi anemia. *Am. J. Hum. Genet.* 96, 1001–1007.
- Hsu, P.D., Scott, D.A., Weinstein, J.A., Ran, F.A., Konermann, S., Agarwala, V., Li, Y., Fine, E.J., Wu, X., Shalem, O., et al. (2013). DNA targeting specificity of RNA-guided Cas9 nucleases. *Nat. Biotechnol.* 31, 827–832.
- Hsu, P.D., Lander, E.S., and Zhang, F. (2014). Development and applications of CRISPR-Cas9 for genome engineering. *Cell* 157, 1262–1278.
- Huertas, P., and Aguilera, A. (2003). Cotranscriptionally formed DNA:RNA hybrids mediate transcription elongation impairment and transcription-associated recombination. *Mol. Cell* 12, 711–721.
- Kee, Y., and D'Andrea, A.D. (2012). Molecular pathogenesis and clinical management of Fanconi anemia. *J. Clin. Invest.* 122, 3799–3806.
- Knipscheer, P., Räsche, M., Smogorzewska, A., Enou, M., Ho, T.V., Schärer, O.D., Elledge, S.J., and Walter, J.C. (2009). The Fanconi anemia pathway promotes replication-dependent DNA interstrand cross-link repair. *Science* 326, 1698–1701.
- Kottemann, M.C., and Smogorzewska, A. (2013). Fanconi anaemia and the repair of Watson and Crick DNA crosslinks. *Nature* 493, 356–363.
- Langevin, F., Crossan, G.P., Rosado, I.V., Arends, M.J., and Patel, K.J. (2011). Fancd2 counteracts the toxic effects of naturally produced aldehydes in mice. *Nature* 475, 53–58.
- Lecona, E., and Fernández-Capetillo, O. (2014). Replication stress and cancer: it takes two to tango. *Exp. Cell Res.* 329, 26–34.
- Li, X., and Manley, J.L. (2005). Inactivation of the SR protein splicing factor ASF/SF2 results in genomic instability. *Cell* 122, 365–378.
- Lossaint, G., Larroque, M., Ribeyre, C., Bec, N., Larroque, C., Décaillot, C., Gari, K., and Constantinou, A. (2013). FANCD2 binds MCM proteins and controls replisome function upon activation of s phase checkpoint signaling. *Mol. Cell* 51, 678–690.
- Luebben, S.W., Kawabata, T., Johnson, C.S., O'Sullivan, M.G., and Shima, N. (2014). A concomitant loss of dormant origins and FANCC exacerbates genome instability by impairing DNA replication fork progression. *Nucleic Acids Res.* 42, 5605–5615.
- Luna, R., Jimeno, S., Marín, M., Huertas, P., García-Rubio, M., and Aguilera, A. (2005). Interdependence between transcription and mRNP processing and export, and its impact on genetic stability. *Mol. Cell* 18, 711–722.
- Meetei, A.R., de Winter, J.P., Medhurst, A.L., Wallisch, M., Waisfisz, Q., van de Vrugt, H.J., Oostra, A.B., Yan, Z., Ling, C., Bishop, C.E., et al. (2003). A novel ubiquitin ligase is deficient in Fanconi anemia. *Nat. Genet.* 35, 165–170.
- Montes de Oca, R., Andreassen, P.R., Margossian, S.P., Gregory, R.C., Taniguchi, T., Wang, X., Houghtaling, S., Grompe, M., and D'Andrea, A.D. (2005). Regulated interaction of the Fanconi anemia protein, FANCD2, with chromatin. *Blood* 105, 1003–1009.
- Niedzwiedz, W., Mosedale, G., Johnson, M., Ong, C.Y., Pace, P., and Patel, K.J. (2004). The Fanconi anaemia gene FANCC promotes homologous recombination and error-prone DNA repair. *Mol. Cell* 15, 607–620.
- Oberbeck, N., Langevin, F., King, G., de Wind, N., Crossan, G.P., and Patel, K.J. (2014). Maternal aldehyde elimination during pregnancy preserves the fetal genome. *Mol. Cell* 55, 807–817.
- Rass, U., and West, S.C. (2006). Synthetic junctions as tools to identify and characterize Holliday junction resolvases. *Methods Enzymol.* 408, 485–501.
- Rickman, K.A., Lach, F.P., Abhyankar, A., Donovan, F.X., Sanborn, E.M., Kennedy, J.A., Sougnez, C., Gabriel, S.B., Elemento, O., Chandrasekharappa, S.C., et al. (2015). Deficiency of UBE2T, the E2 Ubiquitin Ligase Necessary for FANCD2 and FANCI Ubiquitination, Causes FA-T Subtype of Fanconi Anemia. *Cell Rep.* 12, 35–41.
- Rosado, I.V., Niedzwiedz, W., Alpi, A.F., and Patel, K.J. (2009). The Walker B motif in avian FANCM is required to limit sister chromatid exchanges but is dispensable for DNA crosslink repair. *Nucleic Acids Res.* 37, 4360–4370.

- Rose, K.M., Bell, L.E., and Jacob, S.T. (1977). Specific inhibition of chromatin-associated poly(A) synthesis in vitro by cordycepin 5'-triphosphate. *Nature* 267, 178–180.
- Roy, D., Zhang, Z., Lu, Z., Hsieh, C.L., and Lieber, M.R. (2010). Competition between the RNA transcript and the nontemplate DNA strand during R-loop formation in vitro: a nick can serve as a strong R-loop initiation site. *Mol. Cell Biol.* 30, 146–159.
- Sartori, A.A., Lukas, C., Coates, J., Mistrik, M., Fu, S., Bartek, J., Baer, R., Lukas, J., and Jackson, S.P. (2007). Human CtIP promotes DNA end resection. *Nature* 450, 509–514.
- Sato, K., Ishiai, M., Toda, K., Furukoshi, S., Osakabe, A., Tachiwana, H., Takizawa, Y., Kagawa, W., Kitao, H., Dohmae, N., et al. (2012). Histone chaperone activity of Fanconi anemia proteins, FANCD2 and FANCI, is required for DNA crosslink repair. *EMBO J.* 31, 3524–3536.
- Schlacher, K., Wu, H., and Jasin, M. (2012). A distinct replication fork protection pathway connects Fanconi anemia tumor suppressors to RAD51-BRCA1/2. *Cancer Cell* 22, 106–116.
- Schwab, R.A., and Niedzwiedz, W. (2011). Visualization of DNA replication in the vertebrate model system DT40 using the DNA fiber technique. *J. Vis. Exp.* 56, e3255.
- Schwab, R.A., Blackford, A.N., and Niedzwiedz, W. (2010). ATR activation and replication fork restart are defective in FANCM-deficient cells. *EMBO J.* 29, 806–818.
- Seki, S., Ohzeki, M., Uchida, A., Hirano, S., Matsushita, N., Kitao, H., Oda, T., Yamashita, T., Kashiwara, N., Tsubahara, A., et al. (2007). A requirement of FancL and FancD2 monoubiquitination in DNA repair. *Genes Cells* 12, 299–310.
- Shen, B., Zhang, W., Zhang, J., Zhou, J., Wang, J., Chen, L., Wang, L., Hodgkins, A., Iyer, V., Huang, X., and Skarnes, W.C. (2014). Efficient genome modification by CRISPR-Cas9 nickase with minimal off-target effects. *Nat. Methods* 11, 399–402.
- Sirbu, B.M., Couch, F.B., Feigerle, J.T., Bhaskara, S., Hiebert, S.W., and Cortez, D. (2011). Analysis of protein dynamics at active, stalled, and collapsed replication forks. *Genes Dev.* 25, 1320–1327.
- Skourti-Stathaki, K., and Proudfoot, N.J. (2014). A double-edged sword: R loops as threats to genome integrity and powerful regulators of gene expression. *Genes Dev.* 28, 1384–1396.
- Skourti-Stathaki, K., Proudfoot, N.J., and Gromak, N. (2011). Human senataxin resolves RNA/DNA hybrids formed at transcriptional pause sites to promote Xrn2-dependent termination. *Mol. Cell* 42, 794–805.
- Sollier, J., Stork, C.T., García-Rubio, M.L., Paulsen, R.D., Aguilera, A., and Cimprich, K.A. (2014). Transcription-coupled nucleotide excision repair factors promote R-loop-induced genome instability. *Mol. Cell* 56, 777–785.
- Taniguchi, T., Garcia-Higuera, I., Andreassen, P.R., Gregory, R.C., Grompe, M., and D'Andrea, A.D. (2002). S-phase-specific interaction of the Fanconi anemia protein, FANCD2, with BRCA1 and RAD51. *Blood* 100, 2414–2420.
- Tresini, M., Warmerdam, D.O., Kolovos, P., Snijder, L., Vrouwe, M.G., Demmers, J.A., van IJcken, W.F., Grosveld, F.G., Medema, R.H., Hoeijmakers, J.H., et al. (2015). The core spliceosome as target and effector of non-canonical ATM signalling. *Nature* 523, 53–58.
- Tuduri, S., Crabbé, L., Conti, C., Tourrière, H., Holtgreve-Grez, H., Jauch, A., Pantescio, V., De Vos, J., Thomas, A., Theillet, C., et al. (2009). Topoisomerase I suppresses genomic instability by preventing interference between replication and transcription. *Nat. Cell Biol.* 11, 1315–1324.
- Tuschl, T. (2006). Cotransfection of luciferase reporter plasmids with siRNA duplexes. *CSH Protoc.* Published online June 1, 2006. <http://dx.doi.org/10.1101/pdb.prot4342>.
- Wagner, J.M., and Karnitz, L.M. (2009). Cisplatin-induced DNA damage activates replication checkpoint signaling components that differentially affect tumor cell survival. *Mol. Pharmacol.* 76, 208–214.
- Walden, H., and Deans, A.J. (2014). The Fanconi anemia DNA repair pathway: structural and functional insights into a complex disorder. *Annu. Rev. Biophys.* 43, 257–278.
- Walter, D., Lier, A., Geiselhart, A., Thalheimer, F.B., Huntscha, S., Sobotta, M.C., Moehle, B., Brocks, D., Bayindir, I., Kaschutnig, P., et al. (2015). Exit from dormancy provokes DNA-damage-induced attrition in haematopoietic stem cells. *Nature* 520, 549–552.
- Wang, W. (2007). Emergence of a DNA-damage response network consisting of Fanconi anaemia and BRCA proteins. *Nat. Rev. Genet.* 8, 735–748.
- Xue, Y., Li, Y., Guo, R., Ling, C., and Wang, W. (2008). FANCM of the Fanconi anemia core complex is required for both monoubiquitination and DNA repair. *Hum. Mol. Genet.* 17, 1641–1652.
- Yu, K., Chedin, F., Hsieh, C.L., Wilson, T.E., and Lieber, M.R. (2003). R-loops at immunoglobulin class switch regions in the chromosomes of stimulated B cells. *Nat. Immunol.* 4, 442–451.

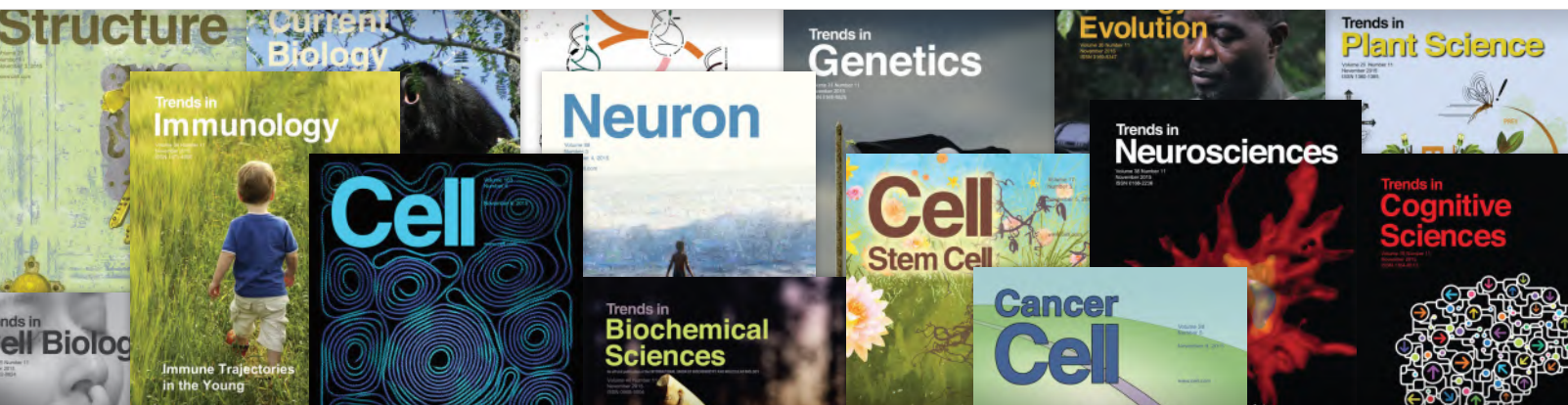


**DON'T BE THE  
LAST TO KNOW**

**Give your research a boost with alerts from Cell Press. You'll be glad you did.**

Get first access with immediate, regular electronic table of contents (eToCs) alerts delivered directly to your desktop, free of charge, that keep you informed of breakthroughs in your field.

Exciting extra features like video abstracts, podcasts, and blog posts give you additional depth and context and you can access news and commentary, normally not accessible online, in advance of publication.



Register today  
Visit [cell.com/alerts](http://cell.com/alerts)

**CellPress**

QUALIFIED ANTIBODIES | MADE IN THE USA | VALIDATED IN THE USA

#%&@  
YES!

**BETHYL**  
LABORATORIES, INC  
Really Good Antibodies

### Heck Yes!—Great Reactions Start with Really Good Antibodies

That's because every antibody is manufactured and validated on-site using a unique process that verifies target specificity with paired antibodies raised against distinct protein epitopes. We've heard our customers' great reactions for over 40 years and now we'd like to hear what you'll say.

Request a free trial size antibody by visiting [bethyl.com/8855](http://bethyl.com/8855)

Terms & Conditions Apply. Please see webpage for complete details.

©2016 Bethyl Laboratories, Inc. All rights reserved.

QUALIFIED ANTIBODIES | MADE IN THE USA | VALIDATED IN THE USA

OH MY  
#Y\$&!

**BETHYL**  
LABORATORIES, INC

Really Good Antibodies

### Oh My Gosh!—Great Reactions Start with Really Good Antibodies

That's because every antibody is manufactured and validated on-site using a unique process that verifies target specificity with paired antibodies raised against distinct protein epitopes. We've heard our customers' great reactions for over 40 years and now we'd like to hear what you'll say.

Request a free trial size antibody by visiting [bethyl.com/8855](https://bethyl.com/8855)

Terms & Conditions Apply. Please see webpage for complete details.